THE ROLE OF DMRT1 IN POSTNATAL TESTIS DIFFERENTIATION

By

Valentine A. Agbor

B.Sc., University of Buea, 2002;
M.S., New Mexico Highlands University, 2006

Submitted to the graduate degree program in Molecular and Integrative Physiology
and to the Graduate Faculty of the University of Kansas
in partial fulfillment of the requirements for the degree of
Doctor of Philosophy

Dissertation Committee:

Leslie L. Heckert, Ph.D., Chair

Joseph S. Tash, Ph.D.

Kenneth R. Peterson, Ph.D.

T. Rajendra Kumar, Ph.D

V. Gustavo Blanco, M.D., Ph.D.

Dissertation defended: August 31, 2012

The Dissertation Committee for Valentine A. Agbor

certifies that this is the approved version of the following dissertation:

THE ROLE OF DMRT1 IN POSTNATAL TESTIS DIFFERENTIATION

Dissertation Committee:

Leslie L. Heckert, Ph.D., Chair

Date Approved: September 4, 2012

Abstract

DMRT1 (doublesex and maleabnormal-3 related transcription factor-1) is a transcription regulator that is expressed in Sertoli cells and germ cells of the testis, where it directs mammalian postnatal testis differentiation. It is currently the only mammalian gene within the sex determination and sex differentiation genetic pathways that is evolutionary conserved and shares a cysteine-rich DNA binding motif (DM-domain) with doublesex in the fruit fly and maleabnormal-3 in the roundworm. The work presented in this dissertation revealed numerous novel roles of DMRT1, including Sertoli cell-specific rescue, structural function in the testis, cell-specific pathways and targets, and a probable regulation by NANOS2 in germ cells; thus providing important insight into how DMRT1 regulates testis development. Recombinogenic engineering was invaluable in the generation of a novel Sertoli cell-rescue (*Dmrt1*$^{-/-;tg}$) mouse model, which is a DMRT1-deficient germ cell model that was produced by breeding *Dmrt1*-null (*Dmrt1*$^{-/-}$) mice with *Wt1-Dmrt1* transgenic mice. The *Wt1-Dmrt1* transgenic mice express a rat *Dmrt1* cDNA in gonadal supporting cells by directing it from the Wilms' tumor locus carried on a yeast artificial chromosome transgene. Characterization of the Sertoli cell rescue mice revealed Sertoli cell-specific function of DMRT1 in the maintenance of seminiferous tubule morphology, autonomous and non-autonomous dose-dependent gene regulation, Sertoli cell differentiation, maintenance of testis size and sperm progressive motility, organization of testis-specific adherens junctions and maturation of Leydig cells and thus regulation of testosterone production. Furthermore, cell-specific direct and indirect pathways and targets regulated by DMRT1 in Sertoli cells and germ cells were identified using global gene expression profiles combined with ChIP-Seq. Analyses of the gene profiles identified potential functions for DMRT1 in vesicular transport, ubiquitination and RNA binding. Similarly, analysis of ChIP-Seq data identified 150

targets with the majority of DMRT1 binding sites located in introns, indicating that DMRT1 preferentially binds to distal regulatory regions. Finally, direct protein-protein interaction was shown between DMRT1 and NANOS2, an evolutionary conserved RNA-binding protein that plays a key role in male germ cell differentiation, by inhibiting entry into meiosis. NANOS2 was shown to act upstream, interact, partially co-localize and repress the *in vitro* transcriptional activity of DMRT1 in germ cells. Overall, these experiments uncovered several questions and new cell-specific roles of DMRT1 in testis differentiation. These findings and their implications are discussed further in this dissertation within the general scope of reproductive biology and the more defined scope of postnatal testis differentiation.

Acknowledgement

This dissertation symbolizes my negligible contribution that nourishes an infinite dedication to science, which is congenital and supported by my mentor, Dr. Leslie Lynn Heckert, whose leadership was invaluable to this chef-d'oeuvre. Her thoughtfulness and tolerance to let me learn through mistakes; her patience to teach me to think, plan, write and perform as a scientist is highly appreciated and I am truly indebted.

Gratitude goes to my parents, siblings, cousins, nieces, nephews, girlfriend and in-laws whose encouragement kept the candle burning during good and bad times.

Student life would have been boring without the countless lifetime friends I have made during graduate school, especially Elizabeth Dille and Jitu George, this life-changing experience has come and gone, but our shared relationships have made us resilient and will last forever.

For the numerous student groups and governing bodies that I was involved with, especially the Physiology Society provided valuable distractions and opportunities to improve my leadership skills. This opportunity was conceivable because of the incessant support for the graduate student community by Dr. Paul Cheney, Chair of the Department of Molecular and Integrative Physiology. Moreover, for the administrative staff members of the University who spent uncountable hours working together with these groups to improve the student experience at the University of Kansas Medical Center.

I am grateful to the members of Dr. Heckert's laboratory, past and present, with and from whom I have learned so much including: Dr. Brian Hermann, Dr. Ning Lei, Kaori Hornbaker, Dr. Tatiana Karpova, Dr. Ravichandran Kumarasamy, Dr. Mathew Anway, Dr. Shixin Tao,

Anindita Chatterjee, Daren Rice, Dr. Barbara Sotolongo, Lovella Tejada, Jitu George and Elizabeth Dille.

My sincere gratitude to those whose technical assistance greatly influenced the success of the experiments reported in this dissertation including Dr. David Albertini, Dr. William Kinsey, Barbara Fegley, Clark Bloomer, Dr. Sumedha Gunewardena, Dr. Stan Svojanovsky, Dr. In-Hee Lee and Dr. Mahesh Visvanathan.

I am appreciative for the continuous assistance from staff members of the Department of Molecular and Integrative Physiology and Center for Reproductive Sciences, past and present including: Jennifer Wallace, Linda Carr, Shari Standiferd, Liz Meng, Linda Spears and Barbara Shull without whom this work would not have come to fruition.

Finally, I am indebted to my student advisory committee, whose impartial feedbacks, recommendations and guidance were invaluable in accomplishing my research aims, experimental design, and professional development; all of which were vital elements of my graduate education.

Table of contents

List of Figures and Tables

Chapter 1: Introduction

Chapter 2: A Wt1-Dmrt1 transgene restores DMRT1 to Sertoli cells of *Dmrt1*$^{-/-}$ testes; a novel model of DMRT1-deficient germ cells

List of Abbreviations

^{3}H ..... ……Radioactive hydrogen (tritium)

A

ade .....Adenine

AMH ..... Anti-mullerian hormone

Ano4.....Anoctamin 4

ANOVA .....Analysis of variance

Aqp5..... Aquaporin 5

AR ..... Androgen receptor

ATM..... Ataxia telangiectasia-mutated gene

B

BAC .....Bacterial artificial chromosome

Bax .....BCL2-associated X protein

Bcat ..... Branched-chain amino acid aminotransferase protein

Bcl2 ..... B cell leukemia/lymphoma 2

Bmp4.....Bone morphogenetic protein 4

Bmp8b..... bone morphogenetic protein 8b

Boll.....bol, boule-like (Drosophila)

BTB.....Blood testis barrier

C

Cadm1 .....Cell adhesion molecule 1

can..... Arginine permease

CASA.....Computer assisted semen analysis

cDNA .....Complementary DNA

Cfi ..... Complement factor i

ChIP-chip ...Chromatin immunoprecipitation with microarray technology

ChIP-qPCR ....Chromatin immunoprecipitation followed by quantitative polymerase chain reaction

ChIP-Seq …Chromatin immunoprecipitation with massive parallel DNA sequencing

Cidea……..Cell death-inducing DNA fragmentation factor; alpha subunit-like effector A

c-Kit . ….c-kit proto-oncogene protein/ Steel factor receptor

Cldn11.....Claudin 11

Clec12b ..... C-type lectin domain family 12, member B

CO_2.....Carbon dioxide

CoA ..... Coenzyme A

Cpne8 .....copine VIII

Crabp II .....……Cellular retinoic acid binding protein II

Cre..... Cre recombinase

Cyp26b1 .....Cytochrome P450, family 26, subfamily b, polypeptide 1

D

DAPI .....4',6-diamidino-2-phenylindole

DAVID.....…Database for Annotation, Visualization and Integrated Discovery

Dax1 ...Congenital adrenal hypoplasia on the X chromosome, gene 1

Dazl ..... Deleted in azoospermia-like

Dhh..... Desert hedgehog

DM .....DNA binding motif

DMRT1……doublesex and maleabnormal-3 related transcription factor 1

DMRT1A2….doublesex and maleabnormal-3 related transcription factor 1A2

DMRT2……doublesex and maleabnormal-3 related transcription factor 2

DMRT3……doublesex and maleabnormal-3 related transcription factor 3

DMRTA1. ... doublesex and maleabnormal-3 related transcription factor A1

DMRTB1. ... doublesex and maleabnormal-3 related transcription factor B1

DMRTC1 ... .doublesex and maleabnormal-3 related transcription factor C1

DMRTC2 ... .doublesex and maleabnormal-3 related transcription factor C2

DNA..... Deoxyribonucleic acid

DNase I ..... Deoxyribonuclease I

Dnd.....Dead end homolog

dpc.....days post coitus

dsx..... doublesex

DTT.....Dithiothreitol

E

Egr1..... Early growth response 1

Emb.....Embigin

Emx2.....Empty spiracles homolog 2

ES.....Ectoplasmic specialization

ESD..... Environmental sex determination

Espin .....….Ectoplasmic specialization associated protein

ExoCarta .....….Exosome protein, RNA and lipid database

F

Fbln2 .....Fibulin 2

Fcgrb2 ....…Fc fragment of IgG, low affinity IIb, receptor

Fgf8 .....Fibroblast growth factor 8

Fgf9 .....Fibroblast growth factor 9

Fgfr2..... Fibroblast growth factor receptor 2

FITC .....Fluorescein isothiocyanate

Foxl2 .....Forkhead box L2

Foxq1 ..... Forkhead box Q1

FSH .....Follicle stimulating hormone

Fshr ...Follicle stimulating hormone receptor

G

GATA1 .....GATA binding protein 1

Gata4/Fog2...……GATA binding protein 4 / Friend of GATA binding protein 2

GC .....Germ cell

GCDmrt1KO..... Germ cell-specific Dmrt1 knockout

GCNA1 .....Germ cell nuclear antigen 1

Gdf9 .....Growth differentiation factor 9

GDNF……...…….....Glial cell line derived neurotrophic factor

Gfra3….Glial cell line derived neurotrophic factor family receptor alpha 3

Gja3.....Gap junction protein, alpha 3

Gpr37 .....G protein-coupled receptor 37

GSD..... Genetic sex determination

Gtsf1..... Gametocyte specific factor 1

H

h ……..Hour

H2Aa…….....Histocompatibility 2, class II antigen A, alpha

H3K27me3... ……Trimethylation of histone H3 at lysine 27

H3K9me2.....Dimethylation of histone H3 at lysine 9

HEPES .....4-(2-hydroxyethyl)-1-piperazineethanesulfonic acid

his.....Histidine

Hoxa10 .....Homeobox A10

Hoxa11 .....homeobox A11

HPRT1 ..... Hypoxanthine phosphoribosyl transferase 1

HRP .....Horseradish peroxidase

Hspb8 ..... Heat shock protein 8

I

Ifitm3..... Interferon induced transmembrane protein 3

IGF-1 ..... Insulin-like growth factor 1

IL-6 .....Interleukin 6

Insl3.....Insulin-like 3

K

kb.....Kilo bases

kDa.....Kilo daltons

KOH.....Potassium hydroxide

Krt18 .....Cytokeratin 18

Krt8 .....Cytokeratin 8

L

Lect1 .. Leukocyte cell derived chemotaxin 1

LH .....Lutenizing hormone

Lhx1 .....LIM homeobox protein 1

Lin28 .....….RNA binding protein Lin-28 homolog A (C. elegans)

lys.....Lysine

M

M……Molar unit

MACS ...Model-based Analysis of ChIP-Seq

Mage-K1 ..RIKEN cDNA 4930550L24 gene

MATa..... Silenced mating-type protein A1

MEME.....Multiple Em for Motif Elicitation

μm ..... micrometer (micron)

Mid1…… .....Midline 1; Tripartite motif-containing protein 18 (Trim18)

min ..... Minutes

MIS ..... Meiotic inducing substance

mM..... milliMolar

MMLV .... Moloney Murine Leukemia Virus

Morc.....Microrchidia

MPS..... Meiotic preventing substance

N

Na_3V0_4 ..... Sodium orthovanadate

NaCl .....Sodium chloride

Nanog.....Homeobox transcription factor Nanog

NANOS2..... nanos homolog 2 (Drosophila)

Nanos3 .....nanos homolog 3

Ncoa2 .....Nuclear receptor coactivator 2

ncRNA .....Noncoding ribonucleic acid

NECTIN-2…..Poliovirus receptor-related 2 (Pvrl2)

NECTIN-3...….Poliovirus receptor-related 3 (Pvrl3)

NFAT .....Nuclear factor of activated T-cells

Nfx2 ..... Nuclear export factor 2

Ngn3.....Neurogenin 3

Nkx3-1 .... NK-3 transcription factor, locus 1

Nlgn1..... Neuroligin 1

nm .....nanometer

Ntm .....Neurotrimin

O

Ocln.....Occludin

Oct4.....Octamer-binding protein 4 (Pou5f1)

P

P ……Postnatal day

PAS…. ..... Periodic acid Schiff's

Pax2.....Paired box gene 2

pBKS.....pBKS plasmid

PBST.....Phosphate buffer saline-tween20

PCNA.....Proliferating nuclear antigen

PCR..... Polymerase chain reaction

PFGE..... Pulse field gel electrophoresis

PGC..... Primordial germ cell

piRNA..... Piwi-interacting RNA

Piwil2 ..... Piwi-like homolog 2 (Drosophila)

Plekhg1 ..... .Pleckstrin homology domain containing, family G (with RhoGef domain) member 1

Plzf .... zinc finger protein 145; Kruppel-like, expressed in promyelocytic leukemia); zinc finger protein

Pramel3 ..Preferentially expressed antigen in melanoma-like 3

Prdm1.... .B lymphocyte-induced maturation protein 1 (Blimp1)

Prdm14.....PR domain zinc finger protein 14

Q

qPCR .....Quantitative Polymerae chain reaction

R

RA..... Retinoic acid

Rarres1 ..... Retinoic acid receptor responder (tazarotene induced) 1

Rbym1a1 .....RNA binding motif protein; Y chromosome; family 1; member A1

Ret..... ret proto-oncogene

RF.....Rescue factor

RNA ..... Ribonucleic acid

RNase.....Ribonuclease

Rspo1.. .....R-spondin homolog (Xenopus laevis)

RT-PCR…Reverse transcription-polymerase chain reaction

S

SC.....Sertoli cell

SCDmrt1KO .....Sertoli cell-specific Dmrt1 knockout

SDS-PAGE .....Sodium dodecyl sulfate polyacrylamide gel electrophoresis

SF1 .. Steroidogenic factor 1 (Ad4bp, Nr5a1)

Smad4 ..... .mothers against decapentaplegic homolog 4

Smad5/8 ....Mothers against decapentaplegic homolog 5/8

Sohlh1 .....…Spermatogenesis and oogenesis specific basic helix-loop-helix 1

Sox2 .....SRY-box containing gene 2

Sox9Sry-related high mobility group (HMG) box containing gene 9

Sp1 .....Trans-acting transcription factor 1

Sp3 .....Trans-acting transcription factor 3

Spag1.....Sperm associated antigen 1

SRY..... …Sex determining Region of Y chromosome

Ssea-1....Stage-specific embryonic antigen 1

Stella .... ……..Developmental pluripotency-associated 3 (DPPA3)

Stk31 .....Serine threonine kinase 31

Stk4 .....Serine/threonine kinase 4

Stra8 .....Stimulated by retinoic acid gene 8

sxl ..... sex lethal

Sycp1..... Synaptonemal complex protein 1

T

T ……Testosterone

T3 ..... Thyroid hormone

Taf7 ..TAF7 RNA polymerase II, TATA box binding protein (TBP)-associated factor

Taok3 .....serine/threonine-protein kinase TAO3; thousand and one amino acid protein 3

Tnap .....Alkaline phosphatase, liver/bone/kidney

Tnnt2 ..... Troponin T2; cardiac

TOMTOM..... Motif comparison tool

Trim34..... Tripartite motif-containing 34

TRITC.... ..... Tetramethyl Rhodamine Isothiocyanate

trp .....Tryptophan

Tuba3a..... Tubulin, alpha 3A

U

UCSC ..... University of California at Santa Cruz

uL ..... Microliter

ura ..... Uracil

Usp9y .....Ubiquitin specific peptidase 9, Y chromosome

UTR.....Untranslated region

V

VDR/RXR..... …….Vitamin D Receptor/Retinoic Acid X Receptor

W

Wnt3 ……..Wingless-related MMTV integration site 3

Wnt4..... ……Wingless-related MMTV integration site 4

Wt1..... Wilms' tumor 1

Y

YAC ..... Yeast artificial chromosome

Z

ZO-1 ..Tight juction protein 1 (TJP1 or ZO1)

Chapter 1: Literature Review

Introduction

This section provides reviews on reproduction, sex determination and differentiation, germ cell and Sertoli cell development, DMRT1 and DM family, hypothesis, specific aims and biological significance of the current study.

Reproduction

Reproduction is a fundamental biological process that ensures propagation of extant organisms. Asexual and sexual reproduction are the two main mechanisms of procreation. In asexual reproduction, an organism divides into one or more analogous or identical copies of itself with no genetic input from another organism. This method of propagation predominates within single cell organisms like bacteria and is exemplified by parthenogenesis in lower plant species. In sexual reproduction, an organism produces an offspring that inherits a combination of genetic material contributed by two members of the species. Sexual reproduction is limited to higher plants, higher invertebrates and all vertebrates, and always entails special male and female reproductive structures and gametes. This requires sex determination, which refers to the decision of restricting the development of an offspring to either a male or a female pathway, and sex differentiation, which consists in the development of a male or female phenotype (Figure 1).

Types of sex determination systems

Different sex determination systems have been documented for various phylogenetic groups that can be classified into two main categories namely, genetic (chromosomal) and non-genetic (environmental factors) [1] .

Environmental sex determination (ESD)

This occurs when there is direct correlation between specific environmental conditions (temperature, nutrients) and the sex of a progeny. This suggests that the sex of the embryo is not predetermined at fertilization, but arises later, based on specific external conditions during the critical sex determination stage, as the zygote develops. In certain species, like fish, turtles, lizards and crocodiles, the females and males have identical genetic composition and sex determination is controlled by external factors like environmental hormones, visual signals and hatching temperatures [2, 3]. For instance, in crocodilians and most turtles, the temperature at which the egg is incubated determines sex. In the European pond turtle, an incubation temperature below 28^{o}C produces phenotypic males, whereas an incubation temperature above 29.5^{o}C produces phenotypic females [4, 5]. Other environmental factors that influence sex determination include the proximity of related species and the duration of daylight (photoperiod). Proximity to related species was observed to determine sex in the echiurid marine worm (*Bonellia spp*), whereby isolated planktonic larvae developed into females while larvae that dwell near females developed into males. In the brackish water shrimp (*Gammarus spp*), long and short days produce males and females, respectively [5, 6].

Genetic sex determination (GSD)

In genetic or chromosomal sex determination, genes inherited from donors (parents) at fertilization determine the sex of the embryo. This suggests that there is a preexisting commitment to a specific sex that cannot be normally reversed subsequently by environmental factors. In groups like mammals, insects, birds, snakes and amphibians, differences in male and female genetic makeup result in a dominant gene that drives sex determination. Genetic sex determination in these species generally uses chromosome combinations of XY, ZW, XO or

haplodiploid. After sex is determined at insemination, sex differentiation is directed to the male or female pathway by sex determining genes [2, 3, 5, 6].

In fruit flies (*Drosophila melanogaster*), sex is determined by the X chromosomes to autosomes (X/A) ratio. In *Drosophila*, each cell in the embryo senses the X/A ratio through the activity of a master regulator that drives sexual dimorphism [7]. Early transient expression of the *sex-lethal* (*sxl*) splicing regulator is observed in XX embryo, and permanent expression of functional *sxl* eventually activates synthesis of the female-determining variant of *doublesex* (*dsx*) through a sex-specific alternative mRNA splicing mechanism [5]. Expression of *sxl* is lower in XY embryos that results in the synthesis of the male-specific spliced isoform of *dsx*. The Y chromosome in fruit flies is dispensable during sex determination but contains genes that are indispensable for male fertility. Thus, an XO fruit fly has a male phenotype, but it is infertile [5].

Among species that propagate by genetic sex determination, the mechanism of this biologic process has been extensively studied in birds (chicken) and placental mammals (humans and mice) (Figure 1), which display heterogametic sex and are capable of producing two types of gametes. Birds (*Gallus gallus*) use a ZZ/ZW system, where animals that inherit two Z chromosomes (homogametic) become male, and those that inherit both a Z and a W chromosome (heterogametic) become female. The W chromosome is smaller, has few bona fide genes while the Z chromosome is larger, and carries the key candidate testis-determining factor, DMRT1. The Z chromosome shares extensive conserved syntenic segments with human chromosome 9, where its human ortholog resides [8]. *DMRT1* dosage was higher in ZZ embryos than in ZW embryos; and it was suggested that higher doses of *DMRT1* in avian embryo direct male development, whereas lower doses promote female development [8, 9].

Mammals use the XX/XY system (Figure 1), where males are heterogametic; carrying an X and a Y chromosome, and females are homogametic; carrying two X chromosomes [2]. In mammals, sex determination is typically categorized by three sequential steps [2]. First, genetic or chromosomal sex is established by the presence or absence of the Y chromosome in the fertilized oocyte. Thus, the genetic sex determines the sex of the developing gonad, such that the presence of the Y chromosome directs development of the testes, while its absence commits the gonad to the ovarian fate. Second, the gonadal sex or primary sex determination along the testicular pathway requires the presence of the testis determining factor or *Sry* (Sex determining Region of the Y chromosome) on the Y chromosome (Figure 1). The absence of *Sry* on the Y chromosome results in progenies that genetically are males, but have ovaries. Thus, the presence or absence of *Sry* determines gonadal fate. Third, phenotypic sex or secondary sex differentiation is determined by the sex of the gonad, which provides the embryo's hormonal environment necessary to develop male or female sexual characteristics, respectively [10].

Other genes implicated in mammalian sex determination

SRY is expressed in the gonad precursor and it is limited to the period in which testes begin to form. Unlike sxl, the master regulator in *Drosophila* that mediates sexual dimorphism in every cell, SRY is confined only to gonadal tissue and does not required germ cells to be present. Thus, *Sry* is all that is needed from the Y chromosome to form a testis and the expression of SRY in a XX background induces male development [11-14]. In addition to *Sry*, many other components of mammalian sex determination and /or gonadal development have been identified, mostly from gene knockout experiments in mice, and evaluation of human patients with sexual disorders or sex-reversed phenotypes. These studies revealed a repertoire of genes that include Dosage-sensitive sex reversal, congenital adrenal hypoplasia, on the X chromosome, gene 1

(*Dax1*), *Dmrt1*, *Emx2*, *Fgf9*, *Gata4/Fog2*, *Lhx1*, *Lhx9*, *Nr5a1* (*Sf1*), *Wt1*, *Sox9*, *Wnt4* and insulin family genes. The majority of these genes encode for transcription regulators that influence key steps during gonad development. But, genes like *Wnt4*, *Fgf9* and the insulin family genes are signaling molecules, which are vital in the recruitment and differentiation of different cell types [15-17]. Functional studies of the expression profiles of these genes revealed various steps in the development of the gonad, which are regulated in a hierarchical manner.

Sexual differentiation in Mammals

Sexual differentiation depends on the hormonal environment and can be divided into two phases. Primary sexual differentiation refers to differentiation events that occur during embryonic development such as development of the internal reproductive organs and external genitalia. Secondary sexual differentiation is the response of multiple tissues to the hormones (Figure 1) produced by the functioning gonads to complete the sexual phenotype, for example the secondary sexual characteristics that occur with puberty. In mammals, expression of *Sry* in the undifferentiated gonad directs development to the testicular pathway (Figures 1 and 2). The supporting cells in the testis start synthesizing two hormones, anti-Müllerian hormone (AMH) produced by Sertoli cells, and testosterone produced by Leydig cells. AMH causes regression of the Müllerian duct, while testosterone and its derivative, dihydrotestosterone, induce formation of ancillary male reproductive organs. In the absence of *Sry* in females, the ovarian pathway is activated by a different set of master regulators and the supporting cells (granulosa and theca cells) in the ovary produce estrogen, which upholds development of the uterus, oviducts, and cervix from the Müllerian duct [6, 15, 18-20].

Gonad development

The indifferent gonads

In mammals and birds, the gonads of each sex begin as a common precursor known as the bipotential gonad or undifferentiated genital ridge (Figure 2). Prior to sex determination in mice and during the first two days, the expanding gonadal ridge is composed of undifferentiated cells derived from the coelomic epithelium that proliferate and migrate to the mesenchyme derived from the mesonephros. Blood vessels develop from the mesonephros, and the gonadal ridge becomes vascularized more in the male than in the female. At approximately 9 days post coitus (dpc) in the mouse embryo, indifferent or bipotential gonads (genital ridges) are first noted as thickenings in the mid-portion of the intermediate mesoderm (i.e. ventrolateral surface of the mesonephroi), consisting of germ cells in both XX and XY embryos (Figure 2) [21, 22]. The somatic components are derived from layers of cells that proliferate and expand from the underlying mesonephroi and coelomic epithelium [22]. Overall, the supporting, steriodogenic and the partial connective cell lineages of the indifferent gonad have a dual potential and follow a dimorphic fate once gonadal sex is determined [23, 24].

Unlike the somatic components, the germ cells originate from the proximal epiblast (primary ectoderm) and, whereas, the male germ cells are not required for testis formation, their female counterparts are needed for ovarian differentiation since their absence elicits masculinization of the ovaries [25-31]. The Wolffian duct (mesonephric duct), mesonephric tubules, adrenal glands and the urinary system are also derived from the mesonephroi. Murine studies revealed *Lhx1*, *Emx2* and *Pax2* genes are essential for stabilization of the intermediate mesoderm and formation of the urinogentital ridge; while *Sf1* and *Wt1* are required for the

differentiation of the gonadal ridge. Gene knockout studies in mice revealed that animals with deletions in the *Wt1* or *Sf1* gene lacked gonads and kidneys or lacked gonads and adrenals, respectively [32, 33]. As the gonad develops, the induction of male or female-specific factors drive the undifferentiated genital ridge to differentiate along the path of the testis or ovary (Figure 2) [32-37]. Overall, sex determination in the mammalian germ line is reduced to choose to enter meiosis, which leads to the ovarian pathway, or arrest in mitosis, which favors the testicular pathway. During this developmental process, the formation of primordial somatic and germ cell components are equally important as genetic makeup and sex-specific differentiation aspects in the establishment of an ovary or testis.

The Testis

The discovery of *Sry* provides important insight on the genes involved in testis development. Thus, a transient wave of SRY expression increases expression of SOX9, which directs the gender-specific regulation that culminates with the development of Sertoli cells in the male gonadal ridge and the development of the testis [11, 12, 27, 38-40]. Sertoli cells also produce AMH and Inhibin B. AMH induces regression of Müllerian ducts and inhibits formation of the fallopian tubes, uterus and vagina. Inhibin B selectively suppresses follicle stimulating hormone (FSH) secreted by the pituitary. After Sertoli cells are formed, they coalesce with peritubular myoid cells that migrate from the mesonephros to form the testis cords, which are the precursors of seminiferous tubules, at 12 days post coitus (dpc) in mice [41]. Formation of testis cords coincides with the block to meiotic entry in the male gonadal ridge. Also, male germ cells (prospermatogonia) are arrested in the G_0/G_1 phase of the cell cycle at about 12.5 and 13.5 dpc, but resume proliferation a few days after birth. Leydig cells appear in the interstitial region, are derived from mesenchymal-like stem cell [42], and secrete testosterone required for the

development of Wolffian structures including epididymis, vas deferens and seminal vesicles. Dihydrotestosterone is a byproduct of testosterone that induces virilization of the external genitalia [43, 44]. After the sex is determined, genes including *Dhh, Insl3, Hoxa10, Hoxa11, Dmrt1, Fgf9, Gata4/Fog2, Sf1, Sox9* and *Wt1* stay on to promote testicular development [15, 17, 45-51].

The ovary

Not much is known about differentiation into the female pathway and it is thought to be the default pathway of gonad development. Thus in the absence of *Sry*, an ovary develops, likely due to the innate ability of germ cells to enter meiosis in the absence of an inhibiting signal from Sertoli cells or the lack of stabilization of the Wolffian duct. After formation of the ovary, genes including *Gdf9, Foxl2* and *Fshr* are required to ensure female germ cell survival and normal follicle development. The supporting cells derived from cells of the underlying mesonephroi differentiate into granulosa cells. Like the interstitial cell population in the males, the cells in the interstitial compartment in the females differentiate into the theca and stromal cells that form a steriodogenic sheath external to the basement membrane of the primordial follicle. These supporting cells in the ovary produce estrogen and inhibin α and β required to maintain development of the female pathway. Genetic studies in mice showed that *Dax1, Wnt4, Foxl2, Rspo1* and *β-catenin* are predominantly ovary-promoting genes [15, 17, 45-51]. At 13.5 dpc, female germ cells enter meiotic prophase and pass through leptotene, zygotene and pachytene before entering quiescence at the diplotene stage, where they are surrounded by a single layer of flattened granulosa cells to form primordial follicles just before birth [42, 52]. Meiotic entry of female germ cells is critical for the somatic components to commit to the ovarian fate [26-28]. This observation is supported by studies that showed that the XX gonad readily

transdifferentiated into a testis when germ cells were absent and that meiotic female germ cells inhibited testis differentiation and cord formation when introduced into an XY gonad, after 12.5 dpc [26]. The meiotic inhibitors are thought to originate from Sertoli cells [53]. Entry into meiosis is regulated by meiotic preventing substance (MPS) and meiotic inducing substance (MIS) [54]. Current views indicate that retinoic acid (RA) made in the mesonephros exerts MIS action in the fetal ovary, whereas the P450 enzyme (*Cyp26b1*), produced in somatic cells of the embryonic male testis, degrades RA and delays meiotic entry by male germ cells [54, 55]. *Stra8* is induced by RA and regulates the G1 mitotic to meiotic transition in female primordial germ cells [56].

Germ cell development

Early specification of primordial germ cells

The laboratory mouse has been an invaluable tool in our understanding of sex differences and origins of mammalian gonads. In mice, primordial germ cells (PGCs) are induced in the pluripotent epiblast by signals from bone morphogenetic proteins (*Bmp4 and Bmp8b*), which originate in the extraembryonic tissues and visceral endoderm [57-61]. The ability of PGCs to respond to BMPs occurs at a time-point coincident with the expression of *Wnt3* [62]. BMP signals are transduced by *Smad5/8*, which translocate into the nucleus with *Smad4* and induce expression of *Fragilis* (*Ifitm3*), a member of the interferon-inducible family gene, in the epiblast and *Prdm1 (Blimp1)* in PGC precursor cells at one end of the short axis before gastrulation [63, 64]. After gastrulation, the PGC precursors locate to the posterior proximal region, where they undergo specification to form the founder population of *Stella*-positive PGCs. The pluripotent proximal epiblast cells respond to signals from the extraembryonic tissues and begin to express

Fragilis as they acquire the ability to form PGCs, although only a small minority of them will become germ cells. At 6.25 dpc, about six cells in the prospective posterior proximal site of the embryo belonging to the *Fragilis*-positive cell population and that are in direct contact with the overlying extraembryonic endoderm start expressing *Blimp1* and *Prdm14*, which are transcriptional repressors of histone methyltansferase belonging to PR-domain proteins and are considered to be PGC determining factors [65, 66]. These cells are recognized as being restricted to the germ cell lineage. *Prdm1* is partially accountable for inhibiting the somatic program in primordial germ cells while promoting the formation of germ cell features. In the *Prdm1*-and-*Prdm14*-expressing germ cells, genes derived from the mesoderm such as *Fgf8*, *Brachyury* and *Snail* are down-regulated, whereas genes associated with pluripotency, including *Stella* (*Dppa3*), *Lin28, Oct4, Tnap, c-Kit, Ssea-1, Sox2* and *Nanog* are up-regulated [64, 67-70]. Overall, the transcriptional programs directed by *Prdm1* and *Prdm14* inhibit primordial germ cells from taking on the somatic fate through a successful epigenetic reprogramming mechanism that favors reactivation of pluripotency marker genes [70, 71].

Primordial germ cell maintenance and migration

By 7-7.5 dpc, midway through gastrulation, PGCs can be observed from their intrinsic and elevated activity level of alkaline phosphatase (*Tnap*)(Figure 3A) [72]. Also, the Pou transcription factor and pluripotent stem cell marker, *Oct4*, is expressed in the epiblast at this time but is restricted to the germ cell lineage at about 8 dpc [73]. It is well established that the precursors of the PGCs are the proximal epiblast cells that are adjacent to the extraembryonic ectoderm rather than cells of the extraembryonic lineage. The germ cell lineage is established only after the precursor epiblast cells have migrated through the primitive streak (from primary endoderm to extraembryonic endoderm) giving rise to the extraembryonic mesoderm, allantois

and about 40 PGCs [43, 74-76]. Briefly, just before the end of gastrulation and 24 hours after establishing PGCs (8-8.5 dpc), the endoderm is invaginated to form the hindgut and, in the process, it carries the PGCs. These cells invade the allantois and the hindgut endoderm, with the fastest PGC arriving the hindgut endoderm at 8.5dpc (Figure 3A). The primordial germ cells become transcriptionally silent at about 8.5 dpc and undergo an elaborate reprogramming of their genome that consists of histone modification, the elimination of dimethylation (H3K9me2) signatures and the augmentation of trimethylation (H3K27me3) marks [77]. By 9-9.5 dpc, PGCs migrate from the ventral to the dorsal side of the hindgut, up the dorsal mesentery and towards the developing genital ridges. Entry of germ cells into the nascent genital ridges continues between 10-11 dpc but by 11.5 dpc (Figure 3B), a distinction between the genital ridges and the mesonephros is formed which blocks subsequent entry of germ cells [43, 75, 76, 78]. Until about 13.5 dpc after entry into the genital ridge, mitotic proliferation continues. At the end of the 2-3 days proliferation period, about 20,000 germ cells are present in the genital ridge, which are derived from an initial pool of 40 PGCs that underwent 12 successive mitotic divisions [43, 75, 76, 78].

Migration of primordial germ cells is complete in about four days (7.5-11.5 dpc) (Figure 3B). Although active migration of primordial germ cells towards the gonadal ridge occurs after 8.5 dpc, the molecular mechanisms that regulate migration and ensure germ cell survival during migration are only partially understood. Murine ablation studies revealed that genes, such as *Fgf8* and *β1-Integrin*, are important for germ cell migration, while genes such as *Dnd*, *Bax*, *Bcl2*, *c-Kit/Steel* and *Nanos3* are vital for PGC survival [79-84].

The postnatal testis

Postnatal Sertoli cell development

The daily sperm production in the adult testis determines the efficiency of spermatogenesis both of which rely on the total number of functional Sertoli cells [85-88]. The number of Sertoli cells available after the developmental perinatal period is critical for establishing both the adult testis size and quantitative daily sperm production [88]. This association exists because each Sertoli cell has a predetermined ability for the number of germ cells it can nurture [88]. Since only immature Sertoli cells proliferate, the final number of Sertoli cells is decided before maturity. Prepubertal, pubertal and adult are the three populations of Sertoli cells that have been characterized, which overlaps with the temporal development of the postnatal mammalian testis.

After the testicular cords are formed, the number of fetal Sertoli cells increase rapidly just prior to birth. After birth, the fetal Sertoli cell, now prepubertal Sertoli cells continue to divide mitotically and stop after the first spermatogonia enters meiosis (at about postnatal day 5 (P5) in mice) [86, 89, 90]. In mice, studies using ^{3}H-thymidine incorporation showed that Sertoli cell proliferation stopped after the cells acquire their mature appearance at P12 [91]. The presence of meiotic and postmeiotic germ cells causes the undifferentiated pre-Sertoli cells to develop into a differentiated and functional Sertoli cells. The transition from the immature proliferative state to the mature non-proliferative state, termed terminal differentiation or maturation, is characterized by: i) the presence of an enlarged tripartite nucleus with a protuberant nucleolus, ii) formation of tight junctions between adjacent Sertoli cells and iii) formation of the adluminal compartment and a fluid-filled lumen [86]. These post-mitotic highly differentiated and complicated

morphological structures are characteristics of adult Sertoli cells. Existing evidence links thyroid hormone (T3), follicle stimulating hormone (FSH), androgen receptor (AR), AMH, and testosterone to the final maturation of Sertoli cells [86]. Furthermore, the absence of meiotic and postmeiotic germ cells were shown to induce secondary changes in the function of Sertoli cells that were similar to those of immature Sertoli cells or features of dedifferentiation of adult Sertoli cells [89, 92-97]. However, in human and murine studies the absence of these differentiated germ cells did not automatically lead to maturation failure by Sertoli cells, but led to temporal delays such as the formation of inter-Sertoli cell tight junctions [86, 98].

Postnatal germ cell development

Male primordial germ cells arrested in mitotic G_0/G_1 phase are called gonocytes; which are evenly spherical, centrally positioned in the seminiferous tubules and detached from the basement membrane [99-101]. Spermatogenesis begins soon after birth and at about postnatal day 0.5 (P0.5) in mice, gonocytes resume mitosis, extend their cytoplasmic processes and radially migrate to the basement membrane [99]. Radial migration is completed between P3 and P6 and is thought to be important for survival of gonocytes, since failure to migrate has been associated with degeneration of germ cells centrally located within the testis cords [102, 103]. Germ cells provide the genetic link between lineages. To fulfill this function, mammalian germ cells self-renew by mitosis to expand and maintain the pluripotent stem cell population, which maintains spermatogenesis in the adult testis [102, 104]. Specifically, the production of haploid gametes in the mammalian testis originates from a small population of stem cells belonging to the undifferentiated spermatogonia (Figure 4). The undifferentiated spermatogonia consist of types A_{single} (A_s, isolated single cells), A_{paired} (A_{pr}, chain of two cells) and $A_{aligned}$ (A_{al}, chain of 4,8,16 or 32 cells) [105-109]. Type A_1 differentiated spermatogonia are derived from A_{al}

population after a series of cyclical events that varies across species [104, 105]. After five successive mitotic divisions, type B-spermatogonia are derived from A_1 spermatogonia. The type B spermatogonia can be detected in the mouse testis by the start of the second postnatal week and their morphology is analogous to those of adult intermediate (In) or B spermatogonia. The B spermatogonia in turn undergo one mitotic and two successive reduction divisions to form the primary spermatocytes and round spermatids, respectively [102, 104]. The round spermatids mature and form sperm cells [108]. In the mouse, spermatozoa are first observed during the first wave of mouse spermatogenesis, at approximately P35. Contrary to normal spermatogenesis which is derived from *Neurogenin 3* (*Ngn3*)-positive undifferentiated spermatogonia, the first wave of mouse spermatogenesis originates directly from gonocytes without going through the *Ngn3*-expressing stage [110].

To date, the biologic processes occurring in embryonic gonadal development have received more attention than the events occurring in the developing immature testis, even though the latter have the potential to provide invaluable information on regulatory pathways or events relevant to germ cell development, Sertoli cell maturation and male fertility. More precisely, the events occurring during the first postnatal week in mice testis are not well characterized. This dissertation focuses on characterizing the events occurring during this time point with special emphasis on the regulatory influence by a key evolutionary-conserved transcription factor, DMRT1; which is present only in the testis and expressed both in germ cells and Sertoli cells.

DMRT1 and DM FAMILY

DMRT1 is a transcriptional regulator that shares an evolutionary conserved cysteine-rich DNA binding motif (DM-domain) with doublesex (dsx) in the fruit-fly, *Drosophila*

melanogaster, and male abnormal-3 (mab-3) in the transparent nematode, *Caenorhabditis elegans*; both of which were shown to regulate sex-specific neuroblast differentiation and yolk protein gene transcription [111-114]. The revelation that the male-specific isoform of dsx (dsx^M) regulated male-specific neuroblast differentiation in *Caenorhabditis elegans* illustrated that these two phylogenetically diverse proteins shared not only structural similarity but functional similarity as well, and suggested a common ancient origin of at least some features of sexual regulation [112]. Given that molecular mechanisms of sex determination are highly variable across species, the above findings revealed the unique situation in which orthologous genes from different phyla retain the same function in sex determination and differentiation. This showed for the first time that pathways for sex determination and differentiation are evolutionary conserved across phyla and suggested that DMRT1, the mammalian ortholog of dsx and mab3, would similarly exhibit conserved functions in sex determination and differentiation.

Function of DMRT1 in humans

The protein characteristics, testis-specific expression and chromosome location of DMRT1 strongly suggested that this protein plays an essential role in testis development [50, 112, 115, 116]. The DM genes in humans were mapped to three distinct loci on chromosomes 1 (1p32-34, containing *DMRTB1* and *DMRT1A2*), 9 (9p21-p24.3 containing *DMRTA1*, *DMRT2*, *DMRT3* (*DMRT1A3*) and *DMRT1*) and 19 (19p13 and 19q13 containing *DMRTC2* and its closest paralog, *DMRTC1*, on chromosome Xq13) [117]. The 9p21-p24.3 locus in the human genome is considered to be evolutionary conserved because it shares extensive syntenic segments with regions on the X chromosome from Platypus (*Ornithorhynchus anatinus)* and regions on the Z chromosome in chicken (*Gallus gallus*) [8, 118]. Also, *DMRTB1*, *DMRTC2*/*DMRTC1* and *DMRT1* carry only a portion of the original sequences of the ancient vertebrate DM gene and are

thus considered to be derivatives that retain roles in sex differentiation [116, 119-121]. Furthermore, XY individuals carrying just one copy of the distal chromosome 9p locus had a greater incidence of reproductive abnormalities with features ranging from indistinct genitalia to complete XY sex reversal, indicating that two copies of the locus are required for ordinary testis differentiation [122, 123]. However, *DMRT1* was mapped outside the missing 9p interval approximately 30kb from the breakpoint identified from two 46, XY female human patients [116]. Further characterization narrowed the deleted region to the most distal portion of 9p and adjacent to 9p24.3, which contains *DMRT1* [119, 124-127]. These findings together with the testis-specific expression of DMRT1 suggested that haploinsufficiency for *DMRT1* may be responsible for the defective testis determination and differentiation [128]. Surprisingly, sequence analysis of transcripts collected from sex-reversed patients failed to identify any mutation or deletion in *DMRT1* [119], suggesting that the testis abnormalities associated with 9p deletions are caused by the loss of other gene(s). A likely candidate gene that could be deleted and associated with testicular abnormalities in 9p deletion would be *DMRT3*, which is located directly downstream of *DMRT1*. The total intergenic sequence of *DMRT3* is less that 4kb and it is plausible that it shares some upstream regulatory sequences with *DMRT1* [116, 129].

Function of DMRT1 in mice

Studies in wild type and mutant mice have contributed significantly to our understanding of DMRT1's expression profile and its requirement for postnatal testis development [50, 119, 130]. During the early stages of gonadogenesis (between 10.5 and 11.5 dpc), DMRT1 is expressed in germ cells and supporting cells of XX and XY gonads (Figure 2A-C), at levels that are sexually indistinguishable [130]. However, by 12.5 dpc, DMRT1 is expressed in a sexually dimorphic manner, with testicular expression predominating in supporting cells and ovarian

expression predominating in germ cells [130]. By 13.5 dpc, DMRT1 expression was absent from pre-granulosa cells of the ovary, while it was robustly maintained in Sertoli cells of the testis. Immediately after birth, at approximately P0.5, DMRT1 was still expressed in Sertoli cells but absent from most germ cells with peak levels attained between P6 and P9 [130].

Functional studies revealed that fetal gonad development was normal in the absence of DMRT1 [50]. In addition, no ectopic structures of the ovary or Müllerian duct-derived structures were identified in *Dmrt1*-null mice. However, postnatal testis development was significantly impaired in *Dmrt1*-null mice, which presented with testicular hypoplasia, disorganization of seminiferous tubules, abnormal Sertoli cell proliferation (failure to differentiate), no radial migration by germ cells, germ cell depletion by P10, and male infertility [50]. Conditional deletions to evaluate DMRT1 cell-specific roles validated many of its earlier-identified functions in addition to providing new insights on DMRT1 in postnatal testis development that indicated Sertoli cells and germ cells have independent requirements for DMRT1, whereas the survival of germ cells is dependent on DMRT1 in Sertoli cells [131]. Thus, DMRT1 in Sertoli cells assists with the cell's differentiation, germ line maintenance, meiotic progression and radial migration [50, 131-136]. Furthermore, DMRT1 was suggested to regulate the mitotic to meiotic transition of spermatogonia by its repression of *Stra8*, which restricts spermatogonial responsiveness to retinoic acid (RA) and consequently meiotic entry, and by its regulation of *Sohlh1*, which implicated DMRT1 as a positive regulator of spermatogonial development [134]. In contrast, *Dmrt1*-null germ cells expressed less STRA8 in the fetal ovary and caused a reduction in the number of primordial follicles in the immature ovary, without any detriment to fertility [137]. Thus, these findings revealed a sex-specific function for DMRT1, whereby it activates *Stra8* in the ovary and represses *Stra8* in the testis. Moreover, conditional deletion of *Dmrt1* in Sertoli

cells demonstrated its role in maintaining Sertoli cell differentiation, as its deletion resulted in the transdifferentiation of Sertoli cells into FOXL2-expressing cells with granulosa cell-like morphology [135]. Finally, about 1400 genes were identified as targets of DMRT1 using promoter arrays [136].

Overall, studies to date support a conserved role of DM genes in sex differentiation and the importance of DMRT1 for the postnatal testis differentiation of mice. However, the studies also raise many additional questions. For example, unlike humans, where deletion at the tip of chromosome 9 resulted in sex reversal, *Dmrt1* deletion or forced expression in female mice produced normal embryonic gonadal development and no sex reversal. The postnatal testicular defect observed might be due to gene redundancy effect provided by other DM gene(s) that are unaffected in the *Dmrt1*-null mice. It may also be attributed to differences in genetic backgrounds across species and a likely deviation of gene function during evolution.

Regulation of Dmrt1's activity

DMRT1's command over spermatogenesis and male fertility underscores the value of understanding the mechanisms that control its expression. While knowledge in this area is far from complete, several excellent studies identified important features of *Dmrt1* transcriptional regulation. Initial analysis of the rat *Dmrt1* gene employed a region of *Dmrt1* that contained its transcriptional start site (TSS) and 5000bp of the 5′- flanking sequence, which was transcriptionally active when transfected into primary Sertoli cell cultures [138]. Mutational analysis of this region identified two regions (between -3280 & -2000 and *Dmrt1* proximal promoter region (-150/+75)) that were important for *Dmrt1*'s transcriptional activity [138]. Further analysis of the first 150bp promoter region identified two elements that activated and two

elements that repressed *Dmrt1*'s transcription. The regulatory regions that activated transcription of *Dmrt1* were bound by three transcription factors namely: Early growth response 1 (*Egr1*), Trans-acting transcription factor 1(*Sp1*) and Trans-acting transcription factor 3 (*Sp3*) [138]. In addition, GATA4 was found to bind three of several regulatory elements identified in the distal promoter region (between -3280 & -2000) and coupled with the expression of DMRT1 in *Fog2*-null mice bolstered a regulatory role for GATA4 in the transcriptional machinery controlled by DMRT1 that's required in the testis, especially during Sertoli cell differentiation [139]. Furthermore, transgenic expression studies, employing transcription regulatory regions of varying length, were used to identify the requirements for cell-specific expression by DMRT1. Transgene evaluation in Sertoli cells and germ cells concluded that distinct *Dmrt1* promoter regions directed expression to Sertoli cells and germ cells [140]. The study also showed that Forkhead box L2 (FOXL2), a known regulator of ovarian differentiation, repressed *Dmrt1* promoter activity via regulatory elements located between the -3.2kb/+2.8kb region [140]. Although these transcription factors contribute to DMRT1's expression, their extensive expression patterns suggest additional, unidentified factors also contribute to the specific expression patterns of DMRT1.

Conclusion

The role of DMRT1 in postnatal testis differentiation is well-established but its cell-specific functions require further investigation [50, 116, 141]. Sertoli cells and germ cells in the testis interact closely, with each mutually affecting the other's development and function. For example, a defect in Sertoli cells severely affects the development and function of germ cells; and likewise, the absence of germ cells negatively affects the differentiation of Sertoli cells. Thus, the functional inferences obtained from the *Dmrt1*-null and the partial deletion of *Dmrt1* in

the conditional knockout studies are confounded by these associations, and attributing phenotypes to Sertoli cells or germ cells become difficult. Therefore, cell-specific assessment of Sertoli cell or germ cell morphology and transcriptome patterns derived from conditional *Dmrt1* mutants compared to *Dmrt1*-null mutants provided an incomplete picture of the activity of DMRT1 on Sertoli cell differentiation or germ cell development. The characterization of cell-specific pathways, biologic processes, gene transcription regulators and mechanism(s) involved in Sertoli cell differentiation and germ cell development require extra methodologies like cell-specific rescues; and this dissertation characterizes a novel mouse model to study the cell-specific function of DMRT1 in the postnatal testis.

Hypotheses and specific aims

The mechanism(s) associated with DMRT1 and the pathways it regulates are unresolved. Thus, the overall hypothesis was to elucidate pathways critical for Sertoli cell differentiation and germ cell growth and maintenance regulated by DMRT1 and its protein-binding partners using mouse models with different cell-specific expression of DMRT1. To investigate this hypothesis, specific aims were proposed to identify biological pathways regulated by DMRT1 that were unique to Sertoli cells and germ cells. This goal relied on the identification of gene expression differences, direct targets and their associated biological processes. In addition, identification of a germ cell-specific partner protein of DMRT1 was the last objective of this project.

Significance

The realization of these goals provide answers for some patients with male infertility, which accounts for 40-50% of human infertility cases with half of the causes unknown [142]. Sterile men are frequently misdiagnosed and their options for treatment are limited to assisted

reproductive technologies (ARTs), which do not require knowledge of the underlying cause. Regrettably, the search for new causes of infertility and treatments has been hindered by the use of ART to avoid diagnosis, but trigger new worries of possible health risks due to inadequate understanding of the causes of male infertility and the lasting impact of such procedures including but not restricted to propagation of genetic defects to offspring. Although genetic factors account for a considerable fraction of male infertility, little progress has been made to untangle the basis of male infertility and highlights the need to encourage research to identify causes of idiopathic male infertility [143]. Therefore, investigation for such causes can be accelerated by widening the number of identified factors and pathways essential for Sertoli cell development, germ cell growth and fertility to facilitate investigation of the cause of the human disease. This project uses murine models and tissues to offer new knowledge on the fundamental biological processes required for optimal testicular environment, fertility and male contraception by identifying factors controlled by DMRT1. The underlying rationale is that, since DMRT1 is indispensable for Sertoli cell maturation, germ cell development and male fertility, and as a transcriptional regulator, it sits at the top of essential biological pathways. Identified downstream targets of DMRT1 probably contribute to the process of sperm production, and since humans and mice share the cascade of downstream genes responsible for testis differentiation, combined with the evolutionary conserved nature of *DMRT1*, will increase the usefulness of newly uncovered factors to facilitate research on possible causes of human male infertility.

Figure 1: Schematic representation of mammalian sex determination and sex differentiation.

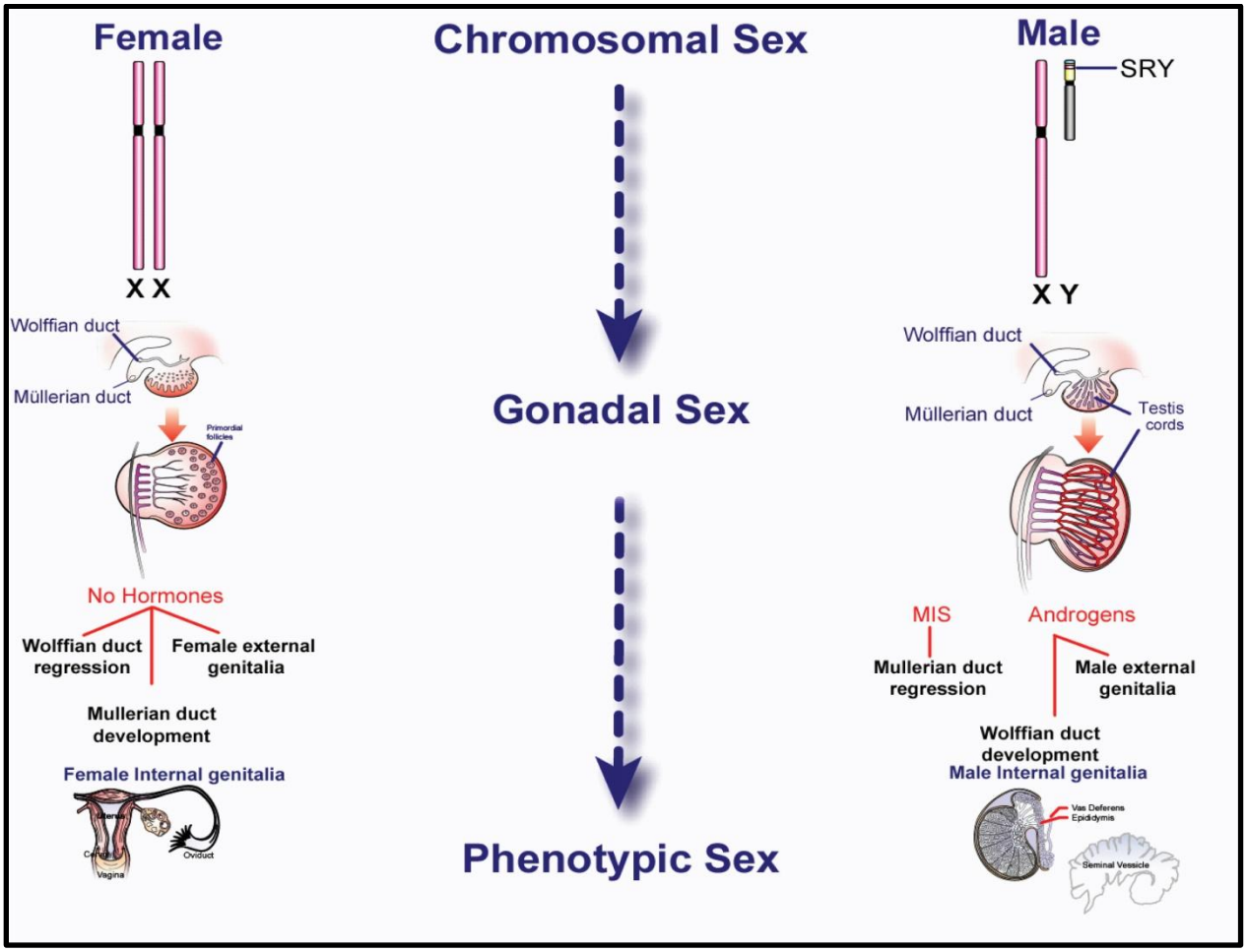

Figure 2: Development of the bipotential gonad. Gonadal primordia develop as paired thickenings of the epithelial layer that lines the body cavity (the ceolomic epithelium), specifically in the region that overlays the ventral–medial surface of the mesonephros. The signals that specify this regional thickening of the coelomic epithelium are unknown, but experiments in mice have identified several genes that have roles in the early growth and maintenance of the gonad in both sexes. **A-C.** Shows expression of DMRT1 in the undifferentiated gonadal ridge at 10.5. **D.** Schematic representation of development of undifferentiated gonad and subsequent sex determination.

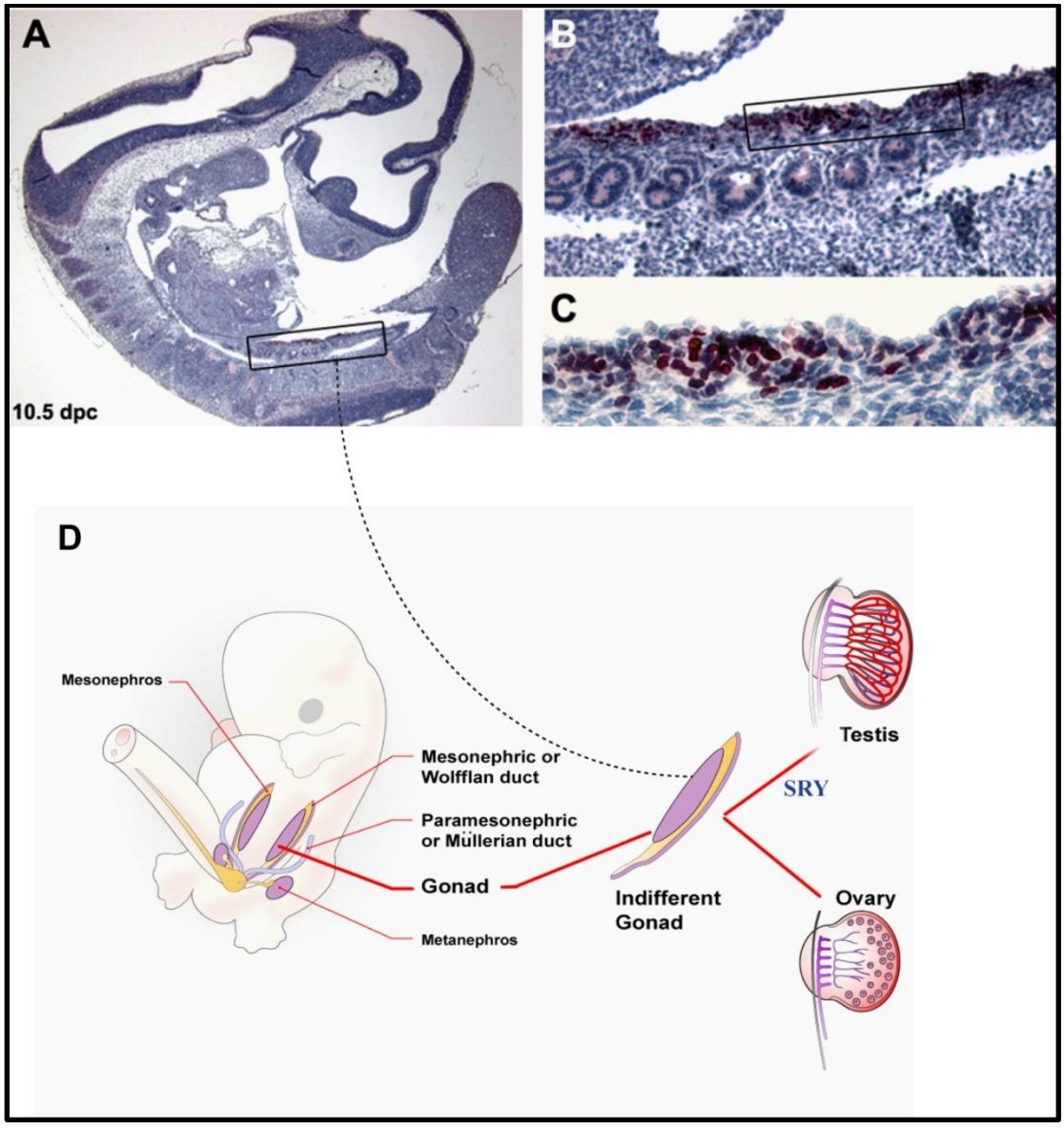

Figure 3: Specification of primordial germ cells and migration. A. Primodial germ cells at the base of the allantois enter the hindgut. Primordial germ cells derive from epiblast during gastrulation (endoderm of the yolk sac) in response to signals from adjacent tissues. Founder pool of mouse germ cells consists of some 40 cells at about 7.25 dpc, located within a cluster of cells expressing high levels of alkaline phosphatase. The cluster lies in the extraembryonic mesoderm at the posterior end of the primitive streak. These founding cells express germ-cell-specific markers such as *Stella* and exhibit the characteristic pattern of TNAP activity that has been used to characterize the germ-cell lineage. These events constitute PGC specification. **B.** Primordial germs migrate from the hindgut into the genital ridges. Complete migration of PGCs takes about 4 days (7.5 dpc to 11.5 dpc) in mice.

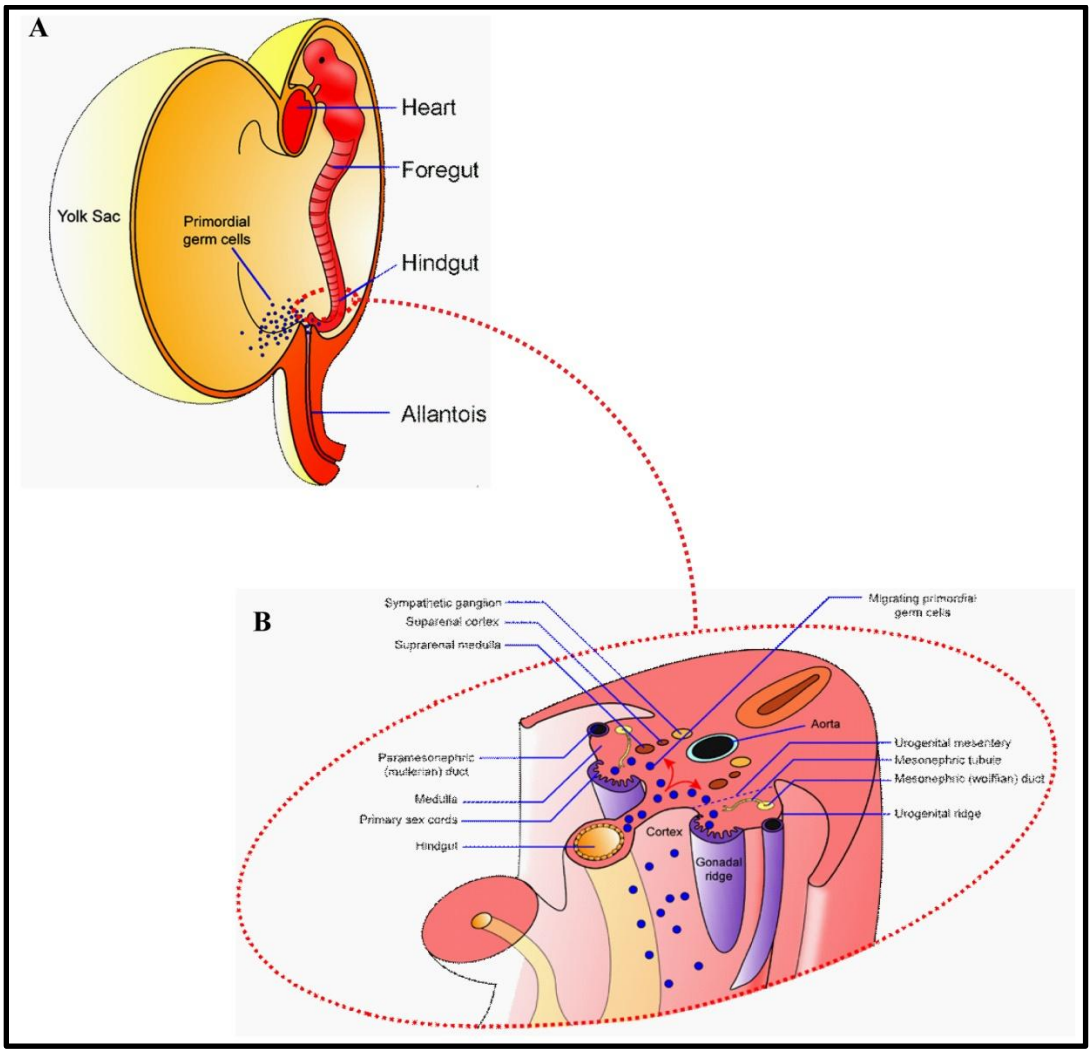

Figure 4: Schematic representation of spermatogenesis. Depicts formation of haploid sperm cells derived from a diploid undifferentiated spermatogonia through successive transformation, mitotic and meiotic processes. Shown also are the cell-specific markers expressed by the undifferentiated and differentiated spermatogonia. The depicted proteins are non-hormonal factors known to modulate the differentiation of germ cells and Sertoli cells in the testis SC = Sertoli cell

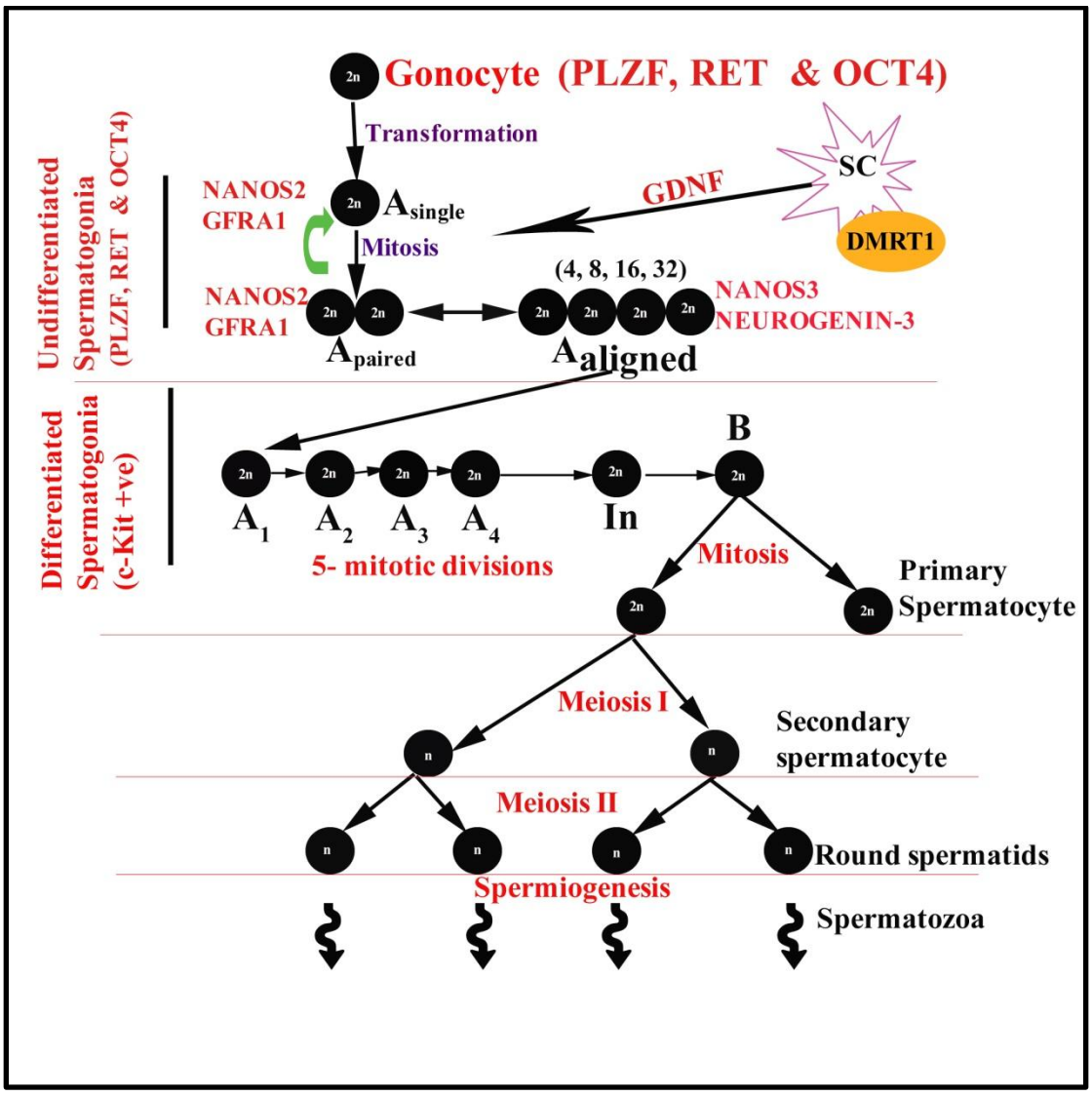

Chapter 2: A *Wt1-Dmrt1* transgene restores DMRT1 to Sertoli cells of *Dmrt1*$^{-/-}$ testes; a novel model of DMRT1-deficient germ cells (Submitted to Biology of Reproduction)

Abstract

DMRT1 is an evolutionary-conserved transcription factor expressed only in the testis, where it is produced in Sertoli cells (SCs) and germ cells (GCs). While deletion of *Dmrt1* in mice demonstrated it is required for postnatal testis development and fertility, much is still unknown about its temporal- and cell-specific functions. This study characterized a novel mouse model of DMRT1-deficient germ cells (rescue (*Dmrt1*$^{-/-;tg}$)) that was generated by breeding *Dmrt1* null mice with *Wt1-Dmrt1* transgenic mice, which express a rat *Dmrt1* cDNA in gonadal supporting cells by directing it from the Wilms' tumor locus carried on a yeast artificial chromosome transgene. Like *Dmrt1*$^{-/-}$ mice, male *Dmrt1*$^{-/-;tg}$ mice were infertile, while female mice were fertile. Expression analyses by qPCR, immunohistochemistry and Western blot showed that exogenous DMRT1 was present in supporting cells of the embryonic gonads of both sex and in Sertoli cells of the testis after birth. Functional analyses of the transgene on a *Dmrt1*$^{-/-}$ background showed that it exhibited copy-number dosage effect on specific genes and could not rescue testis size. However, it did maintain testis size and enhanced sperm progressive motility when expressed on a *Dmrt1*$^{+/+}$ background. Seminal vesicles were absent from *Dmrt1*$^{-/-;tg}$ and *Dmrt1*$^{-/-}$ mice at P42, which was consistent with the low serum testosterone levels observed in these mice. In addition, the seminal vesicles were well-developed in *Dmrt1*$^{-/-;tg}$ mice at P131, suggesting that the development of the reproductive system in these mice was delayed. Morphological analysis of adult testes showed that, compared to *Dmrt1*$^{-/-}$ mice, *Dmrt1*$^{-/-;tg}$ mice have improved seminiferous tubule structure, with lumens present in many cross-sectioned tubules. Features of Sertoli cell maturation were evaluated by electron microscopy, revealing that *Dmrt1*$^{-/-;tg}$ Sertoli cells have not reached complete maturation.

Introduction

Dmrt1 encodes Doublesex and Mab-3 related transcription factor 1, a required regulator of testis differentiation and spermatogenesis that shares homology with *D. melanogaster Doublesex* and *C. elegans Mab-3* through its DM domain, a highly conserved, cysteine-rich DNA-binding motif featured in proteins involved in sex determination and differentiation [3, 112-114, 131, 133, 134, 141, 144-154]. In vertebrates, DMRT1 expression is gonad-specific and favors the testis in a manner that depends on the species and developmental stage, reflecting its diverse roles in sexual development [50, 128, 131-133, 144, 151, 155-158]. In mammals, just prior to birth, DMRT1 expression becomes testis-specific, where it is restricted to undifferentiated spermatogonia and Sertoli cells (SCs) [50, 130-133, 159]. Its dynamic and highly restricted expression profile and similarity to conserved sexual regulators suggested, early on, that DMRT1 played an important role in male reproduction.

In humans, the chromosomal location of *DMRT1* (9p24.3) is associated with a wide spectrum of disorders that suggested *DMRT1* haploinsufficiency causes defects in testis development, but no direct evidence exists connecting human DMRT1 to testis function [160-167]. However, studies from many other species argue strongly for its importance to human fertility, as they demonstrate extensive evolutionary constraints on DMRT1 and its requirement for male reproduction [3, 112, 128, 131-133, 141, 144, 146-155, 157-159, 168-172]. To date, most of our knowledge on DMRT1 comes from studies in mice. *Dmrt1* deletion in mice revealed its requirement for male fertility and important roles in establishment and maintenance of Sertoli cell differentiation and germ cell (GC) expansion and development [131, 133, 135, 173]. The predominant phenotype of *Dmrt1*$^{-/-}$ mice was postnatal male infertility, associated with significantly hypoplastic testes [50, 132]. In contrast, fertility was normal in *Dmrt1*$^{-/-}$ female mice

[50, 173]. In male *Dmrt1*$^{-/-}$ mice, testicular morphology appeared normal through postnatal day 7 (P7), except that, at P2-P5, the tubule centers contained GCs, which, normally have migrated to the periphery by this time [50, 131, 132]. Additional studies indicated DMRT1 in both SCs and GCs contributed to the effects on migration [131]. By P10, GC numbers were significantly decreased, while SC numbers increased and, by P14, GCs were absent and seminiferous tubules were filled with abundant immature SCs [50, 132]. Failure for germ cells to proliferate and differentiate led to depletion of germ cells and were characterized by reduced levels of γ-H2AX and P-H3, which are meiotic and mitotic marker proteins, respectively [132].

Conditional deletion of *Dmrt1* in Sertoli cells demonstrated that DMRT1 acts autonomously to regulate cell maturation and non-autonomously to sustain GCs. In SC-specific *Dmrt1* knockout model (*SCDmrt1KO*), GC morphology, migration and mitosis appeared normal through P7. However, by P9, GCs had accumulated in a disorganized pattern in the lumen and, by P28, they were absent [131]. Sertoli cells also appeared normal through P7, but by P9 were slightly disorganized, and by P14, were noticeably more disorganized. By P28, SCs were positioned throughout the tubule and had an immature phenotype, as indicated by a decrease in AR and GATA1 expression that are markers for SC maturation. More recent studies indicated DMRT1 is needed in SCs to maintain male sexual differentiation, as SC-specific *Dmrt1* deletion caused postnatal loss of the male-promoting factor SOX9 and subsequent expression of the female-promoting factor FOXL2, suggesting DMRT1 loss caused differentiated SCs to reprogram into granulosa cells [135]. The delay between *Dmrt1* deletion, presumably in the fetus, and feminization of the postnatal testis suggests that DMRT1's involvement in maintaining SC differentiation occurs several weeks after birth or its embryonic effects are not erased until then.

Cell-specific effects of DMRT1 in germ cells, indicated that, in males, DMRT1 promotes spermatogonial differentiation by direct regulation of *Sohlh1* and prevents entry into meiosis by repressing *Stra8* expression and retinoid acid signaling [134]. In the fetal ovary, DMRT1 directly activated STRA8 expression and its loss caused improper localization of SYCP3 and γH2AX and reduced primordial follicles in the juvenile ovary, despite normal fertility [173].

While conditional deletions of *Dmrt1* in SCs have demonstrated its role in SC maturation and GC sustenance, its GC specific roles have been more difficult to decipher due to limitations in the models used to delete *Dmrt1* to assess its GC-specific roles. In the *Dmrt1*-deficient germ cell model (*GCDmrt1KO*), a significant number of GCs were positive for DMRT1 due to poor Cre recombinase penetrance of TNAP-Cre; and *Dmrt1*was ectopically deleted in some SCs [131]. Furthermore, another cell-specific deletion model using Ngn3-Cre transgene showed that spermatogonia expressing DMRT1 did not express the transgene until several weeks postpartum [110, 174]. Overall, the available cell-specific deletion models provide an ineffective deletion of *Dmrt1* at early postnatal ages, such as P5-P7, when the spermatogonia stem cell niche is being established. Thus, there is still a need for accurate analysis of DMRT1-deficient germ cells, at times when DMRT1 is implicated in testicular function.

To assess DMRT1 germ cell functions, we employed a transgenic rescue approach that bypasses problems of inefficient gene deletion incurred by poor expression or penetrance of *Cre* recombinase. DMRT1 was overexpressed in mice using the *Wt1* (Wilms' tumor suppressor gene 1) locus in a yeast artificial chromosome (YAC), which directed expression to supporting cells (pre granulosa and pre Sertoli) of the gonad; and mice expressing DMRT1 only in Sertoli cells (DMRT1 Sertoli cell rescue or DMRT1-deficient germ cells) were derived by breeding *Dmrt1*

transgenic with *Dmrt1* null mice. Characterization of the transgene revealed it was expressed only in supportive cell of the gonads from early postnatal stages to adulthood. *Dmrt1* transgene showed dose-dependent regulation for a select group of transcripts in prepubertal mouse testis, maintained testis size and enhanced sperm progressive motility in aging transgenic mice. Seminal vesicles were absent in P42 Sertoli cell rescues which was attributed to a block in Leydig cell function. Finally, the transgene partially rescued the seminiferous tubule morphology and induced a partial maturation state for Sertoli cells in the rescue mice.

Materials and Method

Generation of Wt1-Dmrt1 transgene.

A 620kb YAC containing at least 100kb of the mouse *Wt1* locus was purchased from Research Genetics (YAC620m*Wt1*, address YAC-90-A1, Whitehead I mouse YAC library). A schematic of YAC620m*Wt1* is shown in Figure 1A (top). *Saccharomyces cerevisiae* yeast strain AB1380 (MATa, ura3-52, trp1, ade2–1, his5, lys2–1, can1–100) was grown in Yeast Peptone Dextrose medium and used to propagate the 620-kb YAC containing the mouse *Wt1* gene. YAC-containing yeasts were grown in selective media lacking uracil and tryptophan to maintain the YAC. Propagation was followed as described elsewhere [175].

The targeting vector (pBKS-*Wt1 5′-Dmrt1*-HPRT1-LYS2-*Wt1* 3′) generated using PCR-amplified DNA inserts and standard cloning methodology, is depicted in Figure 1A (middle). The vector contains a rat *Dmrt1* cDNA flanked on its 3′ side by the hypoxanthine phosphoribosyl transferase 1 gene (HPRT1) containing a region of exon 8, exon 9 (contains a polyadenylation site) and intervening sequence, the yeast Lysine 2 gene (LYS2; selectable marker) and 776bp of *Wt1* extending 3′ from its translational start codon. An 825bp fragment encompassing sequences

5′ to the *Wt1* translational start codon was placed upstream of the *Dmrt1* cDNA in the targeting vector. Primers used to PCR-amplify components of the targeting vector are shown in Table 1. HPRT1 and LYS2 inserts were PCR amplified from vectors provided by Dr. Kenneth Peterson and Dr. Alan Godwin, respectively, and are described elsewhere [176, 177]. Accuracy of the targeting vector was confirmed by DNA sequencing.

The targeting vector, pBKS-*Wt1 5′-Dmrt1*-HPRT1-LYS2-*Wt1* 3′, was linearized by digestion with *Cla*I and introduced into YAC 620mWt1-containing yeast (AB1380 strain) by spheroplast transformation [178]. Since AB1380 is auxotrophic for lysine, yeast containing the targeting vector was selected for by growth in the absence of lysine. Restriction endonuclease mapping, pulse field gel electrophoresis and Southern blot analysis were used to identify targeting vectors that integrated correctly (data not shown). Homologous recombination between YAC and targeting vector was confirmed by PCR amplification and DNA sequence analysis, using Wt1-355 and Dmrt1.16A primers that spanned the 5′ integration site. The resulting YAC, *Wt1-Dmrt1*, contains an in-frame insertion of the *Dmrt1* cDNA with *Wt1* coding sequences (Figure 1A, bottom).

Wt1-Dmrt1 and Dmrt1$^{+/-;tg}$ *mice*

Wt1-Dmrt1 YAC DNA was isolated by PFGE, concentrated by two-dimensional gel electrophoresis, released from the gel slice by agarase digestion, and filtered through a 0.22 μm filter as described elsewhere [179, 180]. Transgenic mice were generated through the Transgenic and Gene-targeting Institutional Facility at the University of Kansas Medical Center, using freshly prepared YAC DNA for pronuclear injection into C57B6/SJL F1 zygotes. Two female founders (#s 30 and 37) and one male founder (#13) were obtained and used to generate lines for

the production of transgenic offspring by mating to C57BL/6 mice. *Wt1-Dmrt1* transgenic female mice (lines 30 and 37) were crossed with *Dmrt1*$^{+/-}$ mice (obtained from Dr. David Zarkower and are described elsewhere [50], to create heterozygous transgenic animals (*Dmrt1*$^{+/-;tg}$), which were mated to generate *Wt1-Dmrt1* transgenic mice homozygous for the *Dmrt1* null allele (*Dmrt1*$^{-/-;tg}$). Animals with different transgene copies were generated by crossbreeding lines 30 and 37. However, because transgenic Line 37 had the highest transgene expression, it was predominantly used to generate the data in this study. Genotypes of interest followed typical Mendelian genetics. Mice employed in the studies were of mixed background (primarily 129/SvEv and C57BL/6) and cared for in accordance with National Institutes of Health guidelines; and experimental procedures approved by Laboratory Animal Research Committee at the University of Kansas Medical Center. Mice were maintained on a 12-hour light-dark cycle and given food and water ad libitum.

Mice were genotyped using genomic DNA isolated from mouse tail biopsies, as described elsewhere [181]. Sequences of primers used for genotyping are provided in Table 2. Mice positive for the transgene were identified by PCR of genomic DNA, using either Wt1-355 and Dmrt1.16A or TGIF0088 and TGIF0090 primer pairs. *Dmrt1* alleles were identified using primers TGIF0105 and TGIF0106 for detection of the *Dmrt1*$^{+}$ allele, TGIF0105 and TGIF0107 for detection of the *Dmrt1*$^{-}$ allele. Southern blot analysis was also used for genotyping and transgene copy number determination. In this case, DNA digested with *EcoRI* was resolved by agarose gel electrophoresis, transferred to nylon membrane and hybridized with a probe corresponding to 165bp from exon 5 of *Dmrt1* (generated by PCR using *Dmrt1* exon 5 forward and reverse primer pairs). Embryonic sex was deduced from the presence or absence of *Sry*,

identified by PCR-amplification of genomic DNA (Sry forward and Sry reverse primers). All procedures were as described elsewhere [182] .

Analysis of testis weights and sperm function

Reproductive organs were collected from *Dmrt1*$^{-/-}$, *Dmrt1*$^{-/-;tg}$, *Dmrt1*$^{+/+}$, *Dmrt1*$^{+/+;tg}$ (wild type mice with 1 copy of the transgene) and *Dmrt1*$^{+/+;tg+tg}$ (wild type mice with 2 copies of the transgene) mice. Mice were euthanized by CO_2 anesthesia followed by cervical dislocation. For each genotype, body and testes weights were determined from at least six male mice, ranging in age from P2 to 18 months. Spermatozoa obtained from the cauda of the epididymis from 6-and-12 month old *Dmrt1*$^{+/+}$, *Dmrt1*$^{+/+;tg}$ and *Dmrt1*$^{+/+;tg+tg}$ mice epididymis, were collected in Tyrode's medium, counted, and approximately, $3x10^6$ cells were used for assessment of total and progressive motility by computer assisted semen analysis (CASA), as described elsewhere [183]. Statistical evaluations of changes in testis weight to body weight ratio (TW/BW), total and progressive motility between groups were done by Student T-test ($p<0.05$).

Histology

One testis from postnatal day 7 (P7), 15 (P15), 20 (P20) and 42 (P42) mice were fixed in Bouin's solution at room temperature for 4-24 hr, depending on size. Testes were rinsed twice with 50% and 70% alcohol, cut in half at the sagittal plane, processed and embedded in paraffin according to standard procedures. Five micron (5μm) sections were cut and mounted on slides, cleared in xylene, rehydrated through graded alcohol series and stained with periodic acid Schiff's (PAS) reagent and counterstained with hematoxylin. Testis morphology was analyzed using the Nikon Eclipse 80i microscope (Nikon Inc., Instrument Group, Melville, NY) and

digital images (x200 and x400) collected using Retiga 2000R fast camera and QCapture software (QIMAGING, Surrey, BC, Canada).

Transmission Electron Microscopy.

Testes of *Dmrt1*$^{+/+}$, *Dmrt1*$^{-/-}$ and *Dmrt1*$^{-/-;tg}$ P42 mice were fixed in 2% glutaraldehyde in 0.1M cacodylate buffer, postfixed in 1% osmium tetroxide/0.8% potassium ferrocyanide, stained in uranyl acetate, and embedded in Epoxy-araldite block. Semi-thin, 1μm sections were prepared from each wedge and stained with toluidine blue for examination of tubule morphology by light microscopy. Ultra-thin sections (80nm) were examined at 80 kV using a transmission electron microscope (JEOL 1400EX II; JEOL, Tokyo, Japan) for examination of germ cell and Sertoli cell morphology.

Immunohistochemistry.

Five micron (5μm) sections were cleared in xylene, rehydrated through graded alcohol solutions, and heated in 10mM sodium citrate buffer (pH 6.0) with microwaves (14 min at full power) for antigen retrieval. Sections were blocked using 10% normal goat serum (Zymed Laboratories Inc.) for 60 min at room temperature. For co-staining, primary antibody incubations were carried-out overnight at 4°C in blocking solution using the following dilutions: 1:400 of rabbit anti-DMRT1 antibody; 1:4 of rat antiserum to germ cell nuclear antigen 1 (GCNA1, kindly provided by Dr. G. C. Enders); 1:2000 of mouse anti-Proliferating cell nuclear antigen(PCNA)(PC10, SC56, Lot#G1006); 1:100 goat anti-GATA binding protein 4 (GATA4) (C20, SC-1237X, Lot#J1090); 1:100 goat anti-Androgen receptor (AR); and 1:200 rabbit anti-Cytochrome 450, family 11, subfamily A, Polypeptide 1 (P450SCC). Incubation of the secondary antibody was performed at room temperature for 1 hour with a 1:200 dilution of

fluorophor-conjugated secondary antibodies (Alexa FluorR 488 goat anti-rabbit IgG, Molecular Probes Inc., Eugene; Alexa FluorR 568 donkey anti-rabbit IgG, Molecular Probes Inc., Eugene; Alexa FluorR 488 donkey anti-goat IgG, Molecular Probes Inc., Eugene; Cy™3-conjugated AffiniPure goat anti-rabbit IgG, Jackson ImmunoResearch Laboratories and Cy™3-conjugated AffiniPure goat anti-rat IgG, Jackson ImmunoResearch Laboratories). Samples were then washed 3 times in Phosphate buffer saline-tween20 (PBST) (5 min. each) and glass cover slides mounted using Fluoromount-G (Southern Biotechnology Associates Inc., Birmingham, AL). Digital images were collected as above, using fluorescent filters: DAPI (blue), FITC (green) and TRITC (red). Images were processed using Adobe Photoshop

Serum collection and assay.

Blood was collected, allowed to coagulate for 1hr at room temperature, and centrifuged at 2000 × *g* for 15 min. Serum was transferred to a fresh tube and stored at −80^{o}C. Randomized sera samples were sent to the University of Virginia Center for Research in Reproduction Ligand Assay and Analysis Core, which performed the assays for testosterone, using a mouse testosterone radioimmunoassay (RIA), mouse estradiol, by CalBiotech enzyme immunoassay and Luteinizing hormone (LH), by sandwich immunoradiometric assay (IRMA). Group analyses were performed using one-way ANOVA followed by Tukey's comparisons to detect significant differences between groups ($P < 0.05$).

RT-PCR analysis of transgene expression in transgenic mice

F1 offspring were sacrificed and total RNA isolated from various tissues using TRIZOL reagent, according to manufacturer's procedures (Life Technologies, Gaithersburg, MD) and tissue-specific transgene expression evaluated by RT-PCR, as described elsewhere [184]. One microliter of a 20uL cDNA prep generated from 2ug RNA was used as template in PCR with

primers (listed in Table 2) located in the *Dmrt1* cDNA (Dmrt1 3′) and exon 9 of HPRT1 (HPRT1), which span the HPRT1 intron and allowed differentiation between the expressed transgene and contaminating genomic DNA. Amplified products were examined by agarose gel electrophoresis, with that from the transgene's cDNA yielding a 434bp product and that from genomic DNA yielding a 1102bp product.

Quantitative real-time PCR

Real-time reactions were carried out, as described, using a 7900HT Sequence Detection real time analyzer (Applied Biosystems, Foster City, CA)[185]. Testis RNA was isolated as above from *Dmrt1*$^{-/-}$, *Dmrt1*$^{-/-;tg}$ and *Dmrt1*$^{+/+}$ P7 mice. First-strand cDNA synthesis was performed using 2ug RNA with MMLV reverse transcriptase, following manufacturer's instructions (Invitrogen, Carlsbad, CA). A 1:10 dilution of cDNA was assayed using a SYBR® Green PCR master mix (Applied Biosystems, Foster City, CA) and primers listed in Table 3. Samples and negative control (water) were run in triplicate. C_t melting curves for endogenous RNA ribosomal L7 (*Rpl7)* was used to calculate ΔC_t values for each sample. *Rpl7* C_t values did not vary across genotype and the melting curves for *Rpl7* and the genes assayed gave only a single, unique peak for each primer set. $\Delta\Delta C_t$ values were calculated by subtracting the mean P7 wild type ΔC_t. Fold change was calculated using the ΔΔCt method [186].

Results

Generation of Wt1-Dmrt1 transgenic mice

To establish a mouse model that ectopically expresses DMRT1 in supporting cells of the gonads, a YAC transgene was used to direct expression of DMRT1 to pre-Sertoli and pre-granulosa cells in the embryo. The transgene was generated using a 'knock-in' strategy that

inserted a rat *Dmrt1* cDNA into the mouse Wilms' tumor 1 gene (*Wt1*) located within 620mWt1, a YAC, when previously used as a transgene, expressed only in kidney and gonads (Figure 1, top and [39, 187]). Notably, gonadal expression was restricted to supporting cells and began at a time prior to sex determination. A targeting vector (Figure. 1A middle) was used to insert the *Dmrt1* cDNA into *Wt1* at a specified site in 620mWt1, via homologous recombination. The resulting *Wt1-Dmrt1* transgene contains *Dmrt1*'s *cDNA* (beginning with the DMRT1 AUG start codon) inserted in-frame with WT1's start codon in 620mWt1 (Figure. 1A bottom). Expression of the *Dmrt1* cDNA within *Wt1-Dmrt1* is therefore directed by *Wt1* regulatory sequences. Three founders were obtained and used to develop transgenic lines 13, 30, and 37, all of which produced pups with the correct chromosomal sex. RT-PCR of multiple tissues from newborn and postnatal day 15 (P15) mice showed transgenic *Dmrt1* expressed only in kidneys and gonads, confirming the expected spatial expression of the transgene (Figure 1B-D).

Transgenic DMRT1 is Sertoli cell-specific in Dmrt1$^{-/-;tg}$ testes

Mice with DMRT1 expressed only in Sertoli cells were created by mating transgenic male mice with *Dmrt1$^{-/-}$* female mice, which are fertile. To confirm proper cellular expression of the transgene, immunofluorescence staining was performed for DMRT1 (green) and the specific germ cell marker GCNA1 (red), using testis sections from P7 mice. In *Dmrt1$^{+/+}$* mice, DMRT1 was observed in testicular Sertoli cells and germ cells, the latter of which, when merged, appeared primarily yellow, indicating DMRT1 is present in most P7 germ cells (Figure 2A-C). As expected, no DMRT1-positive cells were seen in *Dmrt1$^{-/-}$* testes (Figure 2D-F) or in *Dmrt1$^{-/-;tg}$* germ cells (Figure 2G-I), which stained only for GCNA1 (Figure 2I). Western blot analysis confirmed that DMRT1 protein was expressed in *Dmrt1$^{-/-;tg}$* but not in *Dmrt1$^{-/-}$* testes (Figure 2J).

Thus, DMRT1 produced from the transgene validates cell-specific expression only in Sertoli cells of the of *Dmrt1*$^{-/-;tg}$ testes.

Transgenic Dmrt1 partially preserves testis morphology but does not rescue testis weights.

As previously reported during characterization of germ cell migration from P0-P7, defects in germ cell radial migration were observed in *Dmrt1*$^{-/-}$ P7 testes. Thus, *Dmrt1*$^{-/-}$ germ cells were confined to the lumen of the seminiferous tubule, while *Dmrt1*$^{+/+}$ germ cells were located on the basement membrane [50, 131, 132, 188]. Notably, germ cells in *Dmrt1*$^{-/-;tg}$ testes also showed defective migration, consistent with similar findings in DMRT1-deficient germ cells [131]. PAS stained P7 *Dmrt1*$^{-/-;tg}$, *Dmrt1*$^{-/-}$ and *Dmrt1*$^{+/+}$ testis sections revealed similar tubule morphology between the three genotypes, with only modest differences noted in organization (Figure 3A-C). However, by P42 *Dmrt1*$^{-/-;tg}$ testes showed notable but partial improvement in tubule morphology relative to *Dmrt1*$^{-/-}$ testes (Figure 3D-L). Thus, histological analyses showed distinct differences in seminiferous tubule organization at P42 and in contrast to *Dmrt1*$^{-/-}$ testes (Figures 3E and 3H), *Dmrt1*$^{-/-;tg}$ testes contained numerous tubules with defined lumens (Figures 3F and 3I, arrowheads). Furthermore, no SC nuclei were observed in the lumen of the tubule in *Dmrt1*$^{-/-;tg}$ (Figure 3I, arrowheads). Because accumulation of fatty acids was difficult to evaluate by PAS staining, toluidine blue staining on 1µm sections (Figures 3J-L) was employed; and whereas the lumen in the *Dmrt1*$^{-/-}$ seminiferous tubules (Figure 3K, asterisk) featured abundant accumulation of lipid droplets in addition to SC nuclei, the lumen of the *Dmrt1*$^{-/-;tg}$ seminiferous tubules (Figure 3L, arrowhead) contained only lipid droplets. The partial restoration of tubule morphology indicated that transgene-derived DMRT1 in Sertoli cells is functional and influences the formation of the basal and apical compartments within the seminiferous tubules.

To better pinpoint the effect of transgenic DMRT1 on testis development and the timeline for deficiency, we compared testis weight to body weight (TW/BW) ratios of *Dmrt1*$^{+/+}$, *Dmrt1*$^{-/-}$, and *Dmrt1*$^{-/-;tg}$ mice at P2, P7, P15, P20, and P42. The TW/BW ratios at P2 were similar between *Dmrt1*$^{+/+}$, *Dmrt1*$^{-/-}$ and *Dmrt1*$^{-/-;tg}$. A small but significant ($p<0.01$) difference was first observed in the *Dmrt1*$^{-/-}$ and *Dmrt1*$^{-/-;tg}$ P7 mice and the TW/BW difference increased with each age, thereafter (Figure 4). No significant difference was observed between TW/BW ratios of *Dmrt1*$^{-/-}$ and *Dmrt1*$^{-/-;tg}$ mice, at all-time points (Figure 4). Thus, loss of *Dmrt1* caused modest changes in TW/BW beginning between P2 and P7 and its return to Sertoli cells, via the transgene, failed to rescue these changes. Given that testis weight strongly correlates to the number of germ cells, the inability of transgenic DMRT1 to preserve testis weights in *Dmrt1*$^{-/-;tg}$ mice confirms the autonomous role of DMRT1 in germ cell maintenance and/or development[131].

Wt1-Dmrt1 copy number influenced testis gene expression.

To determine if DMRT1 levels affect testis gene expression, specific DMRT1-regulated transcripts were quantified from testes carrying different copy numbers of the *Wt1-Dmrt1* transgene. Transcripts were selected from transcriptome data that identified mRNAs with altered expression in P7 *Dmrt1*$^{-/-}$ testes (manuscript in preparation). *Dmrt1* and the selected mRNAs were measured by qRT-PCR, using RNA prepared from *Dmrt1*$^{-/-}$, *Dmrt1*$^{+/+,}$ and *Dmrt1*$^{-/-;tg}$ P7 testis. For *Dmrt1*$^{-/-;tg}$ samples, Southern blot analysis, followed by densitometry and phosphor imaging, was used to identify mice with either one or two copies of the line 37 transgene (Figure 5A). The data revealed dose-dependent expression of transgenic *Dmrt1*, demonstrating that the number of transgenes determined the level of *Dmrt1* mRNA (Figure 5B). The data also identified three distinct categories for responsive genes; resistant, partial and sensitive. Resistant genes (*Mage-K1, Cidea, Rbym1a1, Stk31,* and *Gpr37*) changed significantly in *Dmrt1*$^{-/-}$ *testes*, with or

without the transgene, indicating they are regulated by DMRT1 in germ cells. Genes in the partial category (*Lect1, Nfx2 and Tnnt2*) modestly responded to added transgene, without notable dose-dependency, suggesting a combined requirement for germ cell and Sertoli cell DMRT1. Sensitive genes (*Sycp1, Rarres1, Pramel3,* and *Trim34*) showed a dose-dependent response to the transgene, consistent with a primary dependence on Sertoli cell DMRT1. These findings support using transgene sensitivity to distinguish autonomous from non-autonomous effects of DMRT1.

Transgenic DMRT1 alleviates the age-dependent decrease in testis size and progressive sperm motility observed in wild type mice

Because DMRT1 influences Sertoli cell differentiation, the transgene's influence over age-related changes in testes size and sperm function was evaluated in wild type mice ($Dmrt1^{+/+}$) and mice carrying one or two copies of the transgene ($Dmrt1^{+/+;tg}$ and $Dmrt1^{+/+;tg+tg}$, respectively). The mean body weight (Figure 6A) and mean paired testes weight (Figure 6B) were evaluated at ages 3, 6, 10, 12 and 18 months. Body weights were not changing as no statistical significant differences ($p > 0.05$) were noted between genotypes at each time-point (Figure 6A). Similarly, there was no statistical difference in mean paired testes weights between genotypes at all time-points except at 18 months of age, where the testes weights of $Dmrt1^{+/+;tg}$ and $Dmrt1^{+/+;tg+tg}$ mice were significantly greater ($p<0.001$) than those from $Dmrt1^{+/+}$ mice (Figure 6B). In addition, when the paired testes weights were corrected by their respective body weights (TW/BW ratio), no significant differences were observed between genotypes at 3, 6 and 10 months of age (Figure 6C). However, at 12 and 18 months, the TW/BW ratios were significantly higher in mice carrying the transgene. This finding suggested that Sertoli cell function was preserved, which also preserved the spermatogenic capacity. Thus, CASA revealed

that the decrease in sperm progressive motility observed naturally in 12-month-old wild type mice was partially restored by the presence of the transgene (Figure 6D). The data suggest that the additional DMRT1 in Sertoli cells helped preserve spermatogenesis and sperm function.

Germ cell DMRT1 is needed to maintain adult testosterone levels

To determine if *Dmrt1* impacts the animal's reproductive hormone status, serum testosterone (T) was measured in *Dmrt1*$^{+/+}$, *Dmrt1*$^{-/-;tg}$ and *Dmrt1*$^{-/-}$ mice. Although the difference was only moderately significant ($p = 0.19$), *Dmrt1*$^{-/-}$ mice at P15 had reduced serum T compared to *Dmrt1*$^{+/+}$ mice (Figure 7A). In addition, comparison of *Dmrt1*$^{-/-}$ and *Dmrt1*$^{-/-;tg}$ mice indicated the transgene improved serum testosterone levels at P15 but the increase was not statistically significant ($p = 0.17$). By P20, serum T levels had increased and, surprisingly, were similar in all three genotypes, indicating that the decreased testis size at P20 (Figure 4) did not result from reduced T. By P42, T levels were significantly lower in both *Dmrt1*$^{-/-;tg}$ ($p = 0.04$) and *Dmrt1*$^{-/-}$ ($p = 0.03$) compared to wild type. The drop in testosterone between P20 and P42 was supported by evaluation of the seminal vesicles, which were present in P20 and P42 wild type mice and absent from *Dmrt1*$^{-/-}$ and *Dmrt1*$^{-/-;tg}$ mice only at the P42 time point (Figure 7B). However, the presence of well-developed seminal vesicles at P131 only in *Dmrt1*$^{-/-;tg;37}$ compared to *Dmrt1*$^{-/-}$ mice suggest that the drop in serum testosterone levels was temporary and the *Dmrt1*$^{-/-;tg}$ mice show a delay in the development of reproductive structures (Supplementary Figure 1). Furthermore, the serum levels of LH (Figure 7C) and estradiol (Figure 7D) were examined. Between P15 and P20, T and LH levels rose in *Dmrt1*$^{-/-}$ and *Dmrt1*$^{-/-;tg}$, mice, while between P20 and P42, only T levels dropped significantly. The results suggest that LH regulates T production at P15 and P20 but the regulation is lost by P42. On the other hand, the addition of the transgene caused a rise in estradiol level in *Dmrt1*$^{-/-;tg}$ mice at P15 which was not statistically

different when compared to estradiol levels in *Dmrt1*$^{-/-}$ ($p = 0.15$) or wild-type ($p = 0.24$) mice. From P15 through P42, the levels of estradiol dropped in *Dmrt1*$^{-/-;tg}$ and *Dmrt1*$^{+/+}$ mice but remained constant in *Dmrt1*$^{-/-}$ mice. The results suggest that LH regulates the estradiol level at P15 and the levels at P20 and P42 are derived from the conversion of T.

The above data indicate that, in P15 and P20 *Dmrt1*$^{-/-}$ and *Dmrt1*$^{-/-;tg}$ mice, LH controlled the production of T, but, by P42, despite sufficient LH, T levels dropped, indicating the problem arose from a defect in the testis. Therefore, the testis was examined by immunohistochemistry, using an antibody against CYP11A1 (P450SCC), which is the rate-limiting enzyme for testosterone production and a marker of the Leydig cell population. At P7 (Figure 8A-C) and P15 (Figure 8D-F), Leydig cell numbers appeared similar between testes of each genotype. However, Leydig cell morphology was noticeably different in the *Dmrt1*$^{-/-}$ P15 testis, with more P450SCC-positive cells residing in groups (Figure 8E). By P20 (Figure 8G-I), the number of Leydig cells appeared slightly increased in *Dmrt1*$^{-/-}$ (Figure 8H) and *Dmrt1*$^{-/-;tg}$ (Figure 8I), an impression most likely due to the increased numerical density of Leydig cells (number of Leydig cells per testis volume), given the significantly decreased testis size in the *Dmrt1*$^{-/-;tg}$ and *Dmrt1*$^{-/-}$ mice. In *Dmrt1*$^{-/-;tg}$ and *Dmrt1*$^{-/-}$ P42 mice, the apparent increase was even more exaggerated (Figures 8L & K). In marked contrast to the *Dmrt1*$^{-/-;tg}$ and *Dmrt1*$^{-/-}$ testes at P42, the Leydig cells in *Dmrt1*$^{+/+}$ were larger and accumulated in distinct regions of the interstitium (Figure 8J). These results indicate that the age-dependent hypogonadism resulted, not from a loss in Leydig cell number, but from a defect in Leydig cell function. Since the expression of transgene-derived DMRT1 in Sertoli cells did not correct the problem, the deficiency most likely resulted from DMRT1's absence in the germline.

Germ cell DMRT1 influences Sertoli cell maturation

To determine if the transgene rescues defects in Sertoli cell maturation, proliferation and junctional complex formation, qRT-PCR and immunocytochemistry was used to compare the expression of genes involved in these cellular processes between *Dmrt1*$^{+/+}$, *Dmrt1*$^{-/-}$, and *Dmrt1*$^{-/-;tg}$ testes. To evaluate Sertoli cell maturation, expression of three different genes was evaluated; *Ar* and *Gata1*, which are prominent in mature Sertoli cells, and *Krt18*, which is a marker of immature cells [189, 190] . At P7, *Ar* mRNA levels were not significantly different between *Dmrt1*$^{+/+}$ and either *Dmrt1*$^{-/-}$ or *Dmrt1*$^{-/-;tg}$ mice, while *Gata1* mRNA was reduced ($p<0.005$) in both *Dmrt1*$^{-/-}$ and *Dmrt1*$^{-/-;tg}$ testes (Figure 9). In contrast, *Krt18* was markedly elevated ($p=0.0028$) in *Dmrt1*$^{-/-;tg}$ and *Dmrt1*$^{-/-}$ testes relative to *Dmrt1*$^{+/+}$(Figure 9).

Differentiation of Sertoli cells coincides with formation of the blood-testis barrier, which contains various membrane- and junction-associated inter-Sertoli proteins, such as *OCLN*, *ESPIN*, *CLDN11*, and *TJP1* [191-194]. Transcript levels of the cell junction markers *Ocln, Espin, and Cldn11* were dramatically changed in *Dmrt1*$^{-/-}$, while more modest changes were noted for *Tjp1* (Figure 9). Except for *Espin*, significant changes were noted in both *Dmrt1*$^{-/-}$ and *Dmrt1*$^{-/-;tg}$ mice. Of the four cell junction genes, only *Espin* mRNA levels increased in *Dmrt1*$^{-/-}$ testes (~3 fold; $p < 0.03$) or returned to normal when DMRT1 was returned to Sertoli cells (Figure 9; *Dmrt1*$^{-/-;tg}$). In addition, mRNA levels of *Gata4*, a transcription factor that plays important roles in the development and function of fetal and postnatal Sertoli cells and Leydig cells [195], were significantly increased in both *Dmrt1*$^{-/-}$ and *Dmrt1*$^{-/-;tg}$ testes compared to *Dmrt1*$^{+/+}$ (Figure 9). Notably, of the genes investigated, only *Espin* showed significant sensitivity to DMRT1 in Sertoli cells, indicating that the other genes were primarily influenced by DMRT1 in germ cells.

Expression of AR was examined at a time-point before (P7) and after (P15) Sertoli cell maturation in wild type mice. In mouse testes of all groups, AR was observed in Sertoli cells (arrows), peritubular myoid cells (arrowheads), and Leydig cells (asterisks) (Figure 10). At P7, all three groups showed strong staining for AR in myoid and Leydig cell, while staining was absent from Sertoli cells

(Figure 10A-C). By P15, AR was evident in all or most Sertoli cells of wild type mice, while it was absent or reduced in most Sertoli cells from the *Dmrt1*$^{-/-}$ mice (Figure 10 D & E). Comparison of AR staining in Sertoli cells of *Dmrt1*$^{-/-}$ and *Dmrt1*$^{-/-;tg}$ mice revealed more AR-positive Sertoli cells in mice baring the transgene (Figures 10E & F).

Immunohistochemistry was also used to examine P42 testes for expression of GATA4 and PCNA. Testes sections revealed GATA4 in both Sertoli cells (arrowheads) and Leydig cells (located in the intertubular spaces), while PCNA was largely restricted to germ cells and the occasional Leydig cell (Figure 11A). GATA4 staining was also apparent in spermatids, which, as previously reported, was considered nonspecific staining [189]. In *Dmrt1*$^{-/-}$ testis sections, GATA4 was noted in all cells located within the remaining tubule-like structures and scattered throughout the interstitium. Some cells within the tubules and interstitium stained for both GATA4 and PCNA (Figure 11B, arrows) but most PCNA-positive cells were GATA4 negative and located in the interstitium. In *Dmrt1*$^{-/-;tg}$ testis sections, fewer cells that express only PCNA appeared to partition to the interstitium and cells positive for both GATA4 and PCNA were observed in both the tubules (Figure 11 C, arrows) and interstitium . In the *Dmrt1*$^{-/-;tg}$ mouse testis, two populations of GATA4-positive, PCNA-positive Sertoli cells were identified; one in which GATA4 and PCNA were both nuclear (arrowhead) and the other in which only PCNA was nuclear (asterisks). Sertoli cells co-expressing GATA4 and PCNA were considered immature and proliferating whereas those expressing only GATA4 were considered more mature or differentiated. Sertoli cells in *Dmrt1*$^{-/-}$ mice were still proliferating and thus were considered immature.

Sertoli cell maturation was also assessed by examining nuclear ultrastructure at P7 and P42 (Figure 12: SC and GC nuclei traced by black and white lines, respectively). At P7, Sertoli cell nuclei of *Dmrt1*$^{+/-}$ mice had a regular columnar contour without invaginations and were located away from the basement membrane (Figure 12A, insert). In P7 *Dmrt1*$^{-/-}$ mice, nuclei were more mature in appearance, with an irregular shape and multiple invaginations and more prominent areas of condensed chromatin (Figure 12 B). In P7 *Dmrt1*$^{-/-;tg}$ mice, some rounded, regular-shaped Sertoli cell nuclei, similar to that

observed in the wild type, were observed but the majority appeared as those in P7 *Dmrt1*$^{-/-}$ mice (Figure 12C, arrowheads in insert). At P42, the *Dmrt1*$^{+/+}$ nucleus was ovoid and adjacent to the basement membrane (Figure 12D). The nuclear membrane was irregular and invaginated (arrow in insert, Figure 12 D), while the nucleolus formed a central granular condensed area (Figure 12D). P42 *Dmrt1*$^{-/-}$ nuclei were predominantly round, columnar or ovoid shaped, without invaginations, and located away from the basement membrane of the tubule (Figure 12E). *Dmrt1*$^{-/-}$ nucleoli were found at the periphery of the nucleus and the chromatin was arranged in irregular granular clusters. The morphology of the nuclei in P42 *Dmrt1*$^{-/-;tg}$ mice appeared intermediate to that observed in wild type and *Dmrt1*$^{-/-}$ mice, comprising a mixture of nuclei that were either regular round or irregular ovoid (compare nuclei denoted with asterisks in Figures 12 E and F). Some of these nuclei had invaginations (arrows in insert, Figure 12 F) and nucleoli that formed a central granular condensation area (Figure 12 F, insert). However, most ovoid nuclei had nucleoli located at the periphery of the nuclear membrane and chromatin arranged in irregular granular clusters.

Discussion

Dmrt1 is a putative mammalian ortholog of *Dsx* and *Mab-3*, genes known to be involved in sex determination and differentiation in flies and worms, respectively, and its diverse roles in sex determination and differentiation are well established [3, 50, 112, 128, 131-133, 141, 144, 146-155, 157, 158, 172]. In mammals, DMRT1 functions predominantly after birth, when it becomes male-and-testis-specific and is required for male fertility [50, 131, 133]. At this time, DMRT1 is expressed only in spermatogonia and Sertoli cells where it acts both autonomously and nonautonomously to regulate germ cell proliferation and differentiation and Sertoli cell maturation [50, 130-133, 159]. While many excellent studies have contributed to our understanding of DMRT1's actions in the testes, there remain numerous uncertainties regarding its function, particularly with respect to its cell specific roles. Here we report the development and characterization of a unique mouse model, to facilitate our understanding of DMRT1's specific functions in Sertoli cells and germ cells.

Spatio-temporal expression of Wt1-Dmrt1 transgene

The model employed the *Wt1* locus within a YAC transgene to direct DMRT1 specifically to Sertoli cells of the testis. The use of YACs (or BACs) as transgenes have several advantages over smaller vectors, as they are much less subject to insertion side effects, resulting in expression that depends only on sequences in the transgene [196]. In addition, larger transgenes often express at levels that are copy number dependent, allowing one to adjust levels of expressed product. In the case of the *Wt1-Dmrt1* transgene, its tissue and cellular expression profiles adhered to that of *Wt1* and it induced dose-dependent expression changes in several DMRT1-regulated genes. Transcript measurements of transgenic embryos, as well as previous reports using the original YAC, suggest transgenic DMRT1 was present prior to sex determination, in both male and female gonadal somatic cells, through adulthood. After birth, transgenic *Dmrt1*/DMRT1 was restricted to the kidneys and gonads of both sexes and, in the gonads was limited to the supporting cells [39, 187, 197-199] . Importantly, immunohistochemistry on testis sections from *Dmrt1*$^{-/-}$ mice carrying the transgene showed transgenic DMRT1 expressed only in Sertoli cells of the testis, while Western blot analysis reported levels that matched the endogenous protein. The data, therefore, confirmed that the spatial and temporal expression pattern of DMRT1/*Dmrt1* directed by the YAC transgene matched that reported for endogenous *Wt1*[39, 197, 198].

DMRT1 is not required for murine sex determination but preserves testis function

Expression of exogenous DMRT1 in female mice on a *Dmrt1*$^{+/+}$background did not cause any notable morphological or functional abnormalities during gonadogenesis and female-to-male sex reversal was not observed (data not shown). Thus, consistent with murine *Dmrt1* deletion studies, continuous expression of DMRT1 in pre-granulosa cells did not implicate it in murine sex determination [50, 141]. Eventually, all female transgenic mice, regardless of the genetic background (*Dmrt1*$^{+/+}$, *Dmrt1*$^{+/-}$ or *Dmrt1*$^{-/-}$) reached sexual maturity and were fertile. Male transgenic mice (*Dmrt1*$^{+/+;tg}$) were also fertile and, surprisingly, showed less of the age-related declines in testis size and sperm progressive motility, normally observed in wild type males. The finding suggests that, by preserving Sertoli cell function,

DMRT1 preserved both spermatogenic capacity and sperm function. This role in sex maintenance is supported by a recent study using conditional cell-specific deletion of *Dmrt1* in Sertoli cells (*SCDmrt1KO*). Specifically, cell-specific deletion of *Dmrt1* in Sertoli cells resulted in a normal morphology and SOX9 expression after birth; but by P14, *Dmrt1-null* Sertoli cells started expressing FOXL2, which is normally expressed in the ovary, and by P28, the majority of cells expressing SOX9 were lost while the number of cells that were FOXL2-positive were increased in the seminiferous tubule. Also, similar changes were observed four weeks after the cell-specific deletion of *Dmrt1* in adult mice, leading to the conclusion that loss of *Dmrt1* causes Sertoli cells to be reprogrammed into cells with a granulosa-like or theca-like morphology[135]. Overall, it is still unclear if *Dmrt1* regulates murine primary sex determination but unquestionable that it is vital for postnatal testis differentiation and gonadal sex maintenance.

$Dmrt1^{-/-;tg}$ (or Sertoli cell rescue or germ cell deficiency) mouse model complements existing Dmrt1 cell-specific deletion models.

The *$Dmrt1^{-/-;tg}$* (or Sertoli cell rescue or *Dmrt1*-deficient germ cell) mouse is a Sertoli cell-specific expression model generated by expressing DMRT1 in *Dmrt1-null* Sertoli cells unlike the existing *GCDmrt1KO* models generated by CRE-mediated *Dmrt1* deletion [131, 133, 134]. The *$Dmrt1^{-/-;tg}$* mouse model has the potential to provide novel insight to cell-specific actions of DMRT1 that are impossible to examine using current models, which fail to capture germ cell specific events at early ages afterbirth. For example, existing models cannot precisely evaluate the role of DMRT1 in establishing the germ cell lineage, if the process involves loss of DMRT1 in all germ cells (e.g. expression profiling). Likewise, they cannot assess its specific function in gonocytes prior to puberty, consequently primary processes, like re-activation of DMRT1 in the germ line (P0-P2) and the early events that lead to testis defects (P2-P10), cannot be evaluated [50, 131-133]. More specifically, *Dmrt1* was conditionally deleted from germ cells in previous models using the Cre-LoxP system that employed either TNAP-Cre or Ngn3-Cre [131, 133, 134, 200]. The TNAP-Cre employed was limited by its poor Cre penetrance that resulted in partial

deletion with a portion of germ cells positive for DMRT1. Furthermore, immunohistological analysis showed that deletion using the TNAP-Cre was leaky and nonspecific as DMRT1 was ectopically ablated in some Sertoli cells. Thus, TNAP-Cre cannot be used to correctly profile the cells without accounting for the effective deletion. Likewise, a significant number of spermatogonia that were DMRT1-positive were negative for the Ngn3-Cre transgene until several weeks after birth, which prevented analysis of early germ cell specific events [110, 174]. The restricted co-expression of DMRT1 and NGN3 in prepubertal mice can be appreciated by immunofluorescence of the two proteins in P7 testes, which shows few dual-stained yellow cells [130]. Consequently, the mechanistic, morphological and molecular changes directed by DMRT1 in the germline remains unexploited. In *Dmrt1*$^{-/-;tg}$ mice, DMRT1 is expressed from the *Wt1-Dmrt1* transgene in pre-Sertoli and pre-granulosa cells of the developing gonad and the cells are rescued from DMRT1 deficiency prior to sex determination in the embryo . Thus, complete loss of DMRT1 expression in GCs begins at the onset of gonadogenesis and continues through maturity. Overall, the *Dmrt1*$^{-/-;tg}$ model complements and extends our knowledge of the conditional deletion models by providing understanding from a cell-specific expression perspective that is different from cell-specific deletion standpoint.

Germ cell depletion and abnormal hormonal levels contribute to the hypoplastic testis phenotype in Dmrt1$^{-/-;tg}$ *(rescue) mouse model.*

Like the previously described male *Dmrt1*$^{-/-}$ mice, male *Dmrt1*$^{-/-;tg}$ mice were sterile and characterized by testicular hypoplasia [50]. This phenotype was substantiated in the adult (P42) *Dmrt1*$^{-/-}$ and *Dmrt1*$^{-/-;tg}$ mice by significant reduction in testis weights and serum testosterone levels*;* and estimation of the timeline for the onset of the testicular defect in *Dmrt1*$^{-/-;tg}$ mice like in *Dmrt1*$^{-/-}$ mice suggested it may begin as early as P3. The progressive loss of germ cells noted at P7 which resulted in complete germ cell depletion by P15 (data not shown) in *Dmrt1*$^{-/-;tg}$ like the complete depletion by P10 in the testis of *Dmrt1*$^{-/-}$ mice, most likely contributed to the reduced testis weights [50]. Furthermore, the trends of serum T, LH and estradiol levels in *Dmrt1*$^{-/-}$ and *Dmrt1*$^{-/-;tg}$ mice compared to controls also

suggested strong hormonal influence on the hypoplastic testis phenotype. Specifically, the serum T and LH levels rose between P15 and P20 in all three groups but serum T dropped between P20 and P42 in *Dmrt1*$^{-/-}$ and *Dmrt1*$^{-/-;tg}$ mice while serum LH was similar in all three groups. Although the drop in serum T was substantiated by the absence of seminal vesicles in *Dmrt1*$^{-/-}$ and *Dmrt1*$^{-/-;tg}$ mice at P42, the lack of a significant increase in serum LH as a feedback response to loss of T was likely confounded by the large variability in the LH data. And an obvious increase in serum LH was observed in *Dmrt1*$^{-/-}$ and *Dmrt1*$^{-/-;tg}$ mice when the high values were removed during subsequent data analyses (data not shown). In addition, because Sertoli cells have been shown to transdifferentiate into apparent granulosa cells in *Dmrt1 null* mice [135], the serum levels of the female sex hormone, estradiol; produced by granulosa cells and as an active metabolic product of testosterone, was evaluated. At P15, the addition of the transgene in *Dmrt1*$^{-/-;tg}$ mice caused a significant rise in estradiol levels that was not sustained as the mutant mice aged. Thus, because there was an apparent rise in LH between P15 and P20 it appears the rise in T and estradiol was driven by LH, but between P20 and P42, the drop in T is not dependent on LH. This finding that testosterone levels was maintained only in wild type P42 mice, suggests that DMRT1 activity in germ cells may regulate the development of interstitial Leydig cells which produces testosterone required for the growth of male reproductive organs.

DMRT1 in Sertoli cells maintains tubule integrity

Further evaluation of *Dmrt1*$^{-/-;tg}$ mice reveals Sertoli cell-specific function of DMRT1 in maintaining integrity of seminiferous tubules. The histology of tubule had discernible differences between the *Dmrt1*$^{-/-;tg}$ and *Dmrt1*$^{-/-}$ mice when compared to the wild type controls. Although the seminiferous tubule morphology at P7 was similar across groups as was previously reported [50], the morphology of the seminiferous tubules in the adult *Dmrt1*$^{-/-;tg}$ mouse testes unlike those in *Dmrt1*$^{-/-}$ mice were partially restored. The incomplete restoration of seminiferous tubule morphology when DMRT1 is present in Sertoli cells of *Dmrt1*$^{-/-;tg}$ mice suggest that DMRT1 in germ cells or germ cells themselves are required for total tubule integrity. However, since models devoid of germ cells like $W^{(v)}/W^{(v)}$ mice show good

tubule morphology, it suggests it is not just the absence of germ cells [201]. Thus, it is either that there was not enough DMRT1 provided by the transgene (in this evaluation) or that a conflict arises because DMRT1 is regulated like *Wt1*, not *Dmrt1*, or some other tubule disruption occurs when DMRT1 is present in Sertoli cells or absent in germ cells. This role in tubule integrity is supported by the previous evaluation of Sertoli cells in *SCDmrt1KO* model, generated by DHH-CRE-mediated deletion of *Dmrt1*, which appeared normal through P7, slightly disorganized by P9, and notably disorganized by P14. By P28, SCs were positioned throughout the tubule and seminiferous tubules were disorganized and lacked defined lumens [50, 131].

Wt1-Dmrt1 transgene can be used to demonstrate autonomous and non-autonomous effects of DMRT1.

Expression analysis of DMRT1-regulated genes provided further evidence on the functional effect of the *Wt1-Dmrt1* transgene. In the case of the *Wt1-Dmrt1* transgene, it revealed gene sensitivity derived from different levels of DMRT1 in Sertoli cells. It was demonstrated that exogenous DMRT1 directs dose-dependent gene expression. Three expression groups were identified. The "resistant" (*Mage-K1, Cidea, Rbym1a1, Stk31*and *Gpr37*) category included genes that responded to *Dmrt1* loss but did not change with addition of any amount of transgene. Genes in the "partial" (*Lect1, Nxf2* and *Tnnt2)* category showed modest improvement over the null mice with added transgene, but the response was not dose-dependent. The "sensitive" (*Sycp1, Rarres1, Pramel3,* and *Trim34)* category represented genes that showed significant improvement with transgene addition and, in many cases, a response that was dose-dependent. *Rarres1* was partially restored with one copy, completely restored with two, and further compromised by the addition of more copies. Unlike *Rarres1, Trim34* was best restored with a single copy of the transgene and additional copies further compromised expression. *Pramel3* and *Scyp1* showed similar expression patterns as *Rarres1,* but, all of them only approached full recovery. *Lect1, Nxf2* and *Tnnt2* showed a partial response but failed further recovery with different transgene copies. The genes that responded to each DMRT1 dose indicate *Dmrt1's* activity in the SC is the only influence on that

gene. While those that change partially suggest there is input from *Dmrt1* from both cell types and those that are resistant are dependent on *Dmrt1's* activity in the germ cells. Interestingly, this study identified genes (e.g. *Sycp1*) that are present only in germ cells and are directed by DMRT1's actions in Sertoli cells. The responding gene changes confirmed that there are differences presumably due to *Dmrt1* dosage and to Sertoli cells versus germ cells. These results validate the role of DMRT1 as a dose-sensitive regulator; as was previously shown that it behaves genetically as a dose-sensitive tumor suppressor gene on a 129Sv mouse background, and normal changes in its activity confers vulnerability to malignant cell growth [133]. The gene expression data demonstrate that transgenic DMRT1 is functional and can fully rescue a subset of genes, presumably those directed by Sertoli cell DMRT1, either autonomously or non-autonomously. Overall, the histological and gene expression results show that the *Dmrt1*$^{-/-;tg}$ mice uphold several key requirements that support their use to delineate DMRT1 function and identify the specific effects of DMRT1 in germ cells. First, transgenic DMRT1 is produced only in testicular Sertoli cells and not germ cells. Second, the dosage of exogenous DMRT1 can be managed to match that of the endogenous gene. Lastly, transgenic DMRT1 activity mimics that of the endogenous protein.

Wt1-Dmrt1 transgene influences maturation state of Dmrt1-null Sertoli cells

Sertoli cells are specialized testicular somatic cell that nurtures developing germ cells and are considered to be terminally differentiated after puberty. Terminal differentiation involves loss of proliferative ability, formation of functional inter-Sertoli cell tight junctions, and expression of functions or proteins not present in immature Sertoli cells [86]. In humans, nuclear and general morphology of Sertoli cells coupled with weak or absence of AR expression has been associated with failure to mature [86, 202]. Assessment of markers of Sertoli cell maturation (*Ar* and *Gata1*) and an immature cell marker (*Krt18*) at a prepubertal age showed that development of Sertoli cells in *Dmrt1*$^{-/-;tg}$ and *Dmrt1*$^{-/-}$ mice was compromised [86, 189, 190, 203-207]. In rodents, AR is expressed in peritubular myoid cells and Leydig cells at all stages while its expression is elevated in Sertoli cells prior to their maturation [85]. In this study the transcript and protein levels of *Ar* were similar at P7 in all three groups, whereas at P15 the

expression of AR was reduced in *Dmrt1*$^{-/-}$ and *Dmrt1*$^{-/-;tg}$ compared to *Dmrt1*$^{+/+}$ mice. A similar pattern of expression was previously reported for the *SCDmrt1KO* mice compared to controls whereby up-regulation of AR expression was absent between P5 and P9 but present by P21 [131]. Furthermore, the message for *Gata1* was significantly reduced in *Dmrt1*$^{-/-}$ and *Dmrt1*$^{-/-;tg}$ mice at P7. This is supported by earlier characterization of *Dmrt1-null* mice showing that GATA1 expression was delayed but present in the mutant testes [50]. Likewise, the message for *Krt18* was significantly up-regulated in *Dmrt1*$^{-/-;tg}$ and *Dmrt1*$^{-/-}$ mice relative to *Dmrt1*$^{+/+}$ mice. An impact on Sertoli cell maturation was observable as early as P7 based on the elevated transcript expression of *Krt18* and reduced expression of *Gata1*. Thus, evaluation of these markers suggest that relative to the controls (*Dmrt1*$^{+/+}$ and *Dmrt1*$^{-/-}$), the maturation of Sertoli cells in *Dmrt1*$^{-/-;tg}$ mice is delayed.

In addition, examination of junctional complex proteins revealed that except for *Espin* that was almost normally expressed in *Dmrt1*$^{-/-;tg}$ mice, *Ocln*, *Cldn11* and *Tjp* were reduced in both *Dmrt1*$^{-/-}$ and *Dmrt1*$^{-/-;tg}$ relative to *Dmrt1*$^{+/+}$ mice. Only *Espin* showed significant sensitivity to DMRT1 in Sertoli cells and the other genes are primarily influenced by DMRT1 in germ cells.

Dual staining using Sertoli cell/Leydig cell marker, GATA4, and the proliferation marker, PCNA, was performed to validate the maturation states of Sertoli cells. Sertoli cells in the *Dmrt1*$^{+/+}$ mice did not co-express GATA4 and PCNA, which was indicative of terminal differentiation or acquisition of a mature state. Many Sertoli cells in *Dmrt1*$^{-/-}$ mouse testes co-expressed PCNA and GATA4, which was indicative of an immature or proliferating state. A small number of Sertoli cells in *Dmrt1*$^{-/-;tg}$ mouse testes did not co-express, whereas the majority of Sertoli cells did co-expressed GATA4 and PCNA, which was indicative of an intermediate or partial maturation state.GATA4 expression was persistent and elevated in *Dmrt1*$^{-/-}$ and *Dmrt1*$^{-/-;tg}$ mouse testes as was previously reported elsewhere in the *Dmrt1-null* mice [50]. Interestingly, there were a few Sertoli cells in the *Dmrt1*$^{-/-;tg}$ mouse testes which had GATA4 in the cytoplasm that did not co-localize with PCNA in the nucleus (Figure 11C, asterisks). GATA4 is a transcription factor important in cellular differentiation and their function is believed to reside in the

nucleus. The loss of nuclear localization for GATA proteins was reported in ovarian cancer cells and linked to dedifferentiation [208]. It is likely that the few Sertoli cells located in the lumen that had this cytoplasmic mislocalization were dedifferentiating. .

The above observations were validated by further morphological and ultrastructural analyses using light and electron microscopy, respectively. Sertoli cells display significant structural changes that are linked to pubertal and postnatal developmental processes. They start as small round or oval cells with inconstant contour immediately after birth to complex elongated cells spreading from the basement membrane to the lumen as they age. For example, alterations in the nucleus from birth to puberty show increasing size and complexity. Early in life, Sertoli cells have a regular round or oval nuclei with negligible indentation, finely granular chromatin and small, unremarkable nucleoli. As they age, the nucleus changes into an ovoid to elongated topology that is commonly observed close to the basement membrane. The nuclear contour becomes more irregular with prominent indentations and contains a nucleolus that includes a central condensation area .The nucleolus in mouse is composed of three parts, one central part and two satellite parts. The nuclear matrix is made up of fine particulate matter of many forms namely; granular, fibrillar and fibrous [209]. The Sertoli cell nucleus at P7 in *Dmrt1*$^{+/+}$ mice testis were columnar in shape and immature while those in *Dmrt1*$^{-/-}$ and *Dmrt1*$^{-/-;tg}$ mice were multi-lobulated, had irregular contours, indentations and seems mature. At P42, the SC nucleus in *Dmrt1*$^{+/+}$ was ovoid with irregular indentations and contained a central condensation area. Most of the *Dmrt1*$^{-/-}$ Sertoli cell nuclei were round with regular topology and all the nucleoli lacked a central condensation area but had granular clusters with coarse particulate matter at the periphery of the nuclear envelope. This phenotype is similar to the human condition of long-term estrogen treatment of Sertoli cells but without any germ cells. These defective human Sertoli cells were characterized by round or oval nuclei with most having dense homogenously disturbed chromatin and peripherally located nucleoli. The chromatin appears in irregular granular clusters and in a less condensed state[210]. Nuclei from *Dmrt1*$^{-/-;tg}$ Sertoli cells had a combination of regular ovoid and irregular ovoid topology, with a few nucleoli forming a central granular

condensation area and most carrying fibrillar satellite centers and lacked coarse particulate matter at the nuclear envelope. This suggests that Sertoli cells in *Dmrt1*$^{-/-}$ were reprogrammed with the prepubertal SCs exhibiting mature nuclear characteristics and the postpubertal SCs expressing immature nuclear phenotype. However, the *Dmrt1*$^{-/-;tg}$ mice had a small population of SCs that were normal and a large population of SCs that were also reprogrammed. The above characteristics demonstrated that Sertoli cells in *Dmrt1*$^{-/-;tg}$ mice maintained an intermediate maturation state as they showed partial signs of maturation that were absent in *Dmrt1*$^{-/-}$ mice.

Dmrt1-rescue model shares characteristics with existing human models of male infertility

The phenotype of *Dmrt1*$^{-/-;tg}$ mice resembles that of two mouse models (male 41, XXY and the 41, XX^{Y}*) of human Klinefelter's syndrome (47 XXY) [211-215]. Common phenotypic features include significant germ cell depletion by P7, small testes in adult mice with reduced seminiferous tubule diameter, Sertoli cell-only tubules, Leydig cell hyperplasia and reduced serum testosterone levels. This raises the possibility that the return of DMRT1 to *Dmrt1* null Sertoli cells generates a mouse model that mimics the Klinefelter's phenotype; characterized by the presence of a supernumerary X chromosome, certain endocrine and testicular alterations. However, more experiments are required to further characterize and determine if *Dmrt1*$^{-/-;tg}$ mice exhibit any cognitive and behavioral defects like the Klinefelter's patients.

In conclusion, the Sertoli cell-specific rescue mouse model provides a unique model to identify the role of DMRT1 in the germline if the method requires loss of DMRT1 in germ cells. The present study validates that murine DMRT1 alone is not required for sex determination. However, this study demonstrates that development of Sertoli cell requires DMRT1 from within and DMRT1 in germ cells or just the presence of germ cells to undergo complete differentiation. The DMRT1-deficient germ cells mouse model provides a novel model to study existing phenotypes of idiopathic male infertility.

Figure 1: Generation and tissue-specific expression of the Wt1-Dmrt1 transgene.
A. Generation of the *Wt1-Dmrt1* transgene. The rat *Dmrt1* cDNA was inserted in-frame with the translational start ATG of mouse *Wilms' Tumor Gene 1* within the yeast artificial chromosome YAC 620mWt1. **Top:** YAC 620mWt1; exons = boxed with numbers, URA/Acentric and TRP/Centric = the pYAC4 acentric vector arms with uracil and tryptophan selectable markers, respectively. **Middle:** targeting vector, pBKS-Wt1-Dmrt1-HPRT1-LYS2. Dmrt1 = rat *Dmrt1* cDNA; HPRT1 = exons 8 & 9, intron 8 and polyadenylation site of HPRT1; LYS2 = lysine 2 selectable marker. *Wt1 5′* = 825bp Wt1 5′ untranslated region; *Wt13′*= 776bp of *Wt13′* untranslated region. **Bottom:** *Wt1-Dmrt1* transgene after homologous recombination in yeast (AB1380). **B-D**. RT-PCR of RNA prepared from different organs from male and female transgenic mice. PCR templates comprised of cDNA synthesized in the presence (+) or absence (-) of reverse transcriptase-superscript II. cDNA of the transgene: bottom bands (~450bp) amplified from the template of processed RNA. Genomic DNA: top bands (~1,105 bp) amplified from the template of contaminating genomic DNA. B. Transgene expression in the kidneys and gonads of newborn male and female littermates. Tissues examined are: newborn male and female kidney (K_M & K_F), ovary (O), testis (T) and postnatal day 15 (P15) transgenic testis (T+) C. Expression in P15 male transgenic and wild type littermates. Tissues examined in the transgenic male are: testis (T), brain (B), heart (H), spleen (Sp), Stomach (St), lung (Lu), kidney (K) and liver (Li). Tissues examine in wild-type male are: testis (T-) and kidney (K-). D. Positive and negative controls. The plasmid, pBKS-Wt15′-Dmrt1-HPRT1-LYS2-Wt13′ (P), was used as the positive control for genomic signal, the P15 transgenic testis (T+) previously determined to express Dmrt1-Wt1 transgene was used as a positive control for transgene expression and water (H_2O) used as a negative control for PCR reaction.

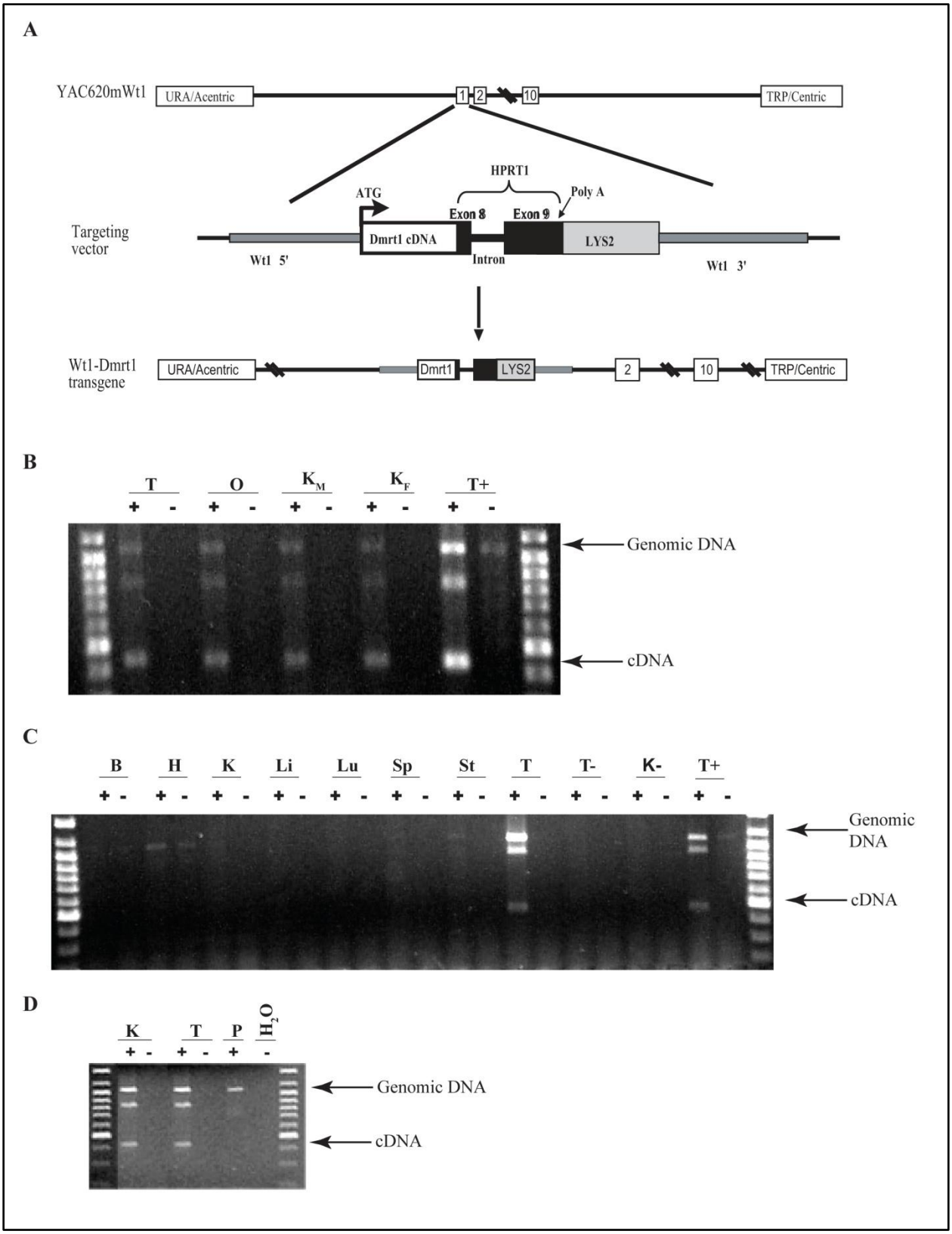
A
YAC620mWt1
URA/Acentric
1
2
10
TRP/Centric
HPRT1
ATG
Poly A
Exon 8
Exon 9
Targeting vector
Dmrt1 cDNA
LYS2
Wt1 5'
Intron
Wt1 3'
Wt1-Dmrt1 transgene
URA/Acentric
Dmrt1
LYS2
2
10
TRP/Centric
B
T
O
K_M
K_F
T+
+ - + - + - + - + -
Genomic DNA
cDNA
C
B
H
K
Li
Lu
Sp
St
T
T-
K-
T+
+ - + - + - + - + - + - + - + - + - + -
Genomic DNA
cDNA
D
K
T
P
H2O
+ - + - + -
Genomic DNA
cDNA

Figure 2: Immunohistochemical analysis of *Dmrt1*$^{+/+}$, *Dmrt1*$^{-/-}$, and *Dmrt1*$^{-/-;tg}$ at postnatal day 7. Testis sections from P7 wild type (A-C), *Dmrt1* $^{-/-}$ (D-F) and *Dmrt1*$^{-/-;tg}$ (G-I) mice were evaluated using fluorescently labeled antibodies against DMRT1 (A, D and G) and GCNA1 (B, E and H). Individual panels for DMRT1 (Green) and GCNA1 (Red) staining, as well as merged panels (C, F, and I), are shown. Yellow stained cells, indicating co-expressed DMRT1 and GCNA1 in germ cells, are observed only in wild type mice (C). DMRT1 expression by western blot (J) from mouse testes from *Dmrt1*$^{+/+}$, *Dmrt1*$^{-/-}$, *Dmrt1*$^{-/-;tg}$, *Dmrt1*$^{+/-}$ and *Dmrt1*$^{+/+;tg}$ mice.

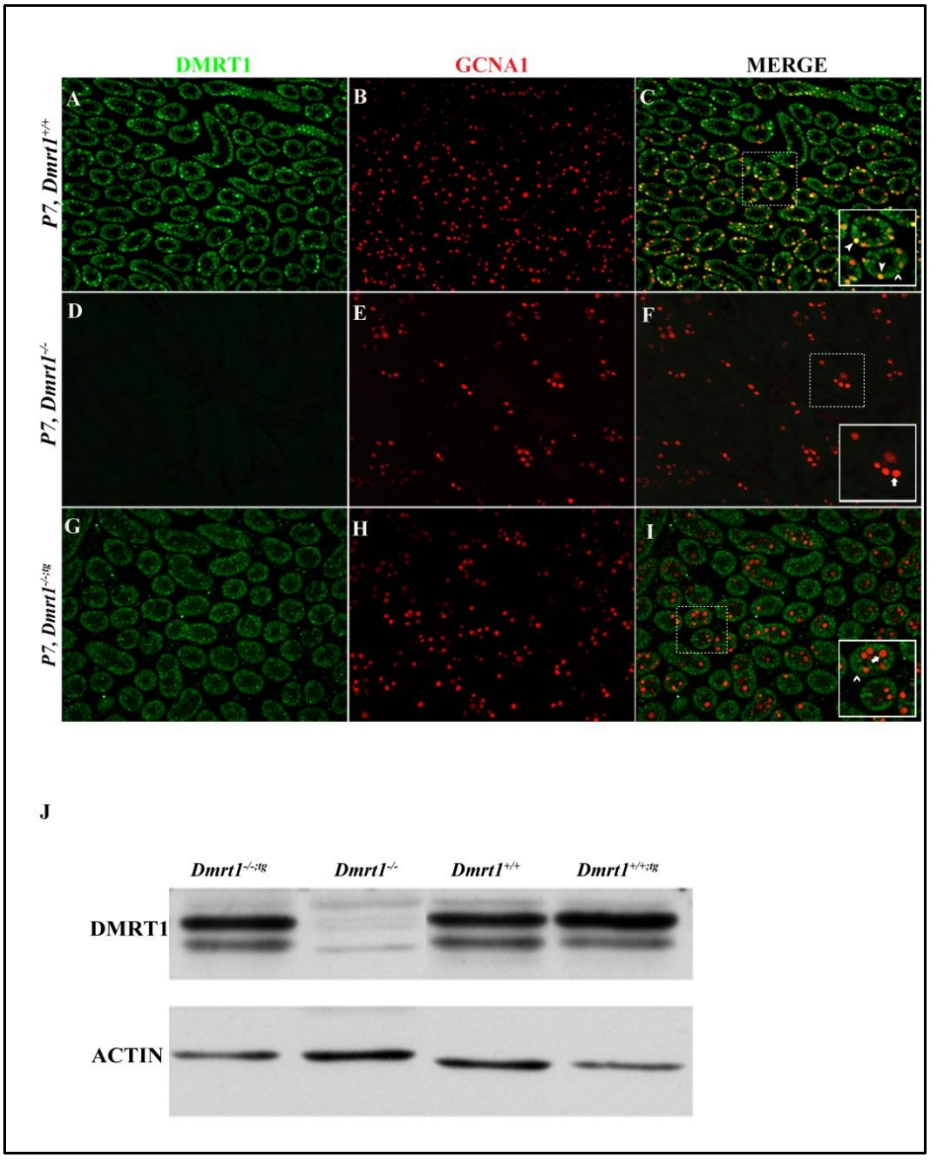

Figure 3: Morphological analysis of testis sections. Periodic Acid Schiff (PAS) staining of P7 & P42 testis section from wild type, *Dmrt1*$^{-/-}$ and *Dmrt1*$^{-/-;tg}$ mice. Return of DMRT1 to Sertoli cells in *Dmrt1*$^{-/-;tg}$ (or SC rescue) mice partially restores seminiferous tubule morphology (C, F and I). **A**, **B** and **C**; P7 testes from wild type, *Dmrt1* $^{-/-}$ and *Dmrt1*$^{-/-;tg}$ mice (20X magnification). **D**, **E**, and **F**; P42 testes from wild type, *Dmrt1* $^{-/-}$ and *Dmrt1*$^{-/-;tg}$ mice (20X magnification). **G**, **H**, and **I** represent higher magnification of boxed regions in G, H, and I (40X magnification). Arrowheads and arrows show the presence of a defined lumen and basal lamina, respectively, in wild type (**G**) and *Dmrt1*$^{-/-;tg}$ (**I**) that are absent in the *Dmrt1* $^{-/-}$(**H**). **J**, **K**, and **L**; P42 testes from wild type, *Dmrt1* $^{-/-}$ and *Dmrt1*$^{-/-;tg}$ mice (40X magnification) stained with toluidine blue. Arrowheads and arrows show the presence of a defined lumen in *Dmrt1*$^{+/+}$ (**J**) and *Dmrt1*$^{-/-;tg}$ (**K**) that are absent in the *Dmrt1* $^{-/-}$(**L**). Seminiferous tubules in *Dmrt1*$^{-/-}$ (**K**) and *Dmrt1*$^{-/-;tg}$ (**L**) have a remarkable number of interstitial Leydig cells and lipid droplets.

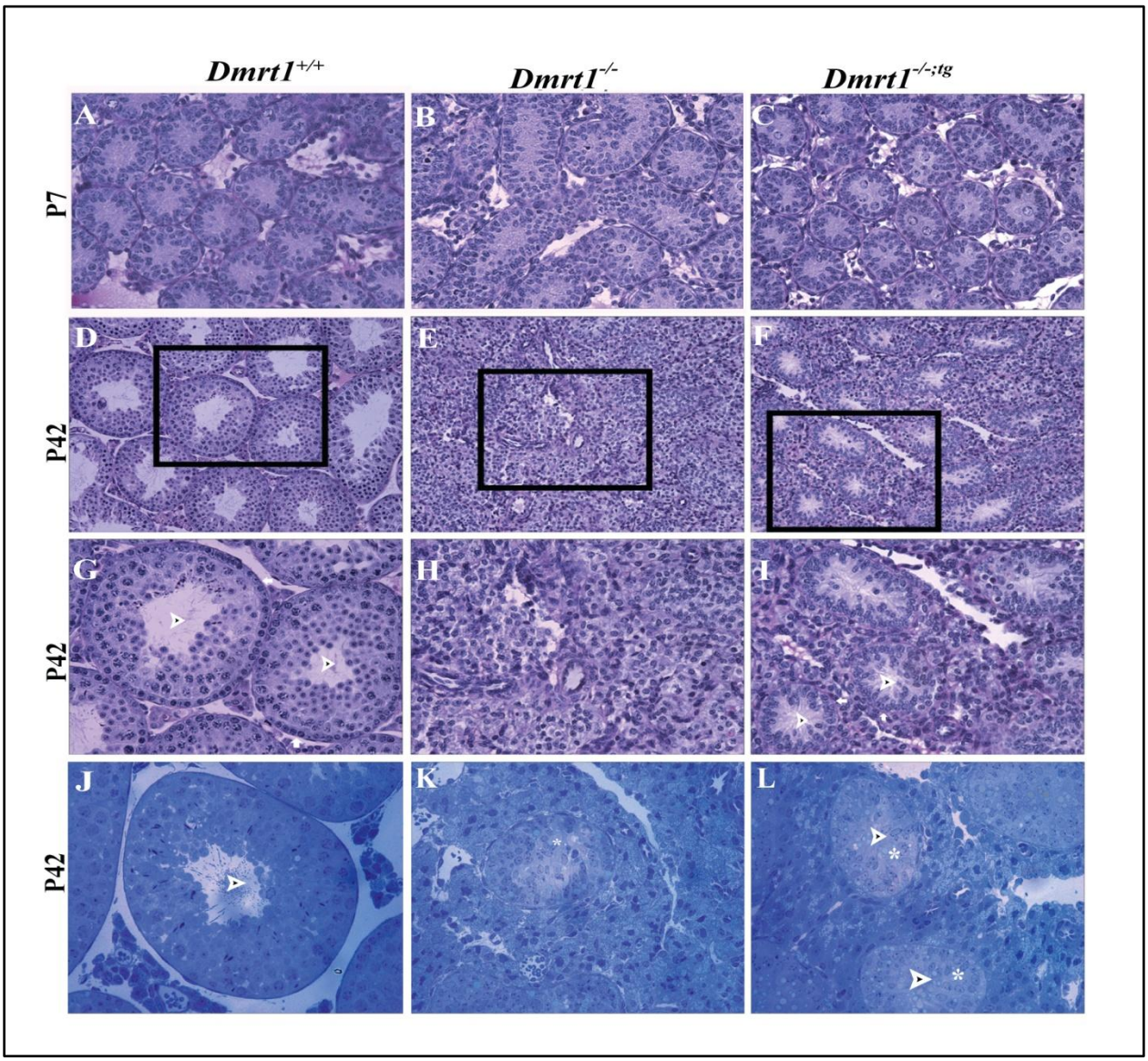

Figure 4: Effect of exogenous DMRT1 on testis size in *Dmrt1*$^{-/-tg}$ mice. Ratios of paired testes to total body weight for *Dmrt1*$^{+/+}$ (black bar), *Dmrt1*$^{-/-}$ (stipple bar), and *Dmrt1*$^{-/-;tg}$ (stripe bar) mice at postnatal days (P): 2 (P2), 7 (P7), 15 (P15), 20 (P20), and 42 (P42). Minimum of three animals were used for each genotype at each time point. Bars represent mean ± SEM of three to 20 animals. *** = $p<0.0001$ (Two tail Student T-Test).

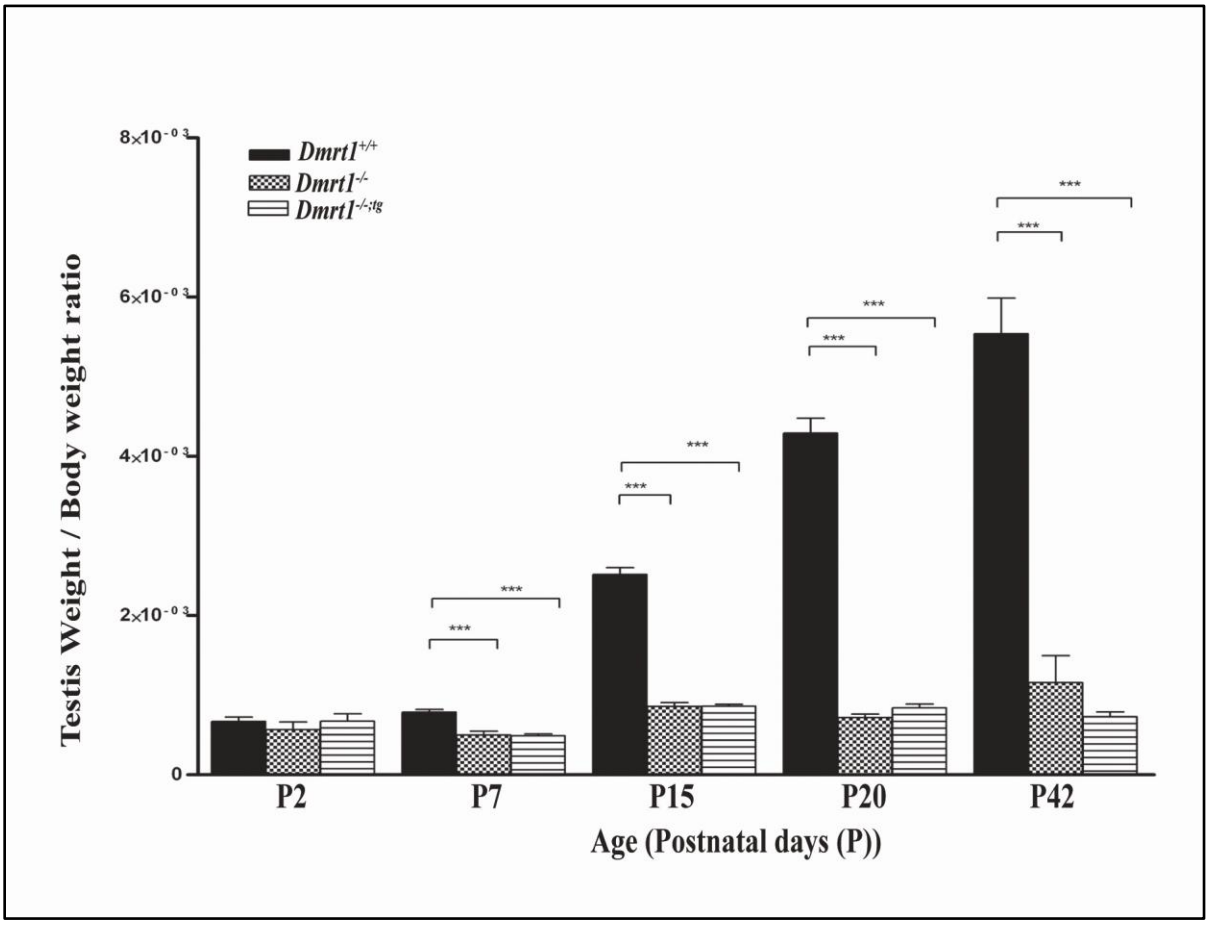

Figure 5: Dosage effects of *Dmrt1* transgene. A. Southern blot analysis to determine transgene copy number for samples used. Analysis of expression of exogenous *Dmrt1* compared to wild type. **B.** Gene expression profiles in mouse testis with different levels of Dmrt1 expressed in Sertoli cells. The data show dose-dependent increases in *Dmrt1* with increased transgene copies. It also shows 3 distinct expression profiles: 1) genes that don not respond to Dmrt1 expressed in Sertoli cells (resistant), 2) genes that respond partially to Sertoli cell *Dmrt1* (Partial), and 3) genes that respond in a dose dependent manner to increasing amounts of *Dmrt1* (sensitive).

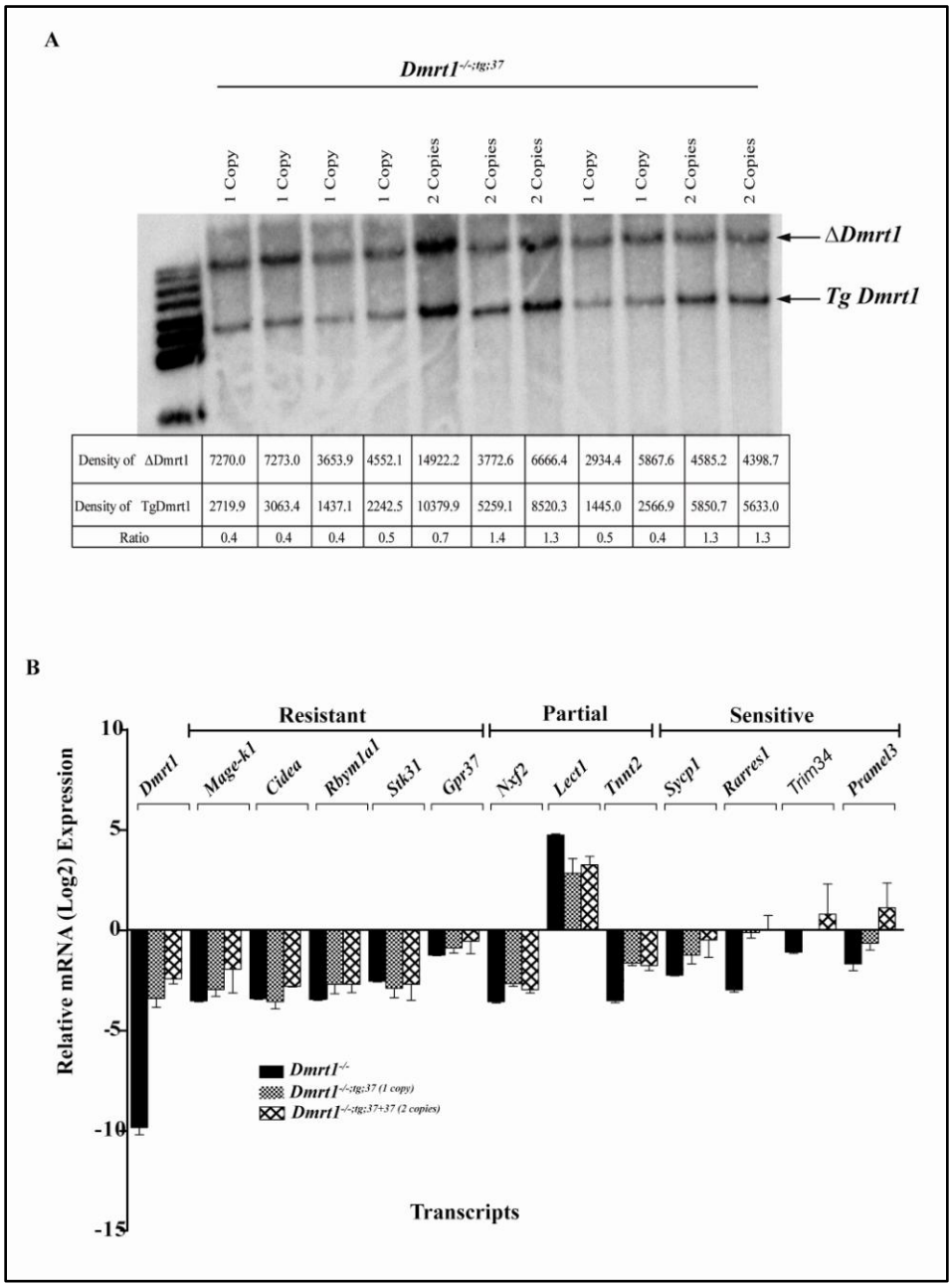

Density of ΔDmrt1	7270.0	7273.0	3653.9	4552.1	14922.2	3772.6	6666.4	2934.4	5867.6	4585.2	4398.7
Density of TgDmrt1	2719.9	3063.4	1437.1	2242.5	10379.9	5259.1	8520.3	1445.0	2566.9	5850.7	5633.0
Ratio	0.4	0.4	0.4	0.5	0.7	1.4	1.3	0.5	0.4	1.3	1.3

Figure 6: Effect of exogenous *Dmrt1* on testes weights and sperm motility. A. Average body weights for *Dmrt1*$^{+/+}$ (black bar), one copy transgenic (*Dmrt1*$^{+/+;tg}$)(stipple bar), and two copy transgenic (*Dmrt1*$^{+/+;tg+tg}$) (stripe bar) at 3, 6, 10, 12, and 18 months of age. **B.** Average paired testes weights for *Dmrt1*$^{+/+}$ (black bar), one copy transgenic (*Dmrt1*$^{+/+;tg}$)(stipple bar), and two copy transgenic (*Dmrt1*$^{+/+;tg+tg}$) (stripe bar) at 3, 6, 10, 12, and 18 months of age. **C.** Ratios of paired testes to total body weight for *Dmrt1*$^{+/+}$ (black bar), one copy transgenic (*Dmrt1*$^{+/+;tg}$)(stipple bar), and two copy transgenic (*Dmrt1*$^{+/+;tg+tg}$) (stripe bar) at 3, 6, 10, 12, and 18 months of age. **D.** Total and progressive motility of sperm from *Dmrt1*$^{+/+}$ and *Dmrt1*$^{+/+;tg}$ at 6 and 12 months of age. Minimum of three animals were used for each genotype at each time point. Bars represent mean ± SEM of three to 20 animals. *** = p<0.0001 (Two tail Student T-Test).

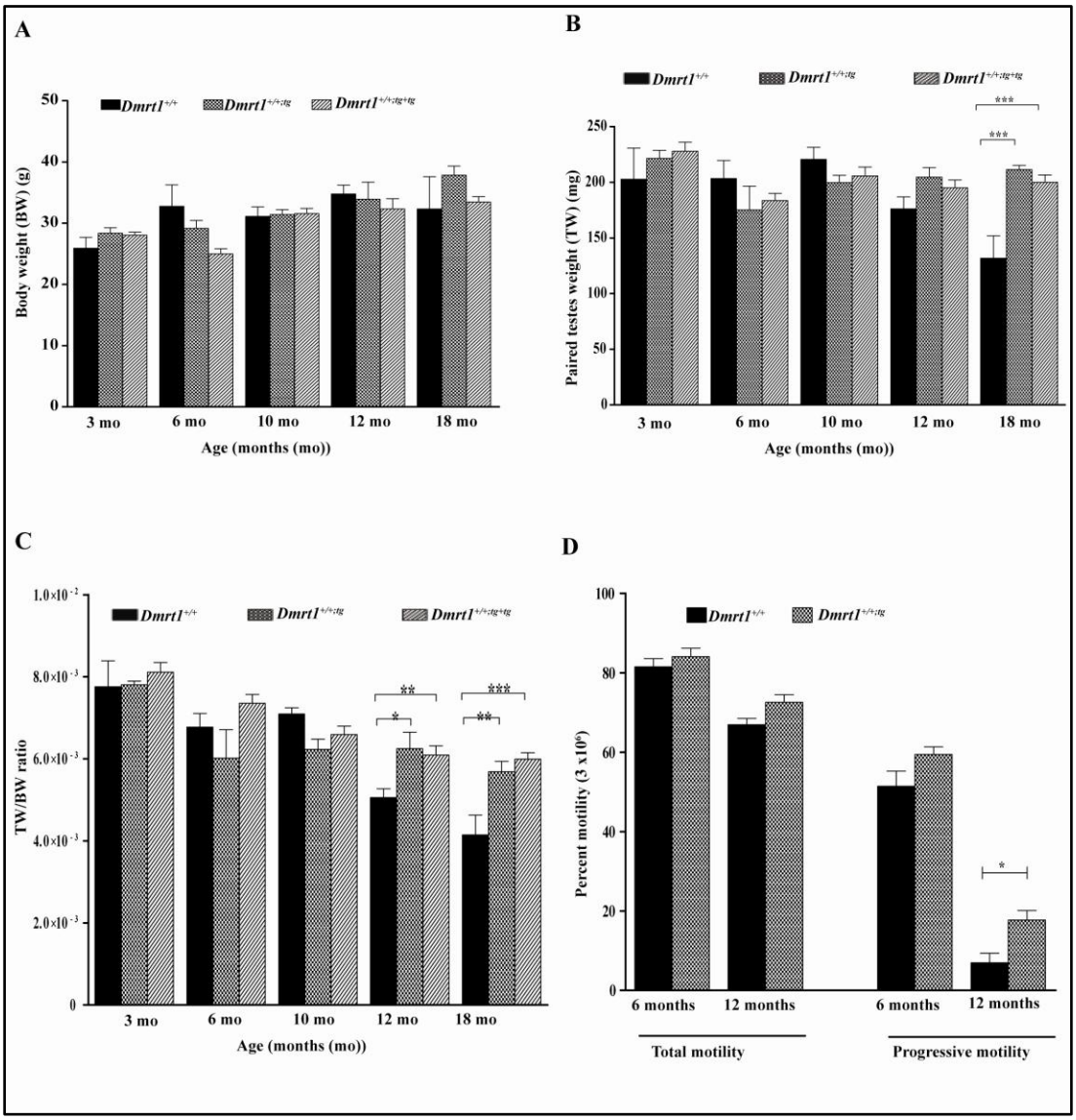

Figure 7: Sex hormone levels and effect on secondary sex organs. A. Serum testosterone levels at P15, P20 and P42 in wild type (black bar), *Dmrt1*$^{-/-}$ (stipple bar), and *Dmrt1*$^{-/-;tg}$ (stripe bar). **B.** Effect of serum testosterone levels on development of seminal vesicles at P20 and P42 in *Dmrt1*$^{+/-;tg}$, *Dmrt1*$^{-/-}$ and *Dmrt1*$^{-/-;tg}$. **C.** Serum LH levels at P15, P20 and P42 in wild type (black bar), *Dmrt1*$^{-/-}$ (stipple bar), and *Dmrt1*$^{-/-;tg}$ (stripe bar). *Bars* represent mean ± SEM of three to 10 animals. **D.** Serum Estradiol levels at P15, P20 and P42 in wild type (black bar), *Dmrt1*$^{-/-}$ (stipple bar), and *Dmrt1*$^{-/-;tg}$ (stripe bar). *Bars* represent mean ± SEM of three to 10 animals. Table below C and D shows pooling of samples used for Serum LH and Estradiol assays.

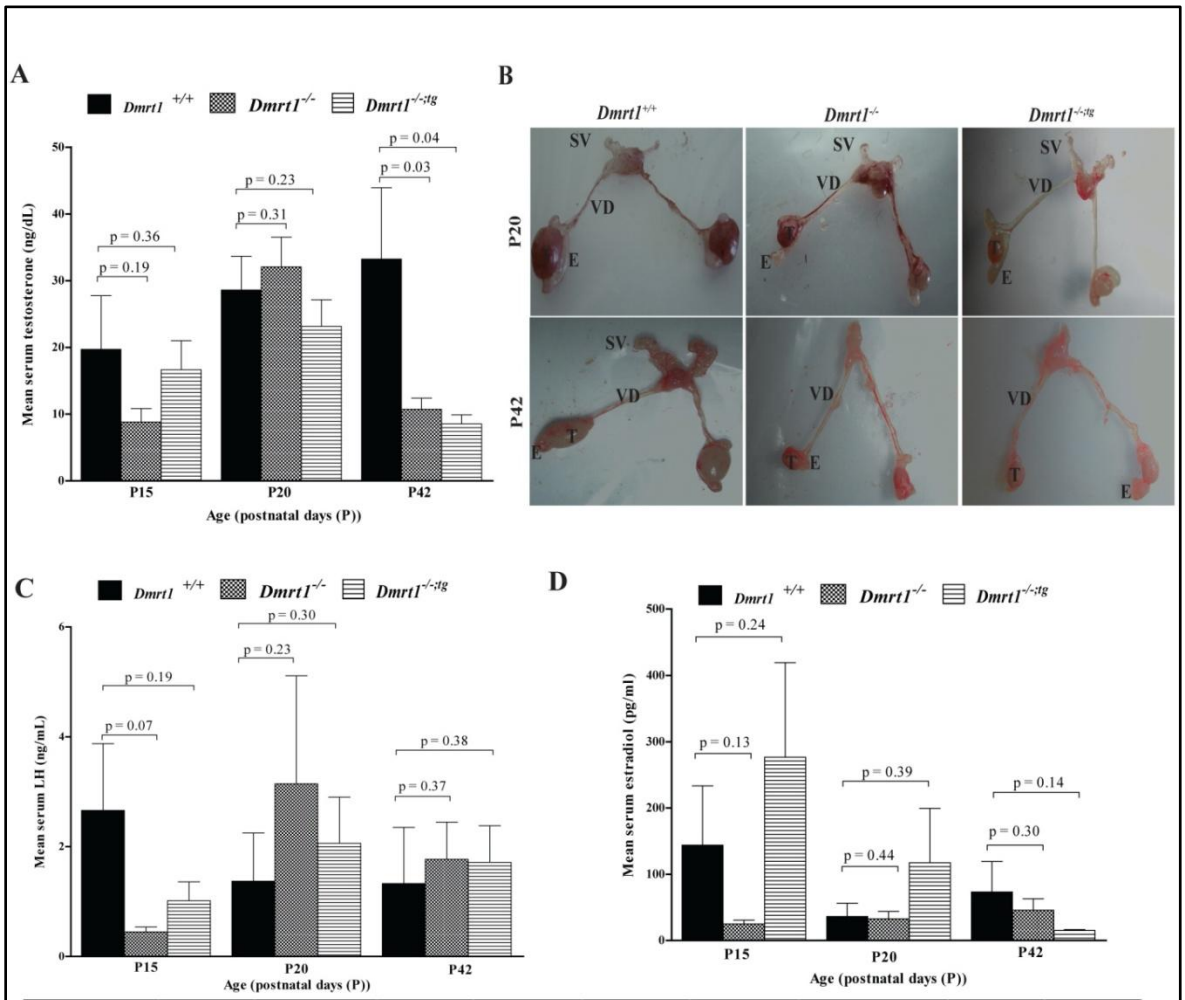

Pooling of mouse serum samples used for LH and estradiol assays

	P15			P20			P42		
	Pool #1	**Pool # 2**	**Pool #3**	**Pool #1**	**Pool # 2**	**Pool #3**	**Pool #1**	**Pool # 2**	**Pool #3**
Dmrt1 $^{+/+}$	54, 56	54, 57	55, 58	27, 39, 45	33, 40, 47	35, 41, 42	14,10, 4	8,11, 24	9, 12
Dmrt1 $^{-/-}$	60, 20	66	67	28, 36, 44	31, 37	34, 38	1, 13, 18, 23	2,16, 21	5,17,22
Dmrt1 $^{-/-;tg}$	8, 52, 63	49, 59, 64	50, 62	26, 32	29, 43	30, 46	6, 19	7, 20	15, 25

Figure 8: Immunohistochemical analysis of adult Leydig cell marker (P450 SCC). *Dmrt1*$^{+/+}$ (A, D, G & J), *Dmrt1*$^{-/-}$(B, E, H & K), and *Dmrt1*$^{-/-;\ tg}$ (C, F, L & I) at P7 (A-C), P15 (D-F), P20 (G-I) and P42 (J-L). Testis sections from mice were evaluated using fluorescently labeled antibodies against P450 SCC. The number of Leydig cells at P42 in the *Dmrt1*$^{-/-}$ (K) and *Dmrt1*$^{-/-;\ tg}$ (L) may be attributed to the shrinking size of the testis and hyperplasia.

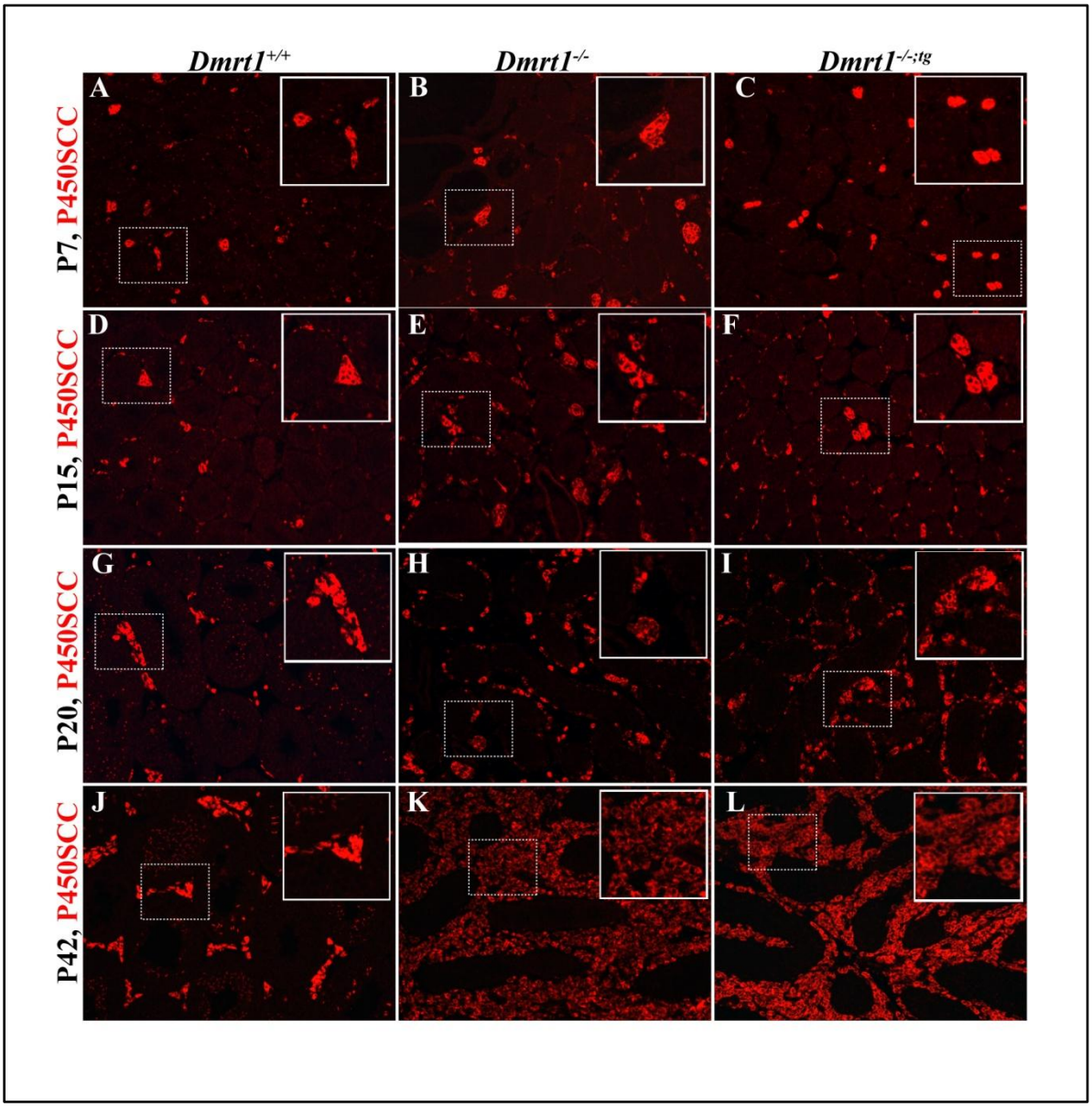

Figure 9: Genes involved in testis function. Quantitative PCR was used to analyze the expression of 10 genes vital for testis function using P7 whole testis mRNA. These included: *Gata1*, *Ar*, and *Krt18* important for SC maturation; *Gata4* important for SC proliferation.*Gata1* was significantly reduced in both *Dmrt1*$^{-/-}$ and *Dmrt1*$^{-/-;tg}$ mice ($p<0.005$). *Ar* was not significantly different in all groups. *Krt18* was significantly elevated in *Dmrt1*$^{-/-}$ and *Dmrt1*$^{-/-;tg}$ mice ($p=0.0028$). *Gata4* was significantly elevated in *Dmrt1*$^{-/-}$ ($p=0.0032$) but not in *Dmrt1*$^{-/-;tg}$ mice. *Espin, Ocln, Cldn11* and *Tjp* are necessary for the formation of the blood-testis barrier . *Ocln, Cldn11,* and *Tjp1* were significantly reduced in both *Dmrt1*$^{-/-}$ and *Dmrt1*$^{-/-;tg}$ mice($p=0.0078$, $p<0.0001$ and $p<0.0001$, respectively). *Espin* was significantly elevated in *Dmrt1*$^{-/-}$ mice ($p<0.03$) but not significant in *Dmrt1*$^{-/-;tg}$ mice.

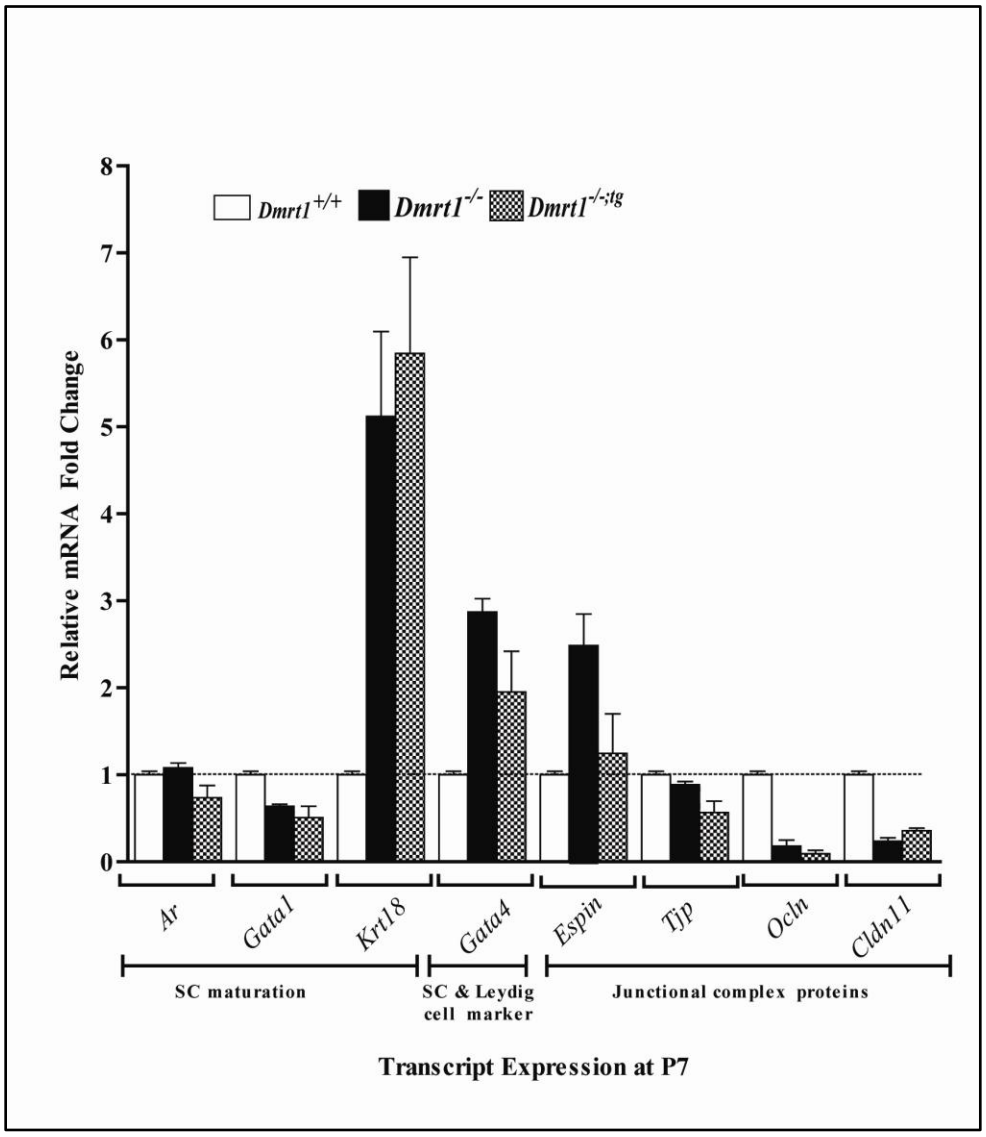

Figure 10: Expression pattern of a protein marker for Sertoli cell maturity. *Dmrt1*$^{+/+}$ (A & D), *Dmrt1*$^{-/-}$(B & E), and *Dmrt1*$^{-/-;\ tg}$ (C & F) at P7 and P15. Testis sections from mice were evaluated using fluorescently labeled antibodies against AR (green) and DAPI (blue) for nuclei stains. Myoid cells are predominantly expressing AR at P7 (arrowheads) in all three groups. The intensity of AR and number of Sertoli cells expressing AR (arrows) in the *Dmrt1*$^{-/-}$ (E) and *Dmrt1*$^{-/-;\ tg}$ (F) is lower at P15 compared to AR expression in the control (D).

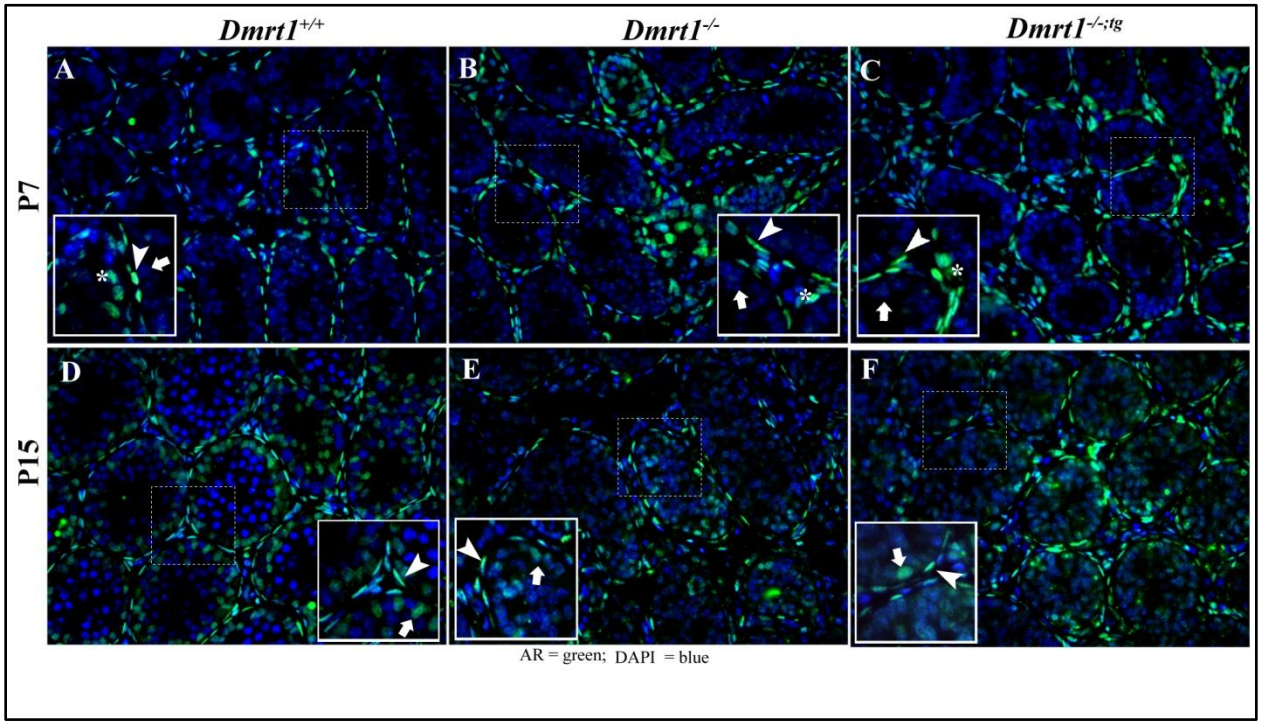

Figure 11: Immunohistochemical analysis of Sertoli cell proliferation in *Dmrt1*$^{+/+}$, *Dmrt1*$^{-/-}$, and *Dmrt1*$^{-/-;tg}$ at postnatal day 42. Testis sections from P42 *Dmrt1*$^{+/+}$ (A-D), *Dmrt1* $^{-/-}$ (E-H) and *Dmrt1*$^{-/-;tg}$ (I-L) mice were evaluated using fluorescently labeled antibodies against GATA4 (A, E and I), PCNA (B, F and J) and DAPI (C,G and K). Individual panels for GATA4 (Green), PCNA (Red), DAPI (blue) and merged panels (D, H, and L), are shown. Arrowheads show the presence of mature Sertoli cells in *Dmrt1*$^{+/+}$ (D) staining green and negative for PCNA that are absent in *Dmrt1* $^{-/-}$ (H) but present in a few Sertoli cell nuclei in *Dmrt1*$^{-/-;tg}$ (L).

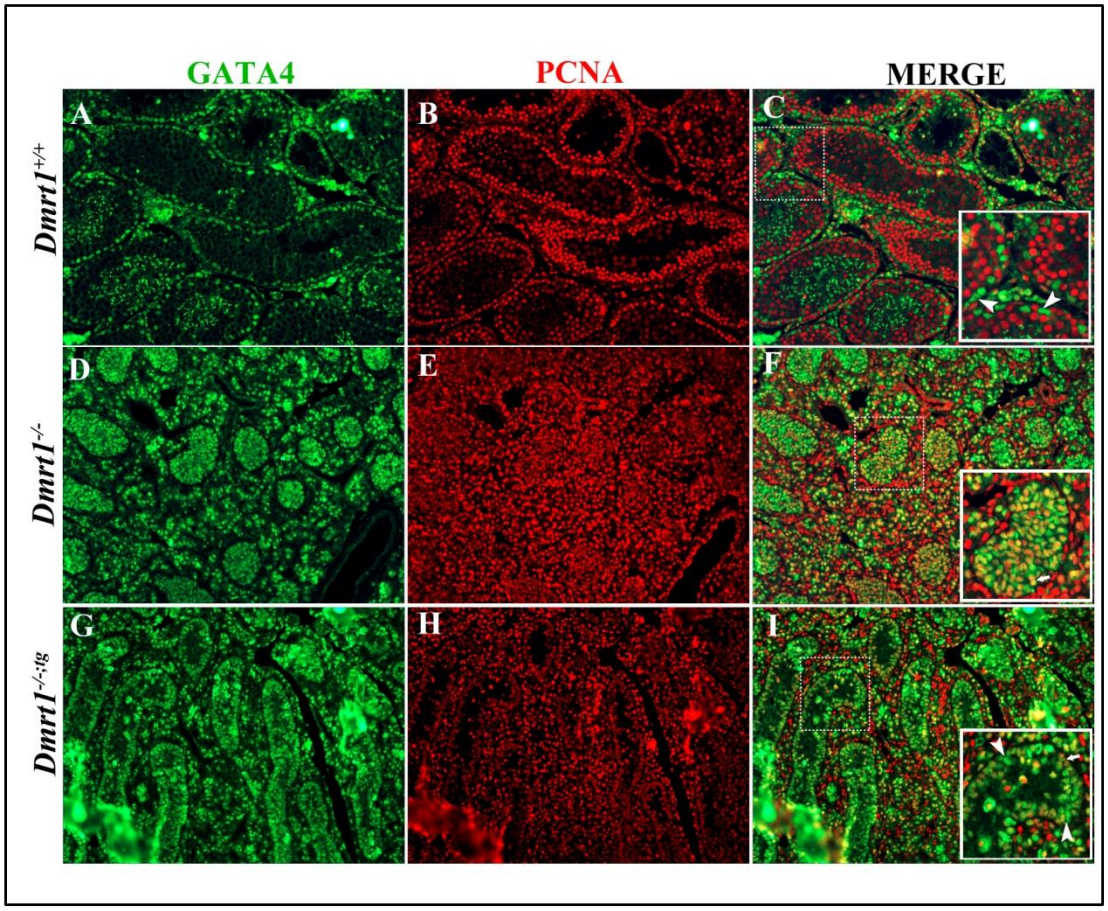

Figure 12: Electron microscopy of Sertoli cell nuclei at P7 and P42. A. Portion of a seminiferous tubule from P7 *Dmrt1*$^{+/-}$ showing normal ultrastructure of Sertoli cell nucleus (insert). Germ cell nuclei have white outlines and Sertoli nuclei have black outlines. The Sertoli cell nucleus is columnar in shape with regular contours and no indentations Magnification x3040; scale bar, 2 μm. **B**. Portion of a seminiferous tubule from P7 *Dmrt1*$^{-/-}$ mice showing abnormal Sertoli cell nuclei. The Sertoli cell nuclei are irregular shaped and multi-lobulated with indentations (arrowheads). Magnification x3040; scale bar, 2 μm. **C.** Portion of a seminiferous tubule from P7 *Dmrt1*$^{-/-;tg}$ mice showing a mixed population of normal and abnormal Sertoli cell nuclei. The normal and abnormal nuclei shared characteristics with *Dmrt1*$^{+/+}$ and *Dmrt1*$^{-/-}$ mice, respectively. Magnification x2280; scale bar, 2 μm. **D**. Portion of a seminiferous tubule from P42 *Dmrt1*$^{+/+}$ mice showing normal ultrastructure of Sertoli cell and germ cells. The Sertoli cell is large and shows considerable amount of perinuclear cytoplasm, an irregular ovoid nucleus with indentation (arrow) and interacting with a spermatogonium and several primary spermatocytes. Nucleolus formed a central condensation area. Magnification x2280; scale bar, 2 μm. **E**. Sertoli cell-only tubule from P42 *Dmrt1*$^{-/-}$ mice showing Sertoli cells with many regular round nuclei scanty amount of cytoplasm (insert). Magnification, x1900; scale bar, 10 μm. **F**. Sertoli cell-only tubule from P42 *Dmrt1*$^{-/-;tg}$ mice showing Sertoli cells with many regular round nuclei and few irregular nuclei with indentations (arrows) and scanty amount of cytoplasm. Nucleolus formed a central condensation area. Magnification, x3040; scale bar, 2 μm.

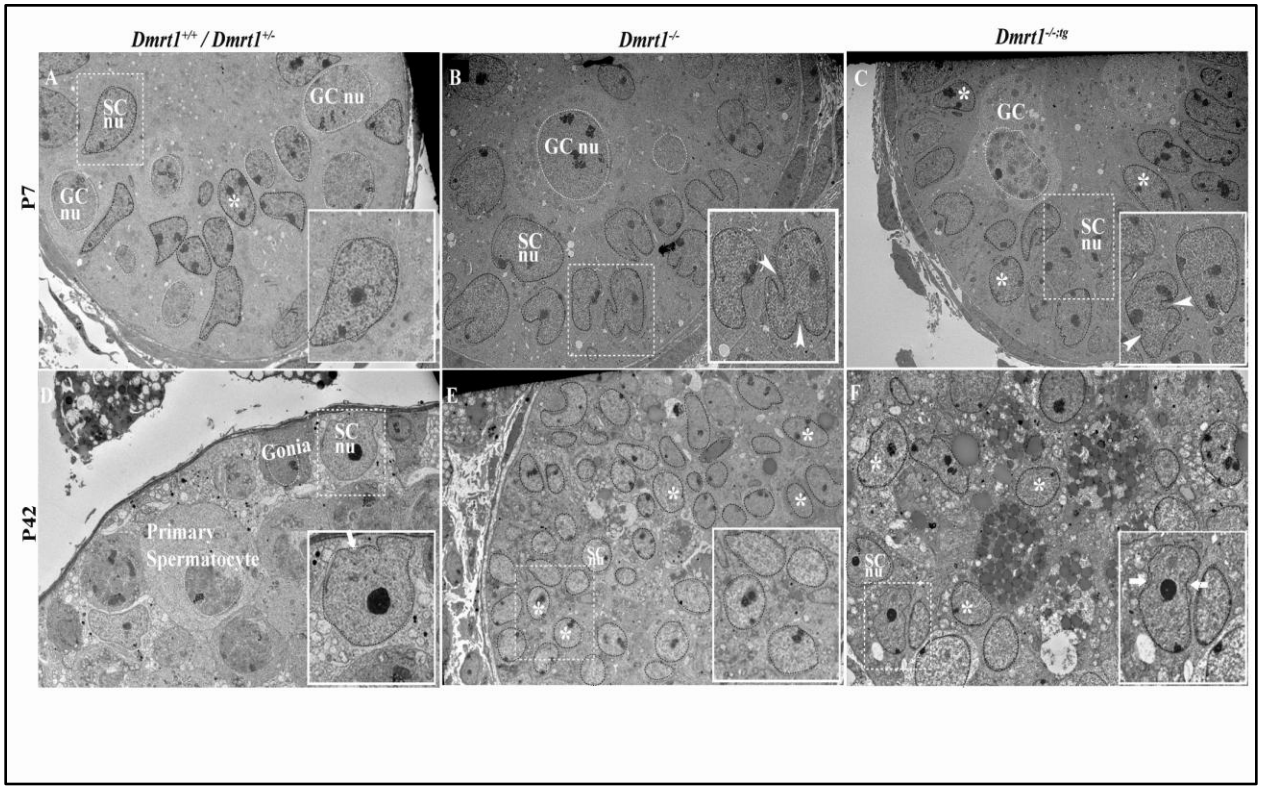

Supplementary Figure 1: Effect of exogenous DMRT1 on secondary sex organs. A. Reproductive organs of *Dmrt1*$^{+/+}$ mice at about 19 weeks after birth **B.** Reproductive organs of *Dmrt1*$^{-/-}$ mice at about 19 weeks after birth **C.** Reproductive organs of *Dmrt1*$^{-/-;tg;30}$ mice at about 19 weeks after birth **D.** Reproductive organs of *Dmrt1*$^{-/-;tg;37}$ mice at about 19 weeks after birth. T = testis, E = epididymis, SV = seminal vesicle, VD = vas deferens

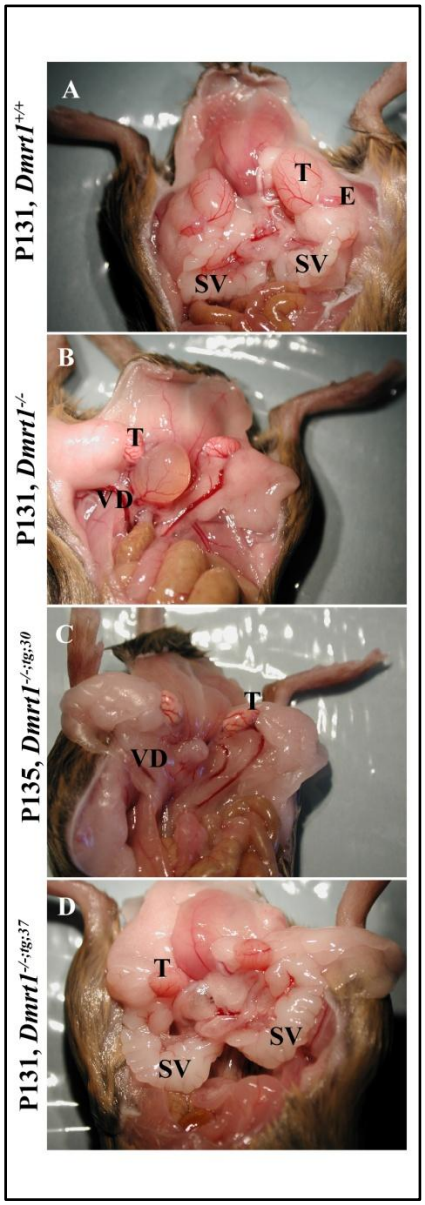

Table 1: Primers used for cloning transgene

Clone	Sequence (5' →3')	Direction	Product size (bp)	Polylinkers
Left arm (Wt1 5′)	GCGC AAGCTTGAGCATCCTGGCTCCTCCTC	F	825	HindIII
	GCGC ACGCGT CGTCGTTAGGCATGAGGTGCGGCTCGG	R		MluI
Right arm (Wt1 3′)	GCGC CCGCGG TTCCGACGTGCGGGACCTG	F	776	SacII
	GCGC CCGCGG ATCGATCCCTAAACCACAGCACCACTC	R		SacII
HPRT1	GCGC TCTAGAGTCGAGGACTTCAGGGATTTG	F	1312	XbaI
	GCGC TCTAGAATTCAAAAAGTGGCGAATT	R		XbaI
LYS2	AGAGAGCGGCCGC CACTTGCAATTACATAAAAAATTCCGG	F	4804	NotI
	AGAGAGCGGCCGC CGCAAGTATTCATTTTAGACCCATG	R		NotI
Dmrt1 m MluI	GCGC ACGCGT TCGGCAAGCCCTCTGCACCG	F	237	MluI
	GCGC ACGCGT AGCCGTGGTTCCTGCAGCGA	R		MluI

Table 2: Primers used for genotyping

	Primer Name	Sequence (5' →3')	Direction	Product size (bp)
Genotyping of Transgenic founders	Wt1 -355	GCCTCAGAACCCAGGAGAG	F	873
	Dmrt1 .16A	GTGAGGAACCTCCGTCGG	R	
Sex Genotyping	SRY Forward	AAGCGCCCCATGAATGCATT	F	250
	SRY Reverse	CGATGAGGCTGATATTTATA	R	
Genotyping of Transgenic pups	TGIF0088	GTCCTCTGAACCTAGCAGCTACG	F	689
	TGIF0090	CCATGGAGACTTTCTAACTGCTCCTG	R	
Transgene expression in Transgenic mice	*Dmrt1 3'*	CACAGGGTATTAGGAGGCTTG	F	434
	HPRT1	GGCCTATAGGCTCATAGTGCAA	R	
Genotying of $Dmrt1^{+/+}$ allele	TGIF0105 (KOs 1N)	GATCTATCTGGAGCCAGGTGGTAG	F	277
	TGIF0107 (KOs 2N)	TGCACACGTGCACCCTCGCCATCG	R	
Genotying of $Dmrt1^{-/-}$ allele	TGIF0105 (KOs 1N)	GATCTATCTGGAGCCAGGTGGTAG	F	420
	TGIF0106 (KOs 3N)	TCATGGCAGCTCTCCCAGTGGAGC	R	
Probe to identify positive YAC *Wt1-Dmrt1* clones	*Dmrt1* ΔMluI Up	GCGCACGCGTTCGGCAAGCCCTCTGCACCG	F	237
	Dmrt1 ΔMluI Down	GCGCACGCGTAGCCGTGGTTCCTGCAGCGA	R	
Probe for Tg Dmrt1 copy number determination	*Dmrt1* exon 5 forward	GCCCAGCAGTCAAGATTCTG	F	165
	Dmrt1 exon 5 reverse	CGACTCAGTTCACAGGGTATT	R	

Table 3: Primers used for gene expression analysis by quantitative PCR

Transcript	Sequence	Tm	Direction	Product Length (bp)
Dmrt1	CCTTACGTGCCTGCTCAGACT	58	F	64
	ACTGGGTGGCGGCTCTCT	59	R	
Cidea	TGGACACCGGGTAGTAAGTATGTC	58	F	85
	AGCCTGTATAGGTCGAAGGTGACT	58	R	
Rbym1a1	CAC TCT CGG GAA GAA AGT GC	60	F	172
	CAT AGC GGT TGT TTC CAC CT	60	R	
Stk31	AGC AGC CAG AAG GTT TTT GA	60	F	194
	TGG ATC TTT TGC AGC ACT TG	60	R	
Nxf2	TGC AGC GAT TCA AGA ATT TG	59	F	267
	CTT GCC CTC ATT CTG GAG AG	59	R	
Lect1 (ChM1)	CGTTTTGCTGGAGGAGAGAAGT	59	F	109
	ATGATCTTGCCTTCCAGTTCAGA	59	R	
Tnnt2	ATC CCC GAT GGA GAG AGA GT	60	F	260
	CTG TTC TCC TCC TCC TCA CG	60	R	
Rarres1	ATACCTGACAGTCATGGACACATTG	59	F	91
	GTCTTCTCCCACATCACGTATGAG	59	R	
Gpr37	ACT TGC CGT TAT CTG GGT TG	60	F	193
	ATA CCA CCA AAG CCT TGC AC	60	R	
Trim34	CTG GAC CCT GGG AGT TTA CA	59	F	110
	CCC AGT AGC CAT TCT GTG GT	59	R	
Pramel3	TTC CTG CAT GTG AAT TTG GA	59	F	121
	AAG ATG AAG CTT GGG GGT CT	59	R	
Ar	TGGCGGTCCTTCACTAATGTC	59	F	72
	TGCGGTACTCATTGAAAACCAA	59	R	
Gata1	GTCAGAACCGGCCTCTCATC	58	F	59
	TGCCTGCCCGTTTGCT	58	R	
Krt18	CTT GCT GGA GGA TGG AGA AG	58	F	72
	CTG CAC AGT TTG CAT GGA GT	58	R	
Gata4	GGGCCAACCCTGGAAGAC	59	F	67
	GACACACTCTCTGCCTTCTGAGAA	59	R	
Espin	TTACATGCAGACCAAGAACAAGCT	59	F	64
	CCACCTTGGGCTCCTTGAG	59	R	
TJP	GCAATGGAGGAAACAGCTATATGG	60	F	61
	AACCCAGGAGCCCTGTGAA	59	R	
Ocln	CTGGACATTTTGCTCATCATAAAGA	58	F	102
	GTTTGAATTCATCAGGTCTGTAAGGA	59	R	
Cldn11	GGACGAACTGGGCTCCAA	58	F	104
	TGCACGTAGCCTGGAAGGA	59	R	
Sycp1	GTT CCG TTC CAT GTC GTC TT	58	F	104
	TGT GAA GGG CTT TTG CTT CT	59	R	
Rpl7	CAACAAGGCTTCAATTAACATGCT	59	F	59
	GGGTACCCCCATGCAATG	59	R	

Chapter 3: DMRT1 in Sertoli cells regulates the organization and formation of ectoplasmic specialization

Abstract

Ectoplasmic specializations (ES) are testis-specific adherens junctions formed between the cytoplasm of adjacent Sertoli cells or between Sertoli cells and maturing spermatids. Since these junctions are a sign of maturation and the evolutionary conserved transcription factor, DMRT1, is known to facilitate and maintain Sertoli cell differentiation, it was hypothesized that DMRT1 perhaps may participate in the organization and maintenance of these junctions. In this study, electron microscopy and immunohistological localization of known ES-associated proteins (ESPIN, NECTIN-2 and NECTIN-3) were used to evaluate Sertoli cell ESs in 42-day-old mice expressing different levels of DMRT1 (wild types, *Dmrt1*$^{+/+}$; *Dmrt1-null*, *Dmrt1*$^{-/-}$; and Sertoli cell rescue, *Dmrt1*$^{-/-;tg}$). In the *Dmrt1*$^{-/-}$ seminiferous tubules, the ES proteins, ESPIN, NECTIN-2 and NECTIN-3 were observed in poorly organized patches and electron micrographs indicated that gap junctions were the predominant junctions present. Notably, transgenic expression of DMRT1 to Sertoli cells of *Dmrt1*$^{-/-}$ mice (*Dmrt1*$^{-/-;tg}$) restored ES organization as revealed by expression of ESPIN, NECTIN-2 and NECTIN-3. In addition, electron micrographs of *Dmrt1*$^{-/-;tg}$ testis sections showed both adherens and gap junctions similarly represented within the seminiferous epithelium. Taken together, the findings indicate that DMRT1 in Sertoli cells is needed for the formation and regulation of the ESs.

Introduction

Double-sex and male abnormal-3 (mab3) related transcription factor 1 (DMRT1) is an evolutionary conserved transcription factor that shares homology with double-sex (dsx) in *Drosophila melanogaster* and male abnormal-3 (mab3) in *Caenorhabditis elegans* [112-114]. DMRT1 in mammals is required for male fertility and produced only in the testes, where it is expressed both in Sertoli cells (SC) and germ cells (GC) [115, 119, 128, 145, 150, 159, 216-218]. In mice, its role is associated with postnatal Sertoli cell differentiation and the growth and maintenance of germ cells [50, 130, 131, 133, 159, 219]; whereas in humans, it is implicated in prenatal testis development and sex determination [163-167].

Conditional deletions and cellular expression profiles in mice have provided important mechanistic insight on DMRT1's cell-specific functions. In Sertoli cell-specific *Dmrt1* knockout mice (*SCDmrt1KO*), Sertoli cells over-proliferated and failed to polarize, while germ cell meiosis was incomplete [131]. However, unlike $Dmrt1^{-/-}$ mice, radial migration, re-initiation of mitosis and initiation of meiosis were not hampered. In contrast, to studies with *SCDmrt1KO* mice, studies in mice with conditional germ cell deletions of *Dmrt1* (*GCDmrt1KO*) have been less informative, primarily due to features of Cre recombinase transgene method employed. In particular, the initial transgene directed by TNAP showed poor penetrance and ectopic expression in Sertoli cells, while another captures only events associated with the second wave of spermatogenesis [131, 134]. Notably, we previously reported the characterization of a new mouse model, which is functionally comparable to conditional deletion of Dmrt1 in germ cells and does not depend on the efficacy of Cre recombinase (Chapter 2). Characterization of these mice (i.e. Sertoli cell rescue, $Dmrt1^{-/-;tg}$), which express DMRT1 from a transgene in Sertoli cells of $Dmrt1^{-/-}$ mice, revealed new roles for DMRT1 in tubule integrity, maintenance of testis size

and sperm progressive motility and supported its previous known role in Sertoli cell maturation (Chapter 2). The studies presented here employed these mice to further explore the role of DMRT1 in Sertoli cell differentiation, by examining how DMRT1 affects a specific feature of Sertoli cell maturation, namely junctional complex formation and/or organization [220-223].

Cell-cell adhesion is vital to the formation and maintenance of multicellular structures complex organisms. A cohort of cell adhesion molecules has evolved to assist in the growing complexity and specialization of cell-cell interactions in higher eukaryotes. The interaction between three main types of junctions (desmosomes, tight junctions, adherens junctions), located at the apical lateral surfaces of adjacent epithelial cells, forms junction complexes that contribute to cell polarity, maintain epithelial cell integrity and control paracellular diffusion [223]. In the testis, Sertoli cells, which are epithelial in origin, and germ cells, are the two principal cell types of the seminiferous epithelium, a tubule-like structure that is the site of germ cell development [224-227]. These testicular epithelial cells are large asymmetrical structures that extend from the base to the center of the tubule and define the overall structure of the seminiferous epithelium, which is divided into basal and adluminal compartments by a barrier (the blood-testis barrier, BTB) formed between adjacent Sertoli cells near the base of the epithelium [224, 227]. The BTB is a specialized structure comprised of tight junctions, basal tubulobulbar complexed, desmosome-like junctions, and one of two testis-specific adherens junctions known as ectoplasmic specialization (ES) [191, 226, 228]. Ectoplasmic specializations are characterized by the presence of actin filament bundles sandwiched between the Sertoli cell plasma membrane and the cisternae of smooth endoplasmic reticulum [225, 228]. Proper formation and function of the BTB is essential for normal spermatogenesis to occur, as it establishes Sertoli cell polarity, creates the specialized milieu necessary for germ cell development and provides an

immunological barrier that isolates post-meiotic antigens from the systematic circulation [229, 230]. In addition to the BTB-associated basal ES formed between adjacent Sertoli cells, a second testis-specific adherens junction, the apical ES, exists between Sertoli cells and developing spermatids [191, 226, 228]. The role of the apical ES is unknown but it has been implicated in several functions such as sperm head shaping, spermatid-Sertoli cell attachment stabilization, sperm release, spermatid orientation, and providing a scaffold for microtubules [231-234].

There is considerable evidence documenting the ultrastructure of ESs in the testis, but little molecular knowledge is available on how these intercellular junctions are regulated. In the current study, various mouse models, having different expression levels and cellular distribution of DMRT1 (*Dmrt1*$^{+/+}$, *Dmrt1*$^{-/-}$ and *Dmrt1*$^{-/-;tg}$), demonstrated that DMRT1 is needed in Sertoli cells to regulate and establish ES. NECTIN-2, which normally localizes to Sertoli cell- Sertoli cell ES, was greatly reduced or absent from the ES of *Dmrt1*$^{-/-}$ mice, while its expression returned with the transgenic addition of DMRT1 to Sertoli cells of *Dmrt1*$^{-/-}$ mice. Furthermore, we report here that NECTIN-3, known to be expressed only at apical ES was strongly induced with transgenic addition of DMRT1 to Sertoli cells of *Dmrt1*$^{-/-}$ mice, which were devoid of germ cells by 14-days of age (Chapter 2).

Materials and Methods

Animals and antibodies

Dmrt1$^{-/-}$ mice, provided by Dr. David Zarkower and *Dmrt1*$^{-/-}$ mice carrying the Wt1-Dmrt1 transgene (*Dmrt1*$^{-/-;tg}$) are reported elsewhere ([112], Chapter 2). All animal procedures were approved by the Laboratory Animal Research Committee at the University of Kansas Medical Center and performed in accordance with National Institutes of Health guidelines.

Immunohistochemistry

Six-week old testis samples from *Dmrt1*$^{+/+}$, *Dmrt1*$^{-/-}$ and *Dmrt1*$^{-/-;tg}$ mice (three samples per genotype) were immersions fixed in Bouin's solution at room temperature for 24 h. Tissues were rinsed twice with 50% and 70% alcohol and fixed testes cut in half at the sagittal plane, processed and embedded in paraffin according to standard procedures. Five-micron (5 μm) sections were cut and mounted on slides, cleared in xylene, rehydrated through graded alcohol series and heated in 10 mM sodium citrate buffer (pH 6.0) with microwaves (14 min at full power) for antigen retrieval. Sections were blocked using 10% normal goat or donkey serum (Zymed Laboratories Inc.) for 60 min at room temperature. Five sections were analyzed per mouse.

Primary antibody incubations were carried out overnight at 4°C in blocking solution. The sections were probed with: anti-ESPIN, anti-NECTIN-2, anti-NECTIN-3, anti-DMRT1, anti-GCNA1 serum or anti-ACTIN antibody. Anti-ESPIN antibody was a rabbit polyclonal and a gift from Dr. Rajendra Kumar. Rabbit anti-NECTIN-2 antibody (AB87220) and rabbit anti-NECTIN-3 antibody (AB63931) were gifts from Dr. Joseph Tash. Goat anti-Actin (L19) antibody (sc1616) was purchased from Santa Cruz Biotechnology, Inc. (Santa Cruz, CA, USA). Rabbit anti-DMRT1 antibody was custom made by Covance Inc. (Denver, PA, USA) using a C-terminal peptide of DMRT1 [130]. Rat anti-GCNA1 serum was kindly provided by Dr. George. C. Enders.

After washing with PBST, sections were incubated with fluorescently labeled secondary antibody for 1 hour at room temperature. The secondary antibodies employed were Alexa FluorR 488 goat anti-rabbit IgG (Molecular Probes Inc., Eugene), Alexa FluorR 568 donkey anti-rabbit IgG (Molecular Probes Inc., Eugene), Alexa FluorR 488 donkey anti-goat IgG (Molecular

Probes Inc., Eugene), Cy™3-conjugated AffiniPure goat anti-rabbit IgG (Jackson ImmunoResearch Laboratories) or Cy™3-conjugated AffiniPure goat anti-rat IgG (Jackson ImmunoResearch Laboratories). Samples were washed 3 times in PBST (5 min. each) and glass cover slides mounted using Fluoromount-G (Southern Biotechnology Associates Inc., Birmingham, AL). Digital images were collected using a 20x or 40x objective lens and fluorescent filters (FITC, TRITC and DAPI) on a Nikon Eclipse 80i microscope (Nikon Inc., Instrument Group, Melville, NY), a Retiga 2000R fast camera and a QCapture software program (QIMAGING, Surrey, BC, Canada) and processed using Adobe Photoshop.

Transmission Electron Microscopy

The testes of *Dmrt1*$^{+/+}$, *Dmrt1*$^{-/-}$ and *Dmrt1*$^{-/-;tg}$ P42 mice were immersion fixed with 2% glutaraldehyde in 0.1 M cacodylate buffer, postfixed in 1% osmium tetroxide/0.8% potassium ferrocyanide, stained in uranyl acetate, and embedded in epon –araldite blocks. Ultra-thin (80nm) sections were examined at 80 kV using a JEOL 1400EX II (JEOL, Tokyo, Japan) transmission electron microscope. For electron microscopic analysis, ES structures were identified as actin bundles sandwiched between Sertoli cell plasma membrane and smooth endoplasmic reticulum [229, 235, 236]. Low magnification (x1200–8000) was used to examine the basal and adluminal ES in various testes sections.

Results

Immunolocalization of exogenous DMRT1 in Sertoli cells of Dmrt1$^{-/-;tg}$ *mice*

We previously described the construction and generation of a DMRT1-deficient germ cell mouse model, which is *Dmrt1*$^{-/-}$ with a transgene (*Wt1-Dmrt1*) that expresses DMRT1 in Sertoli cells (*Dmrt1*$^{-/-;tg}$;Chapter 2). Initial characterization of DMRT1 expression and testis

morphology was performed on P7 testes. To establish that transgenic expression of DMRT1 was sustained in Sertoli cells of *Dmrt1*$^{-/-;tg}$ mice, immunohistological evaluation was performed on P42 testis sections using antibodies to DMRT1 (green), the germ cell marker GCNA1 (red) and a DAPI counterstain for nuclei. DMRT1 was expressed in both Sertoli cells (green) and spermatogonia (white/yellow) of *Dmrt1*$^{+/+}$ animals, while meiotic and postmeiotic germ cells were negative for DMRT1 (Figure 1A-D). As expected, no DMRT1-positive cells were observed in *Dmrt1*$^{-/-}$ testes (Figures 1E-H), while *Dmrt1*$^{-/-;tg}$ testes (Figures 1I-L) continued to express DMRT1 in Sertoli cells (Figure 1L, arrowhead). Both *Dmrt1*$^{-/-}$ and *Dmrt1*$^{-/-;tg}$ P42 testes were depleted of germ cells (Figures 1F and J).

Colocalization of ESPIN and ACTIN in DMRT1-deficient mouse testes

To evaluate organization and formation of ESs, ESPIN immunohistochemistry was performed. ESPIN is an actin-binding/bundling protein and adaptor protein of apical and basal ESs. Immunolocalization of ESPIN (Figure 2 A, E and I) and actin (Figure 2; B, F and J), with DAPI counterstaining for nuclei (Figure 2; C, G, K), was performed in P42 testes from *Dmrt1*$^{+/+}$ (Figure 2 A-D), *Dmrt1*$^{-/-}$ (Figure 2 E-H) and *Dmrt1*$^{-/-;tg}$ (Figure 2 I-L) mice. In *Dmrt1*$^{+/+}$ testes, ESPIN was observed as curvilinear and arching structures at the basal aspect of the seminiferous epithelium, representing its association with specialized tight junctions (Figure 2A, arrowhead). In addition, ESPIN staining was observed amid groups of elongating spermatids that are arranged in columns within seminiferous epithelium (Figure 2A, asterisk). The co-localization of ESPIN and ACTIN at the basal aspect and in the columns established ESPIN at adherens junctions (Figure 2 D, arrowhead). The reactivity at the basal aspect represents basal ES (Figure 2A, arrowhead) and those in the lumen represent apical ESs (Figure 2A, asterisk). ESPIN expression in *Dmrt1*$^{-/-}$ mice (Figures 2 E) appeared in irregular patches, without any recognizable

polarity, in the adlumen compartment of the seminiferous tubule and was absent at the basal aspect and colocalized partially with ACTIN (Figure 2 H). ESPIN was also absent at the basal aspect in *Dmrt1*$^{-/-;tg}$ testes but the adlumenal staining appeared more regular than that of *Dmrt1*$^{-/-}$ mice and stretched in a neuron-like manner (Figure 2 I) with notable co-localization with ACTIN (Figure 2 H, arrowhead), which was consistent with their presence at adherens junctions. However, no ESPIN immunolocalization was present at the basement membrane of *Dmrt1*$^{-/-;tg}$ testes, suggesting that complete polarization of basal ES require the expression of DMRT1 in germ cells or general presence of germ cells in the seminiferous tubules while the polarity/structure of apical ES require DMRT1 expression in Sertoli cells.

Localization of NECTIN-2 and NECTIN-3 in DMRT1-deficient testes

To further characterize the role of DMRT1 in the formation and organization of the ES, expression was examined for NECTIN-2 and NECTIN-3, two proteins associated with ES [223, 237-241]. Localization of NECTIN-2 (Figure 3; A, D, G), NECTIN-3 (Figure 4; A, D, G) and counterstain with DAPI for nuclei (Figures 3 and 4; B, E, H) in P42 mouse testes from *Dmrt1*$^{+/+}$ (Figures 3 and 4; A-C), *Dmrt1*$^{-/-}$ (Figures 3 and 4; D-F) and *Dmrt1*$^{-/-;tg}$ mice (Figures 3 and 4; G-I) were determined by immunofluorescence.

NECTIN-2 is expressed at basal and apical ESs and was used to validate the expression of ESPIN. Similar to ESPIN, NECTIN-2 immunoreactivity showed the presence of the ES protein was present at the inter-Sertoli cell junctions of *Dmrt1*$^{+/+}$ mouse testis, as curvilinear structures associated with tight junctions at the basal compartment of the seminiferous epithelium (Figures 3A & 3C, arrowhead). In addition, NECTIN-2 staining was observed as dots at the luminal edge of the seminiferous tubules, where round and elongating spermatids interact

tightly with the plasma membrane of Sertoli cells (Figure 3A, asterisk). In the testis of *Dmrt1*$^{-/-}$ mice, NECTIN-2 expression was lost from the adlumenal and basal compartments (Figures 2F). However, in *Dmrt1*$^{-/-;tg}$ testes, NECTIN-2 expression was significantly present and collected towards the center of the tubule similar to that observed for ESPIN in these mice (compare Figures 3G and 2I). Its absence from the basal compartment suggested that DMRT1 in Sertoli cells was not sufficient to localize NECTIN-2 to the basement membrane but could maintain NECTIN-2 expression in the adluminal compartment (Figure 3I). This result confirms that Sertoli cell DMRT1 partially regulates organization of ES within the seminiferous tubules.

NECTIN-3 is expressed only at apical ESs and between Sertoli cells and elongating spermatid. NECTIN-3 immunoreactivity was absent at the basal aspects of *Dmrt1*$^{+/+}$ mouse testis (Figure 4A-C). However, NECTIN-3 staining was observed amongst a group of elongating spermatids arranged in columns near the lumen of the seminiferous tubule (Figure 4C, arrowhead). Unlike NECTIN-2 and ESPIN, NECTIN-3 expression was absent in *Dmrt1*$^{-/-}$ mice (Figures 4D-F), suggesting a difference in background. However, similar to ESPIN and NECTIN-2, NECTIN-3 expression in *Dmrt1*$^{-/-;tg}$ mice appeared elevated along the luminal side of the tubule and lost from the basement membrane (Figure 4G-I). The result further supports a role of Sertoli cell DMRT1 in the formation and organization of ESs in the testis.

Electron Microscopic Analysis of Sertoli cell ectoplasmic specialization

To further evaluate the role of DMRT1 in regulating ESs, ultrastructural analysis was performed to compare structures of this testis-specific adherens junction in seminiferous tubules of *Dmrt1*$^{+/+}$, *Dmrt1*$^{-/-}$ and *Dmrt1*$^{-/-;tg}$ mice. In *Dmrt1*$^{+/+}$ testis, basal ESs were identified by actin filament bundles sandwiched between the Sertoli cell membrane and a cistern of the endoplasmic

reticulum and their association with neighboring tight junctions of the blood-testis barrier (Figure 5A). Similarly, apical ESs were observed between elongating spermatids and its supporting Sertoli cells by the presence of actin filament bundles sandwiched between an engorged cistern of endoplasmic reticulum and the membrane of a Sertoli cell (Figure 5B). Thus, the ultrastructural of *Dmrt1*$^{+/+}$ testes indicated the presence of an intact and highly selective blood-testis barriers that conferred polarity to the seminiferous tubule. In contrast, ESs and tight junctions were not observed between adjacent Sertoli cells of *Dmrt1*$^{-/-}$ mice (Figure 6A). However, abundant desmosomes were noted between adjacent Sertoli cells (Figure 6 B), suggesting that the blood-testis barrier is comprised largely of desmosome and their selectivity is speculated to be low, with cell polarity completely absent. In the *Dmrt1*$^{-/-;tg}$ mice, tight junctions were absent but ESs that formed in the adlumen were abundant between adjacent Sertoli cells and formed away from the basal (Figure 7A) but around the apical (Figure 7B) sites of the seminiferous tubules. This suggest that the blood-testis barrier is comprised of adherens junctions and desmosomes (not shown), attributing cell polarity and selectivity that we speculate will be intermediate between that of *Dmrt1*$^{+/+}$ and *Dmrt1*$^{-/-}$ mice.

Discussion

Spermatogenesis, the generation of haploid spermatozoa from diploid spermatogonia, represents one of the best-studied differentiation processes in biology. This transfiguration of the germline relies on numerous complex interactions between Sertoli cells and differentiating germ cells, which take place within the seminiferous epithelium and requires its integrity and polarization. Proper function and structure of the epithelium depend on its integrity and polarization and, in turn, on the junctional complexes that form between the apical-lateral surfaces of adjacent cells. Cellular junctions consists of multiprotein complexes of which three

major types exist in vertebrates including anchoring junctions (adhesion junctions, desmosomes, hemidesmosomes), communicating junctions (gap junctions) and occluding junctions (tight junctions) [223]. In the testicular seminiferous epithelium, a distinct actin-associated adhesion junctions, ESs, have been characterized between adjacent Sertoli cells and between a Sertoli cell and a developing spermatid, each type referred to as the basal and the apical ESs, respectively [226, 235].

In this study, the role of DMRT1 in the formation and organization of ES was evaluated by examining the junctions in the seminiferous tubules of mice with different cellular complements of DMRT1. Our previous studies showed that DMRT1 expression from a *Wt1-Dmrt1* transgene was restricted to Sertoli cells on a *Dmrt1*-null background (*Dmrt1*$^{-/-;tg}$ mice or *Dmrt1* rescue) at P7. This *Dmrt1* rescue mouse model revealed Sertoli cell-specific functions for DMRT1 in the maintenance of seminiferous tubule integrity, testis size and progressive sperm motility, as well as validation of its role in Sertoli cell maturation (Chapter 2). Our current study shows that DMRT1 from the transgene is maintained in Sertoli cells of P42 *Dmrt1*$^{-/-;tg}$ mouse testes and maintained seminiferous tubule structure but not germ cells. Our model is an alternative to the conditional deletion of *Dmrt1* in germ cells in *GCDmrt1KO* mouse model and does not depend on the Cre-LoxP technology (using either TNAP-Cre (Tissue Non-specific Alkaline Phosphatase-Cre) or Ngn3-Cre (Neurogenin3 Cre)) but rather on the return of DMRT1 to a single cell type [131, 133, 134, 200]. In contrast to our current model, the Cre-LoxP technology employed in the conditional models showed poor Cre penetrance and DMRT1 was not deleted in all germ cells. While characterization of the occluding junctions in *Dmrt1*-null mice revealed that *Dmrt1* mutant testes fail to form Sertoli cell tight junctions [132], no data is available on the formation of anchoring or communicating junctions by Sertoli cells in *Dmrt1*-

null or *Dmrt1* conditional deletion mouse models. Thus, the current study is the first of its kind to examine associations between Sertoli cell-specific expression of DMRT1 and formation/organization of ES.

The ESs are testis-specific adherens junction, which are components of the blood-testis barrier and required for spermatid maturation. The current study showed that DMRT1 is required for proper expression and localization of these adherens junctions, as, in its absence, constituents of the ESs were significantly reduced or lost from the seminiferous epithelium. However, when DMRT1 was returned to Sertoli cells of *Dmrt1*$^{-/-}$ mice, i.e. absent only from germ cells, expression of the junction proteins returned but was distributed differently from that observed in wild type mice. Expression of NECTIN-2, NECTIN-3 and ESPIN together with electron micrographs revealed that these ES proteins returned and were abundant in the seminiferous epithelium of *Dmrt1*$^{-/-;tg}$ mouse testes. The extensive ES proteins in the *Dmrt1*$^{-/-;tg}$ mouse testes epithelium accumulated in the adluminal compartment of the seminiferous tubule and formed between adjoining Sertoli cells (Figure 2I, 3G, 4G). This observation of ES protein accumulating in the lumen of *Dmrt1*$^{-/-;tg}$ mice testes in the absence of germ cells, may be attributed to the continuous interaction between the cell membrane processes of neighboring Sertoli cells that forms the required framework for the deposition of these multiprotein complexes. NECTIN-3 was shown to be expressed in spermatids [241, 242], but considerable expression of NECTIN-3 was observed in the absence of elongating spermatids in the seminiferous epithelium of *Dmrt1*$^{-/-;tg}$ mouse testes suggesting that either NECTIN-3 is also expressed in Sertoli cells or NECTIN-3 can be ectopically expressed in the absence of elongating spermatid. In addition, except for ESPIN, which was expressed in irregular patches, the *Dmrt1*$^{-/-}$ mice testes showed weak NECTIN-2 expression and no NECTIN-3 expression. Since it was difficult to differentiate

between weak and no NECTIN-2 expression, it is likely that the weak NECTIN-2 expressions observed in *Dmrt1*$^{-/-}$ mouse seminiferous tubules were non-specific. The expression of all three ES proteins depends on DMRT1 as they were either completely absent of significantly reduced in *Dmrt1*-null mouse testes. In addition, it appears that the apical localization is intact but the basal localization is not or maybe the apical localization is the default in the absence of a basal ES. Thus, failure to localize at basal ES due to the lost tight junction formation favors apical localization of ES proteins. Overall, the phenotype of the *Dmrt1*$^{-/-}$ mice is similar to the absence of fully organized Sertoli cell junctional complexes in hpg Sertoli cells, incompletely formed Sertoli cell junctional complexes in the 12–14-day-old mouse and in the diethylstilbestrol-treated mouse testis [220, 243, 244]. The junctional specialization formed in the *Dmrt1*$^{-/-;tg}$ mice technically can be referred to as basal ES; since, they are formed between adjoining Sertoli cells even though they are localized apically.

Tight junctions are an important component of the BTB and a vital indicator of Sertoli cell polarization and maturation [193]. Tight junctions and adherens junctions play vital roles in determining polarity of a cell [132, 245]. The absence or presence of tight junctions was examined using immunofluorescence and electron microscopy. Similar curvilinear profiles for ESPIN and NECTIN-2 were observed at the basal aspect that contributed to adult Sertoli cell junctional complexes in P42 *Dmrt1*$^{+/+}$ mice that were absent in P42 *Dmrt1*$^{-/-}$ and *Dmrt1*$^{-/-;tg}$ mice. Also, staining for ZO-1, a marker for tight junctions, formed curvilinear structures at the basal aspect of seminiferous tubules in *Dmrt1*$^{+/+}$ mice that were absent in tubules from *Dmrt1*$^{-/-}$ and *Dmrt1*$^{-/-;tg}$ mice; indicating absence of tight junctions (data not shown). These results were supported by the identification of "kisses" of plasma membrane on electron micrographs from *Dmrt1*$^{+/+}$ mice denoting tight junctions (Figure 5A) that were absent in micrographs of *Dmrt1*$^{-/-}$

and *Dmrt1*$^{-/-;tg}$ mice. The expression at the basal aspect is analogous to expression patterns of OCCLUDIN (OCLN) and CLAUDIN11 (CLDN11), two molecules associated with the formation of tight junctions at the BTB [246-249].

In a similar study by Fahrioglu et al [132], the expression of tight junction proteins (ZO-1, OCLN and CLDN11) in *Dmrt1*$^{-/-}$ mice were examined immediately after birth (P2) and through the first wave of spermiation (P36) [132]. Previous studies showed ZO-1 was abundantly expressed in testes of *Dmrt1*$^{-/-}$ mice from P2 through P20, but was disorganized and localized only to the lumen of seminiferous tubule [132]. The tight junction proteins, CLDN11 and OCLN were also absent from *Dmrt1*-null testes at P14 and P20. Our data at P42 suggest that DMRT1 is required for expression of all ES proteins and Sertoli cell-specific DMRT1 expression in *Dmrt1*$^{-/-;tg}$ seminiferous tubules returns expression of ES proteins but fail to localize them to tight junctions because they are still compromised.

Autoimmune recognition of differentiating germ cells is avoided by their translocation from the basal to the immune-privileged adluminal compartment by breaking apical junctional complexes maintained by Sertoli cells and rejoining them at the basal end of a migrating germ cell without jeopardizing the blood-testis barrier. Tight junctions, ES and desmosomes are the three main components of the blood-testis barrier. Knowing the dependent association between adherens and tight junctions, our findings on the dependent action of DMRT1 on NECTIN-2 and ESPIN expression at basal ESs suggests that DMRT1 is essential for establishing the BTB. Like other studies of testis ES, we found that ESPIN and NECTIN-2 localized basal ES at the BTB and with the apical ES associated with spermatids [246, 250-252]. Similarly and as shown previously, electron micrographs of *Dmrt1*$^{+/+}$ mice showed adherens junctions in association with tight junctions formed between adjacent Sertoli cells. However, similar to mice with

testicular feminization, *Dmrt1*$^{-/-}$ mice had small testes, small diameter of seminiferous tubule, large number of lipid droplets and abundant junctional complexes (desmosomes) [253]. In contrast, in addition to desmosome, numerous adherens junctions were identified in *Dmrt1*$^{-/-;tg}$ mice, which also had small testes, large number of lipid droplets and reduced diameter of the seminiferous tubule. Overall, based on the expression of ES protein staining and identification of junctional structures, the blood-testis barrier in *Dmrt1*$^{+/+}$ mice comprised of tight junctions, adherens junctions and desmosome (not shown) was speculated to be intact and highly selective, whereas, those in *Dmrt1*$^{-/-}$ or *Dmrt1*$^{-/-;tg}$ mice were made up only of desmosomes and speculated to be very permeable or composed of adherens junction and desmosome (not shown) and speculated to have an intermediate selectivity, respectively. However, junctional permeability experiments will be required to validate these observations.

In conclusion, this study provides new insights into cell-specific functions for DMRT1 in polarization and compartmentalization within the seminiferous epithelium, phenotypes of Sertoli cell-only pathological condition and putative cytoskeletal regulated signaling pathway essential for the formation and organization of testis-specific adherens junctions.

Figure 1: Immunolocalization of DMRT1 and GCNA1 in postnatal day 42 (P42) mouse seminiferous tubule. Testis sections from *Dmrt1*$^{+/+}$ (**A-D**), *Dmrt1* $^{-/-}$ (**E-H**) and *Dmrt1*$^{-/-;\,tg}$ (**I-L**) mice were evaluated using fluorescently labeled antibodies against DMRT1 (green; **A**, **E** and **I**), GCNA1 (red; **B**, **F** and **J**) and counterstained with DAPI for nuclei (blue; **C**, **G** and **K**). **D**, **H** and **L** shows merged images. Yellow stained cells (arrow), indicating co-expression of DMRT1 and GCNA1 in germ cells, are observed only in *Dmrt1*$^{+/+}$ mice (**D**). Arrowheads show DMRT1 expression in Sertoli cells of *Dmrt1*$^{+/+}$ (**D**) and *Dmrt1*$^{-/-;tg}$ (**L**) mice. Final magnification for micrographs is x400.

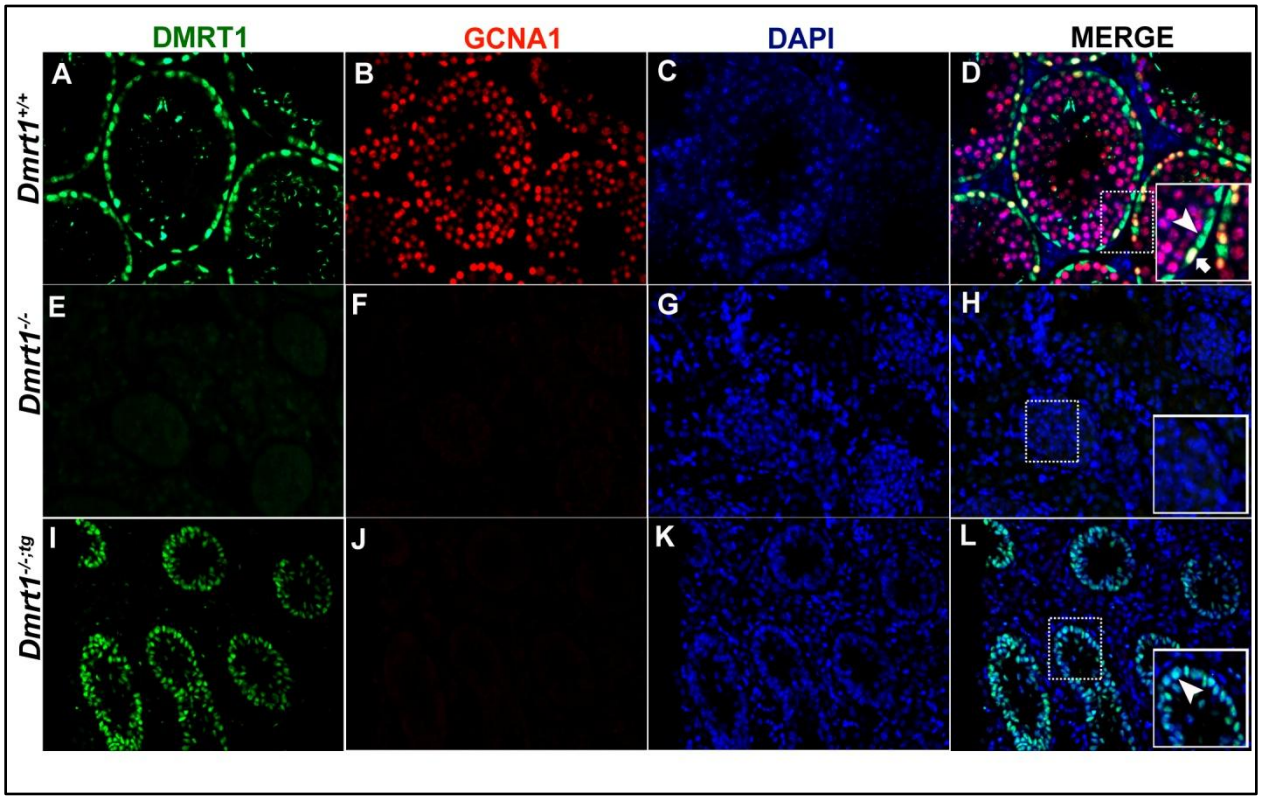

Figure 2: Colocalization of ectoplasmic specialization associated protein, ESPIN. ESPIN (**A**, **E** and **I**) and ACTIN (**B**, **F** and **J**) on P42 testes sections from *Dmrt1*$^{+/+}$ (**A-D**), *Dmrt1* $^{-/-}$ (**E-H**) and *Dmrt1*$^{-/-;tg}$ (**I-L**) mice. ESPIN colocalizes with ACTIN in *Dmrt1*$^{+/+}$ (**D,** arrowhead) and *Dmrt1*$^{-/-;tg}$ (**L,** arrowhead) but not in *Dmrt1*$^{-/-}$ (**H**) mice. Final magnification for micrographs is x400.

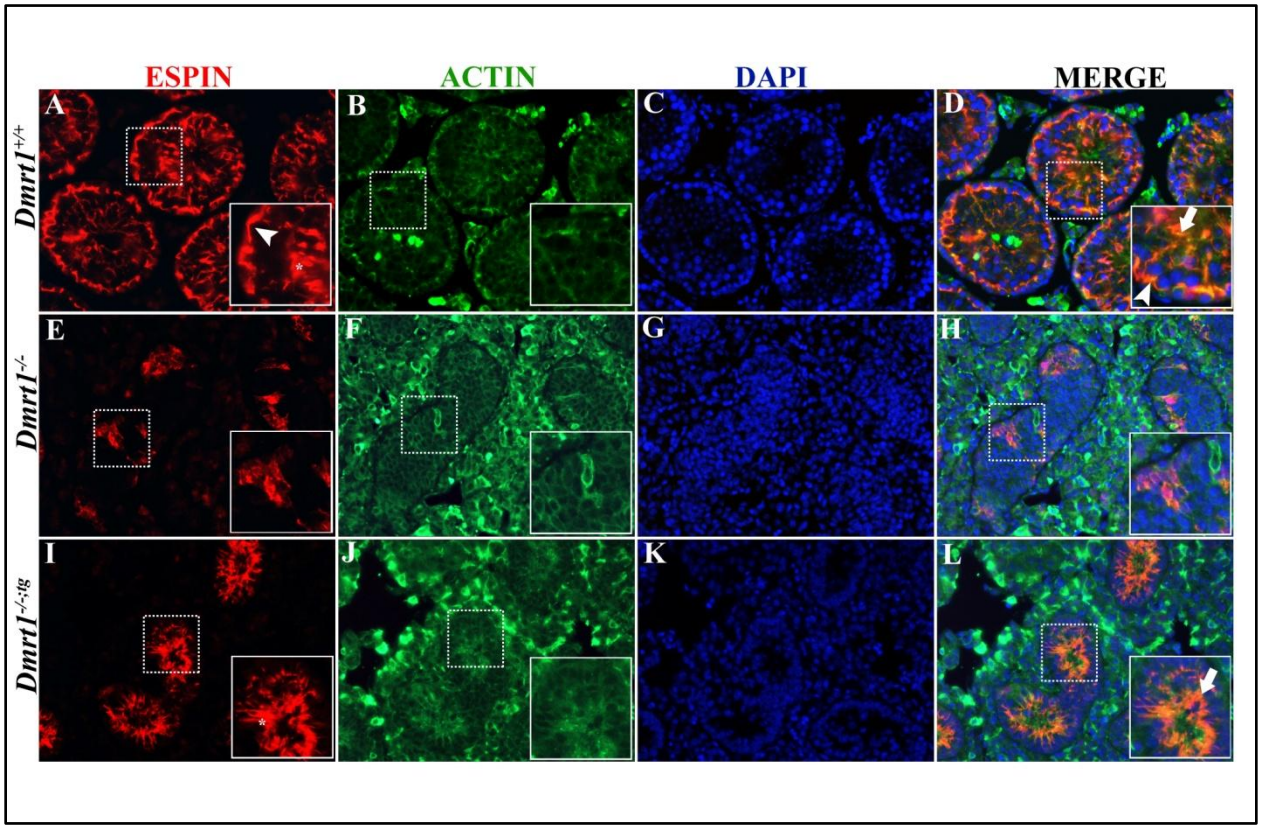

Figure 3: Immunohistochemical localization of NECTIN2. NECTIN-2 (red; **A**, **D** and **G**) and counterstained with DAPI for nuclei (blue; **B**, **E** and **H**) on testes sections at P42 in *Dmrt1*$^{+/+}$ (**A**-**C**), *Dmrt1* $^{-/-}$ (**D**-**F**) and *Dmrt1*$^{-/-;tg}$ (**G**-**I**) mice. Arrowheads in **G** and **I** depicts NECTIN-2 expression between adjacent Sertoli cells. Arrowhead in **F** shows absence of NECTIN-2 expression. Final magnification of micrographs is x400.

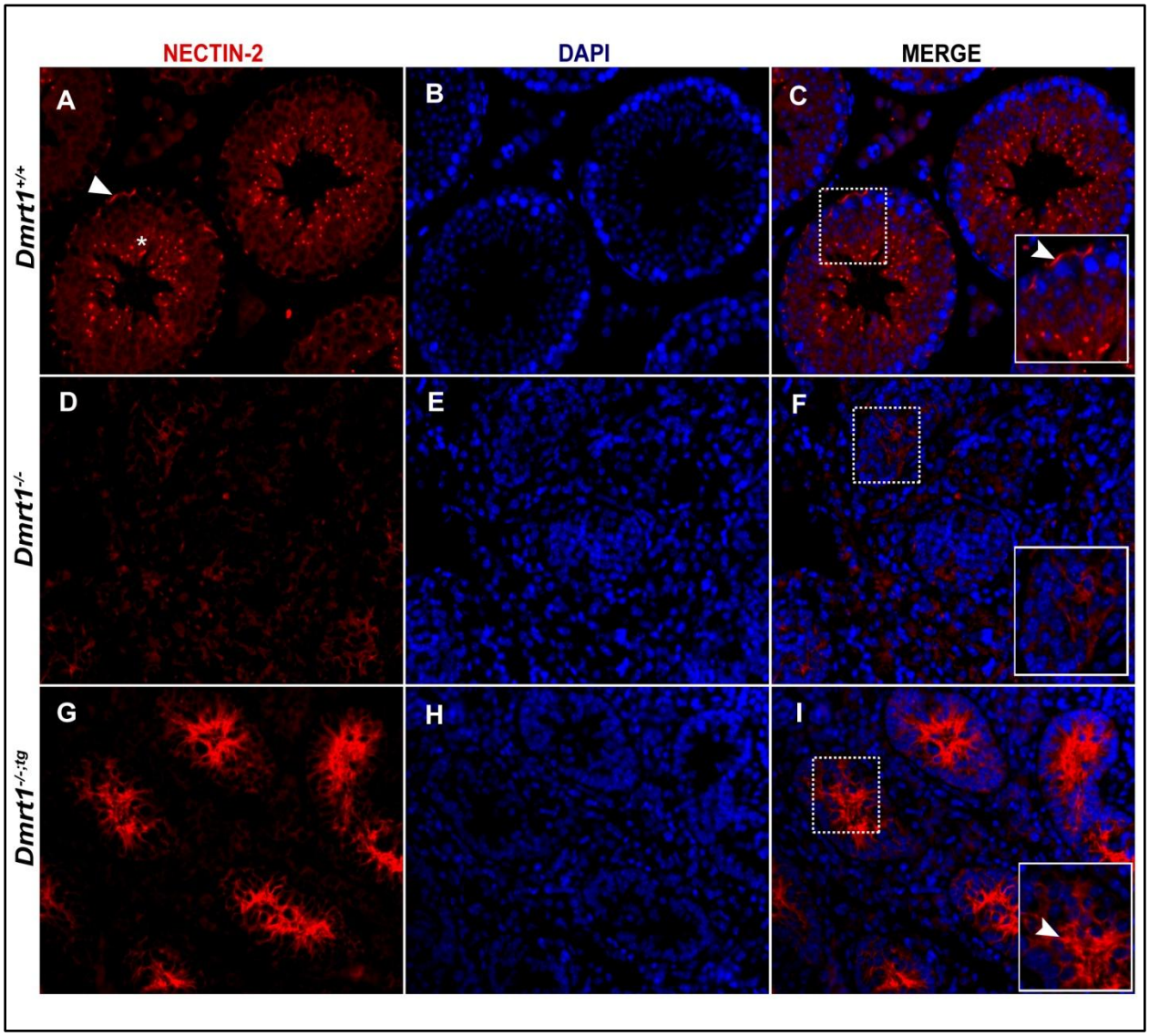

Figure 4: Immunohistochemical localization of NECTIN-3. NECTIN-3 (red; **A**, **D** and **G**) and counterstained with DAPI for nuclei (blue; **B**, **E** and **H**) on testis sections at P42 in *Dmrt1*$^{+/+}$ (**A-C**), *Dmrt1* $^{-/-}$ (**D-F**) and *Dmrt1*$^{-/-;tg}$ (**G-I**) mice. Arrowheads in **G** or **I** depicts ES formation between Sertoli cell and developing germs or between adjacent Sertoli cells, respectively. Final magnification of micrographs is x400.

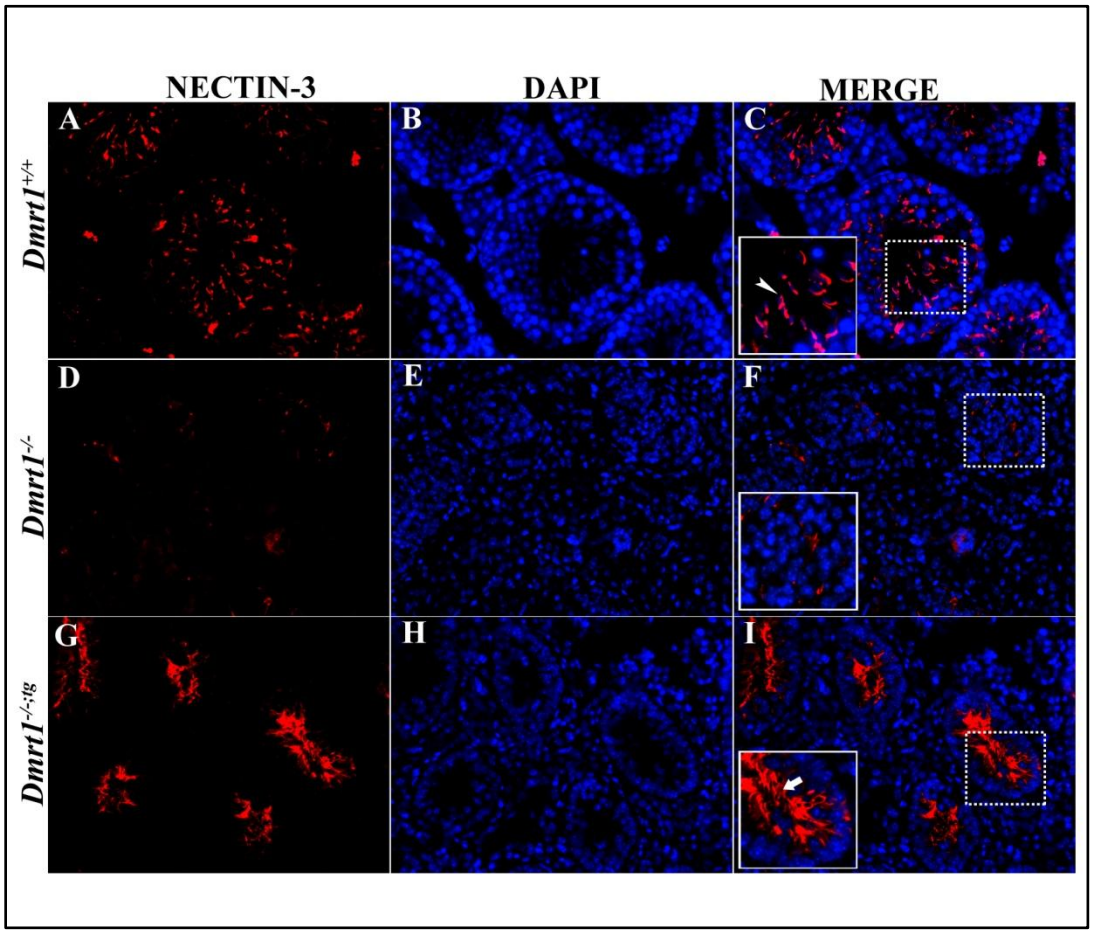

Figure 5: Electron microscopy of Sertoli cell ectoplasmic specialization in testes sections of P42 *Dmrt1*$^{+/+}$ mice. A. Basal ES in normal testis. Actin filament bundles are sandwiched between cisternae of endoplasmic reticulum and cell processes of adjoining Sertoli cells, and together with neighboring tight junctions form the blood-testis barrier. Magnification, x30400; scale bar, 100 nm. **B**. Apical ES in normal testis. The ES is seen in the cytoplasm of a Sertoli cell opposite an elongating spermatid. Magnification, x38500; scale bar, 500nm.

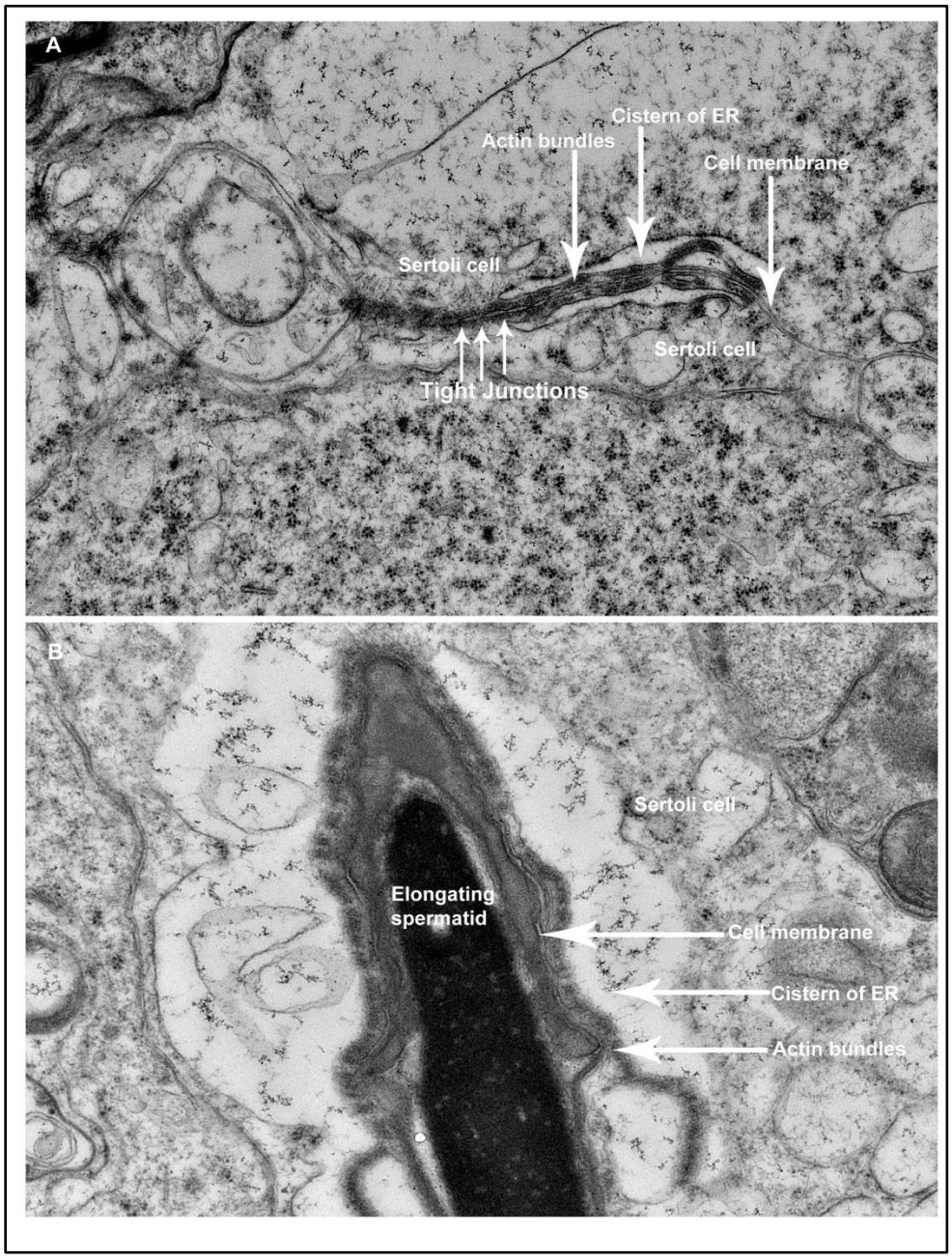

Figure 6: Electron microscopy of Sertoli cell ultrastructure in testes sections of P42 *Dmrt1*$^{-/-}$ mice. A. Absence of basal ES structures between adjoining Sertoli cells in *Dmrt1*$^{-/-}$ seminiferous tubules. Magnification, x30400; scale bar, 500nm. **B**. Desmosomes (arrow) were present between neighboring Sertoli cells in *Dmrt1*$^{-/-}$ testes. Magnification, x38200; scale bar, 100nm.

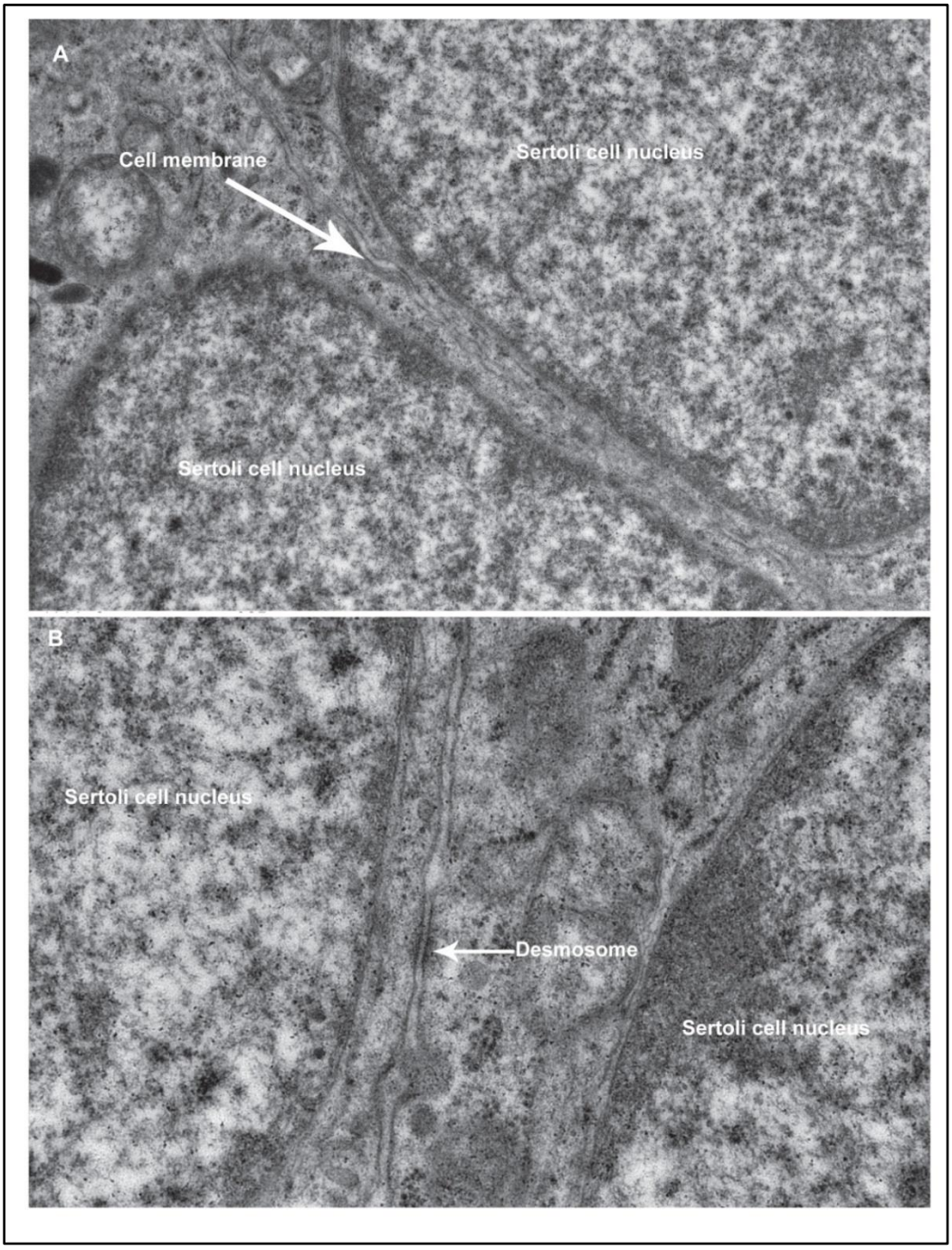

Figure 7: Electron microscopy of Sertoli cell ectoplasmic specialization in testes of P42 *Dmrt1*$^{-/-;tg}$ mice. A. Presence of basal ES structures between adjoining Sertoli cells in *Dmrt1*$^{-/-;tg}$ at the basement membrane of seminiferous tubules. Magnification, x19500; scale bar, 500nm. **B**. Presence of basal ES structures between adjoining Sertoli cells in *Dmrt1*$^{-/-;tg}$ at the lumen of the seminiferous tubules. Magnification, x38200; scale bar, 500nm.

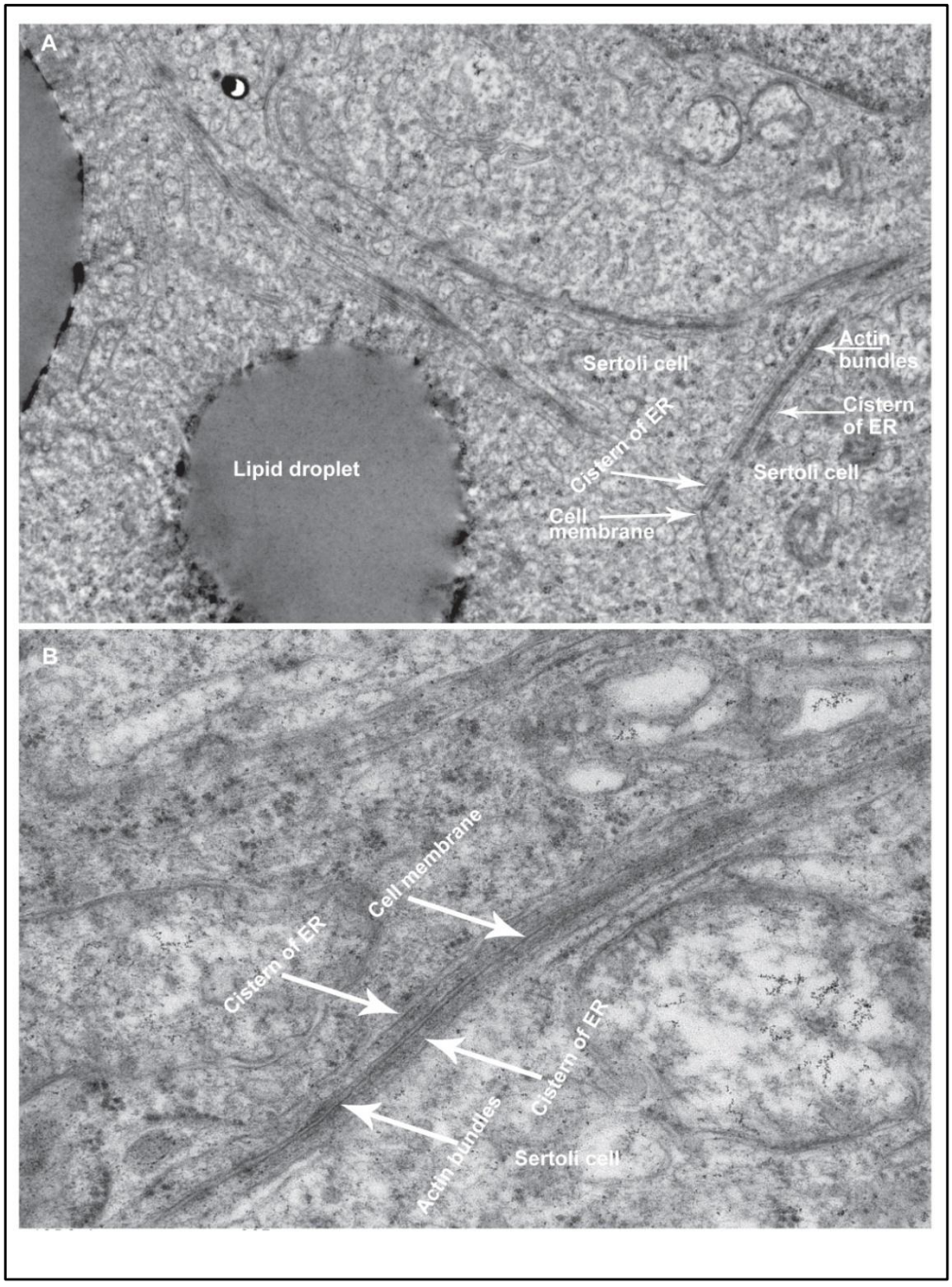

Chapter 4: DMRT1 regulates distinct pathways and targets in Sertoli cells and germ cells

Abstract

The *Doublesex* and *Mab-3* related transcription factor 1 (DMRT1) is a testis-specific transcription factor required for germ cell development and Sertoli cell differentiation. To explore the functional role of DMRT1 in germ cells and Sertoli cells, genome-wide DMRT1 binding sites, identified by ChIP-Seq, were evaluated together with testis gene expression profiles from different models of DMRT1-deficiency. Microarray analyses were performed on postnatal day 7 testes from wild type, *Dmrt1*$^{-/-}$, and Sertoli cell-specific DMRT1 rescue (*Dmrt1*$^{-/-;tg}$) mice. This revealed 609 differentially expressed genes, with at least two fold change and $p \leq 0.05$, in *Dmrt1*$^{-/-;tg}$ testes and 791 in *Dmrt1*$^{-/-}$ testes. Ingenuity Pathway Analysis (IPA) identified top pathways and associated biological processes in differentially expressed genes that were shared and distinct to *Dmrt1*$^{-/-}$ and *Dmrt1*$^{-/-;tg}$ testes and representing changes mediated by DMRT1 in germ cells and Sertoli cells, respectively. Functions associated with genes directed by DMRT1 in germ cells include spermatogenesis, male gamete generation and sex differentiation, whereas functions directed in Sertoli cells included cell-cell contact, male infertility, RNA and kinesin binding. Further functional annotation using DAVID and ExoCarta on a select group of differentially expressed genes revealed potential functions for DMRT1 in ubiquitination and vesicular transport. ChIP-Seq and ChIP-qPCR identified and validated genome-wide DMRT1 binding sites using P10 and, P7 and P10 mouse testes, respectively. Approximately 150 binding peaks were inspected manually on the UCSC Genome Browser, identifying many novel DMRT1 binding sites with desired peak qualities. Putative target genes were designated based on proximity to the binding sites, which, for 87% of the genes, were located in introns. In addition, integration of the microarray and binding peak data identified 52 additional putative targets of DMRT1 and revealed indirect and direct pathways regulated by DMRT1. VDR/RXR activation

and pantothenate and CoA biosynthesis were direct pathways regulated by DMRT1 in germ cells and Sertoli cells, respectively. In summary, the study identified new cell-specific targets and pathways that are regulated by DMRT1 in Sertoli cells and germ cells.

Introduction

Dmrt1 encodes a transcriptional regulator, DMRT1, that shares homology to dsx and mab3; two evolutionary conserved proteins that regulate comparable aspects of sexual differentiation in *Drosophila Melanogaster* and *Caenorhabditis elegans*, respectively [112-114]. These orthologs share a cysteine-rich DNA binding motif, the DM domain, illustrating the existence of a shared gene lineage and preserved molecular pathways essential for sexual differentiation [146]. In vertebrates, DMRT1 expression is restricted to the gonads, where it is expressed in both Sertoli cells and germ cells, and required for testis differentiation [115, 128, 141, 145, 150, 159, 216-218]. Human *DMRT1* has been implicated in sex determination by comparative genetic mapping, which associated the region of chromosome 9 containing *DMRT1* to XY sex-reversed and testicular dysgenesis [119]. In mice, neither *Dmrt1* ablation nor forced expression studies provided evidence for DMRT1 in sex determination but the reprogramming of Sertoli cells to granulosa cells in *Dmrt1*$^{-/-}$ testes did reveal its role in maintaining sex differentiation ([50, 135]; Ning et al., unpublished). In addition, evaluation of *Dmrt1*$^{-/-}$ mice showed DMRT1 is important for germ cell migration, survival and proliferation, Sertoli cell differentiation, and seminiferous tubule organization [50, 131, 133].

DMRT1 is indispensable for spermatogenesis and is an evolutionary conserved transcription factor, suggesting that it may sit at the top of a hierarchy of genes that control key spermatogenic pathways. Therefore, identifying the genes and pathways will significantly advance our understanding of male fertility. In order to understand how DMRT1 contributes to spermatogenesis, it is necessary to identify the relationship between DMRT1 and the genes directed within its network, which requires knowledge of DMRT1's target genes (i.e. those under its direct regulation) and the various biological pathways they affect.

Various cell-specific *Dmrt1*-deletion models contributed more insight on the biological processes and pathways of DMRT1 in the testis. DMRT1's cell specific role is best understood for the Sertoli cells. The DMRT1-deficient germ cell model (Sertoli cell rescue (*Dmrt1*$^{-/-tg}$)) showed that DMRT1 in Sertoli cells is required for the maintenance of testis size, sperm progressive motility and tubule integrity, regulation of Sertoli cell maturation and localization of ES proteins (Chapter 2). These were consistent with findings from the *SCDmrt1KO* conditional deletion mouse model, which had DMRT1 deleted only in Sertoli cells, revealing importance in tubule integrity and Sertoli cell maturation as DMRT1-deficient Sertoli cells fail to polarize and differentiate. Functions for DMRT1 in germ cells were revealed in the *SCDmrt1KO* mice testes including postnatal mitotic reentry by spermatogonia, unimpaired migration from the lumen of the seminiferous tubule to the periphery and meiotic entry by primary spermatocyte that was not completed [131]. The inability of primary spermatocyte to complete meiosis in the *SCDmrt1KO* testes suggested that DMRT1 in Sertoli cells is needed to complete meiosis, demonstrating a non-autonomous action of DMRT1 on germ cells. The biological processes that were impaired and unhindered in Sertoli cells and germ cells of *SCDmrt1KO* mice testes represent the autonomous action of DMRT1 on Sertoli cells and germ cells, respectively. While much is known about the biological processes regulated by DMRT1, many of the mechanistic, direct targets and cell-specific details are missing.

To this end, chromatin immunoprecipitation (ChIP) and gene expression changes resulting from *Dmrt1* deletion have been instrumental in identifying DMRT1 target genes and regulated pathways, respectively. DMRT1 binding peaks were identified at the proximal promoter regions of 1,439 genes using ChIP-chip and the associated DMRT1 binding sites identified using motif searches; and a limited number of these targets were differentially

expressed when *Dmrt1* levels were perturbed after postnatal re-initiation of DMRT1 expression (P1 & P2) or when levels of DMRT1 are at a maximum (P9) [132, 136]. By integrating the data, many known testis regulators, including *Claudin11, Sox2, Stra8, Ar, Vinculin, Gja3, Gfra3,* and *Sohlh1,* were implicated as direct targets of DMRT1 [136]. Furthermore, network analysis ascribed pathways represented by the identified DMRT1 target genes, which included androgen, focal adhesion kinase, IL-6, phosphatase and tensin homolog (PTEN), and insulin-like growth factor 1 (IGF-1), FSH, retinoic acid, GDNF, eicosanoid, and tachykinin 2 pathways [132, 136]. However, this study probed only proximal promoter sequences thus putative DMRT1 target genes regulated by distal binding were not identified. Furthermore, only about 1/10th (143/1439 targets) of the putative genes mapped close to a binding site were misregulated in microarray analyses supporting their regulation by DMRT1.

The present study used previously characterized mouse models of *Dmrt1* deficiency to examine cell-specific DMRT1-regulated pathways. In addition to $Dmrt1^{-/-}$ mice, the study employed a transgenic model of germ cell DMRT1 deficiency, which expresses DMRT1 only in Sertoli cells in $Dmrt1^{-/-}$ mice (i.e. $Dmrt1^{-/-;tg}$ mice; Chapter 2) and therefore function can be ascribed to the entire germ cell population at times when spermatogenesis is initiated and the niche is formed. Pathway analysis revealed roles in VDR/RXR activation, IL-4 signaling and immune response enriched in germ cells, whereas cell-cell contact and RNA binding were enriched in Sertoli cells. Genome-wide analysis of DMRT1 binding sites by ChIP-Seq of chromatin from postnatal day 10 (P10) $Dmrt1^{+/+}$ and $Dmrt1^{-/-}$ testes identified many new DMRT1 target genes, which have roles in RNA transport and regulation, cell cycle, cell adhesion and protein transport.

Materials & Methods

Animals

Generation and characterization of *Dmrt1*$^{-/-}$ and *Dmrt1*$^{-/-;tg}$ mice have been described elsewhere ([50]; Chapter 2). All animal procedures were approved by the Laboratory Animal Research Committee at the University of Kansas Medical Center and performed in accordance with National Institutes of Health guidelines.

RNA isolation and Microarray analysis

Total RNA was isolated from 12 postnatal day 7 (P7) mouse testes, four each from knockout (*Dmrt1*$^{-/-}$), wild type (*Dmrt1*$^{+/+}$) and rescue (*Dmrt1*$^{-/-;tg}$), using Trizol reagent (Invitrogen) following the manufacturer's guidelines. Isolated RNA was quantified using NanoDrop (ND-1000, Thermo Scientific) and quality checked using the Agilent 2100 Bioanalyzer with the RNA 6000 Nano LabChip. Microarray analysis was performed by the Microarray and Bioinformatics core at the University of Kansas Medical Center. Briefly, five microgram (5µg) of total RNA was biotinylated using GeneChip Expression 3′-Amplification IVT labeling kit (Affymetrix, Cleveland, OH). The Mouse Genome 430 2.0 GeneChip arrays (Affymetrix, Cleveland, OH) were hybridized with amplified RNA (cRNA), washed in the Fluidics Station 400 (FS400) (Affymetrix, Cleveland, OH) using the EuKGE-WS2v5 protocol, and scanned, using the default settings, using the GeneChip Scanner 3000 7G Reader (Affymetrix, Cleveland, OH).

Expression data analysis

Raw data analyses were performed using Partek® genomic suite, version 6.4 (Partek Inc., St. Louis, MO) and pairwise comparisons performed between *Dmrt1*$^{-/-}$ and *Dmrt1*$^{+/+}$, *Dmrt1*$^{-/-;tg}$

and *Dmrt1*$^{+/+}$ or *Dmrt1*$^{-/-}$ and *Dmrt1*$^{-/-;tg}$ samples. Background was adjusted using Robust Multi-array Average (RMA) algorithm, data normalized using the Quantile normalization algorithm, and probe intensity levels summarized using the Median polish method [254-256].

To identify differentially expressed genes, a 3-step filtering process was used for each comparison (*Dmrt1*$^{-/-}$ / *Dmrt1*$^{+/+}$, *Dmrt1*$^{-/-;tg}$ / *Dmrt1*$^{+/+}$ or *Dmrt1*$^{-/-}$ / *Dmrt1*$^{-/-;tg}$). The p-values were calculated using R package and functions in the 'limma' Bioconductor package [257]. The false discovery rate (FDR) was calculated using adjusted p-values corrected for multiple comparisons as described elsewhere[258]. Transcripts with expression fold differences less than 2 (i.e. differences with log2 values between -1 and 1), moderate t-test p-values greater than 0.05 or a false discovery rate (FDR) greater than 0.1 were excluded [259].

Pathway analysis

Functional and pathway analyses of differentially expressed genes were performed by Ingenuity Pathway Analysis software (IPA; Ingenuity® Systems, www.ingenuity.com). Prior to importing the gene refseq accession numbers to IPA, germ cell and Sertoli cell-specific differential gene changes were identified using a parameter called the rescue factor (RF). The RF was calculated using the formula, $\mathrm{RF} = 1 - (\frac{\frac{Res}{Wt}}{\frac{Ko}{Wt}})$, where *Res/Wt* was fold changes in *Dmrt1*$^{-/-;tg}$ probes after normalizing to the equivalent *Dmrt1*$^{+/+}$ probes and *Ko/Wt* was fold changes in *Dmrt1*$^{-/-}$ probes after normalizing to the equivalent *Dmrt1*$^{+/+}$ probes. An arbitrary scoring scale ranging from a minimum of negative one (-1) to a maximum of one (1) was utilized to categorize these genes. Genes with and RF > 0.5 were considered either partially (0.5<RF<1.0) or fully (RF = 1.0) rescued, with the latter representing genes regulated by DMRT1 only in Sertoli cells. Genes with an RF < 0.5 were considered to be largely or entirely regulated by DMRT1 in germ

cells. Functional annotation was performed using IPA, the Database for Annotation, Visualization and Integrated Discovery (DAVID; [260]) and ExoCarta (Exosome protein, RNA and Lipid data base;[261, 262]).

Chromatin Immunoprecipitation (ChIP)

ChIP was performed using chromatin from freshly isolated *Dmrt1*$^{+/+}$ and *Dmrt1*$^{-/-}$ P10 mouse seminiferous tubules as described elsewhere [263-265]. Briefly, tubules were prepared by sequential treatments of collagenase, DNase I, and trypsin, followed by sedimentation and low speed centrifugation, resulting in a cell preparation largely consisting of Sertoli cells and spermatogonia. DMRT1 antibody production and characterization were reported elsewhere and preliminary studies confirmed DMRT1 immunoprecipitation before and after formaldehyde treatment ([130] and data not shown). Immunoprecipitated and input DNAs were processed and and analyzed by CoFactor Genomics (St. Louis, MO) using Illumina Pipeline version SCS2.8.0 paired with OLB 1.8.062. Sequence was aligned using Novoalign version 2.07.05 (Novocraft Technologies, Selangor, Malaysia) and Bowtie [266] and normalized reads from both alignments were used with CLC Genomics Workbench (CLC Bio, Cambridge, MA) and MACS to identify peaks [267]. This uncovered roughly 150 peaks specific to the *Dmrt1*$^{+/+}$ IP DNA, which were considered potential DMRT1 binding sites. Sequence tags (BAM files) from all four samples (*Dmrt1*$^{+/+}$, *Dmrt1*$^{-/-}$ IP and input) were visualized on the UCSC Genome Browser, together with peak annotations to mark potential binding sites, which were manually curated to assess spatial spread, strand symmetry and peak density enrichment of *Dmrt1*$^{+/+}$ IP sample compared to negative controls (*Dmrt1*$^{-/-}$ IP, *Dmrt1*$^{+/+}$ input, *Dmrt1*$^{-/-}$ input) [268-271].

Quantitative real-time PCR

To validate ChIP-Seq and microarray results, real-time reactions were carried out as described elsewhere using a 7900HT Sequence Detection real time analyzer (Applied Biosystems, Foster City, CA)[185]. For microarray validation, RNA was isolated from *Dmrt1*$^{-/-}$, *Dmrt1*$^{-/-;tg}$ and *Dmrt1*$^{+/+}$ P7 testes and first-strand cDNA synthesized using 2ug RNA and MMLV reverse transcriptase (Invitrogen (Carlsbad, CA), following the manufacturer's instructions. Default cycle parameters were used to amplify a 1:10 dilution of cDNA with SYBR® Green PCR master mix (Applied Biosystems, Foster City, CA) and primers (supplementary Table 1). Samples were run in triplicate and included water as negative controls. C_t melting curves for ribosomal L7 (*Rpl7)* cDNA was used to calculate ΔC_t values for each sample. *Rpl7* C_t values did not vary across genotype and the melting curves for *Rpl7* and all analyzed genes gave a single peak that validated the absence of primer-dimer formation. $\Delta\Delta C_t$ values were calculated by subtracting the mean P7 wild type ΔC_t. Fold change was calculated using the $2^{-\Delta\Delta Ct}$ method [186].

Validation was performed on forty DMRT1 binding sites identified by ChIP-Seq. Quantitative real-time PCR was performed as above but with chromatin as template and primers spanning the binding site (Supplementary Table 2). For ChIP validation chromatin was prepared from P7 and P10 *Dmrt1*$^{+/+}$ and *Dmrt1*$^{-/-}$ testes.

DNA motif Analysis

Motif identification was performed on the top 5 identified DMRT1 binding sites, using MEME Suite sequence analysis tools [272]. MEME was run using default settings and the projected number of motifs was manually set to equal the number of input sequences. Similarity searches were performed using TOMTOM to compare the predicted binding motif to the existing

in vitro Dmrt1 binding sequence ([TCA][TGA]G[ACT][TA]ACA[TA]TGT[TA][GT][CTAG]) [273, 274].

Integrative Analysis

To identify direct targets of DMRT1, two separate analyses were performed to evaluate genes whose expression were altered in *Dmrt1*$^{-/-}$ or *Dmrt1*$^{-/-;tg}$ testes and contained a mapped DMRT1 binding peak within its proximal, distal or intronic regulatory region. Manual analysis was performed by integrating the differential gene expression obtained in *Dmrt1*$^{-/-}$ and *Dmrt1*$^{-/-;tg}$ samples (Table 2) with either previously published DMRT1 ChIP-chip binding site data ([a-c] in Tables 2, 3 and 4) (http://www.dmrt1.umn.edu/) or with our current ChIP-Seq data ([d-g] in Tables 2) to help predict true DMRT1 target genes [136]. In addition, ChIP-Array (http://jjwanglab.org/ChIP-Array), web-based free-software that integrates ChIP-Seq and microarray data was used as described elsewhere [275]. Briefly, 5537 peaks, with at least twenty tags located in binding site, were uploaded to ChIP-Array, which can identify sequences located within 8kb upstream and 2kb downstream of a gene's transcription start site (TSS). In order to identify all potential DMRT1-targets, all genes with a fold change greater than one (fold change ≥ 1) in *Dmrt1*$^{-/-}$ and *Dmrt1*$^{-/-;tg}$ testes were included in the analyses. The parameters for the ChIP-Array were set to -8kb to +2kb for regulatory region range, p-value for position weighted matrix scan was 10^{e-4}, p-value for conservation filtering was 0.01 and UCSC gene browser was selected search platform.

Results

Gene expression changes in P7 testes from Dmrt1$^{-/-}$ and Dmrt1$^{-/-;tg}$ mice.

Microarray analysis was used to obtain gene expression profiles from *Dmrt1*$^{-/-}$, *Dmrt1*$^{+/+}$, and *Dmrt1*$^{-/-;tg}$, generated by expressing DMRT1 to *Dmrt1*-null Sertoli cells using a *Wt1-Dmrt1* transgene, mouse testes at postnatal day 7, a time-point when germ cell radial migration is complete, spermatogenesis is beginning, and cellular levels of DMRT1 are at a maximum ([130]; as published in the dataset GSE926 [276]). Pairwise comparisons of the expression profiles from *Dmrt1*$^{+/+}$ and either *Dmrt1*$^{-/-}$ or *Dmrt1*$^{-/-;tg}$ identified 791 and 609 differentially expressed transcripts, i.e. with ≥ 2 fold change and $p < 0.05$, in *Dmrt1*$^{-/-}$ and *Dmrt1*$^{-/-;tg}$ samples, respectively (Table 1). Pairwise comparison of *Dmrt1*$^{-/-}$ and *Dmrt1*$^{-/-;tg}$ samples identified 37 differentially expressed transcripts in *Dmrt1*$^{-/-}$ relative to *Dmrt1*$^{-/-;tg}$. The results showed that transgenic return of DMRT1 to Sertoli cells restored expression of 219 transcripts whose expression was altered by at least 2fold or more in the testes of *Dmrt1*$^{-/-}$ mice.

In order to identify cell-specific gene expression changes, microarray data were examined for the most sensitive transcripts that were shared between or unique to the *Dmrt1*-null and *Dmrt1*-rescue testes. Given that the *Dmrt1*-null and *Dmrt1*-rescue testes both lacked DMRT1 in germ cells, gene expression changes that were identical, (or nearly so), in both groups were considered germ cell-specific (Figure 1), while gene expression profiles that were lost when DMRT1 expression was restored to Sertoli cells of *Dmrt1*$^{-/-}$ mice or unique to *Dmrt1*$^{-/-}$ mice, i.e. when DMRT1 is absent in both Sertoli cells and germ cells, were considered Sertoli cell-specific. After excluding duplicates from the 791 and 609 differentially expressed genes that met the cutoff criteria in *Dmrt1*$^{-/-}$ and *Dmrt1*$^{-/-;tg}$ testes samples, 704 and 516 genes were mapped to the IPA database, respectively. Comparative analyses on the mapped genes revealed 450 genes were equally changed in both *Dmrt1*$^{-/-}$ and *Dmrt1*$^{-/-}$ samples, indicating they were associated with DMRT1 actions in germ cells. In addition, 320 genes were rescued by the transgene, as they

were changed only in *Dmrt1*$^{-/-}$ samples, and were associated with DMRT1 activity in Sertoli cells (Figure 1). A second more stringent method was used to evaluate cell-specificity. In this case, a rescue factor (RF) was assigned to 718, 15 and 37 genes with RF < 0.5, RF < 1 and RF =1, respectively, were considered to be germ cell-specific, shared by germ cells and Sertoli cells, and Sertoli cell-specific, respectively. The results suggested that manual analysis is capable of identifying cell-specific differences that could be missed using computer-based methods.

To confirm gene expression profiles obtained by microarray experiments, quantitative PCR was performed on a subset of mRNA of genes characterized to be germ cell or Sertoli cell-specific. Microarray and qRT-PCR results were compared for 11 downregulated and 10 upregulated genes (Figure 2). The overall expression trend of down-regulated (Figure 2A) and up-regulated genes (Figure 2B) obtained in microarrays correlated with the expression trend observed in qPCR. For instance, *Dmrt1* was reduced 10 and 5 fold, *Clec12b* was reduced 7 and 4 fold, *Rarres1* was reduced 4 and 1.7 fold and *Lect1* was induced by 4.5 and 4 fold, in *Dmrt1*-null and *Dmrt1*-rescue testes, respectively. Thus, the qRT-PCR results support the microarray analyses and its ability to detect cell-specific gene expression changes is response to DMRT1 loss.

To gain insight on the temporal effects of DMRT1, gene expression profiles from this study were compared to those of previously reported for P1/P2 *Dmrt1*$^{-/-}$ and P9 *GCDmrt1KO* testes [132, 136]. Comparison of P7 *Dmrt1*-null testis transcriptome to those at P1 and P2, revealed about 40.3%, 42% and 17.5% were absent at P1/P2 (311 out of 770), showed a similar (up or down; 322 out of 770) and opposite (137 out of 770) trend at P7 and P1/P2, respectively. This suggested that almost half of the differential gene profiles present at P7 *Dmrt1*-null testes were silent at P1/P2. Similarly, comparison of differentially expressed genes between P7 *Dmrt1*-

rescue and P9 *GCDmrt1KO* testes revealed 72 genes were unchanged in P9 *GCDmrt1KO*, 2 were unchanged in P9 *GCDmrt1KO* and P7 *Dmrt1*-rescue testes, and 35 were unchanged in P7 *Dmrt1*-rescue but changed at P9 *GCDmrt1KO* testes. In addition, 660 changed in both P7 *Dmrt1*-rescue and P9 *GCDmrt1KO* testes, of these, 434 changed in a similar direction of which 402-showed change that is more robust at P7 *Dmrt1*-recue than P9 *GCDmrt1KO* testes. The results suggested that a significant number of transcripts in the *Dmrt1*-null samples at turned-on at P7 that were off at P1/P2 and the P9 *GCDmrt1KO* sample, generated by *Ngn3*-Cre-mediated conditional deletion of *Dmrt1* in germ cells, and P7 *Dmrt1*-rescue sample, generated by returning DMRT1 to *Dmrt1*-null Sertoli cells, share a significant gene expression profile.

Characterization of DMRT1 binding sites and putative target genes

ChIP-Seq was used to identify DMRT1 binding sites on a genome-wide scale. The UCSC Genome Browser (http://genome.ucsc.edu/cgi-bin/hgGateway) was used to visualize BAM and annotated peak files and the top scoring peaks unique to $Dmrt1^{+/+}$ immunoprecipitated sample (~150) were manually curated to assess spatial spread, strand symmetry and peak density of the $Dmrt1^{+/+}$ immunoprecipitated sample relative to the negative controls ($Dmrt1^{-/-}$ chip, $Dmrt1^{+/+}$ input, $Dmrt1^{-/-}$ input). Binding site characteristics (chromosome and relation to predicted gene) showed that 87% of DMRT1 binding sites mapped within introns, 6.5% mapped within 3′ end and 6.5% within an intron and 5′ end (Table 3A). Thirty-one genes in-close proximity to the peaks enriched for $Dmrt1^{+/+}$ immunoprecipitated sample were confirmed by ChIP-qPCR. All genes except *Taok3* were found to be enriched in the $Dmrt1^{+/+}$ immunoprecipitated DNAs compared to the IgG immunoprecipitated DNAs using real time quantitative PCR (*qChIP, Table 3B). The average binding affinity for qPCR in the $Dmrt1^{+/+}$ immunoprecipitated DNAs was 11 fold over IgG immunoprecipitated DNAs and range between 4 and 20 fold (Table 3A).

The results suggested that the false discovery rate for peaks identified in this study was about 3%.

To predict putative *in vivo* binding motifs for DMRT1, MEME and TOMTOM analyses were performed on the top five DMRT1 binding site sequences[272, 273]. Using MEME, two motifs, logo one (CAG[AT]C[AT]G[AT]CA[CT][AG]TGT[GT]) and logo two (CG[GC]A[CA]T[GC]G[TA]GCGA), were identified with an elevated statistical significance (E-value = $3.4E^{-7}$). Similarities in ACA and TGT nucleotide bases were observed between the *in vitro Dmrt1* consensus logo ([TCA][TGA]G[ACT][TA]ACA[TA]TGT[TA][GT][CTAG]) (Figure 3A) and logo one (CAG[AT]C[AT]G[AT]CA[CT][AG]TGT[GT])(Figure 3B) . Using TOMTOM to search for transcription factors similarities in binding sites to logo two (CG[GC]A[CA]T[GC]G[TA]GCGA) revealed the binding sites ([AGT][AT]TGTTGC[GCA][ATG][ATG][TG][TGCA]) for male abnormal3 (mab3), with 77% (10 out of 13) binding site similarity (Figure 3C).

Pathway comparison of P7 Testes

To categorize the functions of genes specifically regulated by DMRT1 in germ cells and Sertoli cells, the RF was used to select genes for IPA. From the list of 718 genes that were assigned to germ cells with RF < 0.5, canonical pathway analysis using IPA revealed enrichment of VDR/RXR and RAR activation, ATM and FLT3 signaling, role of Nanog in pluripotency and immune response pathways (IL-4 and NFAT; Table 4A, upper panel). Pathways enriched in the 37 genes with RF = 1, which were assigned to Sertoli cells included lipid (sphingolipid and glycerolipid) metabolism, biosynthesis (methyl group amino acids, pantothenate and CoA) and bladder cancer signaling (Table 4A, lower panel). Functional clustering using IPA revealed

enrichment of male gamete generation, apoptosis, cell adhesion, sex differentiation and morphogenetic processes in germ cells (Table 4B, upper panel), whereas infertility, cell-cell contact, cholesterol ester metabolism, RNA and kinesin binding were processes enriched in Sertoli cells (Table 4B, lower panel).

DAVID was used to obtain gene ontology terms and pathways for subset of genes identified by comparing gene expression profiles from *Dmrt1*-null testes at P1/P2 and P7 or P7 *Dmrt1*-rescue and P9 *GCDmrt1KO* testes (Table 5). For the genes absent in P1/P2 *Dmrt1*-null testes, biological processes including piRNA metabolic processes, RNA binding and nuclear RNA export factor complex were represented, whereas pathways including ubiquitin (Ubl) conjugation and axon guidance were enriched (Table 5A). Processes and pathways that were enriched in subset of genes with opposite or similar gene expression changes at P1/P2 and P7 included male gamete generation, sex differentiation, regulation of protein localization, apoptosis, p53 signaling, cell cycle, antigen processing and presentation, and cell adhesion molecules pathways (Tables 5 B and C). The subset of genes absent in P7 *Dmrt1*-rescue sample were implicated in the organization of the cytoskeleton and in panthotenate and CoA biosynthesis, while those absent in P9 *GCDmrt1KO* samples were important in cell-cell junction and p53 signaling (Tables 5 D and E). In addition, the subsets of genes with opposite or similar gene expression changes in P7 *Dmrt1*-rescue and P9 *GCDmrt1KO* were represented by biological processes and pathways that include lipid localization, cell cycle, cell proliferation, lipid transport, spermatogenesis and protein localization (Tables 5 F and G). Overall, these results showed temporal gene regulation by DMRT1 whereby at P1/P2, DMRT1 directs male gamete generation, cell cycle and protein localization, which were maintained at P7 and P9. At P7, functions in lipid localization, lipid transport and cell-cell junction are turned on that were

absent at P1/P2 but sustained at P9. Apoptosis was predominant at P1/P2 and P7 but absent at P9. Unique functions in piRNA metabolic processes, cell-cell junction and RNA binding were enriched only at P7; and at P9, the regulation of cytoskeleton organization was enriched.

To further understand and reveal potential novel functions for DMRT1, DAVID and ExoCarta was used to identify functional clusters within a subset of about 100 genes (Table 6). The functions that were enriched include cell death/survival, pluripotency marker, cell junction, exosomes, adhesion, meiosis, RNA binding, migration, integrin binding, cancer and ubiquitination (Table 6). Ubiquitination was implicated by marked changes in several genes encoding MAGE cancer testis antigens (MAGE11, K1, & B16) and TRIM E3 RING ubiquitin ligases (TRIM71, 12, & 34). Vesicle transport was implicated when it was noted that 13 genes misregulated in *Dmrt1*-null testes were previously identified components of exosomes, vesicles used for intercellular communication that transfer membrane components and nucleic acid between cells (ExoCarta). Remarkably, mRNAs for all except *Foxq1, Gfra1, Rarres1, Tuba3a, Cadm1* and *Piwil2* increased with *Dmrt1* loss, and included *Dppa3, Cpne8, Mid1, Aqp5, H2Aa, BM117570* (long ncRNA), *Hspb8, Krt18, Krt8, Cfi, Rsp9, Ano4, and Fbln2* (Table 6). Return of DMRT1 to Sertoli cells entirely restored *Cpne8, BM117570, Mid1* and *Rarres1*, partially restored *Rsp9* expression and did not restore the rest. The results revealed functions relevant to testis biology including ubiquitination and vesicular transport that have not been associated to DMRT1 until now.

Direct targets of DMRT1

To identify direct targets and pathways of DMRT1, integrative analyses were performed using P7 testes gene expression profiles and ChIP-Seq. Two methods were used to integrate the

ChIP-Seq and microarray data to identify putative DMRT1 targets. The first method consists of manually evaluating the a subset of 770 differentially expressed genes in this study for the desired peak quality in the ChIP-Seq analyses. This analysis revealed 30 targets that were differentially expressed and contained a DMRT1 binding site (Table 7). Of these, *Usp9y*, *Plekhg1* and *Boll* were novel targets identified by ChIP-Seq analyses (Table 7). The importance of these direct targets in testis development is highlighted by the roles of *Boll* and *Usp9y* in germ cell differentiation and male infertility, respectively [277, 278]. The basis of second method was the same to the first but it utilized a web-based freeware, the ChIP-Array, to integrate and query the gene expression (7403 probe sets) and ChIP-Seq (5537 MACS peaks) data. This analysis identified 58 direct targets (Figure 4) and six of these targets (*Tlr7, Unc45a, Clec1a, Zfp606, Ccnf, Kcnh1*) were previously identified as DMRT1 targets elsewhere [136].

Pathways and processes directly regulated by DMRT1

The list of target genes (Table 3 B) was also evaluated for functional associations but because the number of functionally annotated target genes was small, limited information was gained from standard bioinformatics. Therefore, biological profiles were developed from information extracted from the literature and homology to known proteins. This identified several biological areas highly represented by DMRT1 target genes (Table 3B). These included cell adhesion/structure (Group 1), RNA processing/metabolism (Group 2; binding, transport, and regulation), protein modification/transport (Group 3), and DNA damage and repair (Group 4). Within these, cilia biogenesis, cell cycle control, and cell migration were also emphasized. Other areas (composite Group 5) included cell signaling/communication and lipid metabolism. These results favored the elucidation of pathways and processes directly influenced by DMRT1 in Sertoli cells and germ cells.

Discussion

The mammalian testis is the primary site for spermatogenesis and is comprised of four main cell types that include Sertoli cells and germ cells. The development of germ cells and maturation of Sertoli cells are known to be regulated by the transcription factor, DMRT1 [50, 131, 133]. Thus, studying the cell-specific roles of DMRT1 in Sertoli cells and germ cells is of great importance. The present study used cell-specific DMRT1 expression mouse models to systematically study functions of *Dmrt1* in Sertoli cells and germ cells.

Microarray identified global gene expression changes

The expression of DMRT1 in both Sertoli cells and germ cells makes it an extraordinary transcription factor with cell-specific regulatory capabilities for differential expression of direct or indirect target genes. DMRT1 exhibits auto-regulation and its mRNA levels were reduced by 97 and 92 fold in germ cells from *Dmrt1*$^{-/-}$ and *Dmrt1*$^{-/-;tg}$ testes, respectively. The gene expression change for *Dmrt1* was assigned to germ cells for the purpose of analysis because peak expression of DMRT1 that occurs between P6-P9 coincides with increased expression contributed by the multiplying number of spermatogonia, which accounts for a significant amount of total DMRT1 levels ([130]; dataset GSE926 [276]). Thus, the fold difference in *Dmrt1* mRNA level in both *Dmrt1*-null and *Dmrt1*-rescue testes was not statistically significant, but the five-fold enrichment in the *Dmrt1*$^{-/-;tg}$ testes was sufficient for translation and expression of DMRT1 in Sertoli cells that partially restored tubule morphology and integrity in the adult male mice as previously described elsewhere (Chapter 2). Furthermore, the mRNA levels of *Dmrt1* and 19 other genes were confirmed by qPCR (Figure 2). The results revealed a similar expression trend but the magnitude fold change obtained by qPCR was inferior in most cases to those obtained by microarrays. Examples of genes differentially expressed in germ cells and

validated by qRT-PCR include *Clec12b, Lin28, Cidea Plzf, Cfi* and *Lect1*, while that regulated in Sertoli cells was *Rarres1*. *Clec12b* belongs to a C-type lectin-like family and serves as a receptor in myeloid cell function during activation of an immune response [279]. *Lect1* is a cartilage matrix protein shown to inhibit angiogenesis and suppress T-cell responses [280]. *Rarres1* is a tumor suppressor gene shown to regulate differentiation and proliferation of adipose tissue-derived mesenchymal stem cells [281].

The pattern of cell-specific global gene expression profiles regulated by transcription factors like DMRT1 typically occurs through age-dependent activation or repression of the transcription of its target genes. Evaluation of the global gene expression profiles at P1/P2 and P9 revealed 118, 759 and 852 genes were misregulated in *Dmrt1*-null, *SCDmrt1KO* and *GCDmrt1KO* testes, respectively [132, 136]. Consistent with these previous studies, evaluation of P7 *Dmrt1*$^{-/-}$ and *Dmrt1*$^{-/-;tg}$ testes revealed that 791 and 608 genes were misregulated (Figure 1 and Table 1), respectively. The trend suggest that the number of genes regulated increases from P1/P2 to P7 to P9 and overlaps with the increasing cellular levels of DMRT1, which peaks between P6 and P9 in the mouse testes ([130]; GSE926 dataset [276]). In addition, the results in this current study suggested that the return of DMRT1 to *Dmrt1*-null Sertoli cells via a *Wt1-Dmrt1* transgene reduced the number of genes that were misregulated in Sertoli cells. Furthermore, comparing the gene expression profiles of the *Dmrt1*-null testes at P1/P2 revealed that of the total number of genes that met the cutoff criteria in the P7 *Dmrt1*-null testes, 40.31 % and 42% were absent and misregulated at P1/P2, respectively (Table 2B). Likewise, comparison of the gene expression profiles of P9 *GCDmrt1KO* and P7 *Dmrt1*-rescue revealed that 5% of genes misregulated at P9 were absent at P7, 9% of genes misregulated at P7 were absent at P9 and 56% of the genes were misregulated at P7 and P9 (Table 2C). Examples of genes that were

misregulated from P1 through P9 include the continuous increased expression of *Cfi* and decreased expression of *Nkx3-1*, both of which are expressed in germ cells, and thus confirms their role in blocking the transition of primordial germ cells to gonocytes as was previously observed elsewhere [132]. Overall, the various mouse models of cell-specific DMRT1 expression share significant similarities in global gene expression profiles, despite differences in age of the biological samples and method used for cell-specific targeting (conditional deletion vs. transgene expression).

Novel DMRT1-targets identified by ChIP-Seq

Continuous efforts have been made to identify DMRT1-target genes and thus the functions of DMRT1. However, varied conclusions have been drawn using different models. Using ChIP-chip, 1434 targets were identified on P9 testes derived from cell-specific mouse models generated by Cre-mediated conditional deletion of *Dmrt1* in germs cells (*GCDmrt1KO* or GC-KO; used *Ngn3*-Cre) and Sertoli cells (*SCDmrt1KO* or SC-KO; used *Dhh*-Cre) compared to Cre controls [136]. Consistent with previous findings, ChIP-Seq analyses in this study identified approximately two hundred binding sites that were enriched in the $Dmrt1^{+/+}$ immunoprecipitated sample compared to all negative controls ($Dmrt1^{-/-}$ chip, $Dmrt1^{+/+}$ input, $Dmrt1^{-/-}$ input) as previously described elsewhere (Figure 4 and Tables 3 and 7; [268, 269]). The three negative controls, while reducing the total number of peaks identified, significantly improved the quality of the data by eliminating false positives and thus enriching for the most promising DMRT1 binding sites. Surprisingly, most DMRT1 binding sites were found within introns (87%) (Table 3A), suggesting it functions predominantly through distal enhancers. Many putative targets are relatively uncharacterized, while others have known or implicated functions in spermatogenesis (e.g. *Gfra1*, *Boll* and *Spag1*) and neurogenesis (e.g. *Gfra1*, *Ntm*, *Nlgn1*) [279, 282-287]. In

contrast to a previous study that identified about 1400 targets, all identified binding sites in this current study are novel; having escaped detection by previous methods that used promoter arrays [136]. Further evaluation of DMRT1-associated binding sites using the top five DNA binding site sequences revealed a close match to the *in vitro* DNA-binding motif, having 40% conservation of the nucleotides (Figure 3B). More similarity searches using TOMTOM identified a second motif closely related to male abnormal-3 (mab3), which had a 77% similarity to the putative DMRT1 binding site (Figure 3C). These results suggest that DMRT1 interacts directly by binding to a defined regulatory element. These results differ but are consistent to similar findings that analyses of potential DMRT1 regulatory element identified atleast two regions with 70% and 77% similarity to the characterized *in vitro* sequence [136].

Different biological processes are regulated by DMRT1

The biological processes regulated by DMRT1 in Sertoli cells and germ cells were identified using IPA, DAVID and ExoCarta. Evaluation of pathways in genes misregulated in *Dmrt1*-null revealed a tendency for DMRT1 to influence the transcription of genes involved in pathways of pluripotency, immune response, VDR/RXR activation ATM and IL-4 signaling; and lipid metabolism and pantothenate and CoA biosynthesis in Sertoli cells (Table 3A). Functions enriched in germ cells include maturation of male gamete generation, spermatogenesis, and sex differentiation, whereas functions enhanced in Sertoli cells include RNA binding, infertility, cell-cell contact and kinesin binding (Table 3B). These findings are consistent with those from previous studies which showed enrichment of biological processes that included antigen presentation, retinoic acid signaling, FSH receptor, GDNF and tachykinin 2 signaling, eicosanoid and nuclear receptor metabolism, immune response and pluripotency [132, 136]. However, although the pathways at P1/P2 were informative and deduced from pre-existing knowledge of

testicular targets and pathways, they were not statistically significant due to the limited number of focus molecules associated with each pathway. For instance, GDNF pathway was enriched because *Ret* and *Gfra1* were differentially express or retinoic acid signaling was overrepresented due to altered expression of *Crabp II.* Thus, although genes like *Ret*, *Gfra1*and *Crabp II* were differentially expressed in our study, their associated pathways were not statistically significant in the IPA database.

Further analyses using DAVID and ExoCarta revealed the potential role for DMRT1 in ubiquitination and vesicular transport. Ubiquitination was implicated by marked changes in several genes encoding MAGE cancer testis antigens (MAGE11, K1, & B16) and TRIM E3 RING ubiquitin ligases (TRIM71, 12, & 34) and by the recent report showing MAGE and TRIM proteins interact to mediate substrate ubiquitination [288]. Vesicular transport was highlighted when mRNA of 13 genes found to be expressed in exosomes were misregulated in *Dmrt1*-null testes (Table 6). These results open-up more questions on the possible regulatory and communication mechanisms between and/or within Sertoli cells and germ cells. Thus, it is plausible that DMRT1 uses ubiquitination to regulate differentiation of Sertoli cells or exosomes for communication between Sertoli cells and germ cells. However, further experiments will be needed to test these hypotheses.

In addition, biological processes enriched in DMRT1-targets and regulated genes were examined to help conceive a hierarchy for the DMRT1 network. This identified commonalities used to predict biological areas most relevant to DMRT1 function and consequently its control over spermatogenesis. Four areas were identified: 1) protein processing/transport, 2) cell adhesion/cytoskeletal regulation, 3) RNA processing, and 4) DNA recombination/repair. Protein

processing/transport derives from features of up-regulated genes (glycosylated, secreted/membrane proteins) that connect to Group 3 target genes via functions in protein modification (glycosylation, peptidase, thiol exchange) and vesicle-mediated transport. Cell adhesion/cytoskeletal regulation emerged from correlations between up-regulated gene processes (morphogenesis, cell junctions, cytoskeletal regulation) and Group 1 targets. Down-regulated genes were highly enriched for genes involved in RNA processing (binding, metabolism, expression) and DNA recombination/repair; two groups represented by target genes (Groups 2 and 4, respectively).

Integration of the gene expression profiles and binding site data followed by functional analyses facilitated the identification of pathways and processes directly regulated by DMRT1 in Sertoli cells and germ cells. For example the requirement of *Bcat* and *Stk4* in pantothenate and CoA biosynthesis, makes this pathway to be directly controlled by DMRT1 in Sertoli cells. Whereas the involvement of *Fcgrb2*, *Taf7*, *Ncoa2*, and *Fgfr2* in the role of NFAT in immune response, pluripotency and nuclear horme activation and metabolism make these pathways to be directly regulated by DMRT1 in germ cells. Some of these pathways are consistent with those previously reported [136].

In conclusion, the present study shows that DMRT1 regulates distinct pathways and processes in Sertoli cells and germ cells by regulating the basal transcription of its target genes. In addition, expression of DMRT1 in germ cells directly regulated pathways involved in immune response, pluripotency, and ATM signaling; and functions in male gamete generation, spermatogenesis and sex differentiation. On the other hand, its expression in Sertoli cells drives pathways of lipid metabolism and pantothenate and CoA biosynthesis, while also influencing

infertility, cell-cell contact, RNA and kinesin binding. These biological processes and their associated genes have been inferred by *in silico* modeling methods using fixed database information and as such can only be regarded as a source of hypotheses. Most of these associations are acceptable in a variety of physiological and diseased states, but does not establish that the genes in these pathways interact in a similar fashion *in vivo*. Thus, functional testing will be needed to evaluate these individual molecular relationships directed by DMRT1 that are essential for germ cell development and Sertoli cell differentiation.

Figure 1: Strategy for identifying cell-specific gene expression changes using the Ingenuity Pathway Analysis (IPA) software.

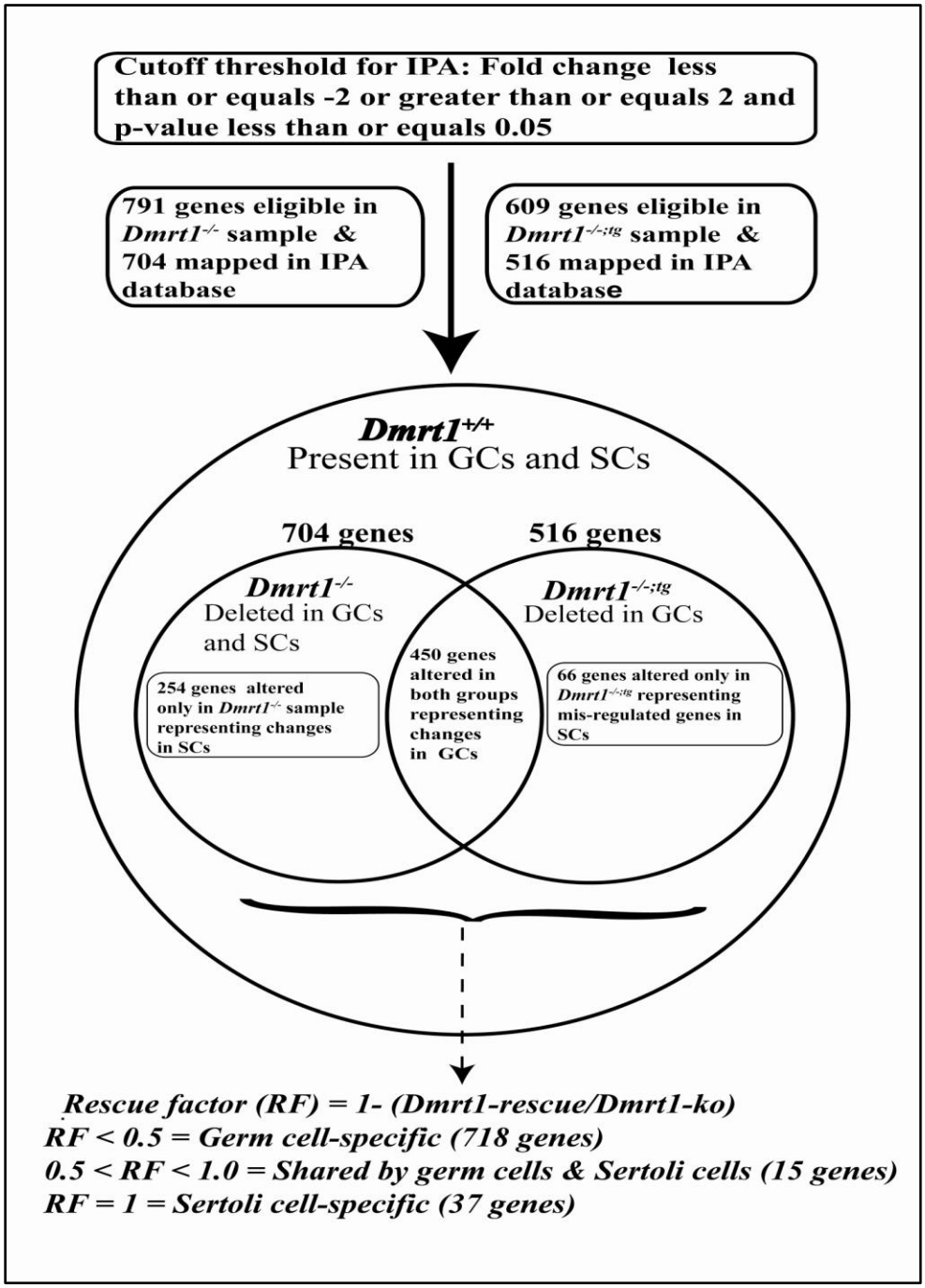

Figure 2: Validation of differentially expressed transcripts by quantitative PCR. A. Down-regulated genes in microarray maintained a similar expression pattern by qPCR in *Dmrt1*$^{-/-}$ or *Dmrt1*$^{-/-;tg}$ relative to *Dmrt1*$^{+/+}$ samples. **B.** Expression patterns of up-regulated genes were similar comparing microarray and qPCR in *Dmrt1*$^{-/-}$ or *Dmrt1*$^{-/-;tg}$ relative to *Dmrt1*$^{+/+}$ samples. Stippled and striped bars are microarray expression in *Dmrt1*$^{-/-}$ and *Dmrt1*$^{-/-;tg}$ samples, respectively, relative to microarray expression in *Dmrt1*$^{+/+}$ samples. Black and clear bars are qPCR expression in *Dmrt1*$^{-/-}$ and *Dmrt1*$^{-/-;tg}$ samples, respectively, relative to microarray expression in *Dmrt1*$^{+/+}$ samples.

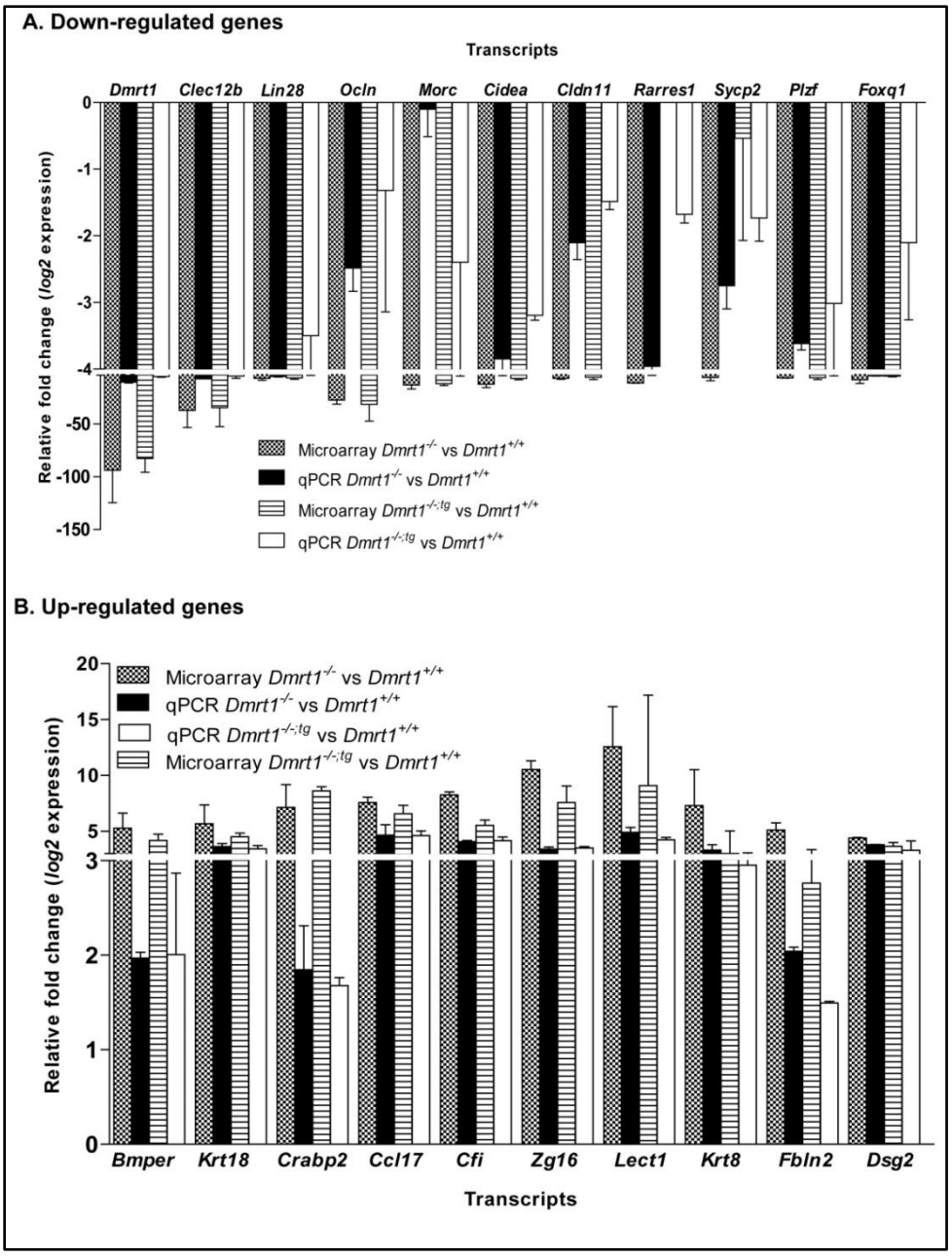

Figure 3: Comparison of DMRT1 in vitro identified consensus binding sequence to putative binding sites identified using MEME and TOM TOM.

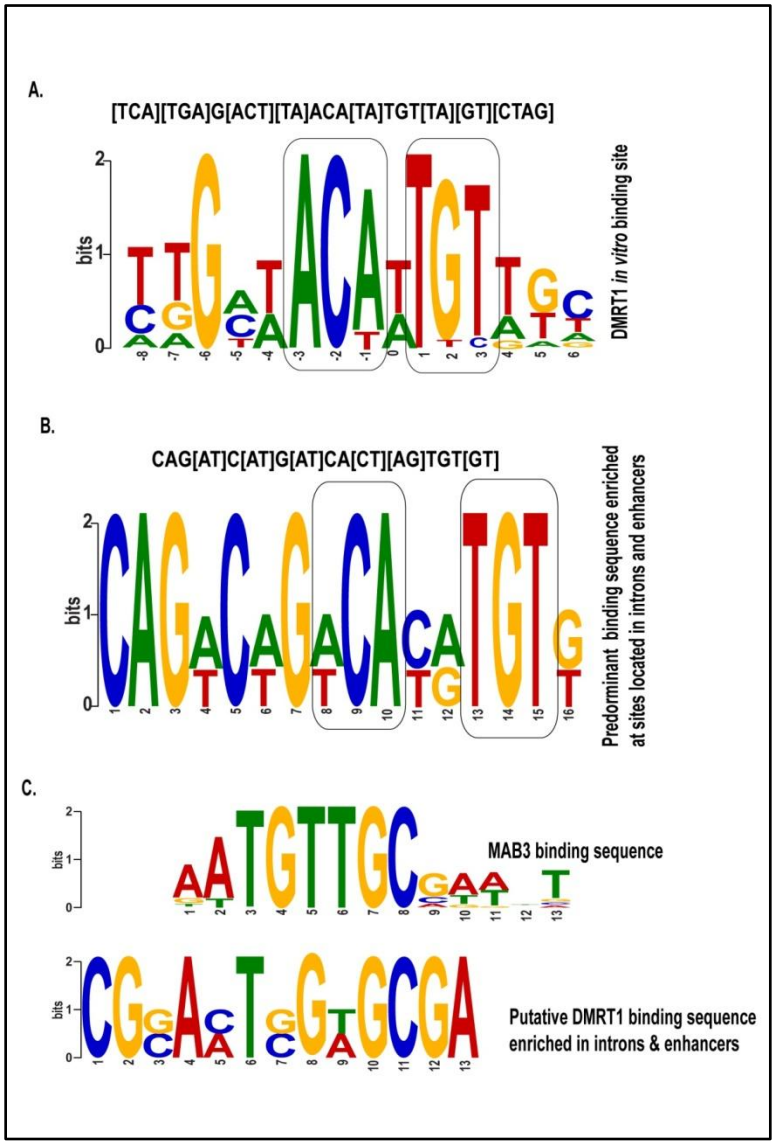

Figure 4: DMRT1 targets identified using ChIP-Array.

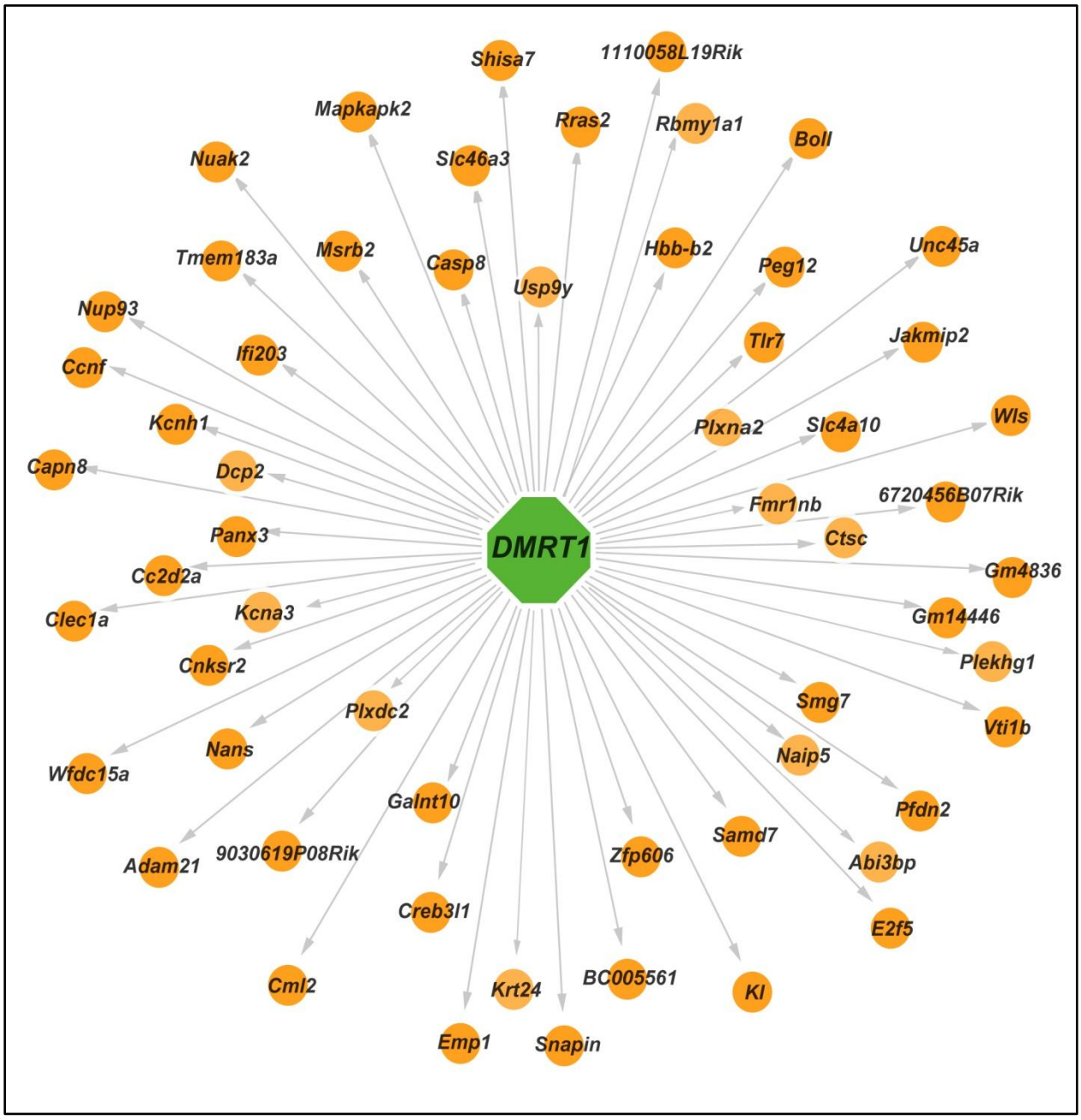

Table 1: Summary of fold changes and number of differentially regulated genes by microarray from *Dmrt1*$^{-/-}$ or *Dmrt1*$^{-/-;tg}$ samples compared to *Dmrt1*$^{+/+}$ samples.

Comparison	Fold change ≥3.0	Fold change > 2.0	2 > Fold change ≥1.00
Significantly elevated in *Dmrt1*$^{-/-;tg}$ vs *Dmrt1*$^{+/+}$	34 genes	138 genes	3346 genes
Significantly reduced in *Dmrt1*$^{-/-;tg}$ vs *Dmrt1*$^{+/+}$	139 genes	298 genes	3455 genes
Significantly elevated in *Dmrt1*$^{-/-}$ vs *Dmrt1*$^{+/+}$	59 genes	167 genes	3874 genes
Significantly reduced in *Dmrt1*$^{-/-}$ vs *Dmrt1*$^{+/+}$	190 genes	375 genes	3543 genes
Significantly elevated in *Dmrt1*$^{-/-}$ vs *Dmrt1*$^{-/-;tg}$	0 genes	7 genes	1627 genes
Significantly reduced in *Dmrt1*$^{-/-}$ vs *Dmrt1*$^{-/-;tg}$	9 genes	21 genes	1161 genes

Table 2: Transcripts (769 genes) differentially regulated in germ cells and Sertoli cells that met the cutoff criteria and represents genes shared by or unique to *Dmrt1*$^{-/-}$ and *Dmrt1*$^{-/-;tg}$ testes. Up or down denotes similar gene expression trend reported in previous studies. Letters a-g denotes gene has been identified as a target of DMRT1 by ChIP-chip or ChIP-Seq. **A.** List of 769 genes comparing expression of Dmrt1-null at P7 to previous results at P1/P2 and comparing Dmrt1-rescue expression at P7 to those of GCDmrt1KO previously published at P9. **B.** Summary of transcript expression trends at P7 and P1/P2 in *Dmrt1*-null testes. **C.** Summary of transcript expression trends between *Dmrt1*-rescue and *GCDmrt1KO* testes.

A	**P7 *Dmrt1* -null / *Dmrt1* - Wt**	**P1 *Dmrt1* - null / *Dmrt1* - Wt**	**P2 *Dmrt1* - null / *Dmrt1* -Wt**	**Comparison of *Dmrt1* - null testes expression at P7 and P1/P2**	**P7 *Dmrt1* - rescue / *Dmrt1* - Wt**	**P9 *GCDmrt1KO* / *GCDmrt1KO* - Ctrl**	**Comparison of P7 *Dmrt1* - rescue and P9 *GCDmrt1KO***		
Symbol	**P7 Fold Change**	**P1 Fold Change (Data from Fahrioglu et al., 2007)**	**P2 Fold Change (Data from Fahrioglu et al., 2007)**	**Up, down, absent at P1/P2, absent at P7**	**P7 Fold Change**	**P9 Fold Change (data from Murphy et al., 2010)**	**Up, down, absent at P9, absent at P7, absent at P7 and P9 (compared to P7 *Dmrt1* -null)**	**P7 Relative factor (RF) = 1-((Res/Wt)/(Ko/Wt))**	**Comparison to previous to ChIP-chip (a-c) and current ChIP-Seq (d-g) data**
DMRT1	-97.38	-16.74	-16.79	down	-91.07	-2.21	down	**0.06**	
CLEC12B	-38.67			absent at P1/P2	-32.42	-1.79	down	**0.16**	
MAGEA11	-29.40			absent at P1/P2	-13.95	-1.33	down	**0.53**	a
Ocln	-26.67	-7.23	-12.27	down	-23.82	-1.48	down	**0.11**	
NKX3-1	-18.56	-5.05	-3.52	down	-11.60	-1.45	down	**0.38**	
CYTIP	-14.26	-2.18	-2.89	down	-8.26	-1.57	down	**0.42**	
MORC1	-12.41			absent at P1/P2	-11.94	1.22	up at P9	**0.04**	
CIDEA	-12.07	-5.25	-8.38	down	-6.73	-1.26	down	**0.44**	
RARRES1	-11.50			absent at P1/P2			absent at P7 and P9	**1.00**	
TRIM71	-10.40			absent at P1/P2	-10.86	-1.37	down	**-0.04**	
SH3GL2	-9.43	-3.09	-4.98	down	-4.25	-1.78	down	**0.55**	
TEX11	-9.23			absent at P1/P2	-2.92	-1.06	down	**0.68**	
ZBTB16	-9.22	-2.37	-1.88	down	-8.94	1.03	up at P9	**0.03**	
RIPK4	-8.47			absent at P1/P2	-7.06	-1.60	down	**0.17**	a
NEFM	-8.47	-1.64	-1.33	down	-9.03	1.18	up at P9	**-0.07**	
FOXQ1	-7.67	-4.03	-2.83	down	-5.18	-1.59	down	**0.33**	
DDX4	-7.51	1.04	-1.24	up at P1 and down at P2	-4.95	1.08	up	**0.34**	C
CADM1	-7.36	-1.96	-2.03	down	-6.61	-1.06	down	**0.10**	
RNF17	-7.28			absent at P1/P2	-2.98	1.37	up	**0.59**	
RSPO2	-7.26	1.24	1.39	Up at P1/P2	-7.61	-1.95	down	**-0.05**	
RBMY1A1	-7.09			absent at P1/P2	-2.63		absent at P9	**0.63**	e,f
TBC1D30	-6.81			absent at P1/P2	-4.97	-1.41	down	**0.27**	
CLDN11	-6.71	-1.25	-1.69	down	-5.27	-1.23	down	**0.21**	a
VDR	-6.71	-1.55	-1.74	down	-6.00	-1.29	down	**0.11**	b
SCARA3	-6.54			absent at P1/P2	-5.19	-1.66	down	**0.21**	
HLA-A	-6.42	-1.21	-1.05	down	-5.89	-1.15	down	**0.08**	
Acaa1b	-6.40	1.16	1.33	Up at P1/P2	-5.57	-1.02	down	**0.13**	
NXF3	-6.06			absent at P1/P2	-3.45	-1.78	down	**0.43**	
JAKMIP1	-5.98			absent at P1/P2	-5.94		absent at P9	**0.01**	
SALL4	-5.90	-1.20	-1.05	down	-9.01		absent at P9	**-0.53**	
FGF13	-5.89	-2.13	-2.54	down		-1.33	absent at P7	**1.00**	
AFP	-5.71	1.46	2.43	Up at P1/P2	-4.86	1.16	up at P9	**0.15**	
TSPAN17	-5.68			absent at P1/P2	-5.23	-1.63	down	**0.08**	
RBM44	-5.61			absent at P1/P2	-3.54	1.31	up at P9	**0.37**	
STARD4	-5.61			absent at P1/P2	-4.97	-1.05	down	**0.11**	
IGF2BP1	-5.60	-1.26	-1.29	down	-5.13	-1.19	down	**0.08**	
EGR2	-5.58	-1.97	-3.15	down	-5.72	-1.51	down	**-0.02**	
GFRA1	-5.50	-2.15	-2.44	down	-4.86	-1.23	down	**0.12**	
GPR37	-5.39	1.92	1.25	Up at P1/P2	-2.65	-1.52	down	**0.51**	
TNNT2	-5.38	1.00	-1.53	up at P1 and down at P2	-1.53	-1.10	down	**0.71**	
ASB9	-5.37			absent at P1/P2	-4.97	-1.45	down	**0.07**	
RICTOR	-5.37			absent at P1/P2	-4.04	1.04	up at P9	**0.25**	
DAZ2	-5.37	-1.10	-1.06	down	-3.50	1.04	up at P9	**0.35**	
PIP5K1B	-5.31	-1.94	-1.78	down	-4.40	-1.26	down	**0.17**	
SYCP2	-5.30			absent at P1/P2	-1.80	1.70	up	**0.66**	
ACSS1	-5.20	-1.72	-1.70	down	-4.43	-1.55	down	**0.15**	
MEIG1	-5.18	-1.43	-1.09	down	-6.22	-1.11	down	**-0.20**	
TBX22	-5.12			absent at P1/P2	-5.05	-2.30	down	**0.01**	b
C20orf54	-5.11			absent at P1/P2	-3.71	-1.19	down	**0.27**	
TKTL1	-5.11	1.11	1.13	Up at P1/P2	-2.36	1.20	up at P9	**0.54**	
GLIS3	-5.09			absent at P1/P2	-4.71	1.04	up at P9	**0.08**	f

LIN28A	-5.06			absent at P1/P2	-4.83	1.22	up at P9	**0.04**	
TUBA3E	-5.05	-1.15	-1.47	down	-4.01		absent at P9	**0.21**	
DDX25	-5.00	1.16	1.11	down	-6.05	-1.09	down	**-0.21**	c
LPAR3	-4.93			absent at P1/P2	-5.25	-2.18	down	**-0.07**	
NTN4	-4.92			absent at P1/P2	-3.56	-1.16	down	**0.28**	
PPHLN1	-4.88			absent at P1/P2	-4.09		absent at P9	**0.16**	
PIWIL2	-4.88			absent at P1/P2	-4.98	1.31	up at P9	**-0.02**	
WNK3	-4.83			absent at P1/P2	-4.38		absent at P9	**0.09**	
ENPP2	-4.82	-1.46	-2.33	down	-5.28	-1.87	down	**-0.10**	
TOX	-4.76			absent at P1/P2	-4.93	-1.37	down	**-0.04**	
CLIC6	-4.75			absent at P1/P2	-5.90	-1.39	down	**-0.24**	a
BASP1	-4.70	1.09	1.14	Up at P1/P2	-4.93	-1.99	down	**-0.05**	
TCFL5	-4.67			absent at P1/P2	-4.03	1.37	up at P9	**0.14**	
SLC25A31	-4.62			absent at P1/P2	-2.84	1.17	up at P9	**0.38**	
RAB11FIP4	-4.61			absent at P1/P2	-4.46	-1.11	down	**0.03**	
NMT2	-4.59	-1.21	-1.47	down	-3.44	-1.01	down	**0.25**	
SCML2	-4.53			absent at P1/P2	-2.82	-1.11	down	**0.38**	
LPPR4	-4.46			absent at P1/P2	-2.61	-1.49	down	**0.41**	
Taf7l	-4.40			absent at P1/P2	-2.27	1.06	up at P9	**0.48**	
DOCK3	-4.34			absent at P1/P2	-4.52	1.86	up at P9	**-0.04**	
MOV10L1	-4.33			absent at P1/P2	-3.44	1.47	up at P9	**0.20**	
FOXC2	-4.31	-1.86	-1.70	down	-5.22	-1.42	down	**-0.21**	
CDO1	-4.27	-1.21	-1.48	down	-2.92	-1.71	down	**0.32**	
FOXF1	-4.25	-1.11	-1.04	down	-4.76	-1.41	down	**-0.12**	
TCL1A	-4.23	-1.20	-1.33	down	-4.72	1.79	up at P9	**-0.11**	
BIK	-4.20	-1.44	-1.38	down	-3.59	-1.80	down	**0.15**	
JAKMIP2	-4.19			absent at P1/P2	-2.99	-1.01	down	**0.29**	
TSC22D3	-4.10			absent at P1/P2	-3.31		absent at P9	**0.19**	
RIMKLB	-4.10	-1.15	-1.40	down	-3.12	-1.08	down	**0.24**	
NXF2	-4.08			absent at P1/P2	-2.53		absent at P9	**0.38**	
FKBP6	-4.05			absent at P1/P2	-3.35	-1.06	down	**0.17**	b
SLC1A6	-4.04	-4.15	-3.48	down	-2.84	1.04	up at P9	**0.30**	
ELAVL2	-4.01	1.20	-1.10	up at P1 and down at P2	-4.17	-1.32	down	**-0.04**	
NEUROG3	-3.99	-1.15	1.32	Down at P1 and up at P2	-4.25	-1.14	down	**-0.07**	
FRZB	-3.98	1.03	-1.01	up at P1 and down at P2	-4.16	-2.42	down	**-0.05**	
SOX3	-3.98	-1.17	1.85	Down at P1 and up at P2	-3.86	1.09	up at P9	**0.03**	
CRABP1	-3.95	1.08	1.32	up	-3.72	1.06	up at P9	**0.06**	
ADH4	-3.94	-3.25	-5.06	down	-3.77	-1.73	down	**0.04**	a
PCGF5	-3.93	-1.15	-1.16	down	-3.84	-1.20	down	**0.02**	
SYT9	-3.91	-1.11	-2.06	down	-5.13	-1.80	down	**-0.31**	C
FGD6	-3.91			absent at P1/P2	-3.41	1.11	up at P9	**0.13**	a
BARD1	-3.90	1.16	-2.09	up at P1 and down at P2	-3.38	-1.34	down	**0.13**	a
GMFB	-3.89	1.56	1.31	up	-3.33	1.19	up at P9	**0.14**	
ARAP2	-3.88			absent at P1/P2	-3.29	-2.20	down	**0.15**	
TULP2	-3.84	-2.20	-2.48	down	-3.42	-1.34	down	**0.11**	
TSPAN8	-3.79	-1.24	-1.09	down	-3.15	-1.34	down	**0.17**	
ID4	-3.75			absent at P1/P2	-4.87	-1.33	down	**-0.30**	
MMD	-3.75			absent at P1/P2	-4.14	-1.31	down	**-0.10**	
DPPA4	-3.65	1.11	-1.06	up at P1 and down at P2	-3.34		absent at P9	**0.09**	b
PDHA2	-3.64	-1.08	-1.31	down		2.36	absent at P7	**1.00**	
RHPN2	-3.63	-1.07	-1.02	down	-3.45	-1.15	down	**0.05**	
HHEX	-3.61	-1.29	-1.03	down	-3.49	-1.29	down	**0.03**	
SUV39H2	-3.60	1.12	-1.02	up at P1 and down at P2	-2.54	-1.09	down	**0.29**	c
SPINLW1	-3.59			absent at P1/P2	-2.52	-1.85	down	**0.30**	a
HMGA1	-3.59	-1.27	-1.04	down	-3.65	-1.07	down	**-0.02**	
PHTF2	-3.58	1.14	-1.01	up at P1 and down at P2	-3.00	-1.00	down	**0.16**	
CCNB1	-3.58			absent at P1/P2	-3.21		absent at P9	**0.10**	
ATP11C	-3.57			absent at P1/P2	-2.92	-1.04	down	**0.18**	
Tex19.1	-3.56	-1.06	1.26	Down at P1 and up at P2	-3.19	1.29	up at P9	**0.10**	
ZNF808	-3.53			absent at P1/P2	-3.30		absent at P9	**0.07**	
ARL5B	-3.53			absent at P1/P2	-3.07	-1.34	down	**0.13**	
SPTA1	-3.52	-10.29	-11.56	down		-1.16	absent at P7	**1.00**	
TNIK	-3.51			absent at P1/P2	-3.59		absent at P9	**-0.02**	
SOX11	-3.51	-1.08	1.18	Down at P1 and up at P2		-1.49	absent at P7	**1.00**	
COL4A3BP	-3.50			absent at P1/P2	-2.65	-1.26	down	**0.24**	
TDRKH	-3.49			absent at P1/P2	-2.63	1.29	up at P9	**0.25**	
SOHLH2	-3.44			absent at P1/P2	-2.19	1.47	up at P9	**0.36**	c
EPB41L3	-3.43			absent at P1/P2	-3.27	-1.02	down	**0.05**	b
ERO1L	-3.43	1.10	-1.11	up at P1 and down at P2	-3.22	1.13	up at P9	**0.06**	
STAG3	-3.42	-1.01	2.72	Down at P1 and up at P2	-1.87	1.37	up at P9	**0.45**	
ZIC3	-3.41	-1.96	-1.83	down	-3.20	-2.98	down	**0.06**	b
API5	-3.41	1.03	-1.13	up at P1 and down at P2	-2.54	1.05	up at P9	**0.25**	
XPO4	-3.38			absent at P1/P2	-2.97	-1.35	down	**0.12**	
UPP1	-3.38	1.06	1.37	up	-3.12	1.36	up at P9	**0.08**	
STRA8	-3.37	-2.62	-2.80	down	-1.64	1.18	up at P9	**0.51**	b
ADAD1	-3.35	-1.09	-1.09	down	-2.22	1.61	up at P9	**0.34**	
DCK	-3.32	1.17	-1.12	up at P1 and down at P2	-2.71	-1.09	down	**0.18**	

MBP	-3.32	-1.50	-1.50	down	-4.10		absent at P9	**-0.24**	
RCC2	-3.31	-1.50	-1.16	down	-3.21	-1.01	down	**0.03**	
FAR1	-3.31			absent at P1/P2	-2.36	1.24	up at P9	**0.29**	
TAF9B	-3.30			absent at P1/P2	-2.38	1.01	up at P9	**0.28**	
ATF7IP2	-3.28			absent at P1/P2	-2.14	1.04	up at P9	**0.35**	
SYCP1	-3.27	1.16	-1.02	up at P1 and down at P2		1.25	absent at P7	**1.00**	
GDPD1	-3.27			absent at P1/P2	-1.53	1.09	up at P9	**0.53**	
CHTF18	-3.27			absent at P1/P2	-3.48	1.15	up at P9	**-0.06**	
Snhg11	-3.25	1.54	1.25	up	-2.49	-1.03	down	**0.24**	
MGEA5	-3.25	1.06	-1.10	up at P1 and down at P2	-2.75	-1.09	down	**0.15**	
CTNND2	-3.25	-1.07	1.33	Down at P1 and up at P2	-3.78	-2.11	down	**-0.16**	
KLHDC10	-3.23			absent at P1/P2	-3.90	1.14	up at P9	**-0.21**	
USP24	-3.21	-1.19	-1.20	down	-2.59		absent at P9	**0.19**	
LGALS2	-3.17	1.08	1.27	up	-3.04	1.29	up at P9	**0.04**	
MASTL	-3.17			absent at P1/P2	-2.36	-1.12	down	**0.26**	
NNAT	-3.16	-2.65	-2.54	down	-3.07		absent at P9	**0.03**	
FLRT1	-3.16			absent at P1/P2	-2.51	-1.58	down	**0.21**	a
UCHL1	-3.16	1.11	-1.12	up at P1 and down at P2	-2.74	1.26	up at P9	**0.14**	
Cycs/Gm10053	-3.16	-1.61	-1.94	down	-2.77	-1.35	down	**0.12**	
PLXNC1	-3.16			absent at P1/P2	-1.72	-1.36	down	**0.46**	
C10orf46	-3.14	1.02	-1.03	up at P1 and down at P2	-2.95	1.08	up at P9	**0.06**	
ESRP1	-3.10	-1.39	-1.15	down	-2.84	1.12	up at P9	**0.08**	
POU3F1	-3.10	-1.24	-2.12	down	-3.15	1.29	up at P9	**-0.02**	
RNF144B	-3.10			absent at P1/P2	-2.60	-1.25	down	**0.16**	
MTMR7	-3.09	1.44	-1.31	up at P1 and down at P2	-3.26	-1.00	down	**-0.05**	b
EXOSC1	-3.09			absent at P1/P2	-1.45	-1.10	down	**0.53**	
BCL2L11	-3.09	1.39	1.25	up	-2.78	-1.11	down	**0.10**	
NCOA2	-3.06	-1.24	-1.90	down	-2.71	-1.28	down	**0.12**	a
Cyct	-3.05	1.14	-1.28	up at P1 and down at P2	-2.39	1.26	up at P9	**0.22**	
FAM184B	-3.04			absent at P1/P2	-3.64	1.10	up at P9	**-0.20**	
FOXJ3	-3.01			absent at P1/P2	-2.98	1.03	up at P9	**0.01**	
SLK	-3.01	1.08	-1.03	up at P1 and down at P2	-2.80	-1.15	down	**0.07**	
TAF4B	-3.01			absent at P1/P2	-2.39	-1.04	down	**0.20**	
SMG1	-2.99			absent at P1/P2	-2.51	1.40	up at P9	**0.16**	
SGK3	-2.98			absent at P1/P2	-2.21	-1.56	down	**0.26**	
NINL	-2.98			absent at P1/P2	-2.72	-1.13	down	**0.09**	
LRP8	-2.97			absent at P1/P2	-2.90	-1.88	down	**0.02**	
CCDC88C	-2.96			absent at P1/P2	-3.02	-1.05	down	**-0.02**	
FAM105A	-2.96	-2.16	-2.26	down	-2.69	-1.67	down	**0.09**	
RUNDC3B	-2.95			absent at P1/P2	-2.62	1.06	up at P9	**0.11**	
HSPA4L	-2.94	-1.00	1.17	Down at P1 and up at P2	-2.36	1.06	up at P9	**0.20**	
DTL	-2.93	-1.04	-1.24	down	-2.73	1.22	up at P9	**0.07**	
TLE3	-2.93	-1.05	-1.06	down	-2.97	-1.23	down	**-0.02**	a
NR0B1	-2.92	-1.76	-2.01	down	-2.02	-1.55	down	**0.31**	
BOLL	-2.92			absent at P1/P2	-2.80	1.04	up at P9	**0.04**	a
PAQR8	-2.92			absent at P1/P2	-2.47	-1.64	down	**0.16**	
MYO1B	-2.92	1.18	1.33	up	-2.92	-1.15	down	**0.00**	
C21orf91	-2.92			absent at P1/P2	-2.88	1.02	up at P9	**0.01**	
POU5F1	-2.90	-1.49	1.30	Down at P1 and up at P2	-2.78	2.03	up	**0.04**	
GCAT	-2.90	1.16	1.17	up	-2.72	-1.17	down	**0.06**	
KBTBD8	-2.89			absent at P1/P2	-2.22	-1.32	down	**0.23**	
LHX1	-2.89	-1.09	-2.28	down	-2.39	-1.25	down	**0.17**	
SKIL	-2.89	-1.41	-2.21	down	-2.70	1.01	up at P9	**0.07**	
DNER	-2.89			absent at P1/P2	-2.09	-1.40	down	**0.28**	a
SFMBT1	-2.88			absent at P1/P2	-2.60		absent at P9	**0.10**	b
LIPA	-2.87	1.04	-1.26	up at P1 and down at P2		1.26	absent at P7	**1.00**	
GNG12	-2.86	-1.35	-1.52	down	-2.45	-1.19	down	**0.14**	
RET	-2.85	-2.70	-7.27	down	-3.10	-1.33	down	**-0.09**	
ENAH	-2.83			absent at P1/P2	-2.79		absent at P9	**0.02**	
C13orf27	-2.83			absent at P1/P2	-2.47	-1.00	down	**0.13**	
FAM40B	-2.83			absent at P1/P2	-2.66	-1.16	down	**0.06**	
ZFP42	-2.82	1.07	1.44	up	-2.33	1.54	up at P9	**0.17**	
4930486L24Rik	-2.82			absent at P1/P2	-1.63	-1.75	down	**0.42**	
PITPNC1	-2.81	1.03	1.21	up	-3.24	-1.39	down	**-0.15**	
PANK1	-2.81			absent at P1/P2		1.30	absent at P7	**1.00**	
MXD1	-2.81	-1.10	-1.58	down	-1.54	-1.14	down	**0.45**	
DDX21	-2.81	-1.04	-1.25	down	-2.85	1.21	up at P9	**-0.01**	c
CACNG5	-2.80			absent at P1/P2	-3.23	-1.23	down	**-0.16**	
PLEKHG1	-2.79			absent at P1/P2	-2.72	-1.76	down	**0.02**	
KIAA0182	-2.79			absent at P1/P2	-2.82	1.16	up at P9	**-0.01**	
LOC284023	-2.78	-1.30	-1.31	down	-2.91	-1.43	down	**-0.05**	
ELL3	-2.78			absent at P1/P2	-2.96	1.07	up at P9	**-0.06**	
TOLLIP	-2.78	-1.17	-1.14	down	-2.56	1.18	up at P9	**0.08**	
Gm884	-2.77			absent at P1/P2	-2.62	1.09	up at P9	**0.05**	
TSC22D1	-2.77	1.13	-1.09	up at P1 and down at P2	-2.44		absent at P9	**0.12**	
DMC1	-2.76	-1.05	1.46	Down at P1 and up at P2		1.92	absent at P7	**1.00**	
RAB20	-2.76	-1.46	-2.21	down	-2.08	-1.22	down	**0.24**	

CHP2	-2.75			absent at P1/P2	-1.75	-1.38	down	**0.37**	
EIF5A2	-2.75			absent at P1/P2	-2.78	1.17	up at P9	**-0.01**	
CDKN2A	-2.75	-1.25	1.13	Down at P1 and up at P2	-2.61	-1.45	down	**0.05**	
KCNG2	-2.75			absent at P1/P2	-1.97	-1.40	down	**0.28**	
EMB	-2.74	-2.56	-4.00	down	-2.39	1.14	up at P9	**0.13**	
SH3BGRL2	-2.72	1.09	-1.78	up at P1 and down at P2	-2.28	1.29	up at P9	**0.16**	
TMEM100	-2.71			absent at P1/P2	-1.55	1.31	up at P9	**0.43**	
ORC1	-2.71	1.03	-1.30	up at P1 and down at P2	-2.27		absent at P9	**0.16**	
ZSWIM5	-2.70			absent at P1/P2	-2.74	-1.29	down	**-0.02**	
AIFM3	-2.68			absent at P1/P2	-2.52	1.09	up at P9	**0.06**	
RPS6KA2	-2.68	-1.90	-2.20	down	-2.68	-1.02	down	**0.00**	
ISLR2	-2.67			absent at P1/P2	-2.68	-1.22	down	**0.00**	
PI4K2B	-2.67			absent at P1/P2			absent at P7 and P9	**1.00**	
SH3D19	-2.67	-1.74	-2.20	down	-2.55		absent at P9	**0.05**	
NAA30	-2.67	-1.13	-1.25	down	-2.17		absent at P9	**0.19**	
MYO5B	-2.67	-1.16	-1.10	down	-2.41	-1.12	down	**0.10**	
TRIM25	-2.66	1.16	-1.09	up at P1	-2.89	-1.06	down	**-0.08**	
PLA2G7	-2.66	-1.40	-1.38	down	-2.17	-1.40	down	**0.18**	a
STRA6	-2.65	-3.68	-1.85	down	-2.74	-1.38	down	**-0.03**	
WDR5	-2.64	-1.06	-1.03	down	-2.41	1.24	up at P9	**0.09**	
PRSS12	-2.63	1.13	-1.08	up at P1 and down at P2	-2.47	-1.08	down	**0.06**	
GSTM2	-2.62			absent at P1/P2	-1.92		absent at P9	**0.27**	
ACTR1A	-2.62	1.36	1.19	up		1.18	absent at P7	**1.00**	
ATF2	-2.61	1.14	-1.04	up at P1 and down at P2	-2.15	1.27	up at P9	**0.18**	
HSPBAP1	-2.61			absent at P1/P2	-2.51	-1.04	down	**0.04**	
KPNA3	-2.61	-1.13	-1.94	down	-2.41	1.31	up at P9	**0.08**	
PSMA8	-2.61			absent at P1/P2	-2.15	1.43	up at P9	**0.18**	
ELOVL2	-2.60	-2.88	-4.56	down	-1.75	-1.46	down	**0.33**	
AK4	-2.59	1.02	-1.05	up at P1 and down at P2	-1.98	-1.37	down	**0.23**	
CRLF1	-2.59	-2.62	-1.72	down	-1.92	1.09	up at P9	**0.26**	
BZW1	-2.58	1.14	-1.17	up at P1 and down at P2	-2.19	-1.03	down	**0.15**	
THAP4	-2.58	-1.33	-1.07	down	-2.85	-1.02	down	**-0.10**	
LRRFIP1	-2.58			absent at P1/P2	-5.70		absent at P9	**-1.21**	
RNF138	-2.58	1.10	-1.10	up at P1 and down at P2	-2.00	1.26	up at P9	**0.22**	
HIF1AN	-2.56			absent at P1/P2	-2.27	-1.03	down	**0.11**	
WAPAL	-2.56			absent at P1/P2	-2.33	-1.00	down	**0.09**	
OSBPL3	-2.55			absent at P1/P2	-2.14	1.13	up at P9	**0.16**	
SEMA4F	-2.55	1.24	-1.02	up at P1 and down at P2	-1.49	-1.08	down	**0.42**	
MAN2A1	-2.55	-1.11	-1.17	down	-2.78	-1.21	down	**-0.09**	a
RORA	-2.54	-1.78	-1.88	down	-2.56	1.12	up at P9	**-0.01**	
GNG13	-2.54			absent at P1/P2	-2.78	1.30	up at P9	**-0.10**	
MNS1	-2.54	1.40	-1.26	up at P1 and down at P2	-2.22	-1.01	down	**0.12**	
PLK4	-2.54	-1.10	-1.29	down	-2.01		absent at P9	**0.21**	
ABCB7	-2.54	1.07	-1.71	up at P1 and down at P2	-2.00		absent at P9	**0.21**	
PIWIL4	-2.54			absent at P1/P2	-2.42	1.03	up at P9	**0.05**	
Chn1	-2.53			absent at P1/P2	-2.05		absent at P9	**0.19**	
HINFP	-2.53	1.08	-1.13	up at P1 and down at P2	-2.39	1.15	up at P9	**0.05**	
CTDSP2	-2.53	-1.11	1.15	Down at P1 and up at P2	-2.57	-1.03	down	**-0.02**	
CAB39L	-2.52	1.03	-1.18	up at P1 and down at P2	-2.02	1.02	up at P9	**0.20**	
LIN7C	-2.52	1.15	-1.32	Down at P1 and up at P2	-2.15	1.26	up at P9	**0.15**	
SMC1B	-2.52			absent at P1/P2		1.63	absent at P7	**1.00**	
PPAT	-2.51	-1.16	-1.39	down	-2.20	1.16	up at P9	**0.12**	
RELN	-2.50	-2.35	-1.05	down	-1.77	1.16	up at P9	**0.29**	
FAM70A	-2.50			absent at P1/P2	-2.17	-1.36	down	**0.13**	
RIF1	-2.50			absent at P1/P2	-1.17	1.00	up at P9	**0.53**	a
OBFC2A	-2.49	-1.49		down	-1.94	1.33	up at P9	**0.22**	
PRR5	-2.49	-1.27	-1.18	down	-1.98	-1.03	down	**0.21**	
G2E3	-2.49			absent at P1/P2	-2.27	1.03	up at P9	**0.09**	
C10orf35	-2.49			absent at P1/P2	-2.92	1.08	up at P9	**-0.17**	
UGT8	-2.49	-1.44	-1.03	down		1.23	absent at P7	**1.00**	
DUSP9	-2.49	1.41	1.77	up	-2.62	1.33	up at P9	**-0.05**	
Nlrp4f	-2.48			absent at P1/P2	-1.98	1.33	up at P9	**0.20**	
RAD9B	-2.48			absent at P1/P2	-1.83	1.09	up at P9	**0.26**	
SPATA5	-2.47	1.02	-1.06	up at P1 and down at P2	-2.13	1.29	up at P9	**0.14**	
SNX6	-2.47	1.00	-1.11	up at P1 and down at P2	-2.19	1.05	up at P9	**0.11**	
EFHC2	-2.47			absent at P1/P2	-1.85	1.47	up at P9	**0.25**	
CAMK1D	-2.47			absent at P1/P2	-1.81	-1.36	down	**0.26**	
MAPK12	-2.46	-1.14	-1.15	down	-2.59	1.12	up at P9	**-0.05**	
STAG1	-2.46	1.11	-1.36	up at P1 and down at P2	-1.94	-1.12	down	**0.21**	c
MPHOSPH9	-2.46	-1.15	-1.33	down	-2.14		absent at P9	**0.13**	
GOSR1	-2.45	-1.05	-1.07	down	-2.08	1.08	up at P9	**0.15**	
FANCD2	-2.44			absent at P1/P2	-2.12	1.25	up at P9	**0.13**	
CDS2	-2.44	-1.01	-1.10	down	-2.34	1.16	up at P9	**0.04**	
TAF7	-2.43			absent at P1/P2	-2.06		absent at P9	**0.15**	b
MFSD2A	-2.43			absent at P1/P2	-2.09	-1.15	down	**0.14**	
DAPK2	-2.42	1.04	-1.00	up at P1 and down at P2	-2.76	-1.11	down	**-0.14**	
USP9Y	-2.42			absent at P1/P2	-1.78	1.44	up at P9	**0.27**	

CAPN6	-2.42	-1.76	-2.49	down	-2.44	1.07	up at P9	**-0.01**	
CORO1C	-2.42	-1.17	-1.16	down	-1.91	1.18	up at P9	**0.21**	a
QPCT	-2.41			absent at P1/P2	-2.10		absent at P9	**0.13**	
EXOC6	-2.41			absent at P1/P2	-2.22	-1.40	down	**0.08**	
INA	-2.41			absent at P1/P2	-2.66	-1.17	down	**-0.11**	
GFPT1	-2.40			absent at P1/P2	-1.92	1.04	up at P9	**0.20**	
CCNG1	-2.39	1.16	-1.03	up at P1 and down at P2	-2.10	1.00	up at P9	**0.12**	
KIF5C	-2.39	1.69	-1.05	up at P1 and down at P2	-2.71	-1.02	down	**-0.13**	
TGFBI	-2.38	2.21	-2.03	up at P1 and down at P2	-2.69	1.07	up at P9	**-0.13**	
RAD18	-2.38			absent at P1/P2	-2.06	1.09	up at P9	**0.13**	
ANKRD57	-2.38	-1.35	-1.69	down	-1.91	-1.21	down	**0.20**	
FSD1	-2.38			absent at P1/P2	-2.44	-1.20	down	**-0.03**	
UBE2T	-2.38	1.11	-1.06	up at P1 and down at P2	-1.62	1.23	up at P9	**0.32**	
TRIM6	-2.37			absent at P1/P2		1.68	absent at P7	**1.00**	c
PLEKHG4	-2.37			absent at P1/P2	-2.26	1.02	up at P9	**0.05**	
SLAIN1	-2.37	-1.49	-1.96	down	-2.35	-1.29	down	**0.01**	
STX3	-2.36	1.93	-1.09	up at P1 and down at P2	-2.27		absent at P9	**0.04**	
ADORA1	-2.36	-2.36	-2.27	down	-1.23	-1.23	down	**0.48**	
RGS17	-2.36			absent at P1/P2	-1.86	-1.82	down	**0.21**	
RADIL	-2.36			absent at P1/P2	-2.46	-1.10	down	**-0.04**	
WIPI2	-2.36	-1.18	-1.15	down	-2.17	1.37	up at P9	**0.08**	
NASP	-2.36	-1.03	-1.41	down	-2.11	1.51	up at P9	**0.11**	
C15orf55	-2.35			absent at P1/P2	-2.43	-1.18	down	**-0.03**	
ART3	-2.35	-1.10	-1.29	down	-2.24	-1.21	down	**0.05**	b
NEB	-2.35			absent at P1/P2	-2.00	-1.10	down	**0.15**	
DDX3Y	-2.34	-1.18	-1.23	down	-1.73	1.74	up at P9	**0.26**	
USP31	-2.34			absent at P1/P2	-1.99	-1.21	down	**0.15**	
YKT6	-2.34	-1.12	-1.28	down	-2.10	1.18	up at P9	**0.10**	
PDE4B	-2.34	-1.11	-1.09	down	-2.10	1.01	up at P9	**0.10**	
DGAT2	-2.33			absent at P1/P2	-2.11	1.46	up at P9	**0.10**	
FYTTD1	-2.33	-1.08	-1.17	down	-1.71	1.29	up at P9	**0.27**	
UXS1	-2.33	-1.17	-1.26	down	-1.92	-1.01	down	**0.18**	
TACC1	-2.32			absent at P1/P2	-1.74	-1.24	down	**0.25**	
FAM84A	-2.32	1.02	-1.09	up at P1 and down at P2	-2.27	-1.80	down	**0.02**	
BRWD3	-2.32	-1.22	-1.01	down	-2.18	-1.32	down	**0.06**	
ZRSR2	-2.32	1.35	1.28	up	-2.15		absent at P9	**0.07**	
KCNA6	-2.31	-1.41	-1.69	down	-1.81	-1.44	down	**0.22**	
DDAH1	-2.31			absent at P1/P2	-1.35	-1.17	down	**0.41**	
KIAA0895	-2.31			absent at P1/P2	-1.92	-1.35	down	**0.17**	
EPCAM	-2.31	1.34	-1.70	up at P1 and down at P2		1.55	absent at P7	**1.00**	
POLR3G	-2.31			absent at P1/P2	-1.89	-1.16	down	**0.18**	
TUBB2C	-2.30	1.03	-1.04	up at P1 and down at P2	-2.15	-1.05	down	**0.07**	
TRPC3	-2.30			absent at P1/P2	-1.57	-1.72	down	**0.32**	
NUPL1	-2.30			absent at P1/P2	-1.76	1.18	up at P9	**0.24**	
TAF7L	-2.30			absent at P1/P2		2.12	absent at P7	**1.00**	
ZDHHC2	-2.30			absent at P1/P2	-1.72	-1.63	down	**0.25**	
ZNF398	-2.30	-1.07	-2.33	down	-1.23		absent at P9	**0.46**	
KCTD20	-2.30	-1.02	-1.04	down	-2.43	-1.06	down	**-0.06**	
RGL1	-2.30	-1.56	-2.07	down	-2.11	-1.43	down	**0.08**	
CCND3	-2.29	1.04	-1.04	up at P1 and down at P2	-1.90	1.27	up at P9	**0.17**	
RAD51C	-2.29			absent at P1/P2	-2.27	1.05	up at P9	**0.01**	
GNA14	-2.29	-1.25	-1.64	down	-2.09	-1.48	down	**0.09**	
SPINT1	-2.29	-1.28	-1.06	down	-2.59	-1.23	down	**-0.13**	
FOXP1	-2.29	1.56	1.22	up	-2.38	-1.25	down	**-0.04**	
ABHD5	-2.29	-1.22	-1.11	down	-2.05	1.11	up at P9	**0.10**	
Mpped2	-2.28			absent at P1/P2	-2.48		absent at P9	**-0.08**	
TFRC	-2.28	-1.29	-1.41	down	-1.79	1.52	up at P9	**0.21**	
PIM1	-2.28	-1.06	1.23	Down at P1 and up at P2	-2.51	-1.05	down	**-0.10**	
SH3GL3	-2.28	-2.39	-2.16	down	-2.08	-1.03	down	**0.09**	
RAB10	-2.27	-1.12	-1.19	down	-1.94	-1.06	down	**0.15**	
EPAS1	-2.27	1.00	1.14	up	-1.95	-1.08	down	**0.14**	
BRIP1	-2.27			absent at P1/P2	-1.56	2.26	up	**0.31**	
4933425L06Rik	-2.27			absent at P1/P2	-1.77	1.70	up at P9	**0.22**	
SHB	-2.27			absent at P1/P2	-1.98		absent at P9	**0.13**	
FZD3	-2.27	-1.20	-1.19	down	-2.08	-1.27	down	**0.08**	
DOCK5	-2.27	-1.26	-1.51	down	-1.88		absent at P9	**0.17**	
RECQL4	-2.27			absent at P1/P2	-2.19	1.01	up at P9	**0.03**	
DMRTB1	-2.27	1.53	-1.92	up at P1 and down at P2	-2.57	-2.20	down	**-0.13**	b
BNC2	-2.27			absent at P1/P2	-1.91	-1.06	down	**0.16**	
DDHD1	-2.26	1.02	-1.02	up at P1 and down at P2	-1.89	-1.12	down	**0.16**	
GABPA	-2.26	-1.22	-1.57	down	-1.79	1.15	up at P9	**0.21**	
ZMYND19	-2.26			absent at P1/P2	-2.01	-1.24	down	**0.11**	
PI4K2A	-2.26	-1.18	1.24	Down at P1 and up at P2		1.03	absent at P7	**1.00**	
TDRD1	-2.26			absent at P1/P2	-2.30		absent at P9	**-0.02**	
C17orf79	-2.25	1.44	1.14	up	-2.20	-1.06	down	**0.02**	
ETNK1	-2.25	1.30	-1.04	up at P1 and down at P2	-1.61	-1.00	down	**0.28**	
ZBED5	-2.24			absent at P1/P2	-2.11	-1.22	down	**0.06**	

TRAIP	-2.24	-1.25	-1.23	down	-2.15	1.48	up at P9	**0.04**	
PTPRR	-2.24	1.68	-1.36	up at P1 and down at P2	-1.98	1.07	up at P9	**0.12**	
MTHFD2	-2.24	1.84	-1.12	up at P1 and down at P2	-1.96	-1.06	down	**0.12**	
SMC5	-2.24			absent at P1/P2	-1.81	1.11	up at P9	**0.19**	
ASNS	-2.23	-1.29	-1.45	down		-1.30	absent at P7	**1.00**	b
ASCL2	-2.23	1.19	1.37	up	-2.41	-1.56	down	**-0.08**	
MYCBP	-2.23	1.39	-1.48	up at P1 and down at P2	-1.96	-1.08	down	**0.12**	
NRAS	-2.22	-1.06	1.24	Down at P1 and up at P2	-2.12	-1.04	down	**0.05**	
EFR3A	-2.22			absent at P1/P2	-1.86	-1.07	down	**0.16**	
ZNF711	-2.22			absent at P1/P2	-2.12	-2.13	down	**0.05**	
HMGN5	-2.22	-1.15	-1.74	down	-1.90	-1.60	down	**0.15**	
SLC31A1	-2.22	-1.54	-1.54	down	-1.76	-1.22	down	**0.21**	
AKT3	-2.22			absent at P1/P2	-1.93	1.14	up at P9	**0.13**	
GSTA3	-2.22	-1.22	-1.42	down	-1.95	-1.78	down	**0.12**	
MDN1	-2.21	-1.01	-1.02	down	-2.18		absent at P9	**0.01**	
SALL1	-2.21			absent at P1/P2	-2.10	-1.42	down	**0.05**	
DCAF7	-2.21			absent at P1/P2	-2.00	1.04	up at P9	**0.09**	
PLEKHA8	-2.21			absent at P1/P2	-2.18	1.06	up at P9	**0.01**	
ZMYM3	-2.20			absent at P1/P2	-1.80	1.03	up at P9	**0.18**	a
PHF17	-2.20	-1.36	-1.33	down	-1.73	1.00	up at P9	**0.22**	
KLHL15	-2.20			absent at P1/P2	-2.01	-2.05	down	**0.09**	
GTF2A1	-2.20	1.03	-1.03	up at P1 and down at P2	-2.18		absent at P9	**0.01**	a
GNAT2	-2.20	-1.07	-1.07	down	-2.21	1.32	up at P9	**-0.01**	
CENPE	-2.19	2.10	3.01	up	-1.59	1.18	up at P9	**0.28**	
C6orf108	-2.19	-1.16	-1.09	down	-2.22	-1.36	down	**-0.01**	
PSME3	-2.19	-1.21	-1.20	down	-2.33	1.05	up at P9	**-0.06**	
RNF114	-2.19	1.66	1.52	up	-1.77	1.17	up at P9	**0.19**	c
LMO1	-2.18	1.02	1.14	up	-2.72	-1.15	down	**-0.24**	
EHD1	-2.18	-1.09	-1.07	down	-1.99	1.12	up at P9	**0.09**	
PDGFC	-2.18			absent at P1/P2	-2.49	-1.22	down	**-0.14**	
SHMT1	-2.18	-1.45	-1.27	down	-2.49	-1.17	down	**-0.14**	
TOX3	-2.18			absent at P1/P2	-2.48	-1.66	down	**-0.14**	
ZBTB44	-2.17			absent at P1/P2	-2.01		absent at P9	**0.07**	
POLR3F	-2.17			absent at P1/P2	-1.86	-1.13	down	**0.15**	
PLEKHF2	-2.17			absent at P1/P2	-2.21	1.06	up at P9	**-0.02**	
REEP1	-2.17	-1.95	-2.03	down	-1.85	-1.27	down	**0.15**	
ARID3B	-2.17	-1.07	-1.06	down	-2.21	1.10	up at P9	**-0.02**	
SLC27A2	-2.17	1.23	1.47	up		-1.36	absent at P7	**1.00**	
LHX8	-2.17	1.78	-1.04	up at P1 and down at P2	-1.81	1.54	up at P9	**0.17**	
EXO1	-2.17	-1.08	-1.21	down	-1.71	-1.06	down	**0.21**	
C12orf5	-2.17			absent at P1/P2	-2.18	-1.01	down	**-0.01**	
DPYSL3	-2.16	-1.11	-1.08	down	-2.23	-1.02	down	**-0.03**	a
HELLS	-2.16	-1.13	-1.50	down	-1.65	1.08	up at P9	**0.24**	
KIF2A	-2.16	-1.03	-1.27	down	-1.96	1.14	up at P9	**0.09**	
CBL	-2.16	-1.09	-1.60	down	-1.62	-1.34	down	**0.25**	
CA6	-2.15	-1.42	-2.77	down	-1.96	1.57	up at P9	**0.09**	
PPRC1	-2.15	-1.23	-1.05	down	-2.24	-1.13	down	**-0.04**	
NDRG4	-2.15	1.38	1.17	up	-2.17	1.13	up at P9	**-0.01**	
ZNF655	-2.15			absent at P1/P2	-1.95	1.05	up at P9	**0.09**	
NUS1	-2.15	1.18	-1.04	up at P1 and down at P2	-1.86	-1.06	down	**0.13**	
CCNB1IP1	-2.15	1.54	-1.05	up at P1 and down at P2	-2.62	1.18	up at P9	**-0.22**	
RIMKLA	-2.15			absent at P1/P2	-2.30	-1.23	down	**-0.07**	
FOXO1	-2.14			absent at P1/P2	-2.44	1.07	up at P9	**-0.14**	
KCNQ5	-2.14			absent at P1/P2	-1.89	-1.58	down	**0.12**	
AKR1B1	-2.14	-1.21	1.13	Down at P1 and up at P2	-1.84	-1.06	down	**0.14**	
C11orf82	-2.14			absent at P1/P2	-1.50	1.18	up at P9	**0.30**	
PADI3	-2.14	-1.03	1.61	Down at P1 and up at P2	-1.85	1.13	up at P9	**0.13**	
TERF1	-2.13	1.10	-1.41	up at P1 and down at P2	-1.70	1.22	up at P9	**0.20**	a
TEX9	-2.13	1.04	-1.05	up at P1 and down at P2	-1.71	1.11	up at P9	**0.20**	
FBXO41	-2.13			absent at P1/P2	-2.33	1.48	up at P9	**-0.09**	
IP6K1	-2.13	1.48	-1.12	up at P1 and down at P2	-2.20	1.18	up at P9	**-0.03**	a
BCAT2	-2.13	-1.91	-1.67	down		-1.01	absent at P7	**1.00**	
LRR1	-2.13			absent at P1/P2	-1.48		absent at P9	**0.30**	
UBFD1	-2.13	-1.17	-1.24	down	-1.92	1.12	up at P9	**0.10**	
GJC1	-2.13	-1.37	-1.26	down	-1.66	1.03	up at P9	**0.22**	
KIAA1468	-2.12			absent at P1/P2	-1.56	1.27	up at P9	**0.26**	
HDGFRP3	-2.12			absent at P1/P2	-1.63	-1.05	down	**0.23**	
CDCA5	-2.12	1.04	-1.09	up at P1 and down at P2	-2.11	-1.00	down	**0.00**	
COL4A3	-2.12	-1.04	-1.35	down	-1.61	-1.01	down	**0.24**	
GAB3	-2.12			absent at P1/P2	-1.58	-1.26	down	**0.26**	
STK10	-2.12	-1.28	-1.23	down	-1.73	-1.19	down	**0.18**	
HOOK3	-2.11			absent at P1/P2	-1.87	-1.15	down	**0.11**	
LATS1	-2.11			absent at P1/P2		-1.22	absent at P7	**1.00**	
DOCK7	-2.11	-1.30	-1.09	down	-1.69	-1.23	down	**0.20**	
TBC1D1	-2.11	1.01	-1.02	up at P1 and down at P2	-1.92	1.13	up at P9	**0.09**	
MYBL2	-2.11	-1.37	-1.29	down	-1.78	-1.19	down	**0.15**	
YWHAB	-2.11	-1.07	-1.04	down	-2.09	1.03	up at P9	**0.01**	

CAMSAP3	-2.10			absent at P1/P2	-2.24	-1.13	down	**-0.07**	
C1orf51	-2.10			absent at P1/P2	-1.86	-1.02	down	**0.12**	
CBLB	-2.10			absent at P1/P2	-2.31	-1.14	down	**-0.10**	
NRCAM	-2.10	-1.76	1.85	Down at P1 and up at P2	-1.89	-1.27	down	**0.10**	
SAR1A	-2.10	1.02	-1.05	up at P1 and down at P2	-1.85	1.31	up at P9	**0.12**	
LPIN2	-2.10	-1.07	-1.65	down		-1.02	absent at P7	**1.00**	
NNMT	-2.10	-1.35	-1.26	down	-1.92	1.52	up at P9	**0.09**	
CDR2	-2.10	1.21	-1.18	up at P1 and down at P2	-2.07	-1.03	down	**0.01**	
CCDC136	-2.10			absent at P1/P2	-1.65	1.03	up at P9	**0.21**	
HEATR1	-2.10			absent at P1/P2	-2.11	1.05	up at P9	**-0.01**	
Prune2	-2.09			absent at P1/P2	-1.71		absent at P9	**0.18**	
PMAIP1	-2.09			absent at P1/P2	-2.54		absent at P9	**-0.22**	
CRLF3	-2.09	-1.04	-1.20	down	-1.80	-1.06	down	**0.14**	
RACGAP1	-2.09	-1.06	-1.28	down	-1.93	1.01	up at P9	**0.08**	a
RNF38	-2.09	-1.05	-1.02	down	-2.18	-1.14	down	**-0.04**	b
CAD	-2.09	-2.63	1.50	Down at P1 and up at P2	-1.75	1.02	up at P9	**0.16**	
MTF1	-2.09	-1.15	-1.09	down	-1.96	1.03	up at P9	**0.06**	
GML	-2.09	-1.50	-1.29	down	-1.76	2.65	up at P9	**0.15**	
DDX46	-2.08	1.03	-1.14	Down at P1 and up at P2	-1.85	1.15	up at P9	**0.11**	
DICER1	-2.08	1.00	1.28	up	-1.97	-1.01	down	**0.06**	
CHPT1	-2.08	-1.36	-1.66	down	-1.59	-1.38	down	**0.23**	
ATP13A3	-2.08	1.03	-1.23	up at P1 and down at P2	-1.94		absent at P9	**0.07**	
ZBTB37	-2.08	-1.03	-1.21	down	-1.63	1.32	up at P9	**0.22**	
KIAA1024	-2.08			absent at P1/P2	-1.97	1.15	up at P9	**0.05**	
TCTE3	-2.08	1.10	-1.08	up at P1 and down at P2	-1.92		absent at P9	**0.08**	
THAP1	-2.08			absent at P1/P2	-1.94	1.06	up at P9	**0.06**	
STAT1	-2.08	1.01	-1.09	up at P1 and down at P2	-1.93	-1.43	down	**0.07**	
RBP4	-2.07	1.15	1.14	up	-1.62	-1.45	down	**0.22**	
CITED1	-2.07	-1.47	-1.31	Down at P1 and up at P2	-1.34	-1.23	down	**0.35**	
VPS13A	-2.07			absent at P1/P2	-2.11	1.23	up at P9	**-0.02**	
ERBB3	-2.07	1.17	1.19	up	-1.88	1.81	up at P9	**0.09**	
NFKBIA	-2.07	-1.59	-1.40	down	-1.80	1.07	up at P9	**0.13**	a
WIPF3	-2.07			absent at P1/P2	-1.80	-1.54	down	**0.13**	
DISP1	-2.07			absent at P1/P2	-1.94	-1.09	down	**0.06**	
RUNX3	-2.06			absent at P1/P2	-2.17	-2.30	down	**-0.05**	
ARIH1	-2.06	-1.05	1.52	Down at P1 and up at P2	-2.18	-1.12	down	**-0.06**	
GRIK3	-2.06			absent at P1/P2	-1.99	1.03	up at P9	**0.03**	
KIF26A	-2.06			absent at P1/P2	-2.17		absent at P9	**-0.05**	
CCNF	-2.06	-1.08	-1.19	down	-1.83	1.13	up at P9	**0.11**	
CPEB1	-2.06	-1.17	2.42	Down at P1 and up at P2		1.31	absent at P7	**1.00**	
TCEA1	-2.06	-1.05	-1.25	down	-1.66	1.16	up at P9	**0.19**	
SLAIN2	-2.05			absent at P1/P2	-1.90	-1.15	down	**0.07**	
TJP2	-2.05			absent at P1/P2	-1.94	1.02	up at P9	**0.06**	
PRKCB	-2.05	-1.05	1.19	Down at P1 and up at P2	-1.48	-1.17	down	**0.28**	
RTKN2	-2.05			absent at P1/P2	-1.93	1.03	up at P9	**0.06**	
CCNA2	-2.05	1.05	-1.08	up at P1 and down at P2	-1.89	1.17	up at P9	**0.08**	
DRP2	-2.04			absent at P1/P2	-1.75	-1.49	down	**0.14**	
BICD2	-2.04			absent at P1/P2	-1.79	1.01	up at P9	**0.12**	
ALDOC	-2.04	1.45	1.45	up	-1.72	1.08	up at P9	**0.16**	
NUP50	-2.04	-1.12	-1.08	down	-1.95	1.06	up at P9	**0.05**	
MYH3	-2.04	1.59	2.38	up	-1.91	1.29	up at P9	**0.07**	
CDCA7	-2.04			absent at P1/P2	-2.00		absent at P9	**0.02**	
DDX19B	-2.04	1.13	-1.01	up at P1 and down at P2	-1.70	1.60	up at P9	**0.17**	a
GALNT12	-2.04			absent at P1/P2	-1.91	1.15	up at P9	**0.06**	
VCL	-2.04	-1.50	-1.72	down	-1.80	-1.12	down	**0.12**	c
CGN	-2.04			absent at P1/P2	-1.54		absent at P9	**0.24**	
RYBP	-2.03			absent at P1/P2	-2.02	1.02	up at P9	**0.01**	
CDC45	-2.03	-1.06	-1.44	down	-1.76	1.17	up at P9	**0.14**	
PCBD1	-2.03	-1.89	-2.75	down	-2.21	-1.10	down	**-0.09**	
SRPK2	-2.03	-1.03	-1.15	down	-1.74	-1.71	down	**0.15**	
C1orf112	-2.03			absent at P1/P2	-1.60	1.30	up at P9	**0.21**	
AP2A2	-2.03	-1.10	1.16	Down at P1 and up at P2	-1.99	1.18	up at P9	**0.02**	
LRIG2	-2.03			absent at P1/P2	-1.90	-1.24	down	**0.06**	
SIX4	-2.03	2.19	1.46	up	-2.18	-1.11	down	**-0.07**	
Bc1	-2.03			absent at P1/P2	-1.78		absent at P9	**0.13**	b
RAD51	-2.03	-1.60	-1.57	down	-1.79	1.15	up at P9	**0.12**	
WIPF2	-2.03			absent at P1/P2	-1.88	1.13	up at P9	**0.07**	
ING5	-2.03			absent at P1/P2	-1.95	1.10	up at P9	**0.04**	
ARHGAP44	-2.03			absent at P1/P2	-1.88	1.12	up at P9	**0.07**	
ZNF264	-2.02			absent at P1/P2	-2.19		absent at P9	**-0.08**	
MXI1	-2.02	-1.09	-1.30	down	-1.90	-1.15	down	**0.06**	
RIPK3	-2.02			absent at P1/P2	-2.10	1.27	up at P9	**-0.04**	
CUL4B	-2.02			absent at P1/P2	-1.82	-1.04	down	**0.10**	
RND2	-2.02	-1.87	-2.00	down	-1.62	1.02	up at P9	**0.20**	
BNC1	-2.02	1.14	1.56	up	-1.81	1.58	up at P9	**0.10**	
MREG	-2.02			absent at P1/P2	-1.75	-1.41	down	**0.13**	
C6orf1	-2.02	-1.10	1.11	Down at P1 and up at P2	-1.79	1.00	up at P9	**0.11**	

ESCO2	-2.02			absent at P1/P2	-1.47	1.18	up at P9	**0.27**	
C11orf70	-2.02			absent at P1/P2	-1.45	-1.18	down	**0.28**	
STK4	-2.02			absent at P1/P2	-1.99	1.04	up at P9	**0.01**	a
MECR	-2.02	1.14	1.32	up		1.13	absent at P7	**1.00**	
BRSK2	-2.01			absent at P1/P2	-2.02		absent at P9	**0.00**	
RAB11FIP3	-2.01			absent at P1/P2	-1.94	-1.24	down	**0.04**	
TMEM87B	-2.01			absent at P1/P2	-1.84	1.20	up at P9	**0.09**	
MPP6	-2.01			absent at P1/P2	-2.10		absent at P9	**-0.04**	
TACR3	-2.01			absent at P1/P2	-1.73	-1.07	down	**0.14**	
SDAD1	-2.01			absent at P1/P2	-2.02	-1.20	down	**-0.01**	
LRBA	-2.01	-1.39	-1.53	down	-1.78	-1.33	down	**0.12**	
GABPB1	-2.01	1.25	-1.19	up at P1 and down at P2	-1.68		absent at P9	**0.16**	
DYRK3	-2.01			absent at P1/P2	-2.07	1.20	up at P9	**-0.03**	b
CDCA7L	-2.01	-1.07	-1.30	down	-1.91	1.04	up at P9	**0.05**	
STK38L	-2.01			absent at P1/P2	-1.81	1.13	up at P9	**0.10**	
INTS6	-2.00	1.13	-1.01	up at P1 and down at P2	-1.62	2.01	up	**0.19**	
DTNA	-2.00	-1.64	-2.10	down	-1.57		absent at P9	**0.22**	
MYNN	-2.00	1.12	-1.01	up at P1 and down at P2	-1.50	-1.03	down	**0.25**	
DUSP6	-2.00	-1.72	-2.11	down	-1.95	-1.16	down	**0.03**	
PKD2L1	-2.00			absent at P1/P2	-1.73	1.65	up at P9	**0.13**	
PDK1	-2.00	-1.09	-1.06	down	-1.95	-1.36	down	**0.03**	
TTK	-2.00	-1.01	-1.40	down	-1.80	-1.08	down	**0.10**	
MEX3C	2.00			absent at P1/P2	1.79	1.08	up	**0.11**	
COL25A1	2.00			absent at P1/P2	1.57		absent at P9	**0.22**	
SPHK1	2.01	-1.18	-1.07	down	2.07		absent at P9	**-0.03**	
MIOX	2.01	-2.05	-1.51	down	1.94	2.24	up	**0.03**	
SESN3	2.01			absent at P1/P2	1.78	1.04	up	**0.12**	
HRK	2.02	-1.11	-1.92	down	1.74	1.27	up	**0.14**	
FAM107A	2.02			absent at P1/P2	1.88	-1.17	down	**0.07**	
STAR	2.02	1.53	-1.04	up at P1 and down at P2	1.96	-1.04	down at P9	**0.03**	
GNMT	2.02	2.04	1.39	up	1.46	1.51	up	**0.28**	
ELOVL6	2.03	1.22	1.54	up	1.67	1.48	up	**0.17**	a
B3GNT2	2.03	-1.12	-1.17	down	2.05	1.37	up	**-0.01**	
GRAMD1B	2.03			absent at P1/P2	1.64	1.20	up	**0.19**	
NAV1	2.03	1.01	-1.10	up at P1 and down at P2	1.82	1.21	up	**0.10**	
KHDRBS3	2.03			absent at P1/P2	2.13	-1.08	down at P9	**-0.05**	
SLC24A2	2.03			absent at P1/P2	1.79	-1.31	down	**0.12**	
TOR3A	2.03	1.40	1.35	up	1.71	1.39	up	**0.16**	
FABP7	2.03	1.45	2.12	up	1.87	1.22	up	**0.08**	c
AK1	2.04	1.47	2.22	up	1.73	1.44	up	**0.15**	
ADAM12	2.04	1.12	1.14	up	1.75	1.06	up	**0.14**	
PLEKHA2	2.04			absent at P1/P2	1.92	1.48	up	**0.06**	
PLEKHA7	2.04	-1.07	1.42	Down at P1 and up at P2	2.04	1.33	up	**0.00**	
CYP4V2	2.05	1.50	1.29	up	1.87	-1.09	down at P9	**0.08**	b
ATP1A2	2.05	1.31	1.33	up	1.47	-1.06	down	**0.28**	
MAPK13	2.05	1.01	1.50	up	1.66	1.31	up	**0.19**	
MMP2	2.05	-1.32	-1.72	Down at P1 and up at P2	1.57	1.22	up	**0.23**	
LRP2	2.05	1.09	1.32	up	1.79	5.22	up	**0.12**	
MATN2	2.05	1.26	1.15	up	2.45	1.45	up	**-0.19**	
RGS7	2.05	1.03	1.18	up	1.66	-1.18	down at P9	**0.19**	
NRP1	2.05	1.42	1.31	up	1.80	1.18	up	**0.12**	
RGN	2.06	1.80	-1.39	up at P1 and down at P2	2.43	1.57	up	**-0.18**	
RNF43	2.06			absent at P1/P2	1.48	2.19	up	**0.28**	
AMH	2.06	-1.31	1.28	Down at P1 and up at P2	1.96	1.28	up	**0.05**	
NR1H4	2.07	1.79	1.21	up	1.77	-1.18	down at P9	**0.14**	
GPR137B	2.07	1.25	1.22	up	1.74	1.08	up	**0.16**	
TXNDC5	2.07	1.05	1.35	up	1.92	1.43	up	**0.07**	
SOCS2	2.07	-1.18	-1.02	down	1.95	1.10	up	**0.06**	
CTTNBP2	2.08			absent at P1/P2	1.87	1.01	up at P9	**0.10**	
UGCG	2.08	1.38	1.31	up	1.76	1.20	up	**0.15**	a
PEX5L	2.08			absent at P1/P2	1.80	1.07	up	**0.14**	
CCDC80	2.09	1.17	1.16	up	1.73	1.25	up	**0.17**	
KIAA1199	2.09			absent at P1/P2	1.60	2.66	up	**0.24**	
ZNF467	2.09	-1.10	-1.10	down	1.88	1.49	up	**0.10**	
GULP1	2.09			absent at P1/P2	1.95		absent at P9	**0.06**	
TGFA	2.09	-1.08	1.14	Down at P1 and up at P2	1.82	1.25	up	**0.13**	
SLC38A1	2.09			absent at P1/P2	2.01	1.48	up	**0.04**	
HAO2	2.09	2.07	1.30	up	2.24	1.28	up	**-0.07**	
SYK	2.09	-1.44	1.48	Down at P1 and up at P2	1.71	1.62	up	**0.19**	c
CRIP2	2.10	1.61	1.15	up	2.07	1.56	up	**0.01**	
LTBP1	2.11	1.24	-1.15	up at P1 and down at P2	1.72	1.10	up	**0.18**	c
LGI2	2.11			absent at P1/P2	1.85	1.31	up	**0.13**	
SEMA3B	2.11	4.34	2.85	up	1.64	1.75	up	**0.22**	
CDKN1A	2.11	-1.81	1.62	Down at P1 and up at P2	1.74	2.51	up	**0.17**	
RTP4	2.11			absent at P1/P2	2.19	1.24	up	**-0.04**	
TMEM51	2.11			absent at P1/P2	2.02	1.88	up	**0.04**	
NDRG2	2.12	1.38	1.40	up	1.70	1.19	up	**0.20**	

RERG	2.12			absent at P1/P2	1.97	1.22	up	**0.07**	
KCNMA1	2.12	1.19	1.26	up	1.87	1.38	up	**0.12**	
FCGR2B	2.12	2.22	1.88	up	2.30	1.27	up	**-0.08**	
COL23A1	2.12			absent at P1/P2	1.77	1.22	up	**0.16**	
TSPAN7	2.12	1.29	1.20	up	1.85	1.30	up	**0.13**	c
CD74	2.13	1.56	1.99	up	1.72	1.35	up	**0.19**	a
CHST11	2.13			absent at P1/P2	1.81	1.18	up	**0.15**	
SLC1A5	2.13	1.18	-1.02	up at P1 and down at P2		-1.01	absent at P7	**1.00**	
TM2D2	2.13	1.13	-1.04	up at P1 and down at P2	1.89	1.09	up	**0.11**	
SMPDL3A	2.14	1.21	1.17	up	1.92	1.61	up	**0.10**	
FXYD1	2.14	1.13	1.19	up	1.75	-1.08	down	**0.18**	
TOB1	2.15	1.47	1.30	up	1.87	1.46	up	**0.13**	
MST4	2.16			absent at P1/P2	2.00	1.02	up	**0.08**	
FLRT3	2.16			absent at P1/P2	1.97	-1.02	down at P9	**0.09**	
CEBPA	2.17	-1.42	-1.19	down	2.05	1.13	up	**0.05**	
C16orf45	2.18			absent at P1/P2	2.16	2.12	up	**0.01**	
CLIP3	2.19	1.15	-1.01	up at P1 and down at P2	1.57	-1.12	down at P9	**0.28**	
IIGP1	2.20			absent at P1/P2	2.02		absent at P9	**0.08**	
PPARGC1B	2.20			absent at P1/P2	1.99	2.83	up	**0.09**	
KCNK1	2.20	1.21	1.18	up	2.60	1.88	up	**-0.18**	a
CDH1	2.20	-1.06	-1.07	down		4.15	absent at P7	**1.00**	
SLC7A8	2.20	1.11	1.32	up	1.70	1.23	up	**0.23**	
P2RX7	2.20	1.01	-1.00	up at P1 and down at P2	1.92		absent at P9	**0.13**	
PLXNB1	2.21			absent at P1/P2	1.98	1.92	up	**0.11**	
PNLIP	2.22			absent at P1/P2		1.70	absent at P7	**1.00**	
PKP2	2.22	2.98	1.67	up	2.00	1.38	up	**0.10**	
SEMA3D	2.23			absent at P1/P2	2.05	-1.11	down	**0.08**	
XDH	2.24	1.83	1.96	up		1.22	absent at P7	**1.00**	
GREB1	2.24			absent at P1/P2		-1.02	absent at P7	**1.00**	
EYA1	2.25	1.17	1.13	up	2.08	2.50	up	**0.07**	
SLIT2	2.25			absent at P1/P2	1.72	1.50	up	**0.24**	
PRLR	2.26	-1.31	1.79	Down at P1 and up at P2	2.12	1.50	up	**0.06**	
BCL11A	2.26			absent at P1/P2	1.65	1.58	up	**0.27**	c
NR2F1	2.27	1.15	1.21	up	1.99	-1.27	down	**0.12**	
IQGAP2	2.27	-1.18	-1.07	down	2.49		absent at P9	**-0.09**	
IGDCC3	2.28	1.09	1.31	up	1.83	1.66	up	**0.20**	
CAPN5	2.28	1.10	-1.01	up at P1 and down at P2	1.66	1.19	up	**0.27**	
CYP17A1	2.28	1.23	-1.07	up at P1 and down at P2	2.12	1.19	up	**0.07**	
MKX	2.30			absent at P1/P2	2.53	1.05	up	**-0.10**	
ITGB5	2.33	1.25	1.45	up	1.85	1.61	up	**0.20**	
KY	2.33			absent at P1/P2	2.23	3.05	up	**0.05**	
NELL2	2.34	1.04	1.29	up	1.40	1.46	up	**0.40**	
KCNT1	2.34			absent at P1/P2	2.30	1.99	up	**0.02**	
HLA-DMB	2.35	6.50	2.28	up	1.96		absent at P9	**0.17**	
SFRP1	2.35	1.07	1.47	up	1.80	1.23	up	**0.23**	
Svs5	2.36	2.10	1.83	up	1.63	1.84	up	**0.31**	
LIN7A	2.36			absent at P1/P2	1.89	1.06	up	**0.20**	
TES	2.37	5.01	1.40	up	2.03	-2.18	down at P9	**0.14**	
RBFOX1	2.37			absent at P1/P2	2.14		absent at P9	**0.10**	
CTSH	2.38	1.26	1.57	up	1.85	1.10	up	**0.22**	
ANGPT2	2.39	1.38	1.28	up	2.08	1.49	up	**0.13**	
SYBU	2.39			absent at P1/P2	1.93	1.25	up	**0.19**	
GABRA1	2.39	1.32	1.30	up	1.70	-1.09	down at P9	**0.29**	
GPC1	2.40	1.03	1.25	up	2.08	1.30	up	**0.13**	
FAM57B	2.40			absent at P1/P2	1.99		absent at P9	**0.17**	
IGF1	2.40	1.16	1.25	up	2.24		absent at P9	**0.07**	
DPF3	2.40	1.33	1.28	up	1.70	1.26	up	**0.29**	
TMPRSS13	2.40			absent at P1/P2	2.17	1.93	up	**0.10**	
OOEP	2.41			absent at P1/P2	1.73	3.24	up	**0.28**	
LEPR	2.41	-1.03	-1.24	down	1.56		absent at P9	**0.35**	
CAMTA1	2.42			absent at P1/P2	1.57	1.30	up	**0.35**	
THBS1	2.42	1.77	1.44	up		1.01	absent at P7	**1.00**	
NTSR1	2.43	1.05	1.36	up	2.02	1.28	up	**0.17**	
PAK3	2.43	1.37	-1.09	up at P1 and down at P2	2.16	-1.10	down at P9	**0.11**	
RASGEF1B	2.43			absent at P1/P2	2.01	1.33	up	**0.17**	
EPHA3	2.43	1.07	-1.01	up at P1 and down at P2		-1.07	absent at P7	**1.00**	
PPM1H	2.44			absent at P1/P2	2.21	2.05	absent at P7	**0.09**	
MDFIC	2.44	1.20	1.20	up	2.26	1.15	up	**0.07**	
ALDH3A1	2.44	1.26	-1.19	up at P1 and down at P2	1.84	1.22	up	**0.25**	
NLRP10	2.45			absent at P1/P2	1.74	1.09	up	**0.29**	
PBX3	2.45	1.17	1.31	up	2.06	1.36	up	**0.16**	
C13orf15	2.46	1.01	1.26	up	2.39	1.36	up	**0.03**	
STC2	2.46	1.25	1.47	up	1.87	1.16	up	**0.24**	
MIA	2.46	1.20	-1.00	up at P1 and down at P2		1.22	up	**1.00**	a
FGF7	2.46	1.51	-1.05	up at P1 and down at P2	1.89	1.23	up	**0.23**	c
DMRT3	2.46			absent at P1/P2	2.11	1.51	up	**0.14**	
SERPINF1	2.46	1.47	1.79	up	1.89	-1.12	down at P9	**0.23**	

FGFR2	2.46	1.86	1.26	up	2.07		absent at P9	**0.16**	
GPD1	2.47	2.38	1.92	up	2.58	1.12	up	**-0.04**	
TNNI1	2.48	1.29	1.48	up		1.42	absent at P7	**1.00**	
ZC3H4	2.48			absent at P1/P2	1.78	-1.10	down	**0.28**	
GMPR	2.53			absent at P1/P2	2.54	1.65	up	**0.00**	
RND3	2.53			absent at P1/P2	2.47	1.52	up	**0.02**	
NOBOX	2.55	1.43	-1.12	up at P1 and down at P2	1.39	9.08	up	**0.46**	
ROBO1	2.56	1.66	-1.06	up at P1 and down at P2	2.17	-1.19	down at P9	**0.15**	
EDA2R	2.56			absent at P1/P2	1.83	-1.04	down at P9	**0.29**	
CNTN4	2.56	2.09	1.31	up	2.10	1.22	up	**0.18**	
CELSR1	2.57	1.44	1.75	up	1.85	1.39	up	**0.28**	
KCND2	2.58	1.23	1.50	up	1.62	1.83	up	**0.37**	
PRMT8	2.59			absent at P1/P2	1.47	8.67	up	**0.43**	
ODZ2	2.59	1.13	1.72	up	2.13	1.51	up	**0.18**	
PIK3R1	2.59	1.32	1.14	up	2.23	1.14	up	**0.14**	
Aldh1a7	2.59	1.37	1.65	up	1.83	-1.15	down at P9	**0.30**	
GABRB3	2.61	1.31	1.36	up	2.19	3.02	up	**0.16**	
TGFB2	2.64	1.37	1.31	up	1.92	1.43	up	**0.27**	
MYOC	2.65	1.12	1.41	up		1.80	absent at P7	**1.00**	
FETUB	2.65			absent at P1/P2	2.18	2.22	up	**0.18**	
THRSP	2.65	1.63	-1.09	up at P1 and down at P2	1.79	1.85	up	**0.33**	
LSAMP	2.67			absent at P1/P2	1.87	1.06	up	**0.30**	
TESC	2.67			absent at P1/P2	2.75	1.93	up	**-0.03**	
TTC39B	2.68	2.50	2.01	up	2.45		absent at P9	**0.08**	
SPEG	2.68	-1.67	1.56	Down at P1 and up at P2	2.29	1.53	up at P9	**0.15**	
FRAS1	2.69			absent at P1/P2	2.27	1.93	up	**0.16**	
VTN	2.71	1.13	1.20	up	1.94	1.93	up	**0.28**	
HTRA1	2.71	1.08	1.25	up	2.32	1.51	up	**0.15**	
MYBPC3	2.72	1.27	1.67	up	1.91	2.37	up	**0.30**	
KCNE1	2.72	-1.43	-1.47	down	2.32	-1.26	down	**0.15**	b
SLC6A15	2.76	1.65	1.16	up	1.97	1.11	up	**0.28**	
CADPS	2.77	1.75	1.55	up	2.14	1.27	up	**0.23**	C
KCNJ3	2.77	2.02	-1.09	up	2.68	1.21	up	**0.04**	
TRIM62	2.78			absent at P1/P2	2.51	1.41	up	**0.10**	
RCN1	2.79	1.19	-1.04	up at P1 and down at P2	1.62	1.27	up	**0.42**	
PIPOX	2.80	1.27	1.30	up	2.36	2.22	up	**0.16**	
HEY1	2.81	1.43	1.48	up	2.19	1.19	up	**0.22**	
SORL1	2.86	1.19	-2.16	up at P1 and down at P2	1.88	-1.42	down at P9	**0.34**	
NFE2	2.87	1.43	1.68	up	2.28	1.87	up	**0.21**	
MMP23B	2.87			absent at P1/P2	2.46	1.99	up	**0.15**	
EPHA4	2.88	1.88	1.15	up	2.13	1.29	up	**0.26**	
RPRM	2.90	2.83	2.04	up	2.52	2.43	up	**0.13**	
CHST8	2.95			absent at P1/P2	1.94	1.29	up	**0.34**	
BHLHE22	2.97			absent at P1/P2	2.16	1.19	up	**0.27**	
HSD17B1	2.98	-1.07	-1.02	down	2.60	1.50	up	**0.13**	
FHOD3	3.00	1.38	1.93	down	2.57	2.15	up	**0.14**	
CPNE8	3.01			absent at P1/P2		-2.05	absent at P7	**1.00**	
ENO3	3.01	1.27	1.66	up	2.00	1.45	up	**0.34**	c
UNC13D	3.02			absent at P1/P2	2.57	2.34	up	**0.15**	
WIF1	3.02			absent at P1/P2	2.59	2.63	up	**0.14**	
PCDH9	3.03			absent at P1/P2	2.88	1.34	up	**0.05**	
LTBP3	3.06	1.15	-1.36	up at P1 and down at P2	2.87	1.30	up	**0.06**	
RBM47	3.09			absent at P1/P2	2.08		absent at P9	**0.33**	
ADCYAP1R1	3.12	-1.24	-1.64	down	2.30	2.16	up	**0.26**	
MRAP	3.16	1.75	1.44	up	2.14	1.47	up	**0.32**	
ZNF521	3.18			absent at P1/P2	2.09		absent at P9	**0.34**	
MMP15	3.18	1.47	1.31	up	2.09	1.48	up	**0.34**	
ASPH	3.20				2.93			**0.08**	
CADPS2	3.21				2.41	-1.29		**0.25**	
ZMIZ1	3.24			absent at P1/P2	3.60		absent at P9	**-0.11**	
PTGDS	3.24	-1.35	1.30	Down at P1 and up at P2	2.71	2.17	up	**0.17**	
CELA3B	3.26			absent at P1/P2	3.27	1.75	up	**0.00**	
NPPC	3.26	2.12	2.66	up	3.23	1.76	up	**0.01**	
KLKB1	3.28	2.84	1.98	up	2.84	1.48	up	**0.14**	
EPPK1	3.32			absent at P1/P2	2.53	1.77	up	**0.24**	
PCSK6	3.34	1.36	1.71	up	2.59	3.22	up	**0.23**	
NETO2	3.38			absent at P1/P2	2.68		absent at P9	**0.21**	
MID1	3.40	-1.16	-1.21	down		1.16	absent at P7	**1.00**	
RPS9	3.48			absent at P1/P2	1.30	1.08	up	**0.63**	
EGFL6	3.48			absent at P1/P2		2.05	absent at P7	**1.00**	
MYO1A	3.57			absent at P1/P2	2.52	2.64	up	**0.29**	
AQP5	3.57			absent at P1/P2	4.06	2.11	up	**-0.13**	
CNGA1	3.63	-1.72	-3.83	down	2.26	1.80	up	**0.38**	
P2RY6	3.63			absent at P1/P2	2.59	1.30	up	**0.29**	
SEMA3A	3.64	1.45	-1.03	up at P1 and down at P2	2.85	1.05	up	**0.22**	
HLA-DRB1	3.64	2.48	2.44	up	2.64	3.77	up	**0.27**	
FABP3	3.65	1.53	1.34	up	3.40	1.61	up	**0.07**	c

SGPP2	3.94			absent at P1/P2	3.60	1.37	up	**0.09**	
HLA-DQA1	4.10	4.22	4.78	up	3.22	2.13	up	**0.22**	
PQLC1	4.20	1.85	1.96	up	2.98	1.58	up	**0.29**	
ANO4	4.28			absent at P1/P2	3.33	-1.08	down at P9	**0.22**	
DSG2	4.34	1.43	1.68	up	3.62	3.19	up	**0.17**	a
HLA-DQB1	4.36			absent at P1/P2	3.40		absent at P9	**0.22**	
FBLN2	4.50	1.22	1.46	up	3.23	2.03	up	**0.28**	
KCNH1	4.64	1.11	1.13	up	3.99	1.63	up	**0.14**	c
SPSB4	4.65			absent at P1/P2	4.17	1.84	up	**0.10**	
TCEA3	4.67	1.83	2.01	up	3.56	1.03	up	**0.24**	
APOC1	4.69	2.11	2.83	up	2.80	2.25	up	**0.40**	
BMP6	4.70	1.63	1.44	up	3.61	1.54	up	**0.23**	b
TMEM178	4.75			absent at P1/P2	3.49	1.75	up	**0.27**	
HSPB8	4.76	2.77	1.65	up	3.44	1.72	up	**0.28**	
DSP	4.95	1.10	-1.12	up at P1 and down at P2	3.56		absent at P9	**0.28**	
BMPER	5.17			absent at P1/P2	3.49	1.09	up	**0.33**	
LRRN1	5.19	2.08	1.55	up	3.46	1.70	up	**0.33**	
KRT18	5.77	1.94	1.71	up	4.86	2.51	up	**0.16**	
PCDH8	6.26			absent at P1/P2	3.40	2.25	up	**0.46**	
KRT8	6.36	2.31	2.07	up	4.05	2.10	up	**0.36**	
CRABP2	6.55	2.28	4.63	up	8.00	9.15	up	**-0.22**	
CCL17	7.71	1.20	2.33	up	6.44	-1.01	down at P9	**0.16**	
CFI	8.21	15.47	11.15	up	5.71	2.80	up	**0.30**	
PNMT	9.69	-1.46	1.30	Down at P1 and up at P2	4.40	-1.16	down at P9	**0.55**	
ZG16	9.89	1.03	-1.03	up at P1 and down at P2	6.90	2.92	up	**0.30**	
LECT1	11.62			absent at P1/P2	6.20	3.95	up	**0.47**	

KEY
a = (Chip-Chip)-DMRT1 Binding to anywhere within the promoter. Peak called in 3 separate experiments (Murphy et al., 2010)
b = (Chip-Chip)-DMRT1 Binding to anywhere within the promoter. Peak called in 2 separate experiments (Murphy et al., 2010)
c = (Chip-Chip)-DMRT1 Binding to anywhere within the promoter. Peak called in 1 experiment (Murphy et al., 2010)
d = ChIP-Seq- Enrichment at 10kb to 5' promoter region
e = ChIP-Seq - Enrichment at intergenic regions
f = ChIP-Seq - Enrichment at intronic regions
g = ChIP-Seq - Enrichment at 3' regions

B

		Dmrt1 -null / *Dmrt1* -Wt	
	Comparison	**P1& P2/P7 (# of genes)**	**Percentage (%)**
	Absent at P1/P2	310	40.31
Opposite	Up at P1 and down at P2	94	12.22
	Down at P1 and up at P2	36	4.68
Shared	Up	132	17.17
	Down	190	24.71
	Up at P1	1	0.13
	Up at P1/P2	6	0.78
	TOTAL	769	

C

		Dmrt1 -rescue/ *Dmrt1* -Wt vs *GCDmrt1KO* / Ctrl	
	Comparison	**P7/P9 (# of genes)**	**Percentage (%)**
	Absent at P7	36	4.68
	Absent at P9	72	9.36
Opposite	Up at P9 and down at P7	198	25.75
	Down at P9 and up at P7	18	2.34
Shared	Up	179	23.28
	Down	264	34.33
	Absent at P7 & P9	2	0.26
	Total	769	

Table 3: DMRT1 binding sites characteristics identified by manual analysis of ChIP-Seq data. A. DMRT1 binding site characteristics. **B.** Top 31 DMRT1 targets grouped into five functional categories. 1 = Cell adhesion/ cytoskeletal regulation, 2 = RNA processing, 3 = protein processing/transport, 4 =DNA recombination/repair and 5 = homeostasis.

A: DMRT1 Binding Site Characteristics

REPRESENTED CHROMOSOMES	
1, 2,3,4, 5, 6, 7, 8, 9, 10, 12, 14, 15, 19, X, Y	
BINDING SITE	
INTRON	87%
3' END	6.5%
5' END + INTRON	6.5%
AVERAGE BINDING AFFINITY (qChIP)	
11X over IgG	
Range = 4X - 20X	

B: 31 Top DMRT1 Binding Sites and Putative Target Characteristics

BINDING		CONFIRMATION	TARGET GENE CHARACTERISTICS			
CHR	GENE	*qChIP	SYMBOL	GROUP	NAME	PREDICTED / KNOWN FUNCTION
chr9	INTRON	20X	Bbs9	1	Bardet-Biedl syndrome 9	Cilia biogenesis
chr15	INTRON	10X	Cdh12	1	Cadherin 12, type 2	Cell adhesion, cell junction assembly
chr19	INTRON	11X	Gfra1	1	GDNF receptor 1	Cell adhesion, migration, differentiation
chr3	INTRON	10X	Nlgn1	1	Neuroligin 1	Cell adhesion, lipid metabolism, vesicle transport
chr9	INTRON	15X	Ntm	1	Neurotrimin	Cell adhesion, cell recognition
chr6	INTRON	20X	Ppp1r9a	1	Protein phosphatase 1, regulatory subunit 9A	Cytoskeleton organization, polarized cell growth
chr5	INTRON	10X	Sez6l	1	Seizure related 6 homolog-like	Cell adhesion
chr1	INTRON	4X	Spag16	1	Sperm associated antigen 16	Cilia biogenesis, gamete production
chr10	INTRON	20X	Bicc1	2	Bicaudal C homolog 1	RNA binding, translation regulator, cilia orientation
chr1	800bp 3'	8X	Pou2f1	2	POU domain, class 2, transcription factor 1	Transcription, cell fate, growth arrest
chr2	INTRON	16X	Rbl1	2	Retinoblastoma-like 1 (p107)	Transcription, cell cycle regulation
chrY	INTRON	14X	Rbmy1a1	2	RNA binding motif protein, Y chr, family 1, A1	RNA processing/splicing
chr1	INTRON;5'	10X	Smg7	2	Smg-7 homolog	RNA transport / regulation NMD
chr1	INTRON	16X	Thoc3	2	THO complex 3	RNA binding / localization
chr2	INTRON	8X	ZNF658	2	zinc finger protein 658	Transcription
chr10	INTRON	8X	Cpm	3	Carboxypeptidase M	Peptide hormone processing, signaling
chr6	INTRON	8X	D6Wsu116e	3	WASH complex subunit FAM21	Retrograde transport (endosome to Golgi)
chr14	INTRON	6X	Enox1	3	Ecto-NOX disulfide-thiol exchanger 1	Disulfide-thiol interchange, cell migration
chr8	INTRON	11X	Galntl6	3	N-acetylgalactosaminyltransferase-like 6	Glycosylation, cell adhesion
chr4	INTRON	12X	Heatr8	3	HEAT repeat containing 8	Intracellular transport
chr10	INTRON	8X	Man1a	3	Mannosidase, alpha, class 1A, member 1	Glycosylation
chr5	INTRON	8X	Vps33a	3	Vacuolar protein sorting 33A	Intracellular trafficking, exocytosis
chr6	12Kb 5'	8X	Anubl1	4	AN1, ubiquitin-like, homolog	DNA repair
chr2	INTRON	8X	Aven	4	Apoptosis, caspase activation inhibitor	DNA damage response / G2/M progression
chr5	INTRON	ND	Taok3	4	TAO kinase 3	DNA damage
chr8	INTRON	13X	BM894861	5	BM894861; BE335740; BX517754	Unknown
chr1	INTRON;5'	8X	Cd247 (nc)	5	Cd247 antigen; T Cell Receptor zeta	Antigen recognition / cell signaling
chr12	INTRON	12X	Dhrs7	5	Dehydrogenase/reductase member 7	Steroid, retinoid, prostaglandin metabolism
chrX	760 bp 3'	7X	Fthl17	5	Ferritin, heavy polypeptide-like 17	Iron transport / storage
chr7	INTRON	10X	Inpp5a	5	Inositol polyphosphate-5-phosphatase A	Calcium mobilization, cell communication
chr4	INTRON	5X	Mup12	5	Major urinary protein 12	Glucose homeostasis
*Fold over IgG					** EXP = mRNA expression in P7 *Dmrt1*$^{-/-}$ testes relative to *Dmrt1*$^{+/+}$ testes	

Table 4: Pathways and processes induced by differential gene expression profiles regulated through *Dmrt1* in Sertoli cells and germ cells. A. Canonical pathways. B. Biological processed.

A

IPA identified functional clusters of genes regulated by DMRT1 in germ cells and Sertoli cells				
Category		Count [a]	% [b]	p-value [c]
Clusters of genes differentially regulated through *Dmrt1* in germ cells				
	VDR/RXR Activation	9	11.1	4.07E-03
	ATM Signaling	7	11.9	7.76E-03
	Mouse Embryonic Stem Cell Pluripotency	8	9.09	1.45E-02
	RAR Activation	13	6.91	2.24E-02
	Role of NANOG in Mammalian Embryonic Stem Cell Pluripotency	9	7.89	3.24E-02
	FLT3 Signaling in Hematopoietic Progenitor Cells	9	12.2	2.34E-03
	Role of NFAT in Regulation of the Immune Response	15	7.58	3.89E-03
	IL-4 Signaling	8	11	5.89E-03
Clusters of genes differentially regulated through *Dmrt1* in Sertoli cells				
	Valine, Leucine and Isoleucine Biosynthesis	2	4.76	5.25E-04
	Pantothenate and CoA Biosynthesis	2	3.28	1.62E-03
	Glycerolipid Metabolism	3	1.92	4.27E-03
	Alanine and Aspartate Metabolism	2	2.44	6.76E-03
	Sphingolipid Metabolism	2	1.77	2.88E-02
	Bladder Cancer Signaling	2	2.2	3.16E-02
	Note. A canonical pathway–based analysis was conducted using the IPA (Ingenuity Systems, www.ingenuity.com) to identify the pathways enriched in genes constitutively induced or suppressed withdifferential expression of *Dmrt1* in Sertoli cells and germ cells. [a]Probe number in a specific pathway. [b]The ratio of the number of genes that were differentially regulated by *Dmrt1* and map to the pathway, divided by the total number of genes that map to the canonical pathway, was calculated. [c]Fisher's exact test was used to calculate the p-value determining that the probability of the association between the genes differentially regulated by Dmrt1 and the canonical pathway was random.			

B

Clustering of associated processes enriched among genes constitutively induced or suppressed by cell-specific action of *Dmrt1* using IPA		
Category		p-value
Clusters of processed among genes differentially regulated by *Dmrt1* in germ cells		
	Spermatogenesis	2.01E-04
	Male gamete generation	2.01E-04
	Sexual reproduction	6.53E-04
	Gamete generation	4.17E-04
	Apoptosis	4.81E-02
	Cell adhesion	2.76E-03
	Reproductive process	9.41E-05
	Reproduction	9.63E-05
	Internal genitalia morphogenesis	4.87E-04
	Sex differentiation	4.76E-02
	Genitalia morphogenesis	3.89E-03
Clusters of processes among genes differentially regulated by *Dmrt1* in Sertoli cells		
	Infertility	1.40E-04
	Cell-To-Cell Signaling and Interaction	3.16E-03
	Cell-cell contact	3.16E-03
	Metabolism of cholesterol ester	3.16E-03
	Kinesin binding	1.61E-03
	RNA binding	4.24E-03

Table 5: Functional annotations for subset of genes derived from comparisons of *Dmrt1*-null, *Dmrt1*-rescue and *GCDmrt1KO* gene expression profiles. A, B, and **C,** represent biological processes enriched in subset of genes comparing P1/P2 and P7 *Dmrt1*-null samples. **D, E, F** and **G** represent biological processes enriched in subset of genes comparing P7 *Dmrt1*-rescue and P9 *GCDmrt1KO* samples.

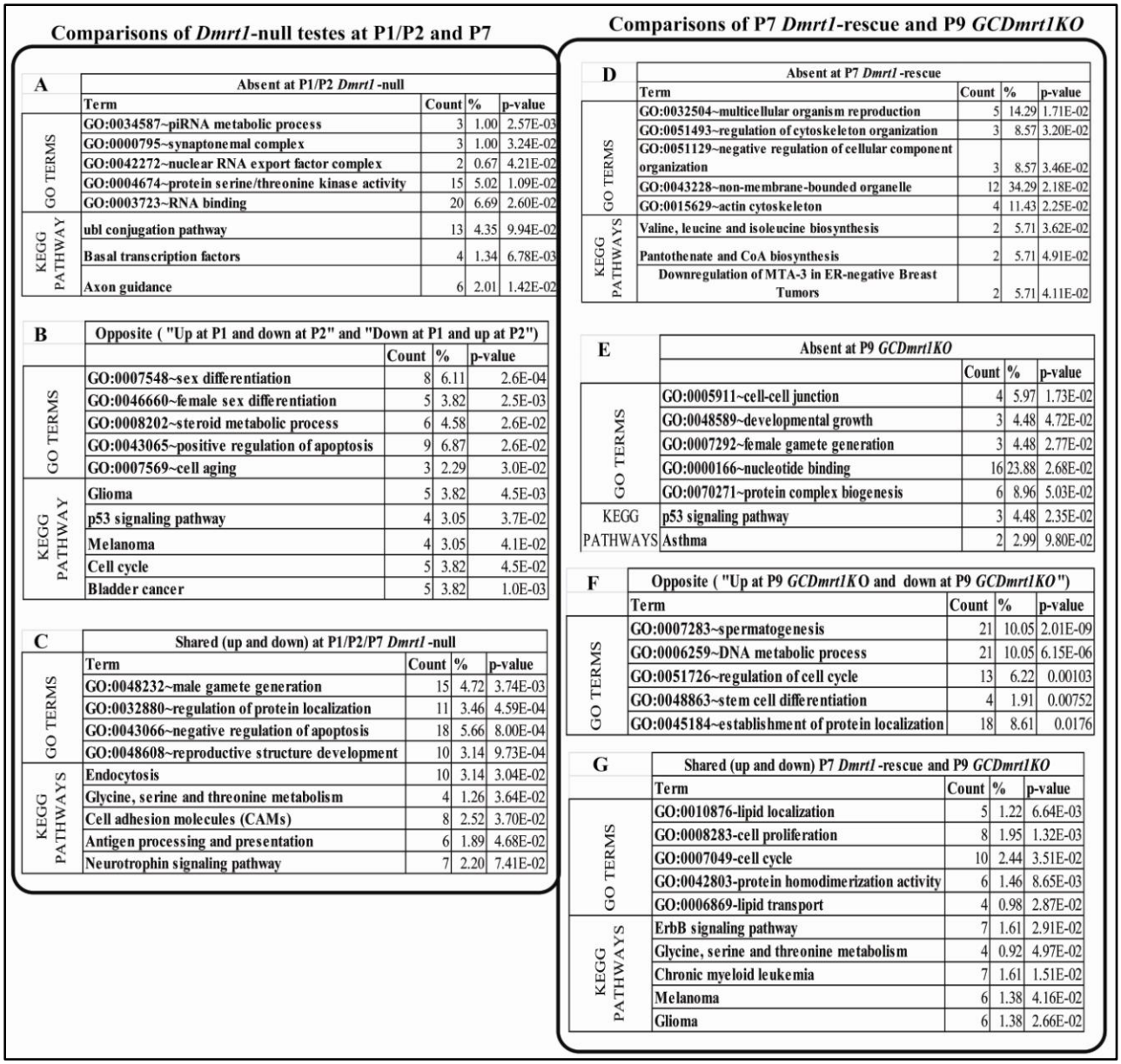

Comparisons of *Dmrt1*-null testes at P1/P2 and P7

A

	Absent at P1/P2 *Dmrt1* -null			
	Term	Count	%	p-value
GO TERMS	GO:0034587~piRNA metabolic process	3	1.00	2.57E-03
GO TERMS	GO:0000795~synaptonemal complex	3	1.00	3.24E-02
GO TERMS	GO:0042272~nuclear RNA export factor complex	2	0.67	4.21E-02
GO TERMS	GO:0004674~protein serine/threonine kinase activity	15	5.02	1.09E-02
GO TERMS	GO:0003723~RNA binding	20	6.69	2.60E-02
KEGG PATHWAY	ubl conjugation pathway	13	4.35	9.94E-02
KEGG PATHWAY	Basal transcription factors	4	1.34	6.78E-03
KEGG PATHWAY	Axon guidance	6	2.01	1.42E-02

B

	Opposite ("Up at P1 and down at P2" and "Down at P1 and up at P2")			
		Count	%	p-value
GO TERMS	GO:0007548~sex differentiation	8	6.11	2.6E-04
GO TERMS	GO:0046660~female sex differentiation	5	3.82	2.5E-03
GO TERMS	GO:0008202~steroid metabolic process	6	4.58	2.6E-02
GO TERMS	GO:0043065~positive regulation of apoptosis	9	6.87	2.6E-02
GO TERMS	GO:0007569~cell aging	3	2.29	3.0E-02
KEGG PATHWAY	Glioma	5	3.82	4.5E-03
KEGG PATHWAY	p53 signaling pathway	4	3.05	3.7E-02
KEGG PATHWAY	Melanoma	4	3.05	4.1E-02
KEGG PATHWAY	Cell cycle	5	3.82	4.5E-02
KEGG PATHWAY	Bladder cancer	5	3.82	1.0E-03

C

	Shared (up and down) at P1/P2/P7 *Dmrt1* -null			
	Term	Count	%	p-value
GO TERMS	GO:0048232~male gamete generation	15	4.72	3.74E-03
GO TERMS	GO:0032880~regulation of protein localization	11	3.46	4.59E-04
GO TERMS	GO:0043066~negative regulation of apoptosis	18	5.66	8.00E-04
GO TERMS	GO:0048608~reproductive structure development	10	3.14	9.73E-04
KEGG PATHWAYS	Endocytosis	10	3.14	3.04E-02
KEGG PATHWAYS	Glycine, serine and threonine metabolism	4	1.26	3.64E-02
KEGG PATHWAYS	Cell adhesion molecules (CAMs)	8	2.52	3.70E-02
KEGG PATHWAYS	Antigen processing and presentation	6	1.89	4.68E-02
KEGG PATHWAYS	Neurotrophin signaling pathway	7	2.20	7.41E-02

Comparisons of P7 *Dmrt1*-rescue and P9 *GCDmrt1KO*

D

	Absent at P7 *Dmrt1* -rescue			
	Term	Count	%	p-value
GO TERMS	GO:0032504~multicellular organism reproduction	5	14.29	1.71E-02
GO TERMS	GO:0051493~regulation of cytoskeleton organization	3	8.57	3.20E-02
GO TERMS	GO:0051129~negative regulation of cellular component organization	3	8.57	3.46E-02
GO TERMS	GO:0043228~non-membrane-bounded organelle	12	34.29	2.18E-02
GO TERMS	GO:0015629~actin cytoskeleton	4	11.43	2.25E-02
KEGG PATHWAYS	Valine, leucine and isoleucine biosynthesis	2	5.71	3.62E-02
KEGG PATHWAYS	Pantothenate and CoA biosynthesis	2	5.71	4.91E-02
KEGG PATHWAYS	Downregulation of MTA-3 in ER-negative Breast Tumors	2	5.71	4.11E-02

E

	Absent at P9 *GCDmrt1KO*			
		Count	%	p-value
GO TERMS	GO:0005911~cell-cell junction	4	5.97	1.73E-02
GO TERMS	GO:0048589~developmental growth	3	4.48	4.72E-02
GO TERMS	GO:0007292~female gamete generation	3	4.48	2.77E-02
GO TERMS	GO:0000166~nucleotide binding	16	23.88	2.68E-02
GO TERMS	GO:0070271~protein complex biogenesis	6	8.96	5.03E-02
KEGG PATHWAYS	p53 signaling pathway	3	4.48	2.35E-02
KEGG PATHWAYS	Asthma	2	2.99	9.80E-02

F

	Opposite ("Up at P9 *GCDmrt1KO* and down at P9 *GCDmrt1KO*")			
	Term	Count	%	p-value
GO TERMS	GO:0007283~spermatogenesis	21	10.05	2.01E-09
GO TERMS	GO:0006259~DNA metabolic process	21	10.05	6.15E-06
GO TERMS	GO:0051726~regulation of cell cycle	13	6.22	0.00103
GO TERMS	GO:0048863~stem cell differentiation	4	1.91	0.00752
GO TERMS	GO:0045184~establishment of protein localization	18	8.61	0.0176

G

	Shared (up and down) P7 *Dmrt1* -rescue and P9 *GCDmrt1KO*			
	Term	Count	%	p-value
GO TERMS	GO:0010876-lipid localization	5	1.22	6.64E-03
GO TERMS	GO:0008283-cell proliferation	8	1.95	1.32E-03
GO TERMS	GO:0007049-cell cycle	10	2.44	3.51E-02
GO TERMS	GO:0042803-protein homodimerization activity	6	1.46	8.65E-03
GO TERMS	GO:0006869-lipid transport	4	0.98	2.87E-02
KEGG PATHWAYS	ErbB signaling pathway	7	1.61	2.91E-02
KEGG PATHWAYS	Glycine, serine and threonine metabolism	4	0.92	4.97E-02
KEGG PATHWAYS	Chronic myeloid leukemia	7	1.61	1.51E-02
KEGG PATHWAYS	Melanoma	6	1.38	4.16E-02
KEGG PATHWAYS	Glioma	6	1.38	2.66E-02

Table 6: Manual analysis identifying genes important in specific spermatogenic processes and regulated entirely or partially by DMRT1 in a cell-specifically. Relative factor (RF) was the difference of one (1) minus the quotient obtained by dividing *Dmrt1*$^{-/-;tg}$/*Dmrt1*$^{+/+}$ fold changes by *Dmrt1*$^{-/-}$/*Dmrt1*$^{+/+}$ fold changes. RF≤ 0.4 = Not rescued, 0.5 ≤ RF≤ 0.7 = partially rescued and RF ≥ 0.8 = completely rescued. All genes with RF<1 were considered germ cell-specific while those with RF = 1 were considered Sertoli cell specific.

GENE	GENE TITLE	KO VS WT	RES VS WT	RF	FXN	Point of Interest	Cell type inference
Tktl1	Transketolase-like 1	-5.11	-2.36	0.5	C,CS	PR	SC,GC
Bcl2-l11	BCL2-like 11 (apoptosis facilitator)	-1.27	-1.38	-0.1	CS	NR	GC
Bmp6	Bone morphogenetic protein 6	4.70	3.61	0.2	CS	NR	GC
Dpf1	D4, zinc and double PHD finger family 1	-1.20	0.00	1.0	CS	ER	SC
Gpr37	G protein-coupled receptor 37	-5.39	-2.65	0.5	CS	PR	SC,GC
Hspb8	Heat shock protein 8 (aka Hsp22)	4.76	3.44	0.3	CS	NR	GC
Tlx1	T-cell leukemia homeobox protein 1	1.19	0.00	1.0	CS	ER	SC
POU3F1	POU domain, class 3, transcription factor 1	-3.10	-3.15	0.0	CS,SCM	NR	GC
Cldn11	Claudin 11	-6.71	-5.27	0.2	CJ	NR	GC
Ocln	Ocludin	-26.67	-23.82	0.1	CJ	NR	GC
Aqp5	Aquaporin 5	4.06	3.57	0.1	E	NR	GC
BM117570	Noncoding exosome RNA	4.35	0.00	1.0	E	ER	SC
Cadm1	Cell adhesion molecule 1	-7.10	-6.61	0.1	E	NR	GC
Cfi	Complement component factor i	8.21	5.71	0.3	E	NR	GC
Cpne8	Copine VIII	3.01	0.00	1.0	E	ER	SC
Foxq1	Forkhead box Q1	-7.67	-5.18	0.3	E	NR	GC
H2-Aa	Histocompatibility 2; class II antigen A; alpha	4.10	3.22	0.2	E	NR	GC
Hspb8	Heat shock protein 8 (aka Hsp22)	4.76	3.44	0.3	E	NR	GC
Rps9	Ribosomal protein S9	3.48	1.39	0.6	E	PR	SC,GC
Tuba3a	Tubulin; alpha 3A	-5.05	-4.01	0.2	E	NR	GC
Ano4	Anoctamin 4 (Tmem 16d)	4.28	3.33	0.2	E	NR	GC
Fbln2	Fibulin 2	4.50	3.23	0.3	E,A	NR	GC
Rarres1	Retinoic acid receptor responde (tazarotene induced) 1	-11.50	0.00	1.0	E, CS,VA	ER	SC
Dsg2	Desmoglein 2	4.34	3.62	0.2	E, CJ	NR	GC
Dsp	Desmoplakin	4.95	3.17	0.4	E, CJ	NR	GC
Piwil2	Piwi-like homolog 2	-4.88	-4.98	0.0	E,M,RB	NR	GC
Krt18	Keratin 18	5.77	4.86	0.2	E,MI	NR	GC
Krt8	Keratin 8	6.36	4.05	0.4	E	NR	GC
Mid1	Midline 1;	3.40	0.00	1.0	E, UC	ER	SC
Dppa3	Developmental pluripotency-associated 3	2.59	3.33	-0.3	E,SCM	NR	GC
Gfra1	Glial cell line-derived neurotrophic factor receptor alpha 1	-5.50	-4.86	0.1	E, SCM	NR	GC
Crabp2	Cellular retinoic acid binding protein II	6.55	8.00	-0.2	E,VA	NR	GC
Maeg	EGF-like-domain, multiple 6	3.48	0.00	1.0	IB	ER	SC
Dazl	Deleted in azoospermia-like	-5.37	-3.50	0.3	M	NR	GC
Tex14	SAM & basic leucine zipper domain containing 1	-5.39	-3.64	0.3	M	NR	GC
Gtsf1	Gametocyte specific factor 1	-7.38	-4.15	0.4	M	NR	GC
Nxf2	Nuclear RNA export factor 2	-4.08	-2.53	0.4	M	NR	GC
Sycp1	Synaptonemal complex protein 1	-3.27	0.00	1.0	M	NR	SC
Sycp2	Synaptonemal complex protein 2	-5.30	-1.80	0.7	M	PR	SC,GC
Tex11	Testis expressed gene 11	-9.23	-2.92	0.7	M	PR	SC,GC
Tex19.1	Testis expressed gene 19.1	-3.56	-3.19	0.1	M	NR	GC
Vdr	Vitamin D receptor	-6.71	-4.61	0.3	M	NR	GC
Morc1	Microrchidia 1	-12.41	-11.94	0.0	M,CS	NR	GC
Mov10l1	Moloney leukemia virus 10-like 1	-4.33	-3.44	0.2	M, RB	NR	GC
Mael	Maelstrom homolog (Drosophila)	-6.50	-4.24	0.3	M, RF	NR	GC
Stra8	Stimulated by retinoic acid gene 8	-3.37	-1.64	0.5	M, VA	PR	SC,GC
Meig1	Meiosis expressed gene 1	-5.18	-6.22	-0.2	M, VA	NR	GC
Ccl17	Chemokine (C-C motif) ligand 17	7.71	6.44	0.2	M	NR	GC
Sgpp2	Sphingosine-1-phosphate phosphotase 2	3.94	3.60	0.1	M	NR	GC
Lect1	Leukocyte cell derived chemotaxin 1	11.62	6.20	0.5	M	PR	SC,GC
Ddx25	DEAD (Asp-Glu-Ala-Asp) box polypeptide 25	-5.00	-6.05	-0.2	RB	NR	GC

GENE	GENE TITLE	KO VS WT	RES VS WT	RF	FXN	Point of Interest	Cell type inference
Tex14	SAM & basic leucine zipper domain containing 1	-5.39	-3.64	0.3	M	NR	GC
Gtsf1	Gametocyte specific factor 1	-7.38	-4.15	0.4	M	NR	GC
Nxf2	Nuclear RNA export factor 2	-4.08	-2.53	0.4	M	NR	GC
Sycp1	Synaptonemal complex protein 1	-3.27	0.00	1.0	M	NR	SC
Sycp2	Synaptonemal complex protein 2	-5.30	-1.80	0.7	M	PR	SC,GC
Tex11	Testis expressed gene 11	-9.23	-2.92	0.7	M	PR	SC,GC
Tex19.1	Testis expressed gene 19.1	-3.56	-3.19	0.1	M	NR	GC
Vdr	Vitamin D receptor	-6.71	-4.61	0.3	M	NR	GC
Morc1	Microrchidia 1	-12.41	-11.94	0.0	M,CS	NR	GC
Mov10l1	Moloney leukemia virus 10-like 1	-4.33	-3.44	0.2	M, RB	NR	GC
Mael	Maelstrom homolog (Drosophila)	-6.50	-4.24	0.3	M, RF	NR	GC
Stra8	Stimulated by retinoic acid gene 8	-3.37	-1.64	0.5	M, VA	PR	SC,GC
Meig1	Meiosis expressed gene 1	-5.18	-6.22	-0.2	M, VA	NR	GC
Ccl17	Chemokine (C-C motif) ligand 17	7.71	6.44	0.2	M	NR	GC
Sgpp2	Sphingosine-1-phosphate phosphotase 2	3.94	3.60	0.1	M	NR	GC
Lect1	Leukocyte cell derived chemotaxin 1	11.62	6.20	0.5	M	PR	SC,GC
Ddx25	DEAD (Asp-Glu-Ala-Asp) box polypeptide 25	-5.00	-6.05	-0.2	RB	NR	GC
Rbm44	RNA binding motif protein 44	-5.61	-3.54	0.4	RB	PR	GC
Rbmy1a1	RNA binding motif protein; Y A1	-7.09	-2.63	0.6	RB	PR	SC,GC
Ddx4	DEAD (Asp-Glu-Ala-Asp) box polypeptide 4	-7.51	-4.95	0.3	RB, SCM	NR	GC
Lin28	Lin-28 homolog (C. elegans)	-5.06	-2.16	0.6	RB, SCM	PR	SC,GC
MAGE 1	RIKEN cDNA 4933402E13 gene	-72.51	-69.75	0.0	UC	NR	GC
Mageb16	Melanoma antigen family B, 16	-10.54	-7.75	0.3	UC	NR	GC
Mage-k1	RIKEN cDNA 4930550L24 gene	-29.40	-13.95	0.5	UC	PR	SC,GC
Trim12	Tripartite motif-containing 12A	-5.52	-4.65	0.2	UC	PR	SC,GC
Trim34	Tripartite motif-containing 34A	-3.57	0.00	1.0	UC	ER	SC
Trim71	Tripartite motif-containing 71	-10.40	-10.86	0.0	UC	NR	GC
Dppa4	Developmental pluripotency associated 4	-3.65	-3.34	0.1	SCM	NR	GC
Glis3	GLIS family zinc finger 3	-5.09	-4.71	0.1	SCM	NR	GC
Ngn3	Neurogenin 3	-3.99	-4.25	-0.1	SCM	NR	GC
PLZF	zinc finger and BTB domain containing 16	-9.22	-8.94	0.0	SCM	NR	GC
Sall4	Sal-like 4 (Drosophila)	-5.90	-9.01	-0.5	SCM	NR	GC
Cidea	Cell death-inducing DNA fragmentation factor, alpha subunit like effector A	-12.07	-6.73	0.4	CS,VA	NR	GC
Rbm44	RNA binding motif protein 44	-5.61	-3.54	0.4	RB	PR	GC
Rbmy1a1	RNA binding motif protein; Y A1	-7.09	-2.63	0.6	RB	PR	SC,GC
Ddx4	DEAD (Asp-Glu-Ala-Asp) box polypeptide 4	-7.51	-4.95	0.3	RB, SCM	NR	GC
Lin28	Lin-28 homolog (C. elegans)	-5.06	-2.16	0.6	RB, SCM	PR	SC,GC
MAGE 1	RIKEN cDNA 4933402E13 gene	-72.51	-69.75	0.0	UC	NR	GC
Mageb16	Melanoma antigen family B, 16	-10.54	-7.75	0.3	UC	NR	GC
Mage-k1	RIKEN cDNA 4930550L24 gene	-29.40	-13.95	0.5	UC	PR	SC,GC
Trim12	Tripartite motif-containing 12A	-5.52	-4.65	0.2	UC	PR	SC,GC
Trim34	Tripartite motif-containing 34A	-3.57	0.00	1.0	UC	ER	SC
Trim71	Tripartite motif-containing 71	-10.40	-10.86	0.0	UC	NR	GC
Dppa4	Developmental pluripotency associated 4	-3.65	-3.34	0.1	SCM	NR	GC
Glis3	GLIS family zinc finger 3	-5.09	-4.71	0.1	SCM	NR	GC
Ngn3	Neurogenin 3	-3.99	-4.25	-0.1	SCM	NR	GC
PLZF	zinc finger and BTB domain containing 16	-9.22	-8.94	0.0	SCM	NR	GC
Sall4	Sal-like 4 (Drosophila)	-5.90	-9.01	-0.5	SCM	NR	GC
Cidea	Cell death-inducing DNA fragmentation factor, alpha subunit like effector A	-12.07	-6.73	0.4	CS,VA	NR	GC

Rescue factor $(RF) = 1 - \left(\frac{\frac{Res}{WT}}{\frac{KO}{WT}}\right)$

RF < 0.5 = not rescued, RF < 1 = partially rescued, and RF = 1 = entirely rescued

KEY		
C = Cancer	VA = Vitamin A metabolism	UC = Ubiquitination/ cancer
CS = Cell death/survival	M = Meiosis	PR = Partially rescued
SCM = Stem cell marker	RB = RNA binding	NR = Not rescued
CJ = Cell junction	IB = Integrin binding	ER = Entirely rescued
E = Exosomes	MI= Migration	SC = Sertoli cell
A = Adhesion	RF = RNA function (piRNA)	GC = germ cell

Table 7: DMRT1-direct targets identified by manual integration of ChIP-Seq and Microarray data.

Gene	Chromosome location	Binding site characteristic	Fold enrichment
Rarres 1	chr3:67,307,300-67,307,600	Intron	3x
Fgf13	chrX:56,605,942-56,606,894	Intron	2x
Sox11	chr12:28,020,179-28,020,706	intergenic	2x
Stag3	chr5:138,743,354-138,743,638	Intron	3x
Mecr	chr4:131,422,504-131,423,228	Intron	7x
Slc27a2	chr2:126,402,961-126,403,511	Intron	2x
Cpeb1	chr7:88,515,303-88,517,449	Intron	3x
Myoc	chr1:164,577,479-164,577,659	intron	2x
Slc1a5	chr7:17,378,575-17,378,980	intron	3x
Crabp2	chr3:87,757,070-87,757,354	intron/exon	6x
cidea	chr18:67,509,260-67,509,651	intron	3x
Actra1	chr19:46,452,799-46,453,197	intron	2x
Magea10	chrX:69,636,152-69,636,303	~300bp 5' end	6x
Ocln	chr13:101,273,115-101,273,554	intron	2x
Ocln	chr13:101,273,170-101,273,557	intron	3x
Ocln	chr13:101,319,728-101,320,144	intron	3x
Ocln	chr13:101,315,114-101,315,192	intron	3x
Dppa4	chr16:48,286,063-48,288,019	intron	3x
Sh3gl2	chr4:84,837,640-84,837,905	5kb 5' end	5x
Tex11	chrX:98,224,055-98,224,440	intron	5x
ripk4	chr16:97,967,003-97,967,738	intron	2x
ripk4	chr16:97,975,923-97,976,397	intron	3x
nefm	chr14:68,731,296-68,731,992	intron	2x
Rnf17	chr14:57,032,220-57,034,846	intron	5x
Rspo2	chr15:43,045,237-43,046,280	intron	1x
Boll	chr1:55,375,489-55,375,774	intron	10x
Plekhg1	Chr10:6470881-6471323	intron	4x
Krt24	chr11:99,140,234-99,141,522	1kb 5' end	4x
Msrb2	chr2:19,293,629-19,295,542	Intron	2x
Kcnh1	chr1:193,999,069-193,999,787	10kb 5' end	3x
Abi3bp	chr16:56,588,988-56,589,431	intron	3x
Creb3l1	chr2:91,834,527-91,835,107	intron	3x
Tmem183a	chr1:136,265,851-136,268,209	8kb 5' end	5x
Nans	chr4:46,499,678-46,500,136	~3kb 5' end	9x
Fmr1nb	chrX:66,009,586-66,009,862	5kb 5' end	5x
Slc46a3	chr5:148,710,063-148,710,375	8kb 5' end	4x
Galnt10	chr11:57,454,160-57,454,669	5kb 5' end	4x
Galnt10	chr11:57,452,590-57,453,288	~8kb 5' end	6x
Gm4836	chrX:27,599,193-27,599,373	~2kb 5' end	10x

Gene	Chromosome location	Binding site characteristic	Fold enrichment
Rras2	chr7:121,223,572-121,226,240	Intron	3x
Jakmip2	chr18:43,851,629-43,852,336	3kb 5' end	7x
Nup93	chr8:96,731,093-96,731,376	8kb 5' end	20x
Plxdc2	chr2:16,265,704-16,265,882	3kb 5' end	4x
Plxdc2	chr2:16,270,192-16,271,188	2kb 5' end	4x
Plxna2	chr1:196,425,457-196,425,703	15kb 5' end	4x
Usp9y	chrY:807,546-807,941	12kb 5' end	15X
Wls	chr3:159,594,294-159,594,496	intron	13x
Naip5	chr13:100,987,411-100,987,757	intron/exon	3x
Naip5	chr13:101,018,815-101,019,025	~2kb 5' end	2x
Kcna3	chr3:106,836,741-106,837,232	2kb 5' end	4x
Dcp2	chr18:44,565,624-44,565,992	intron	4x
Dcp2	chr18:44,530,814-44,531,196	~9kb 5' end	4x
Ctsc	Chr7:95,417,134-95,417,319	12kb 5' end	5x
Snapin	chr3:90,296,122-90,296,321	3kb 5' end	2x
Tlr7	chrX:163,741,907-163,742,124	1kb 3' end	4x
Emp1	chr6:135,311,444-135,311,561	~2kb 5' end	20x
Pfdn2	chr1:173,284,568-173,284,662	intron	2x
Wfdc15a	chr2:164,027,302-164,027,523	~3kb 5' end	4x
Casp8	chr1:58,862,629-58,862,865	intron	2x
Casp8	chr1:58,837,012-58,837,142	12kb 5' end	4x
Peg12	chr7:69,613,605-69,613,768	4kb 5' end	3x
Vti1b	chr12:80,274,320-80,275,247	1kb 5' end	3x
Ki	chr11:101,181,187-101,181,335	intron/exon	2x
1110058l19rik	chr1:24,010,761-24,010,841	intron	6x
Shisa7	chr7:4,781,069-4,781,178	exon	3x
Smg7	chr1:154,764,746-154,764,955	12kb 5' end	4x
Panx3	chr9:37,480,263-37,480,932	12kb 5' end	4x
Samd7	chr3:30,640,823-30,640,997	4kb 5' end	11x
Gm14446	chr19:34,677,431-34,677,555	1kb 5' end	5x
Capn8	chr1:184,489,947-184,490,402	6kb 5' end	4x
Unc45a	chr7:87,479,768-87,480,208	intron	2x
E2f5	chr3:14,595,052-14,595,164	intron	3x
Hbb-b2	chr7:110,966,864-110,967,012	6kb 5' end	4x
Mapkapk2	chr1:132,981,771-132,982,696	intron	3x
Adam21	chr12:82,659,818-82,660,151	exon	4x
Cml2	chr6:85,825,336-85,826,087	6kb 5' end	3x
Cc2d2a	chr5:44,045,531-44,046,208	10kb 5' end	6x
Clec1a	chr6:129,409,087-129,409,309	5kb 5' end	3x
Cnksr2	chrX:154,498,615-154,498,785	10kb 5' end	4x
Ifi203	chr1:175,873,983-175,874,268	5kb 5' end	4X
Nuak2	chr1:134,225,393-134,225,876	Intron	5x
9030619p08rik	chr15:75,268,950-75,269,124	8kb 5' end	3x
Zfp606	chr7:13,059,630-13,059,809	5kb 5' end	4x
6720456b07rik	chr6:113,571,544-113,571,684	5kb 3' end	3x
Bc005561	chr5:104,935,177-104,935,580	2kb 5' end	8x
Bc005561	chr5:104,951,189-104,951,575	~200bp 3' end	4x
Ccnf	chr17:24,382,861-24,383,015	intron	2x

Chapter 5: NANOS2 partially co-localizes and interacts with DMRT1 to modulate its transcriptional activity

Abstract

The doublesex and mab-3 related transcription factor 1 (DMRT1) and nanos homolog 2 (NANOS2) are both evolutionary conserved proteins implicated in germ cell development and maintenance. However, the molecular mechanisms involved are not fully appreciated for either protein. The current study provides evidence that NANOS2 and DMRT1 collaborate to regulate one or several steps in germ cell development. Co-immunoprecipitation experiments demonstrated that DMRT1 and NANOS2 can directly interact with one another. The potential of this interaction was supported by double immunofluorescence staining, which revealed occasional overlap of DMRT1 and NANOS2 cellular expression as indicated by confocal microscopy. Immunofluorescence analyses of *Dmrt1*-null mice revealed that NANOS2 protein was expressed in the absence of DMRT1 and suggested that NANOS2 is upstream of DMRT1. Global gene expression analyses from *Nanos2-null* mice from a previously published study revealed the expression of *Dmrt1* along with other genes vital for germ cell development were up-regulated in the absence of *Nanos2*, validating the spatiality of *Nanos2* relative to *Dmrt1* and illustrating the absence of its evolutionary conserved repressive functions. These findings show that NANOS2 can interact with DMRT1 and regulate its activity. The finding, together with the known roles of NANOS2 and DMRT1 in germ cell development, suggests that the NANOS2-DMRT1 interaction is needed to assure proper progression of germ cells through development.

.

Introduction

Differentiation of mammalian germ cells occurs early during embryonic development and involves the commitment of the sexually indifferent germ cells to either the male or the female pathway. Sex-specific differentiation of germ cells starts after they colonize the nascent genital ridge at about 10.5 days post coitus (dpc) in mice, and germ cells from both sexes maintain the capability to differentiate into either pathway until about 11.5 dpc [44]. Once committed, male germ cells are arrested in the G_0/G_1 phase of the cell cycle at 12.5 dpc and the female germ cells enter meiosis at 13.5 dpc, where they enter quiescence in the late diplotene stage [289].

Both extrinsic environmental signals and intrinsic germ cell factors determine the entry into meiosis. It is well established that the sex of germ cells follows the sex of the supporting cells that surround them, and thus the presence of granulosa cells favors the entry into meiosis by female germ cells, both of whose existence is dependent on the absence of SRY and SOX9 expression in the bipotential gonad [26, 38, 156, 290-292]. Entry into meiosis of the embryonic female germ cells is favored by an intrinsic factor, retinoic acid (RA), known as the meiosis-inducing factor and required in the RA signaling pathway [55, 56, 105]. Evidence show that a down-stream target of RA, a retinoic acid responsive gene, STRA8, is necessary for RA signaling pathway as its deletion prevents preleptotene spermatocytes in *Stra8* knockout mice to enter meiosis [293, 294]. In contrast, differentiation and mitotic arrest of embryonic male germ cells is favored by the early expression of SRY and SOX9 during sex determination and the resultant differentiation of Sertoli cells, which produces CYP26b1; a P450 enzyme that oxidizes RA to an inactive metabolite. The importance of CYP26b1, a meiosis-inhibiting factor, was revealed in *Cyp26b1*-null mice, whereby embryonic male germ cells lacking this enzyme showed an elevated STRA8 expression that culminated in meiotic induction [54, 55]. This phenotype is

consistent to that reported in the *Nanos2*-null mice, in which STRA8 was elevated in embryonic male germ cells that led to initiation of meiosis [295]. This result was validated using female germ cells expressing exogenous NANOS2, which suppressed *Stra8* expression and subsequent progress in meiosis [295]. These findings suggested that NANOS2 suppresses the expression of *Stra8*, which is up-regulated by RA signaling, to prevent meiotic entry by male germ cells; and thus acting as an intrinsic regulator of embryonic male germ cell differentiation [106].

In addition to its role in embryonic germ cell differentiation, NANOS2, an evolutionary conserved zinc finger RNA binding protein expressed in germ cells, is also required for the maintenance of postnatal undifferentiated spermatogonia pool [105, 106]. In the postnatal mouse testis, NANOS2 is expressed only in types A_s and A_{pr} spermatogonia; the subset of undifferentiated spermatogonia that comprise the "actual stem cell" pool with the ability to self-renew [105-107, 109, 296]. It has been shown that NANOS2 favors self-renewal of undifferentiated spermatogonia than their differentiation. This is illustrated by the finding that male germ cells with a *Nanos2* deletion initiate meiosis and STRA8 expression was up-regulated [295]. Like NANOS2, the transcription factor, DMRT1 is also essential for the development and maintenance of germ cells in the postnatal murine testis [50, 131, 133].

DMRT1 is a conserved transcriptional factor that is essential for postnatal testis differentiation. It is testis-specific and expressed both in Sertoli cells and in pre-meiotic spermatogonia [134]. Specifically, deletion of DMRT1 in undifferentiated spermatogonia favors premature switch from a normal mitotic differentiation program to a precipitated meiotic program that culminates in germ cells differentiating into spermatids [134]. These findings led to the conclusion that DMRT1 promotes spermatogonial differentiation by repressing the activation

of *Stra8* through direct transcriptional regulation and ubiquitous inhibition of RA-dependent transcriptional activity [134].

While many excellent studies have contributed to our current understanding of DMRT1's molecular characteristics and role in the testis, some important detail is missing. In particular, there is limited information on what regulates DMRT1 expression or activity in germ cells. Efforts have been placed on identifying the downstream targets of DMRT1 than on identifying upstream regulators that affect its transcriptional activity especially in germ cells.

NANOS2 and DMRT1 are both regulators of male germ cell differentiation by regulating the mitotic to meiotic switch [134, 295]. These proteins may share a partial overlapping function since the deletion of DMRT1 in male germ cells did not induce uncontrolled meiosis [134]. This similarity in function raises the likelihood of a mechanistic link between NANOS2 and DMRT1 in germ cells. In our present study, NANOS2 expression was unaffected in the absence of DMRT1 in both Sertoli cells and germ cells, whereas *Dmrt1* mRNA expression was elevated in the *Nanos2 null* mice. Further analysis revealed that NANOS2 and DMRT1 interact with each other and a NANOS2 mammalian expression vector repressed the transcriptional activity of DMRT1 in *in vitro* experiments. This suggested that NANOS2 acts upstream of DMRT1 and serves as a potential regulator of DMRT1's activity in undifferentiated germ cells.

Materials and Methods

Animals husbandry

The generation of *Dmrt1*$^{-/-}$ (*Dmrt1*-null) and *Dmrt1*$^{-/-;tg}$ (*Dmrt1*-rescue) mice were reported elsewhere ([112] and Chapter 2). All animal procedures were approved by the Laboratory Animal Research Committee at the University of Kansas Medical Center and in

accordance with National Institutes of Health guidelines. Three animals each of *Dmrt1*$^{+/+}$, *Dmrt1*$^{-/-}$ and *Dmrt1*$^{-/-;tg}$ mice at postnatal day 7 (P7) were examined in this study.

Immunohistochemistry

Testes from postnatal day (P7) mice were immersion-fixed in Bouin's solution at room temperature for 24 h. Tissues were rinsed twice with 50% and 70% alcohol. Fixed testes were cut at the sagittal plane in half, processed and embedded in paraffin according to standard procedures. Five-micron (5 μm) sections were cut and mounted on slides. Five sequential sections on slide were analyzed per mouse by immunohistochemistry. Slides containing sections were cleared in xylene, rehydrated through graded alcohol series and heated in 10 mM sodium citrate buffer (pH 6.0) with microwaves (14 min at full power) for antigen retrieval. Sections were blocked using 10% normal goat or donkey serum (Zymed Laboratories Inc.) for 60 min at room temperature. For co-staining, primary antibody incubations were carried out overnight at 4°C in blocking solution. The sections were immunostained with goat anti-NANOS2 and rabbit anti-DMRT1 antibodies. Goat polyclonal anti-NANOS2 antibody (sc-69190) was purchased from Santa Cruz Biotechnology, Inc. (Santa Cruz, CA, USA). Rabbit polyclonal anti-DMRT1 antibody was custom made by Covance Inc. (Denver, PA, USA) using a C-terminal peptide of DMRT1 and its reported elsewhere [130]. After washing with PBST, sections were incubated with fluorescent-labeled secondary antibody (Alexa FluorR 568 donkey anti-rabbit IgG, Molecular Probes Inc., Eugene; Alexa FluorR 488 donkey anti-goat IgG, Molecular Probes Inc., Eugene; Alexa FluorR 568 donkey anti-goat IgG, Molecular Probes Inc., Eugene; and Alexa FluorR 488 donkey anti-rabbit IgG, Molecular Probes Inc., Eugene) for 1 hour at room temperature. Samples were washed 3 times in PBST (5 min. each) and glass cover slides mounted using Fluoromount-G (Southern Biotechnology Associates Inc., Birmingham, AL).

Digital images were collected using fluorescent filters (200x and 400x) on a Nikon Eclipse 80i microscope (Nikon Inc., Instrument Group, Melville, NY), a Retiga 2000R fast camera and a QCapture software program (QIMAGING, Surrey, BC, Canada). Images were processed using Adobe Photoshop.

Co-immunoprecipitation

P7-P10 testes from *Dmrt1*$^{+/+}$ and *Dmrt1*$^{-/-}$ mice were homogenized, using a tooth polisher, on ice in cell lysis buffer (25 mM HEPES-KOH, pH 7.4, 250mM sucrose, 75mM β-glycerophosphate, 1mM DTT,150 mM NaCl, 1 mM Na_3V0_4, 1% Nonidet P-40, 2x complete protease inhibitor (Roche) containing 400 units/ml RNase out). Three hundred microliters (300uL) and 500uL of lysis buffer were used for total testis weight ≤20mg and ≥ 50mg, respectively. Whole testis extracts were collected by centrifugation at 10,000 xg for 10mins at 4^{o}C and supernatant were precleared in 75 uL of Protein A/G plus-agarose (Santa Cruz Biotechnology, Inc.); and then incubated with 2ug of rabbit anti-DMRT1 (Covance) or goat anti-NANOS2 (Santa Cruz Biotechnology, Inc.) on a rotator for 2 h at 4^{o}C. Forty microliters (40uL) of protein A/G agarose were added and incubated for 2h at 4 ^{o}C. Immunoprecipitates were collected by centrifugation at 1000 x g for 5mins at 4 ^{o}C and washed five times with wash buffer (25 mM HEPES-KOH, pH 7.4, 250mM sucrose, 75mM β-glycerophosphate, 1mM DTT, 350 mM NaCl, 1 mM Na_3V0_4, 1% Nonidet P-40, 2x complete protease inhibitor (Roche) containing 400 units/ml RNase out). The agarose beads were boiled at 100^{o}C in 40uL 2x SDS-PAGE loading buffer for 5mins. The eluents were run on a 12% acrylamide gel and analyzed by Western blot. Anti-DMRT1 was used to probe samples immunprecipitated with anti-NANOS2 while anti-NANOS2 (sc69160) was used to probe samples immunoprecipitated with anti-

DMRT1. Donkey anti-rabbit-HRP and Donkey anti-goat-HRP (Jackson Immuno Research) were used as secondary antibodies.

Nanos2 cloning and other vectors

Mouse *Nanos2* transcripts were PCR-amplified with oligodeoxynucleotide primer sets engineered with Bgl II (TTGAGCGCAGATCTTAATGGACCTACCGCCCTTTGA) /Hind III (TTAAGCGGCTCG AGT TATCG CTTGACTCTGCGACC) and Hind III (TTGAGCG CAAGCTTATGGACCTACCG CC CT TTG A) / Xho I (TTAAGCGGCTCGAGTTATCGCTTGACTCTGCGACC) restriction endonuclease sites and double restriction digest performed using Bgl II / Hind III and Hind III / Xho I restriction enzymes, respectively. The cloning vectors, pcDNA3 (Invitrogen, Carlsbad, CA) and pCMV-Tag1 (Agilent Technologies, Santa Clara, CA), were restriction digested with Hind III / Xho I and Bgl II / Hind III, respectively; dephosphorylated with calf intestinal phosphatase (New England Biolabs, Ipswich, MA), and ligated with the Hind III / Xho I and Bgl II / Hind III digested PCR products, respectively, using T4 ligase (New England Biolabs, Ipswich, MA).

Other expression vectors used for transient transfection include EF-FLAG-DMRT1, VP16-DMRT1 and GAL4-VP16 that are all driven by a CMV promoter in the EF-FLAG-pLink, pKH68 and pBudCE4.1(Invitrogen, Grand Island, NY) mammalian expression vectors, respectively. The EF-FLAG-DMRT1 and VP16-DMRT1 expression vectors were gifts from Dr. Vivian Bardwell and the base vectors have been describe elsewhere [274, 297]. The VP16 activation domain was generated by PCR using VP16 forward 2 (GCCGCTCG AGCC GAGGAG GACCTG AACATG GC) and VP16 reverse 2 (CCG GCT CGA GTC ACC CAC CGT ACT CGT CAA T) primers and VP16-mDMRT1 plasmid (Bardwell lab) as template. This PCR product was cloned into the XhoI site of pBudCE4.1 (Invitrogen) to give the plasmid VP-16-pBudCE4.1. The *Gal4* DNA binding domain was generated by PCR using *Gal4* forward

(AGG CGG TAC CAG CTT GAA GCA AGC CTC CTG) and *Gal4* reverse (CTC TCG GTA CCT CCA TGA TGG CGG CTC G) primers and pGBKT7 (Clontech) as template. The resulting PCR product was cloned into the KpnI site of the VP16-pBudCE4.1 vector to produce GAL4-VP16-pBudCE4.1.

Also, the reporter constructs used include 4X-IRE-promoter-Luc and 4X-DM-Luc generated by placing four copies of the binding sequences of DMRT1 upstream of a strong, constitutive SV40 promoter and a minimal promoter (TATA box) that drive luciferase expression in a pGL3-promoter (Stratagene, Agilent Technologies, Santa Clara, CA) and pLuc-MCS (Stratagene, Agilent Technologies, Santa Clara, CA) plasmid reporter vectors, respectively. The control reporter was a pFR-Luc vector (Stratagene, Agilent Technologies, Santa Clara, CA), which contained five copies of upstream activation sequences (5X-GAL4-UAS) for the GAL4 DNA binding domain and was placed in front of an SV40 promoter. Plasmid DNAs were prepared from overnight bacterial cultures using plasmid DNA miniprep columns according to the supplier's protocol (Fermentas, Thermo Fisher Scientific, Inc., Glen Burnie, MD). All resulting clones were sequenced by GENEWIZ, South Plainfield, NJ.

Cell preparation and transient transfection analysis

Preparation and propagation of GC-1 spg (mouse spermatogonia cell line; ATCC #: CRL-2053^{TM}) were as described elsewhere and were cultured in Dulbecco's modified Eagle's medium (Cellgro Mediatech; Fisher Scientific, Pittsburgh, Pa.) supplemented with 10% fetal bovine serum[298]. For transient transfection, GC1 cells were plated at a density of 20,000 cells/well in 24-well culture dishes (Costar, Corning, N.Y.) and transfected with 300ng total DNA and 0.6µl of TurboFect transfection reagent (Fermentas, Thermo Fisher Scientific, Inc., Glen Burnie, MD). Unless otherwise stated, GC1 cells were transfected with 200ng 4X-DM-Luciferase or 4X-IRE-

promoter luciferase constructs along with 0-80ng of EF-FLAG-DMRT1 or VP16-DMRT1, FLAG-NANOS2-MYC or pCDNA3-NANOS2 and their base mammalian expression vectors. Transfection efficiency was controlled by including 20ng of phRL-TK (Promega Corp), which express *Renilla* luciferase from the hSV-TK promoter. For control experiments to determine specificity of NANOS2, GC1 cells were transfected with 200ng 5X-GAL-UAS-Luciferase, 20ng of phRL-TK and 0-80ng of GAL4-VP16, FLAG-NANOS2-MYC and their base mammalian vectors. Overall, Luciferase reporters with response element insert (4X-DM-Luc or 4X-IRE-Luc or 5X-GAL4-UAS-Luc) were co-transfected with a constant amount of expression vector (EF-FLAG-DMRT1 or VP16-DMRT1 or GAL4-VP16) and increasing amounts of FLAG-NANOS2-MYC into cultures of GC1-spg cells. Each transfection was performed in triplicates. Forty-eight hours after transfection, cells were lysed and assayed for both firefly and *Renilla* luciferase activities using the Dual-Luciferase reporter assay system (Promega Corp.), as described previously[138, 299]. The data are presented as the firefly/Renilla luciferase activity ratio of 4X-DM-Luc (or 4X-IRE promoter Luc) in the presence of EF-FLAG-DMRT1 (or VP16-DMRT1) and with or without FLAG-NANOS2-MYC (or pCDNA3-NANOS2) constructs relative to the firefly/*Renilla* luciferase activity ratio of the promoter-alone construct. All transient transfection experiments were repeated at least three times. All plasmid DNAs were prepared from overnight bacterial cultures using a GeneJET^{TM} plasmid miniprep kit according to the supplier's recommendations (Fermentas, Thermo Fisher Scientific, Inc., Glen Burnie, Md.).

Results

Majority of genes involved in spermatogenesis showed opposite regulatory patterns in Nanos2-null and Dmrt1-null mice

There was significant evidence from the literature for an important interaction between NANOS2 and DMRT1 based on shared regulation of similar genes. To explore a potential link between DMRT1 and NANOS2, the gene expression changes were compared in embryonic *Nanos2* knockout and P7 *Dmrt1* mutant (*Dmrt1*$^{-/-}$ and *Dmrt1*$^{-/-;tg}$) testes ([300], Chapter 4). These genes were classified into a group of similar or opposite transcriptional change. Twenty-four (24) out of forty (40) genes examined including *Dmrt1*, *Stra8*, *Dazl*, *Sox3*, *Sohlh2*, *Sycp1*, *Plzf*, *Taf7l*, *Lin28* and *Ngn3* had expression patterns that were opposite in *Nanos2-null* and *Dmrt1-null* mice (Figure 1 and Table 1). For example, the expression of *Dmrt1*, *Stra8*, and *Lin28* were up-regulated when *Nanos2* was deleted, whereas their expression were down-regulated in the absence of *Dmrt1* (Figure 2). On the other hand, the expression of 16 genes including *Dppa3*, *Dppa4*, *Piwi4*, *Morc*, *Gtsf1* and *Emb* had similar transcriptional change; which were either up-regulated or down-regulated in both *Nanos2-null* and *Dmrt1-null* mice (Table 2). Also, whereas *Dmrt1* expression changed significantly in embryonic *Nanos2-null* testes compared to the controls, *Nanso2* expression was unchanged in *Dmrt1-null* testes. This suggested that NANOS2 is potential regulator of *Dmrt1* levels in germ cells and showed that NANOS2 is upstream of DMRT1.

NANOS2 and DMRT1 form a stable interaction

To explore potential interactions between DMRT1 and NANOS2, experiments were executed to determine if NANOS2 was a binding partner of DMRT1. To determine if physical

interaction can exist between these two proteins, *in vitro* methods that disrupted cellular barriers were employed. To this end, DMRT1 and NANOS2 were immunopreciptated from protein extracts of *Dmrt1*$^{+/+}$ and *Dmrt1*$^{-/-}$ P7 testes and the immunoprecitates analyzed for NANOS2 and DMRT1, respectively, using western blot analysis (Figure 2). Western blot analysis of anti-DMRT1 precipitates probed with anti-NANOS2 revealed a major band of about 18kDa corresponding to NANOS2, which was exclusively detected in immunoprecipitates obtained from *Dmrt1*$^{+/+}$ testes and absent in precipitates from *Dmrt1*$^{-/-}$ testes (Figure 2A). Similarly, Western blot analysis of anti-NANOS2 precipitates probed with anti-DMRT1 revealed three major bands in the *Dmrt1*$^{+/+}$ testes that were absent in *Dmrt1*$^{-/-}$ testes (Figure 2B). One of the bands was about 41kDa and corresponded to the expected size of DMRT1, whereas the other two were located about 18kDa. It is likely that the lower bands are proteolytic products of the full-length DMRT1 protein that are in a protein degradation complex, which also interacts with NANOS2.

NANOS2 is localized at nuclear envelope and is upstream of Dmrt1

There was little indication from the literature that NANOS2 and DMRT1 co-localized in the cell, given that DMRT1 is localized in the nucleus while NANOS2 was recently shown to localize in the cytoplasmic and nuclear compartments of HEK293T cells transfected with a NANOS2-MYC-expression vector [301]. To evaluate this possibility of co-localization and provide a hierarchical basis on the molecular mechanisms underlying observed interaction between NANOS2 and DMRT, immunofluorescence was used to localize NANOS2 in cells of postnatal day 7 (P7) testes, using sections from mice with and without DMRT1. In the *Dmrt1*$^{+/+}$ testes, NANOS2 was observed in the cytoplasm of germ cells juxtaposed to the nuclear envelope of the DMRT1-positive nuclei (Figure 3 A-C; arrowhead in Figure 3C). As in the *Dmrt1*$^{+/+}$ mice,

NANOS2 was similarly expressed in testes from *Dmrt1-null* (*Dmrt1*$^{-/-}$) mice, suggesting that NANOS2 is upstream of DMRT1 (Figure 3 D-F). This result validates observations that *Dmrt1* mRNA was induced in embryonic *Nanos2*-null testes and that *Nanos2* mRNA did not change in the embryonic ovaries of female *Dmrt1*-null mice [137, 300]. Furthermore, immunostaining followed by confocal microscopy revealed that DMRT1 and NANOS2 are in close-proximity but did not completely overlap with each other (Figures 4C & 4I, arrowheads). As previously proposed NANOS2 was located in the cytoplasm and partially in the nucleus, where it juxtaposed to the nuclear envelope of the germ cell nuclei and partially co-localized with DMRT1.

NANOS2 modulates DMRT1's transcriptional activity in cultured cells

To investigate whether NANOS2 can modulate DMRT1 transcriptional activity, transient transfection was used to measure the ability of NANOS2 (derived from an expression vector) to alter activity of co-transfected DMRT1, as measured by DMRT1's ability to activate transcription from the two stated reporters (4X-DM-Luc and 4X-IRE-Luc) in immortalized GC1-spermatogonia cells [274]. The 4X-DM-Luc reporter was generated by placing four copies of DMRT1 binding site in front of a TATA box minimal promoter, whereas the 4X-IRE- Luc reporter was generated by inserting four copies of DMRT1 binding site in front of a strong SV40 promoter. In GC1 cells, co-transfection of a DMRT1 expression vector with the 4X-DM-Luc reporter or 4X-IRE-Luc reporter increased the basal activity by approximately 6-fold or 9-fold, respectively (Figures 5A and 5B). Co-transfection of increasing amounts of NANOS2 expression vector caused a dose-dependent decrease and increase in DMRT1-dependent transcriptional activity for the 4X-DM-Luc and 4X-IRE-Luc reporters, respectively (Figures 5A and 5B). To determine if the effect of NANOS2 was specific to DMRT1, co-transfection of a GAL4-VP16

and NANOS2 expression vectors with the 5X-GAL4-UAS-Luc reporter, showed that NANOS2 had not effect on the GAL4-dependent transcriptional activity the reporter vector (5X-GAL4-UAS-Luc; Figure 5C). Thus, the dose-dependent transcriptional activities illustrated by the 4X-DM-Luc and 4X-IRE-Luc exemplifies the activating and repressive roles of DMRT1, respectively, with both roles modulated by NANOS2, suggesting that NANOS2 is a potential regulator of DMRT1's *in vivo* functions in germ cells.

Discussion

The differentiation of postnatal germ cells in the mammalian testis is regulated by a diverse group of genes identified primarily from gene ablations studies in mice. These studies identified a number of genes that, when deleted, block germ cell development, including *Dmrt1*, *Nanos2*, *Nanos3*, *Dazl*, *Gdnf*, *Stra8*, *Cyp26b1*, *Gfra1* and *Sohlh1* [5, 50, 83, 105, 107, 134, 135, 137, 295, 300, 302, 303]. Amongst these genes *Nanos2*, *Dmrt1*, *Dazl*, *Sohlh1*, *Stra8* and *Cyp26b1* are implicated in the mitotic-to-meiotic transition of germ cells and *Nanos3*, *Nanos2*, *Gdnf* , *Gfra1,* are required for the maintenance of spermatogonial stem cell population [55, 105, 106, 134, 303]. Within this list are transcription regulators (DMRT1 and SOHLH1), translation regulators (DAZL, NANOS2 and NANOS3), a transmembrane receptor (GFRA1) and its ligand, GDNF, a neurotrophic factor, an unknown family protein (STRA8) and an enzyme (CYP26B1); all of which are vital to the production of a mature sperm. These genes regulate a sequential series of events that is important for inducing spatiotemporal expression of downstream target genes responsible for specific developmental changes. For example, GDNF secreted by Sertoli cells acts upstream to maintain expression of NANOS2 and their synergistic action is required for maintaining pluripotency of spermatogonia stem cells [105]. Likewise, DMRT1 and NANOS2 were both shown to act upstream of STRA8 and regulate meiotic entry of

spermatogonia [106, 134]. As a testis-specific transcription factor that is invaluable for testis differentiation, DMRT1 holds a vital position in this germ cell developmental pathway and this current study revealed functional and biochemical interactions between NANOS2 and DMRT1 suggesting that they participate within the same pathway; and the gene expression / immunohistochemistry data showed that NANOS2 is upstream of DMRT1. This suggested that NANOS2 plays an important role in modulating the effects of DMRT1, a protein required for germ cell survival and development.

NANOS2 belongs to the evolutionary conserved *Nanos* family that is intrinsic to the male germ cell and encodes an RNA binding protein containing a zinc-finger motif [304]. NANOS1 and NANOS3 are the other two identified murine Nanos homologs that are expressed in the embryonic and adult brain and as well as in adult testis. In the testis, only NANOS3 and NANOS2 are expressed in germ cells were they protect germ cells from undergoing programmed cell death during migration into and after colonization of the male gonadal ridge, respectively [83, 305]. Although nanos2 is not implicated in meiosis or sex differentiation of germ cells in *Drosophila melanogaster*, it was shown to form a complex with pumilio, another RNA binding protein. Together, they repressed the translation of *hunchback*, *cyclin B*, and *hid* transcripts that results in embryonic polarity, mitotic latency and apoptotic suppression, respectively, by binding to the *nanos*-response element (NRE). The NRE (TTTGTTGTGCAAAATTGTACATAAGC-CA) located at the 3′ untranslated region (UTR) of these target transcripts [306-309]. In the developing mouse gonad, ectopic expression of NANOS2 in female gonocytes and its normal expression in primordial male germ cells suppress entry into meiosis while promoting male-specific differentiation [83]. In addition, NANOS2 was found to localize to P-bodies, which accumulate profusely in male gonocyte and are well-characterized RNA degradation sites [300].

Furthermore, P-bodies have been shown to contain translational silent mRNAs, suggesting that NANOS2 not only promotes degradation of transcripts involved in meiosis but also sequesters other transcripts in a translation silent state within P-bodies during the development of the embryo. The sequestered transcripts can be later release from P-bodies and translated to support differentiation as the levels of NANOS2 declines after birth [300]. The deadenylation complex is associated with RNA degradation and in *Drosophila melanogaster*, the mRNA of *hunchback* was deadenylated with the help of nanos that resulted in translational repression without any change in the levels of the mRNA [310].

The relevance of NANOS2 in suppressing the proliferation and differentiation of spermatogonial stem cells was shown through studies in mice that overexpress NANOS2 and with a conditional *Nanos2* deletion [107, 295, 311]. Characterization of *Nanos2* conditional knockout mice, generated using a Tamoxifen-inducible chimeric Cre-ERT2, a fusion protein between a mutated ligand binding domain of the human estrogen receptor (ER) and the Cre recombinase, showed a gradual depletion of spermatogonial stem cells during spermatogonial cell cycles that was exacerbated with age and showed various degree of germ cell loss and complete loss at 8 and 12 weeks after birth, respectively [107]. The shift from undifferentiated to differentiated germ cells, followed by their complete loss, was associated with the loss of PLZF and GFRA1, two well-characterized markers of undifferentiated germ cells [107]. Likewise, the role of NANOS2 in spermatogonial stem cell maintenance was confirmed using gain-of-function experiments. The NANOS2-overexpressing testes were characterized by the accumulation of spermatogonia with diminished levels of NANOS3 or NGN-3 and elevated levels of PLZF and GFRA1 [107]. These results showed vital roles for NANOS2 in posttranscriptional regulation of undifferentiated spermatogonial pool based on existing evidence that its *Drosophila* homolog,

nanos, may function by impeding translation or assisting with the degradation of mRNA target [312, 313].

The observed NANOS2 expression in *Dmrt1*$^{-/-}$ mouse testes, the partial co-localization, *in vitro* interaction with DMRT1, and influence on *Dmrt1* transcriptional activity have significant implications for the roles of DMRT1 and NANOS2 in germ cell development. NANOS2 regulation of *Dmrt1* was first implicated from global gene signatures of *Nanos2-null* mice. Several genes involved in germ cell development including *Dmrt1* and *Stra8* were up-regulated in the absence of NANOS2, whereas these genes were down-regulated when *Dmrt1* was absent ([300], Agbor, Unpublished). NANOS2 was expressed in the absence of DMRT1 in the *Dmrt1*$^{-/-}$ testis indicating that NANOS2 is upstream of DMRT1. This suggested that *Nanos2* is at the top of a germ cell-specific developmental pathway, which includes genes like *Dmrt1* that are required for germ cell maintenance and survival.

Recent findings show that GDNF acts upstream of NANOS2, whereas STRA8 was downstream of NANOS2 and DMRT1 [105, 106, 134]. Thus, a possible signaling cascade would be initiated by GDNF produced in Sertoli cells and transported to germ cells were it acts through its receptor, GFRA1, to maintain the expression of NANOS2. NANOS2 expressed in P-bodies in germ cells represses the translation of *Stra8* alone or interacts with DMRT1 in an unknown complex to repress *Stra8* translation. Alternatively, it is also possible that DMRT1 and NANOS2 employ two separate mechanisms to repress STRA8 expression. Our findings implicate NANOS2 in the regulation of DMRT1 and that loss of *Dmrt1* does not disturb NANOS2 expression, suggesting that DMRT1 is downstream of NANOS2. The studies suggest a pathway

involving the sequential use of GDNF, NANOS2, and DMRT1 to the control of germ cell development.

It was also observed that NANOS2 partially colocalized with DMRT1 *in vivo*, and co-immunoprecipitation showed DMRT1 and NANOS2 interact. It is uncertain however if the interaction is direct or within a larger complex. In addition, transient transfection studies revealed DMRT1 and NANOS2 functionally interact *in situ*. These findings support the postulation that there is a possible mechanistic link between DMRT1 and NANOS2 due to their similarity in the regulation *Stra8* expression and other shared genes involved in postnatal germ cell development [134]. Given that NANOS2 interacts with the CCR-NOT complex and is thought to regulate the deadenylation-mediated RNA degradation in P-bodies provides a possible mechanism by which NANOS*2* regulate the posttranscriptional *Dmrt1* message or its translation [314].

Both NANOS2 and DMRT1 are evolutionarily conserved with prominent expression in male germ cells. *Nanos2* expression is also expressed in the brain with no known function while *Dmrt1* is testis specific but also expressed in Sertoli cells [130, 302, 305]. Since NANOS2 can activate DMRT1 on one promoter and repress it on another, it cannot be doing so by regulating the same RNA. A possible mechanism of interaction will be dependent on the identification and characterization of a murine homolog of nanos response element, which was vital in the repression of *hunchback* in *Drosophila melanogaster*. These short *cis*-acting regulatory elements were found to be sufficient in mediating the repressive action of nanos on *hunchback* and *bicoid.* These regions located in the 3′ untranslated region (UTR) of the gene acted as independent functional units that were active irrespective of the sequence context and relative position within the 3′ UTR [315]. The nanos response element consensus sequence was found to be similar

between *bicoid* and *hunchback* and arranged in two-half homologous regions. The first half was made-up of GUUGU (or GTTGT) nucleotides while the second was comprised of AUUGUA (or ATTGTA) nucleotides [315]. Preliminary analysis of the 3′ UTR region of *Dmrt1* revealed nucleotides at positions 1335-1342 (TTTGTTGT) and positions 1604-1610 (AATTGTA) that were homologous to the independent functional units of NRE identified in *bicoid* and *hunchback.* Two polyadenylation sites of 9 (positions: 2187-2195) and 12 (positions: 1540-1551) nucleotides were identified in the 3′ UTR of *Dmrt1*. The TTTGTTGT conserved consensus sequence was located 212 bases downstream of the stop codon (position 1124-1126), 205 bases upstream of the first polyadenylation site (positions: 1540-1551) and 860bases upstream of the second polyadenylation site (positions: 2187-2195). Likewise, the AATTGTA consensus site was located 486 bases downstream of the stop codon, 53 bases downstream of the first polyadenylation site and 591bases upstream of the second polyadenylation site. Thus, knowing that most RNA binding sites are recognized as folded secondary structures facilitates the convergence of these conserved structural features into the correct spatial orientation that is recognized by *Nanos2*. However, the nature of this interaction awaits further characterization and may reveal vital knowledge on the role of NANOS2 on DMRT1 expression during germ cell development in the testis.

Figure 1: Expression changes of a group of genes that are differentially regulated by NANOS2 and DMRT1. The gray bars represent changes in male gonads lacking *Nanos2* collected at embryonic day 15.5 (E15.5) and evaluated by microarray. The dark bars represent microarray gene expression changes at P7 in mouse testis that were *Dmrt1*-deficient.

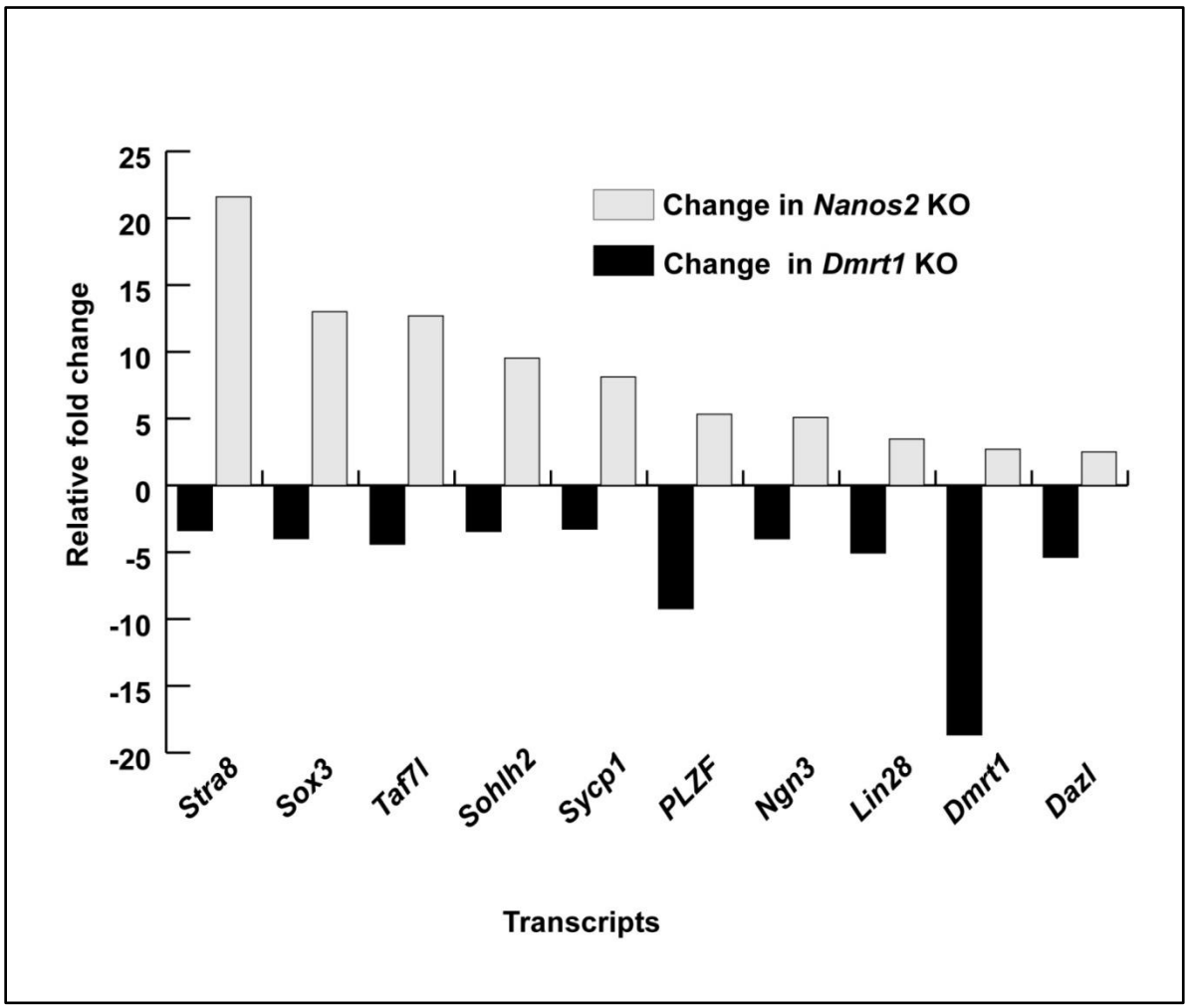

Figure 2: DMRT1 and NANOS2 Co-IP. P10 testis lysates from *Dmrt1*$^{+/+}$ and *Dmrt1*$^{-/-}$ mice were immuno-precipitated (Imppt) with antibodies to either DMRT1 (A) or NANOS2 (B) and analyzed by Western blot analysis to detect NANOS2 (A) and DMRT1 (B). NANOS2 was observed in the DMRT1-imppt complex (A) and DMRT1 in the NANOS2-imppt complex (B). 1= Sertoli cell nuclear extract (SC NE), 2, 3 and 4 = Input flow-through (FT) and immunoprecipitates from *Dmrt1*$^{+/+}$ testes extract, respectively, 5, 6 and 7 = Input flow-through (FT) and immunoprecipitates from *Dmrt1*$^{-/-}$ testes extract, respectively.

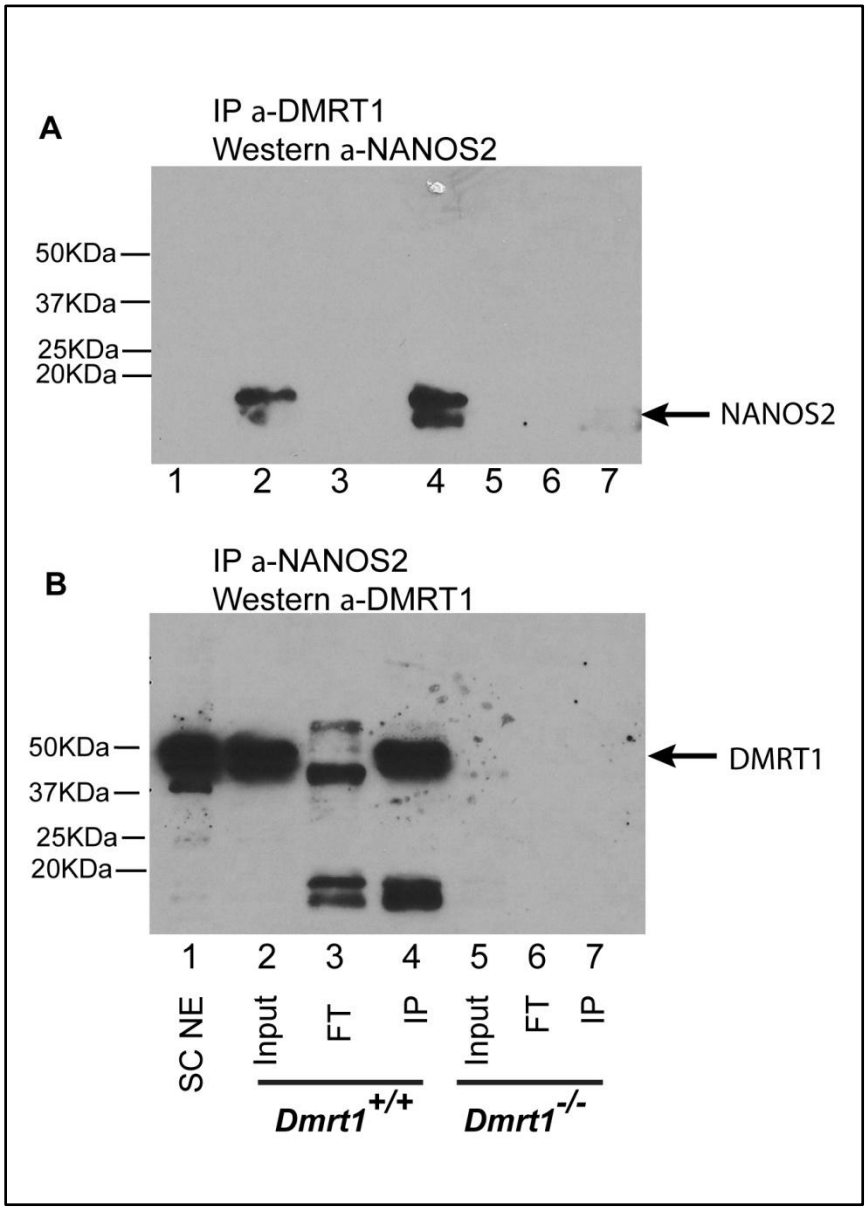

Figure 3: Immunolocalization of DMRT1 and NANOS2 in postnatal day 7 (P7) mouse testis. Testis sections from *Dmrt1*$^{+/+}$ (A-C) and *Dmrt1* $^{-/-}$ (D-F) mice were evaluated using fluorescently labeled antibodies against DMRT1 (green; A and D) and NANOS2 (red; B and E). Panels C and F show merged images. Arrowhead in panel C show partial interaction between NANOS2 in the cytoplasm and DMRT1 in the nucleus of germ cells in *Dmrt1*$^{+/+}$ mice testis. Also note the expression of NANOS2 in the absence of DMRT1 (E). Final magnification for micrographs is x400.

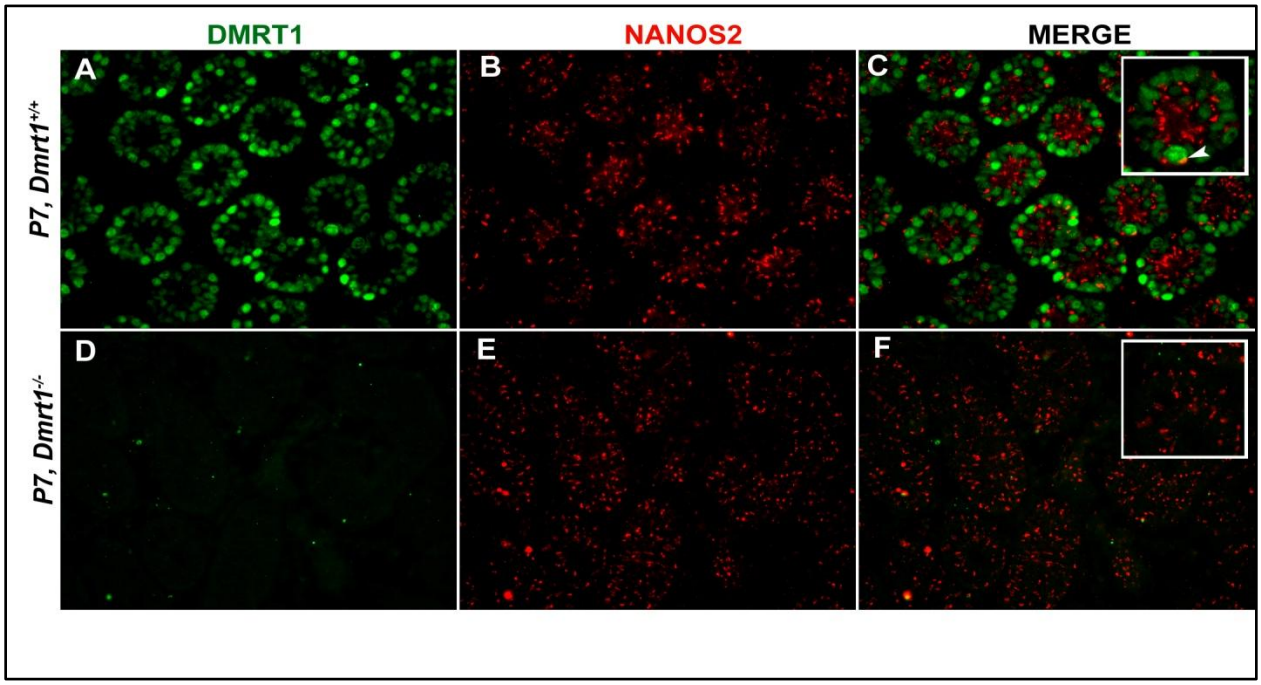

Figure 4: Immunolocalization of DMRT1 and NANOS2 in postnatal day 7 (P7) mouse testis. Testis sections from *Dmrt1*$^{+/+}$ (A-I) mice were evaluated using fluorescently labeled antibodies against DMRT1 (red; A) and NANOS2 (green; B) and counterstained with DAPI for nuclei (blue; D, E and F). Panels C, G, H and I show merged images. Arrowheads in panel C and I show partial interaction between NANOS2 in the cytoplasm and DMRT1 in the nucleus of germ cells in *Dmrt1*$^{+/+}$ mice testis. Final magnification for micrographs is x600.

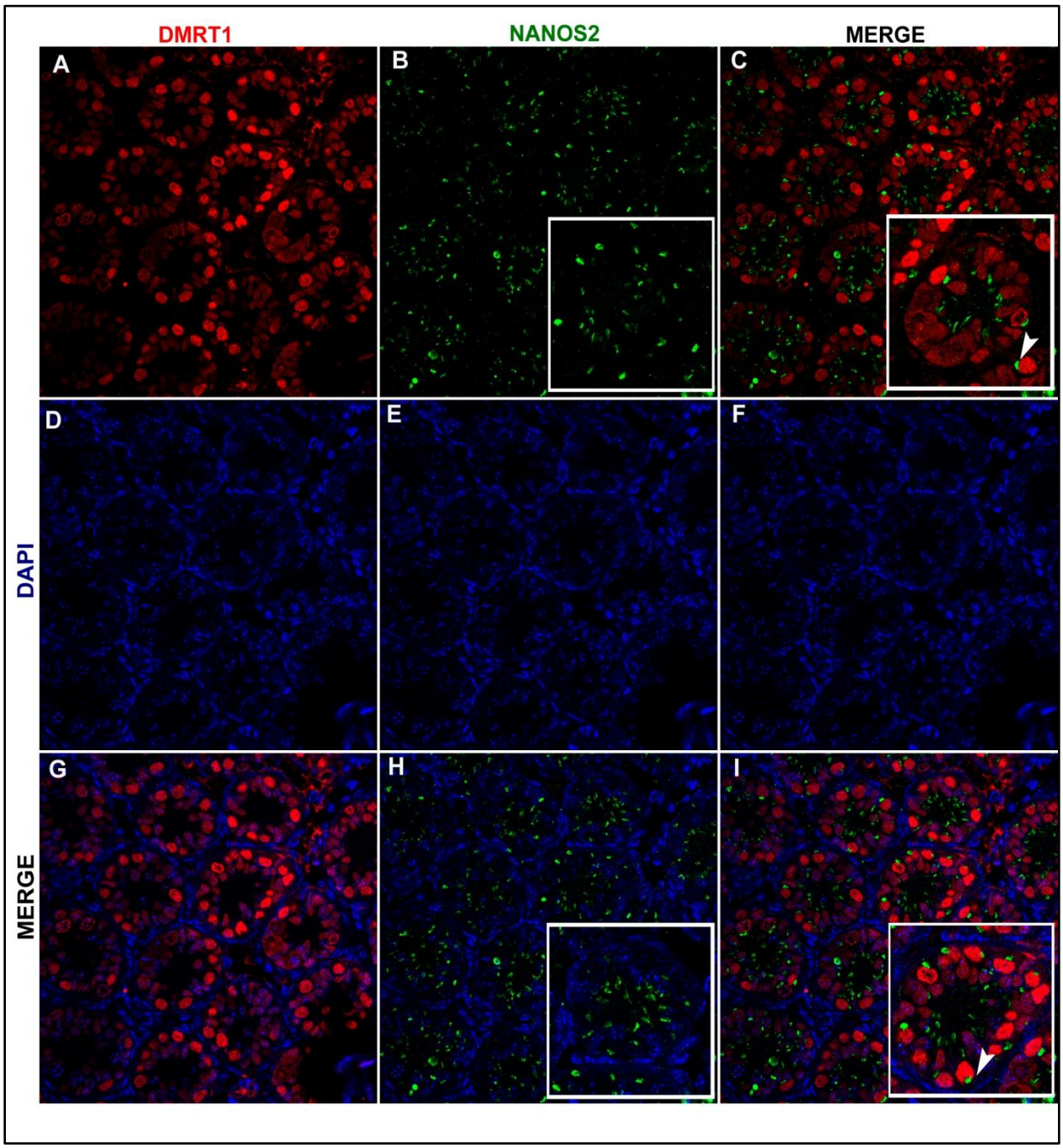

Figure 5: NANOS2 alters the activity of DMRT1. The effect of NANOS2 on DMRT1 and GAL4 transcriptional activity was evaluated by transient transfection of GC-1 cells with various luciferase reporters and expression vectors. **A.** Co-transfection of EF-FLAG-DMRT1, increasing amounts of FLAG-NANOS2-MYC and 4X-DM-Luc, which was generated by placing four copies of DMRT1-response element upstream of a TATA box (minimal promoter). **B.** Co-transfection of VP16-DMRT1, increasing amounts of FLAG-NANOS2-MYC and 4X-IRE-Luc, which was generated by placing four copies of DMRT1-response element in front of an SV40 promoter (strong and constitutive promoter). **C.** Co-transfection of VP16-DMRT1, FLAG-NANOS2-MYC and 4X-DM-Luc (solid bars), and co-transfection of GAL4-V16, FLAG-NANOS2-MYC and 5X-GAL4-UAS-Luc, generated by placing four copies of GAL4 upstream activation sequence (UAS) in front of an SV40 promoter (checkered bars). The ratio of firefly to renilla luciferase activities for each sample was made relative to the firefly/renilla values for the reporters' transfected without expression vectors. Error bars represent standard error of means.

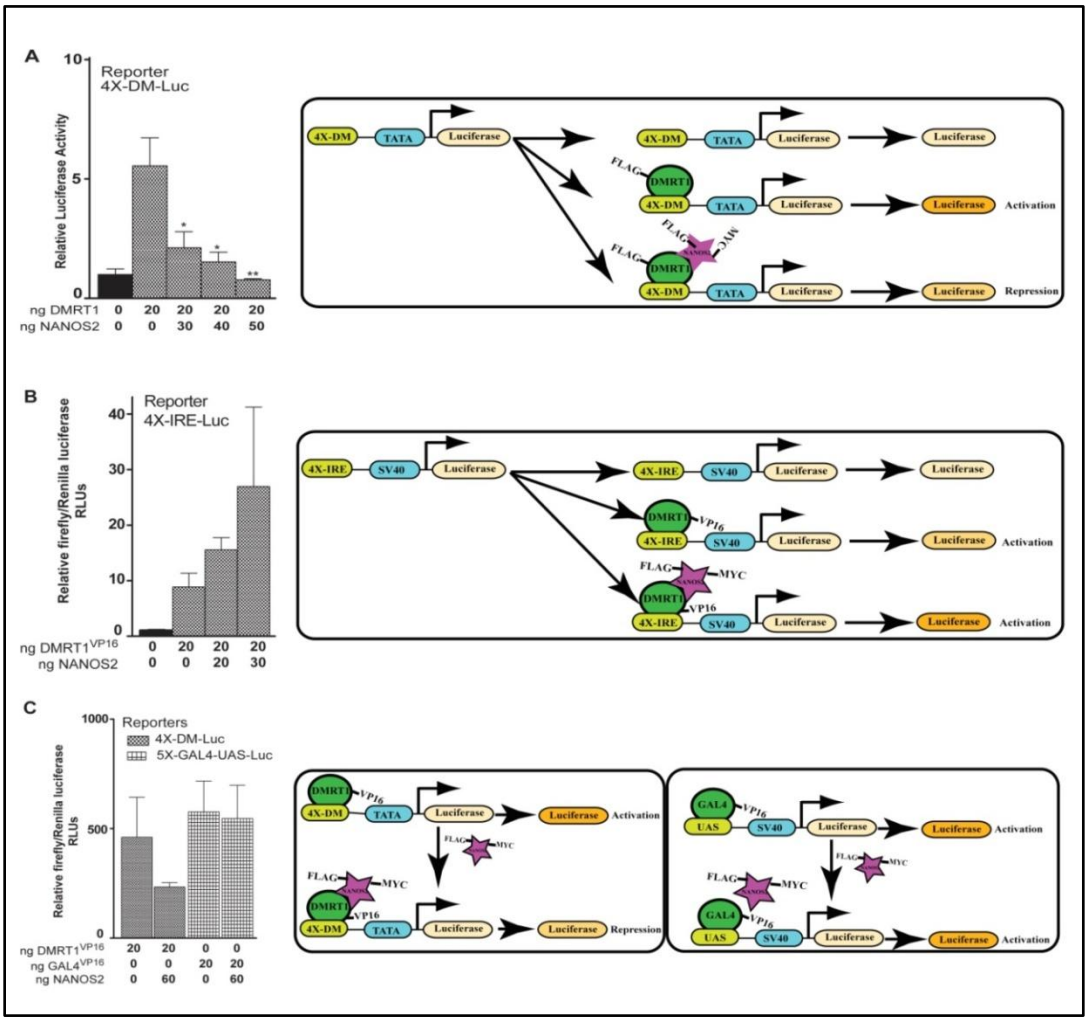

Table 1: Opposite gene expression changes of twenty-four (24) genes regulated by NANOS2 and DMRT1 obtained from *Nanos2*$^{-/-}$ and *Dmrt1*$^{-/-}$ mice.

	GENES	PUBLIC ID	GENE TITLE	Change in *Dmrt1* KO	Change in *Nanos2* KO (Suzuki et al., 2010)
Genes (opposite directional change)	***Stra8***	NM_009292	Stimulated by retinoic acid gene 8 homolog (mouse)	-3.37	21.60
	Sox3	AV306664	SRY-box containing gene 3	-3.98	13.00
	Taf7l	AF285574	TAF7-like RNA polymerase II	-4.40	12.69
	Asb9	AF398970	Ankyrin repeat and SOCS box-containing 9	-5.37	12.55
	Upp1	NM_009477	Uridine phosphorylase 1	-3.38	9.89
	Sohlh2	AK016704	Spermatogenesis-oogenesis specific bHLH 2	-3.44	9.53
	Fmr1nb	AW542416	Fragile X mental retardation 1 neighbor	-3.01	8.62
	Acaa1b	BC019882	Acetyl-Coenzyme A acyltransferase 1B	-6.40	8.27
	Sycp1	AV275615	Synaptonemal complex protein 1	-3.27	8.12
	1700013H16Rik	AK005953		-1.79	6.79
	PLZF	BQ174973	PLZF, Zfp145, lu; Zbt16	-9.22	5.33
	Tex16	NM_031382	Testis expressed gene 16	-3.57	5.16
	Ngn3	AK008017	Neurogenin 3	-3.99	5.09
	Pramel3	NM_031390	Preferentially expressed antigen in melanoma-like 3	-10.39	4.85
	Rimklb	AV271892	Ribosomal modification protein rimK-like family member B	-4.10	4.75
	1700011M02Rik	1700011M02Rik	Dmrtc1a	-7.03	3.95
	Lin28	BB706377	Lin-28 homolog (C. elegans)	-5.06	3.47
	Dmrta1	BB461344	Dmrta1	-18.66	2.71
	Dazl	NM_010021	Deleted in azoospermia-like	-5.37	2.51
	Rimklb	AV271892	Ribosomal modification protein rimK-like family member B	-1.72	2.37
	Phf17	BM119726	PHD finger protein 17, mRNA	-5.30	2.29
	Dsp	AV297961	Desmoplakin	4.95	-2.41
	Ccl17	NM_011332	Chemokine (C-C motif) ligand 17	7.71	-3.00
	Slc1a5	NM_009201	Solute carrier family 1 ; member 5	0.00	-3.10

Table 2: Similar gene expression changes of sixteen (16) genes regulated by NANOS2 and DMRT1 obtained from *Nanos2*$^{-/-}$ and *Dmrt1*$^{-/-}$ mice.

	GENES	PUBLIC ID	GENE TITLE	Change in *Dmrt1* KO	Change in *Nanos2* KO (Suzuki et al., 2010)
Genes (similar directional change)	***Cdh1***	NM_009864	Cadherin 1	2.20	5.95
	Dppa3; Stella	AY082485	Developmental pluripotency-associated 3; Stella	2.59	2.92
	Morc1	NM_010816	Morc1	-12.41	-2.42
	Ripk4	AF302127	Receptor-interacting serine-threonine kinase 4;	-8.47	-2.50
	Ripk4	AF302127	Receptor-interacting serine-threonine kinase 4	-2.10	-3.00
	Afp	NM_007423	Alpha fetoprotein	-5.71	-3.00
	Tdrd1	AF285591	Tudor domain containing 1	-2.26	-3.00
	Emb	BG064842	Embigin	-2.74	-3.01
	Gtsf1	AK005675	Gametocyte specific factor 1	-5.70	-3.05
	Gtsf1	AV045004	Gametocyte specific factor 1	-7.38	-3.48
	Dnd1	BF020021	Dead end homolog 1 (zebrafish)	-3.07	-3.18
	Nefm	NM_008691	Neurofilament; medium polypeptide	-8.47	-3.31
	Map3k12	BQ176966	Mitogen activated protein kinase kinase kinase 12	-2.38	-3.35
	Mns1	NM_008613	Meiosis-specific nuclear structural protein 1	-2.54	-3.42
	Dppa4	BB067210	Developmental pluripotency associated 4	-3.65	-4.23
	Tdrd9		Tudor domain containing 9	-3.70	-5.00
	Piwil4	BB814395	Piwi-like homolog 4 (Drosophila)	-2.54	-7.29
	Tspan8	BC025461	Tetraspanin 8	-3.79	-15.00

Chapter 6: Implications and Future Direction

Introduction

DMRT1 is an evolutionary conserved transcriptional regulator required for postnatal testis development. The mechanism(s) associated with DMRT1 and the pathways it regulates are unresolved. Thus, the overall hypothesis was to elucidate pathways critical for Sertoli cell differentiation and germ cell growth and maintenance regulated by DMRT1 and its protein-binding partners using mouse models with different cell-specific amounts of DMRT1. To investigate this hypothesis, specific aims were proposed to identify biological pathways regulated by DMRT1 that were unique to Sertoli cells and germ cells. This goal relied on the identification of gene expression differences, direct targets and their associated biological processes. In addition, more light was shed on the regulation of the transcriptional activity of DMRT1 in germ cells with the identification of a germ cell-specific partner protein.

The work in this dissertation uncovers many essential features of DMRT1 including cell-specific expression and physiological function in the testis (Chapter 2), importance during ES formation and organization (Chapter 3), distinct cell-specific pathways and direct targets (Chapter 4), and transcriptional and translational regulation in germ cells (Chapter 5), which provided new insights on biological processes modulated by DMRT1 during postnatal testis differentiation. The implications and follow-up experiments of these findings will be discussed in this chapter.

Dmrt1$^{-/-;tg}$ mice (aka *Dmrt1*-rescue)- a novel mouse model of *Dmrt1*-deficient germ cells and male infertility

The *Dmrt1*-rescue mice is a novel DMRT1-deficent germ cell mouse model generated by the return of DMRT1 to *Dmrt1*-null Sertoli cells using a *Wt1-Dmrt1* transgene. Characterization of these mice revealed new functions modulated by DMRT1 in Sertoli cells including maintenance of testis weight and sperm progressive motility, Sertoli cell maturation, serum testosterone levels and seminiferous tubule integrity. Consistent with previous murine *Dmrt1* deletion studies, these results supported roles for this

transcription factor in postnatal testis differentiation but not sex determination like in the *Dmrt1*-null mice, which were characterized by postnatal Sertoli cell defects and germ cell death but not XY sex reversal [50]. Specifically, the adult *Dmrt1*-null male mice were characterized by severe testis hypoplasia, disorganized seminiferous tubules, failed Sertoli cell differentiation, premeiotic germ cell death and sterility, without evidence of ectopic ovarian tissues or Mullerian duct-derived structures. Features like infertility, testicular hypoplasia, germ cell loss and no XY sex reversal were also present in male *Dmrt1*-rescue mice. In contrast, the *Dmrt1*-null females had normal ovaries and were fertile [50]. This finding is consistent with our observations that overexpression of DMRT1 in pregranulosa cells did not cause XX sex reversal on a $Dmrt1^{+/+}$ or $Dmrt1^{-/-}$ background. The ovaries in these transgenic females developed normally and remained fertile in the presence of DMRT1 during gonadal development.

Further characterization of *Dmrt1*-transgenic and *Dmrt1*-rescue mice, which express exogenous *Dmrt1* transgene only in Sertoli cells, validated roles for this transcriptional regulator in postnatal testis differentiation. Specifically, testis size and sperm progressive motility were better in aging transgenic males and in $Dmrt1^{-/-}$ background, the transgene partially restored SC differentiation, tubule morphology and production of adherens junction proteins (Chapter 3). The transgenic studies suggest that more DMRT1 is expressed or the levels are maintained in aging mice that provided a better testis environment, which translated to a better germ cell niche and improved sperm quality. This hypothesis can be tested by setting up fertility experiments to determine fertilization success in 1.5- 2.5 year-old *Dmrt1*-transgenic ($Dmrt1^{+/+;tg}$ and $Dmrt1^{+/+;tg+tg}$) and $Dmrt1^{+/+}$ mice. Consistent with the above results, recent studies using different approaches arrived at the same conclusion for DMRT1 in the maintenance of a testis environment. Notably, cell-specific deletion of *Dmrt1* in Sertoli cells resulted in a normal morphology at birth with normal expression of SOX9; but by P14, *Dmrt1*-null Sertoli cells started to differentiate into granulosa cells, as indicated by the expression of FOXL2, which is normally expressed in the ovary, and by P28, the majority of cells expressing SOX9 were lost while FOXL2 was strongly expressed by cells in the seminiferous tubule [135]. In the same study, similar changes were observed four weeks after *Dmrt1*

was deleted from adult mice, leading to the conclusion that loss of *Dmrt1* causes Sertoli cells to be reprogrammed into cells with a granulosa-like or theca-like morphology accompanied with elevated expression of female-specific genes, enzymes and androgens. With the above findings, it is still unclear if DMRT1 regulates primary sex determination in mice, but invaluable during postnatal testis differentiation and sex maintenance; and it is essential to note that some factors may limit the actual function of DMRT1 when *Dmrt1* is deleted or forced expressed in cell-specific expression studies.

Potential factors affecting role of exogenous DMRT1

The strength of the *Wt1* promoter and gene redundancy are two factors that may have restricted the function of the exogenous DMRT1. It has been shown that the presence or absence of expression of a gene product depends on the strength of the control promoter of interest and the levels of expression of a gene product is directly proportional to the strength of the promoter [316, 317]. In our study, DMRT1 was express from *Wt1-Dmrt1* transgene and thus under the control of *Wt1* promoter elements. Comparing the gene expression profiles of *Dmrt1* and *Wt1* from P6 through P10, as published in the dataset GSE926, which evaluated the global gene expression profiles during mouse postnatal testis development starting immediately after birth (P0) through the first wave of spermiation (P35) (Figure 1;[276]), showed that expression of *Dmrt1* was about two-fold higher than that of *Wt1* expression. However, knowing that in the testis, WT1 is expressed only in Sertoli cells and DMRT1 is expressed in both Sertoli cells and premeiotic germ cells provides an explanation for the difference in *Dmrt1* and *Wt1* expression levels. Germ cell proliferation adds to the number and level of germ cell-specific expression of DMRT1, whereas the levels in Sertoli cells are fixed once the number of Sertoli cells required to maintain spermatogenesis are determined at puberty, at about P12 in mice. Consequently, the Sertoli cell-specific *Dmrt1* expression levels can be deduced to be comparable to the gene expression levels of *Wt1* in Figure 1. The strength of the *Wt1* promoter was previously tested and was used to direct expression of SOX9 in the *Wt1-Sox9* transgenic mouse model; and was found to be powerful and sufficient to produce levels of SOX9 that induced XX-to-XY sex reversal [39]. Consistent with this study, it is evident that *Wt1* directed the

expression of an adequate amount of DMRT1 from the *Wt1-Dmrt1* transgene, which did not induce sex reversal. This also suggested that transgenic DMRT1 is regulated like endogenous DMRT1 but the seminiferous tubule integrity in adult testes from *Dmrt1*-rescue mice were partially restored and different from those of mice models like the W^v/W^v mice, which lack germ cells [190, 318]. It is likely that there is a delay in the action of the exogenous DMRT1 given that *Dmrt1*-null and *Dmrt1*-rescue mice lacked seminal vesicles at P42 but by P120 and above, seminal vesicles were fully formed only in *Dmrt1*-rescue mice (Chapter 1; supplementary Figure 1). Thus, transplantation experiments by transferring germ cell explants into *Dmrt1*-rescue testes will be required to determine the nurturing function of Sertoli cells in this DMRT1-deficient germ cell mice model and in the process validating or refuting the strength of *Wt1* promoter. In addition, an elaborate characterization of the *Dmrt1*-rescue at older ages (starting from P90) will be required to determine the full extent of restoration of tubule integrity directed by exogenous DMRT1.

The effects of gene redundancy provided by other DM domain genes may be the obstructing factors, knowing that other DM domain proteins are expressed both in the embryonic ovaries and testes (DMRT4 and DMRT7) or only in the embryonic testes (DMRT3), may account for the normal sex determination and embryonic testis differentiation observed in *Dmrt1*-null, *Dmrt1*-rescue and *Dmrt1*-transgenic mice [50, 319]. Similar studies on the functional ablation of *Sox9* demonstrated the gene redundancy effect, whereby the specific deletion of *Sox9* in the gonads did not induce XY-to-XX sex reversal until an additional deletion of a closely related gene, *Sox8*, occurred in the male gonads [38]. Thus, double murine deletion studies of *Dmrt3* and *Dmrt1*, which are both testis-specific and neighbors on chromosome 9 in humans, will be required to finally include or exclude DMRT1 as a mammalian sex determining factor.

Phenotypic similarities between adult Dmrt1-rescue mice and mice models of Klinefelter's syndrome

The phenotype of P42 testes in *Dmrt1*$^{-/-;tg}$ mice resembles that of two mouse models (male 41, XXY and the 41, XX^{Y}*) of human Klinefelter's syndrome (47 XXY), with common phenotypic features including significant germ cell depletion by P7, small testes in adult mice with reduced seminiferous tubule diameter, Sertoli cell-only tubules, Leydig cell hyperplasia and reduced serum testosterone levels [211-215]. Thus a novel mouse model of infertility that shares characteristics with Klinefelter's patients; who are characterized by the presence of a supernumerary X chromosome, endocrine deficiencies and testicular alterations; is generated by returning DMRT1 to *Dmrt1*-null Sertoli cells. Klinefelter's syndrome results from the failure of sex chromosomes to segregate during meiosis. Chromosomal non-segregation in meiosis can occur during differentiation of gametes, which leads to aberrant karyotypes resulting in different disease states as long as the alterations induced by the extra chromosomes are not lethal [320-322]. Giving that a delay in the function of DMRT1 is likely present in the *Dmrt1*-rescue testes as suggested by the presence of seminal vesicles at >P120 that were absent at P42, it will be worthwhile to investigate if the similarities to mouse models of Klinefelter's syndrome are maintained at older ages. Nonetheless, more experiments will required to further characterize and determine if P42 *Dmrt1*$^{-/-;tg}$ mice exhibit any cognitive, behavioral and metabolic defects like Klinefelter's patients.

Novel function in formation and organization of testis-specific adherens junction

Although existing findings exclude *Dmrt1* as a potential murine sex-determining factor or as a central gene required for early embryonic regulation of testis differentiation, further characterization of *Dmrt1*-rescue mice validated cell-specific function vital for postnatal testis differentiation. Our findings showed that Sertoli cell-specific return of DMRT1 modulate the expression of proteins required for the formation and organization of ES, a testis-specific adherens junction, as determined by identification of these structures on electromicrographs and by immunohistochemical expression of ES- adapter proteins ESPIN, NECTIN-2 and NECTIN-3 (Chapter 3). The NECTINS are immunoglobulin-like adhesion

molecules that interact with AFADIN, an actin filament-binding protein that connects NECTINS to the cytoskeleton. Three actin-based adherens complexes have be identified at the apical junctional specialization namely: the INTEGRIN-LAMININ, the NECTIN-AFADIN, and the CADHERIN-CATENIN complexes [193]. The association and dissociation of the apical junctional specialization overlaps with the expression of these junctional complexes [323, 324]. This distinctive association in cell–cell interactions may be linked to the dynamic properties of the apical junctional specialization. The NECTIN-AFADIN complex links spermatid to the Sertoli cell through a heterotypic interaction between NECTIN-2, located exclusively on the Sertoli side of the apical ES and NECTIN-3, located on the spermatid side [240]. By binding to I-AFADIN, an F-ACTIN binding protein, the interactions with NECTIN-2 play vital roles in the organization and reorganization of the cytoskeleton during spermiogenesis, since the epithelial organization was totally disrupted in *Afadin* knockout embryonic ectoderm, suggesting that AFADIN regulates the functional state of NECTINS and contributes to the basic organization of cell–cell junctions [325-327]. Similarly, genetic mutation experiments showed that ESPIN constitute a family of actin bundling regulatory proteins with the capacity to alter the organization, dimensions, dynamics and signaling abilities of the actin cytoskeleton [328]. Furthermore, *Nectin-2* knockout induces abnormal development of the spermatid head resulting in misshaped nuclei, presence of mitochondria in the head, and a disorganized middle piece, while *Nectin-3* knockout also induces sterility in the mouse [326, 329]. Thus, *Afadin*, *Nectin-2*, *Nectin-3* and *Espin* mutation studies illustrate the importance of the above interactions in cytoskeletal framework and Sertoli cell-germ cell interaction; and our current findings directly implicate DMRT1 in the formation and/or organization of ES by may be regulating the assembly of the NECTIN-AFADIN complex. Two observations implicate Sertoli cells' DMRT1 in the formation and organization of this cytoskeletal framework. First, ES structure was reduce and absent in *Dmrt1*$^{-/-}$ mice based on protein expression of NECTIN-2 and NECTIN-3, respectively, but induce in tubules of *Dmrt1*$^{-/-;tg}$ mice. Second, immunofluorescence evaluation of ESPIN showed weak and irregular signals in *Dmrt1*$^{-/-}$ tubules compared to the strong and regular signals in *Dmrt1*$^{-/-;tg}$ tubules.

Vinculin (VCL), an actin-binding protein important for adherens junction assembly [330-332], was found to be a direct target of DMRT1 and its expression was misregulated in *Dmrt1*-null testes ([136]; Chapter 4). It is evident that DMRT1 modulates the formation and organization of cytoskeleton by regulating genes like *Vcl*, which facilitates the assembly of adherens junction proteins. Thus, identifying downstream targets, partner proteins and the pathways recruited by VCL at the ES will provide a cytoskeletal assembly pathway directed by DMRT1 in Sertoli cells.

Regulated genes and DMRT1 targets

With a desire to understand DMRT1 functions, mice expressing different cell-specific amounts of *Dmrt1* were generated and their global gene expression profiles analyzed to elucidate the cell-specific functions directed by DMRT1 in Sertoli cells and germ cells. Evaluation of cell-specific differential expression revealed enrichment of genes involved in ubiquitination (*Magek1*, *Mage11*, *MageB16*, *Trim71*, *Trim12*, and *Trim34*), Piwi (P-element-induced wimpy testis)-interacting RNAs (piRNAs (*Piwil2* and *Piwil4*)) and expressed in exosomes (*Cpne8*, *Ano4*, *Rps9*, *Cfi*, *Cadm1*, *Aqp5*, *Foxq1*, *H2-Aa*, *Hspb8*, *Tuba3a*, *Flbn2*, *Rarres1*, *Dsp*, *Piwil2*, *Krt18*, *Krt8*, *Gfra1*, *Crabp2*, *Dppa3*) (Chapter 4); thus providing a platform to speculate on some of the cell-specific roles of DMRT1. It is well established that DMRT1 regulates Sertoli cell differentiation and germ cell development and survival but the mechanisms that determine the cellular fate of proteins involved in these biological processes remains obscure.

MAGE-cancer testis antigens

One way by which the cellular fate of proteins can be determined is through ubiquitination, which is a conserved posttranslational protein modification required during cell proliferation, differentiation, programmed cell death or inflammation [333, 334]. Proteins are modified by the addition of ubiquitin molecules by the sequential action of three enzymes: ubiquitin-activating (E1), ubiquitin-conjugating (E2) and ubiquitin-ligase (E3) enzymes. The proteins tagged with ubiquitin are targets for proteins carrying ubiquitin-binding domains, which determine the cellular fates of the ubiquitinated proteins [335-337].

Several genes encoding MAGE cancer testis antigens (MAGE11, K1, & B16) and TRIM E3 RING ubiquitin ligases (TRIM71, 12, & 34) were differentially expressed in our study (Chapter 4) and a recent report showing MAGE and TRIM proteins interact to mediate substrate ubiquitination, may provide a possible mechanism by which DMRT1 directs differentiation of Sertoli cells [288]. However, characterization of the protein-protein interaction between DMRT1 and MAGE/TRIM ubiquitination complex will be required to establish this posttranslational modification as a process regulated by DMRT1.

Non coding RNA

The quest to identify possible mechanisms utilized by DMRT1 to regulate postnatal testis development also revealed noncoding small RNAs. Small RNAs are vital because of their various biological functions as powerful transcriptional, translational and RNA stability regulators [338]. Small RNAs are classified into three groups based on their origin, modes of action and functions including small interfering RNAs (siRNAs), microRNAs (miRNAs) and piRNAs [339]. piRNAs are expressed during sperm production in the mammalian testis, where they interact with PIWI-family proteins like PIWIL1,PIWIL2 and PIWIL 4 [340-345]. This Piwi-family proteins are a subfamily of Argonaute proteins, previously shown as the essential constituents of the RNA-induced silencing complex (RISC) in siRNA-mediated pathway [343, 346, 347]. The actions of the PIWI proteins can be deduce from their association with RNA helicase like the Tudor-domain-containing family protein (TDRDs), which are suggested to be critical regulators of nuage (germinal granules) assembly involved in piRNA-mediated signaling pathway. TDRD8 (STK31) and TDRD9 have been demonstrated as interacting partners of PIWIL2, and PIWIL4, respectively, in the piwi pathway [346, 348, 349]. Similarly, MOV10L1 another RNA helicase, which is specific to germ cells and contain the complete conserved helicase motif, also interacts with PIWI proteins with a preference for the MILI-piRNA complex than the MIWI-piRNA complex. These interactions are postulated to retain the evolutionary trait in the germline and safeguard RNA in male germ cells against retrotransponsons, thus maintaining the genetic content of a cell [350,

351]. STK31 is expressed postmeiotically and its conserved helicase domain suggests that it may be important in reorganizing sperm chromatin during spermiogenesis [352]. Although the maintenance of germline stem cells was unaffected in *Mov10l1*-null mice, primary spermatocytes activated long-terminal repeat (LTR) and Long interspersed element 1 (LINE1) retrotransposons that culminated in cell death and male infertility [351]. Thus, STK31 and MOV10 L1 are indispensable for spermatogenesis. Results in our study showed that the message levels of *Piwi2*, *Piwi4*, *Mov10L1* and *Stk31* were significantly reduced in the *Dmrt1*-null and *Dmrt1*-rescue mice, when compared to Wild-type mice (Chapter 4). This study revealed that, in the context of wild-type mice, the expressions of *Piwi2*, *Piwi4*, *Mov10L1* and *Stk31* in testicular germ cells are dependent on the transcriptional activity of DMRT1 and provides a putative mechanism for DMRT1-dependent regulation of germ cell development and maintenance.

Vesicular transport and exosomes

Although Sertoli cells and germs cells are the major occupants of the testis, no channel for exchange of information between these cell types have been established. Exosomes or microvesicles are released by most cells under normal physiological conditions and this membrane transfer is being used by some cells for communication [353]. Epididymosomes are exosomes secreted in an apocrine manner and are derived from epididymal epithelium. Proteins associated with the epididymosomes like macrophage migration inhibitory factor (MIF) was identified to be transferred from exosomes to spermatozoa as they transit the epididymis [354]. The revelation that genes shown to be expressed in exosomes like *Cpne8*, *Ano4*, *Rps9*, *Cfi*, *Cadm1*, *Aqp5*, *Foxq1*, *H2-Aa*, *Hspb8*, *Tuba3a*, *Flbn2*, *Rarres1*, *Dsp*, *Piwil2*, *Krt18*, *Krt8*, *Gfra1*, *Crabp2* and *Dppa3* were down-regulated in *Dmrt1*-null and *Dmrt1*-rescue, when compared to *Dmrt1*-wild-types, suggests that exosomes might be the conduit for exchange of information between Sertoli cells and germ cells in the testis. However, more characterization and tracing experiments will be required to substantiate this hypothesis.

DMRT1 targets

In combination with the global gene expression profiles, primary and downstream targets of DMRT1 were identified using ChIP-Seq. The majority of targets identified were novel, as they were not detected in the previously published ChIP-promoter array analyses and may be because the majority of targets had DMRT1 binding sites located beyond the proximal promoter region. Characterization of these binding site sequences revealed two putative sequences with considerable similarities to the *in vitro* binding sequence and mab3 binding site. Direct targets with these binding sites included *Boll*, *Gfra1* and *Usp9y* that are important for germ cell differentiation and male infertility [105, 277, 278]. Further functional analyses revealed cell adhesion and development, cell cycle regulation, protein processing and transport, RNA metabolism and transport, and energy metabolism, to be enriched amongst DMRT1-targets. Overall, these results identified novel targets and putative binding sites of DMRT1.These putative binding sites identified could be confirmed using EMSA and reporter gene activation along with mutated variants of the binding site sequences.

Nanos2, a modulator of DMRT1 expression and function in germ cells

DMRT1 is essential for male development and fertility yet how its activity is regulated; particularly in germ cells was a mystery until now. Our knowledge of what regulates DMRT1 expression is derived almost entirely from studies in Sertoli cells and therefore essentially nothing was known on its regulation in germ cells.

Controversy on the exact role of DMRT1 in mitotic to meiotic transition

NANOS2 is an evolutionary conserved zinc finger RNA binding protein that is expressed in germ cells and required for maintenance of undifferentiated spermatogonia [105, 106]. In mouse testis, embryonic germ cells start expressing NANOS2 at 13.5 dpc and postnatal germ cell expression is restricted to types A_s and A_{pr} spermatogonia; the subset of undifferentiated spermatogonia that includes the “actual stem cell” pool with the ability to self-renew [105-107, 109, 296]. NANOS2 favors the

maintenance of an undifferentiated spermatogonial germ cell pool and thus hinders differentiation by suppressing synthesis and expression of retinoic acid (RA) and STRA8, respectively. Like NANOS2, DMRT1 was recently shown to repress meiosis by controlling the mitotic to meiotic transition of germ cells [134, 295], suggesting they may share a partial overlapping functions since the deletion of DMRT1 in germ cells did not generate excessive meiosis by germ cells [134]. However, the current published role of DMRT1 as meiotic repressors is controversial based on available published and unpublished data on the transcript expression profiles of *Dmrt1* and *Stra8*.

It is evident that DMRT1 in male germ cells regulate the mitotic to meiotic switch but not by repressing retinoic acid (RA) and STRA8 expression as was recently depicted [134]. Based on available transcript expression profiles from postnatal mouse testis time course (P0-P56, GSE926 dataset; [276]), embryonic *Nanos2*-null testes [295, 300], P7 *Dmrt1*-null and *Dmrt1*-rescue testes (Chapter 4), P1 and P2 *Dmrt1*-null [132], *Dmrt1*-null ovaries [137], and except for P9 cell-specific *Dmrt1* knockout testes [134], the transcription activity of DMRT1 on *Stra8* points to activation not repression. Analyses of the global gene expression profiles of the postnatal mouse testis from P0 through P56 (GSE926 dataset; Figure 2A) showed that the lowest gene expression levels for *Stra8* were observed between P0 and P3 when *Dmrt1* levels were at about 33% of its maximum expression level. However, the gene expression levels of *Stra8* increased gradually with increasing *Dmrt1* levels and attained its maximum level at P10 when *Dmrt1* levels were also at maximum. *Dmrt1* gene expression levels peak at P6 and peak levels were maintained until P10. From P14 through P35, the gene expression levels of *Stra8* decreased as *Dmrt1* levels dropped, suggesting that the *Stra8* message was not suppressed [276]. The dependence of *Stra8* gene expression to the expression of DMRT1 has been studied using *Dmrt1*-null mice, where gene expression of testes from these mice at P1, P2, P7 and P9 or ovaries, showed that the levels of *Stra8* were suppressed in the absence of *Dmrt1* ([132, 134, 137]; Chapter 4).

Unfortunately, the above gene expression patterns were discarded in favor of STRA8 expression results obtained using *Ngn3*-Cre-mediated conditional deletion of *Dmrt1* in germ cells [134]. Even though the message for *Stra8* in the P9 mutant testes was not elevated in this study, the finding was overlooked; leading to the conclusion that DMRT1 is a repressor of STRA8 and thus meiosis. Several factors might have contributed to the misinterpretation of their findings. Conditional knockouts are limited by their penetrance as the TNAP-Cre employed in another cell-specific deletion of DMRT1 was limited by its poor Cre penetrance that resulted in partial deletion with a portion of germ cells positive for DMRT1. Thus, immunohistological analysis showed that deletion using the TNAP-Cre was leaky and nonspecific as DMRT1 was ectopically ablated in some Sertoli cells. Thus, TNAP-Cre cannot be used to correctly profile the cells without accounting for the effective deletion. Likewise, a significant number of spermatogonia that were DMRT1-positive were negative for the Ngn3-Cre transgene until several weeks after birth, which prevented analysis of early germ cell specific events [110, 174]. The restricted co-expression of DMRT1 and NGN3 in prepubertal mice can be appreciated by immunofluorescence of the two proteins in P7 testes, which shows few dual-stained yellow cells [130]. Consequently, the activation of *Stra8* by DMRT1 in those populations of germ cells with failed *Dmrt1*deletion in the study was misinterpreted.

In addition, knowing that NANOS2 represses meiosis and consistent with the gene expression profiles of *Dmrt1*-null testes, the transcriptional activation of *Stra8* by DMRT1 is favored by global gene expression profiles of embryonic day 17 (E17) testes from *Nanos2*-null mice, which showed up-regulation of both the *Stra8* and *Dmrt1* gene expression levels [295, 300]. Our current findings that NANOS2 is upstream of DMRT1, partially co-localizes, interacts and modulates the transcriptional activity of DMRT1 in germ cells (Chapter 5) are exciting and provide valuable information required to establish the role of DMRT1 in the mitotic-to-meiotic transition by germ cells. It is likely that the levels of DMRT1 is suppressed and tightly regulated by NANOS2 in the undifferentiated spermatogonia (A_{single} and A_{paired}), which inturn suppresses retinoic acid synthesis and the transcription of *Stra8*, a direct target

of DMRT1 (Figure 2B). As the spermatogonium proliferates and progresses in development, NANOS2 is suppressed while DMRT1 levels are elevated and sufficient to mediate the transcription of *Stra8* and hence meiosis. Thus, we speculate that NANOS2 controls meiosis by suppressing DMRT1's expression in undifferentiated spermatogonial stem cells. However, more transient transfection, knockdown and coimmunoprecipitation experiments will be required to elucidate the mechanism and additional factors involved in DMRT1-mediated activation of mitotic-to-meiotic transition.

What are the putative mechanisms employed by NANOS2 to regulate the transcriptional activity of DMRT1?

DMRT1 expression can be regulated at several different levels. Its synthesis may be suppressed, the synthesized protein may be inactivated or degraded in the cytoplasm and the protein can be mislocalized in the cytoplasm in the absence of specific nuclear localization signals (Figure 3). Existing literature on the translation regulator and RNA binding protein, NANOS2, and the observed interaction and functional findings between NANOS2 and DMRT1 in this current study provide a platform to speculate on potential mechanisms by which NANOS2 regulates the transcriptional activity of DMRT1 in germ cells. NANOS2 was previously shown to localize in the cytoplasmic and nuclear compartments of HEK293T cells transfected with a NANOS2-MYC expression vector [301]. Our current immunostaining of NANOS2 and DMRT1 revealed partial co-localization with NANOS2 affixed to the nuclear membrane with DMRT1 in the nucleus. Furthermore, NANOS2 modulated the transcriptional activity of DMRT1 in transient transfection experiments using GC1 cells. Giving that nuclear localization of NANOS2 has been shown, suggests that NANOS2 translocate to the nucleus either alone or tethered to a binding partner like DMRT1 during its translocation from the cytoplasm to the nucleus. Based on the transient transfection results and given that NANOS2 was localized to the nucleus, the

first possibility for the regulation of synthesis of DMRT1 by NANOS2 could be at the initiation-step of transcription.

Co-transfection of NANOS2 had two independent effects (activation and repression) on DMRT1 transcriptional activity, which was dependent on the promoter context. When the DMRT1 response elements were placed upstream of a constitutive SV40 promoter and co-transfected with NANOS2 and DMRT1, the transcriptional activity of DMRT1 was up regulated as seen with the dose-dependent increase of luciferase activity with increasing NANOS2. This suggests that NANOS2 bound to DMRT1 on the promoter facilitates the recruitment of co-activators, such as NCOA2 and NCOA4 identified as direct targets of DMRT1, with a variety of modification capabilities vital for gene transcription (Figure 3; I) ([136]; Chapter 4). This possibility has been documented for other RNA binding proteins. For example, two members of the U2AF65 family of proteins, RBM39 and RBM 23, regulate gene transcription and alternative splicing mediated by steroid hormones. The RBM proteins co-activated the progesterone receptor in transient transfection assays and altered in a hormone-dependent manner the alternative splicing of a calcitonin/calcitonin gene-related peptide [355]. Suppression of DMRT1 transcriptional activity was the alternative effect obtained when NANOS2 and DMRT1 were co-transfected along with a minimal TATA box promoter that was downstream of the DMRT1-response elements. In this instance, NANSO2 potentially aids in the recruitment of co-repressors which hinders the transcription of a gene (Figure 3; II). An example exists with the non-POU-domain-containing, octamer binding protein (p54nrb) and PTB-associated RNA splicing factor (PSF) initially characterized to be vital factors for pre-mRNA splicing but now have a novel function. They are currently associated with co-repression of steroid receptors. The consensus binding motifs (RVxF) of protein phosphatase 1 (PP1) was shared by p54nrb and PSF,

suggesting that PP1 may regulate phosphorylation state of both co-repressors and thus their role in gene transcription. In the same study, changes in transcriptional suppression of p54nrb and PSF were associated to changes in protein interactions between p54nrb or PSF and transcriptional corepressors like Sin3A and histone deacetylase 1 [356].

The posttranscriptional and posttranslational functions of NANOS2 are well documented and it is conceivable these mechanisms are employed in the regulation of DMRT1 expression (Figure 3; III-V). NANOS2 was found to localized in P-bodies in the cytoplasm of germ cell and are known as sites of RNA degradation and storage, since NANOS2 co-localized with DCP2 and XRN, two proteins expressed in P-bodies [314]. Components of the CCR4-NOT deadenylation complex were the major proteins identified in NANOS2 immunoprecipitations suggesting that members of these protein complex are *in vivo* interacting partners of NANOS2 [314]. Using the *in vitro* deadenylase assay system, it was shown that NANOS2-interacting deadenylase complex had catalytic activity based on the finding that cleavage of poly (A) RNA substrates occurred only in NANOS2 immunoprecipitates [300]. Since NANOS2 promotes the degradation of NANOS2-interacting mRNAs by recruiting the deadenylation complex, it is possible that same mechansism is employed to regulate the synthesis of DMRT1 in germ cells (Figure 3; III). Furthermore, the CCR4-NOT complex has been shown to have other functions including transcriptional, post-transcriptional RNA regulation and protein ubiquitylation [357, 358]. For example, CNOT1 interacts with nuclear receptors while CNOT3 is involved in chromatin remodeling, both of which are vital transcription regulatory mechanisms [359, 360]. These strongly predict by extrapolation a vital role for NANOS2 in modulating DMRT1's transcriptional activity. Moreover, CNOT4 has E3 ligase activity, putting the CCR4-NOT complex in the protein ubiquitylation/proteolytic cleavage pathways [361, 362]. Thus,

proteolytic cleavage can be utilized by NANOS2 for regulation of DMRT1 levels in undifferentiated spermatogonial stem cells (Figure 3; IV). Finally, phosphorylation provides a reversible modification by which NANOS2 can stabilize or destabilize the levels of DMRT1 in germ cells (Figure 3; V). This possibility is exemplified by the Cold-inducible RNA-binding protein (*Cirp*), which binds directly to a dual-specificity tyrosine-phosphorylation-regulated kinase 1B (*Dyrk1b* or *Mirk*) to inhibit its binding to cyclin-dependent kinase inhibitor 1B (*Cdkn1b or p27*) leading to reduced phosphorylation and destabilization of *Cdkn1b* [363].

Conclusion

A cellular model is provided on the functions of DMRT1 in Figure 4, which summarizes the findings in this project. The first and second sections of this chapter was focused on the characterization of a novel *Dmrt1*-deficient germ cell mouse model of male infertility, revealing key cell-specific processes regulated by DMRT1 in Sertoli cells. The cell-specific processes include maintenance of sperm progressive motility and testis size, differentiation of Sertoli cells, gene dosage dependency, maintenance of androgen levels and formation and organization of ES. In the third section, the differential expression of genes involved in ubiquitination, vesicular transport and piRNA pathways, which were top biological processed functions derived from manual analysis were examined. This addressed possible mechanisms for Sertoli cell-germ cell communication, regulation of Sertoli cell differentiation and germ cell development and survival. The last section highlights the shortage of research on the regulation of DMRT1 activity in germ cells and provides the first findings on a putative factor, NANOS2, which regulated DMRT1 transcriptional activity in germ cells. These studies have supplemented the existing knowledge and provided better understanding of the role of DMRT1 in postnatal testis differentiation, and thus fulfilled overall hypothesis and specific aims of this dissertation. However, the project raised many questions on the cell-specific function of DMRT1, which will require further investigation. For example, fertility experiments will be required to determine if overexpression of exogenous DMRT1 in *Dmrt1*$^{+/+}$

mice maintains a better testis milieu and sustains better sperm quality. Next, transplantation of germ cell explants into Sertoli cells of *Dmrt1*-rescue mice will determine the nurturing function of DMRT1-rescued Sertoli cells and validate the strength of the *Wt1* promoter. In addition, identification of downstream targets of VCL, binding partners or pathways involved will show a cytoskeletal assembly biological process directed by DMRT1 in Sertoli cells. Finally, more transient transfections, knockdown (RNAi), coimmunoprecipitation for NANOS2, DMRT1 and STRA8 will be invaluable in validating NANOS2 as a regulator of the transcriptional activity of DMRT1 in germ cells as well as confirming that DMRT1 activates the mitotic to meiotic transition in premeiotic germ cells.

Figure 1: Time course for the expression of Wt1 and Dmrt1 during mouse postnatal testis development. Dataset GSE926 contains published global gene expression profiles collected at P0 through P35 during postnatal mouse testis development. Expression of Wt1 is highest between P3 and P10, whereas *Dmrt1* levels are highest between P6 and P10. During this period of elevated expression for both transcripts, the level of *Dmrt1* is about two-fold higher than the levels of *Wt1*.

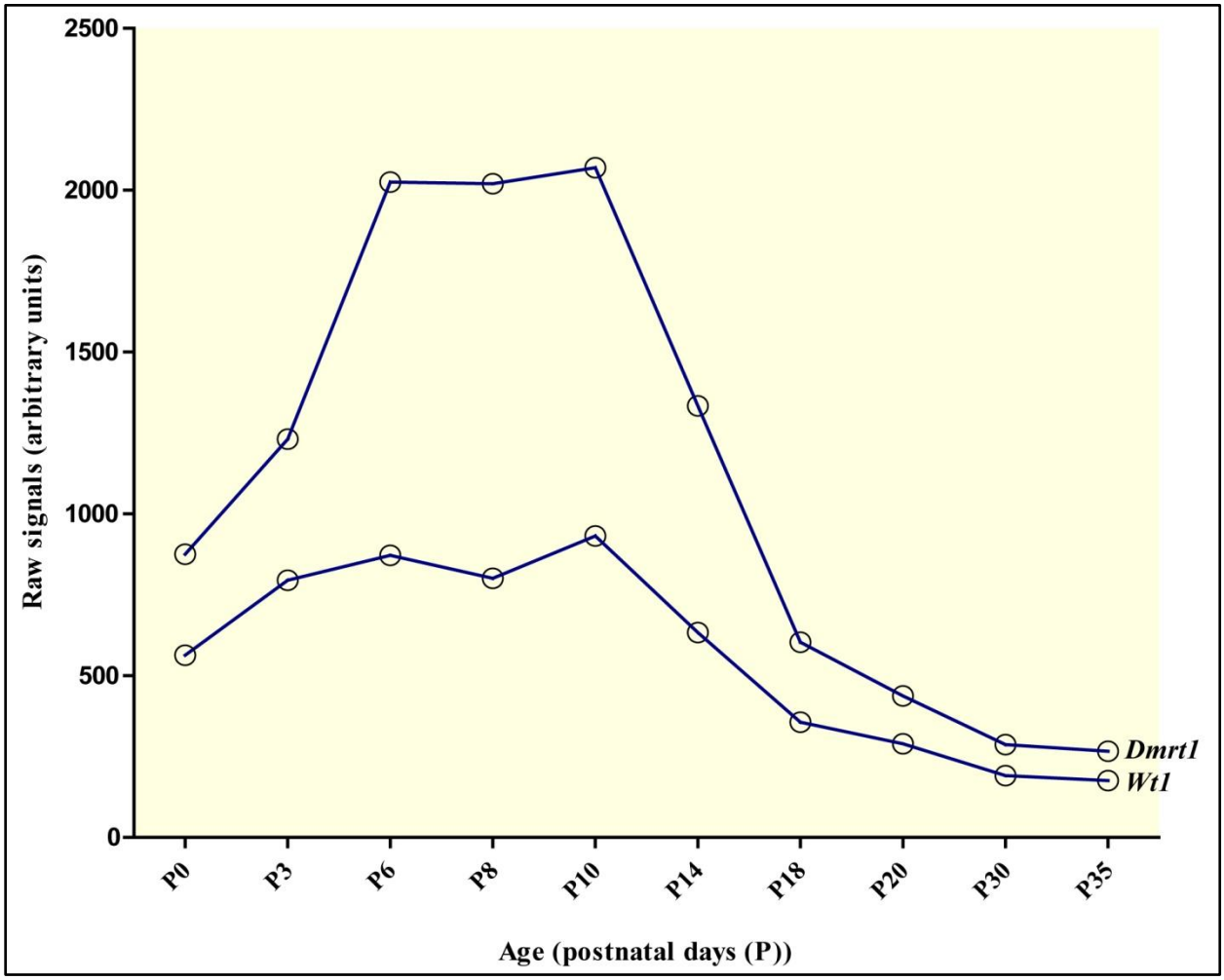

Figure 2: Gene expression of Stra8 and Dmrt1 andputative mechanism of DMRT1-activation of the mitotic to meiotic transition. A. Time course for the expression of *Stra8* and *Dmrt1* during mouse postnatal testis development. Dataset GSE926 contains published global gene expression profiles collected at P0 through P35 during postnatal mouse testis development. **B.** Putative mechanism of DMRT1 activation of the mitotic to meiotic transition of germ cells. NANOS2 regulate meiosis by suppressing DMRT1's expression.

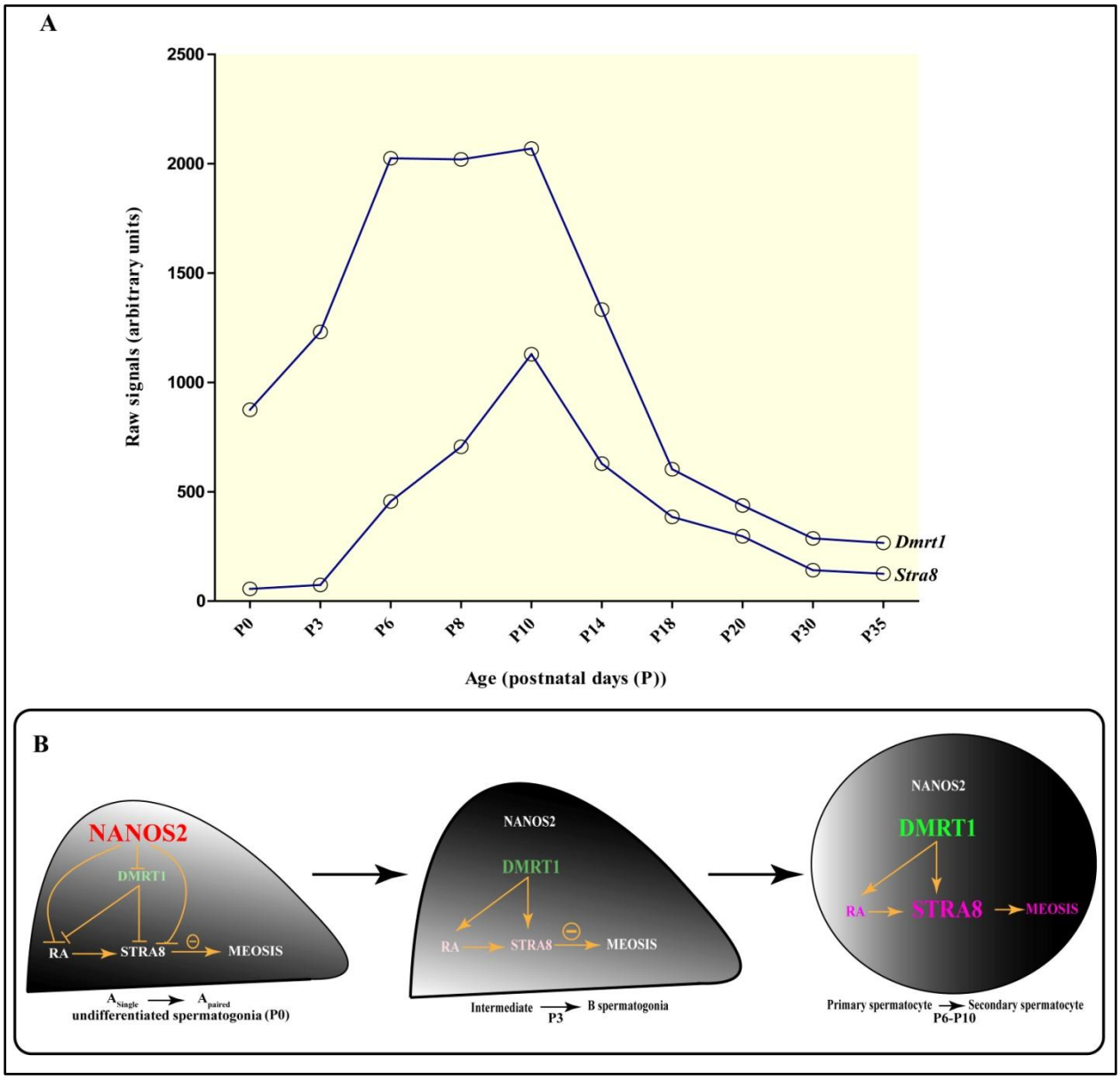

Figure 3: Model depicting potential mechanisms by which NANOS2 modulate the transcriptional activity of DMRT1 in germ cells. In the first situation (**I**), the translocated complex binds to the *Dmrt1*-response element placed in front of a constitutive SV40 promoter and may recruit a co-activator (**J**) and the general transcriptional machinery, which transcribes the gene. In the second situation (**II**), the NANOS2-DMRT1 complex instead recruits an unidentified co-repressor (**F**) to the TATA box minimal promoter region of Dmrt1, inhibits its transcription. In the third situation (III), NANOS2 bound to its unidentified mammalian binding partner (**Z**) and the CCR4-NOT deadenylation complex in the P-body, sequester posttranscriptionally modified *Dmrt1* mRNA in the cytoplasm, where it is degraded resulting in mRNA decay or mRNA is silenced, preventing translation and stored temporally in P-bodies. Finally, in **IV** and **V**, NANOS2 bound to DMRT1 in the cytoplasm can recruit an ubiquitin protein complex (**Y**; in **IV**) or a kinase (**Y**; in **V**) that mediates the ubiquitination or phosphorylation of DMRT1, leading to proteolytic cleavage or inactivation, respectively. **W** is a transcription factor like SOX9 known to regulate transcription of Nanos2, **J** = co-activators (NCOA2, NCOA4 and PPARGC1B) and **P** = phosphate moieties.

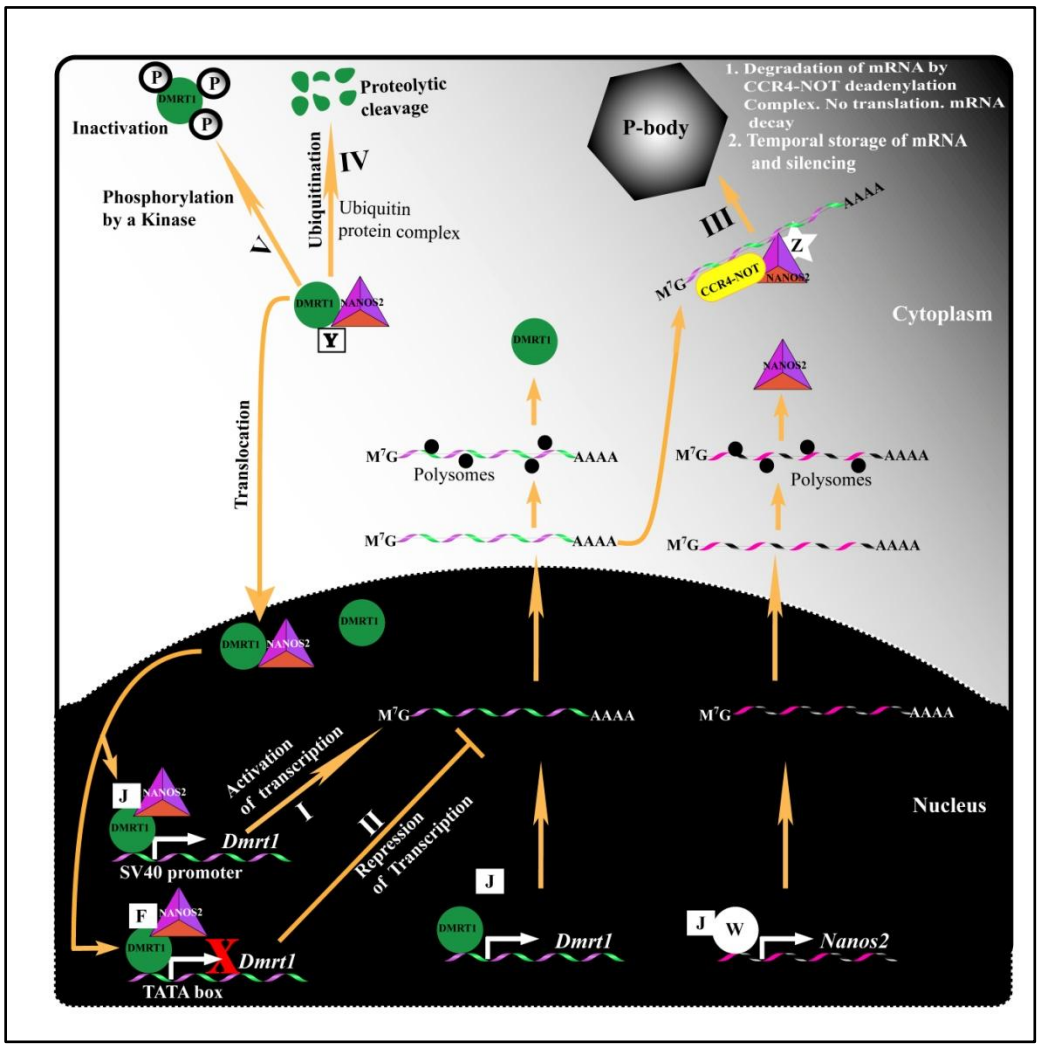

Figure 4: Integration model of DMRT1 activity. A cell model was generated showing predicted locations, subcellular fractions (denoted by shape) and associated functions (denoted by color) of the identified DMRT1 target genes (determined by proximity to confirmed DMRT1 binding sites). Some genes are represented multiple times, as they are located in different parts of the cell. The analysis identified unique functional correlations between target and regulated genes, indicated by the color scheme associated with targets (located in the cell) and the up- and down-regulated gene categories.

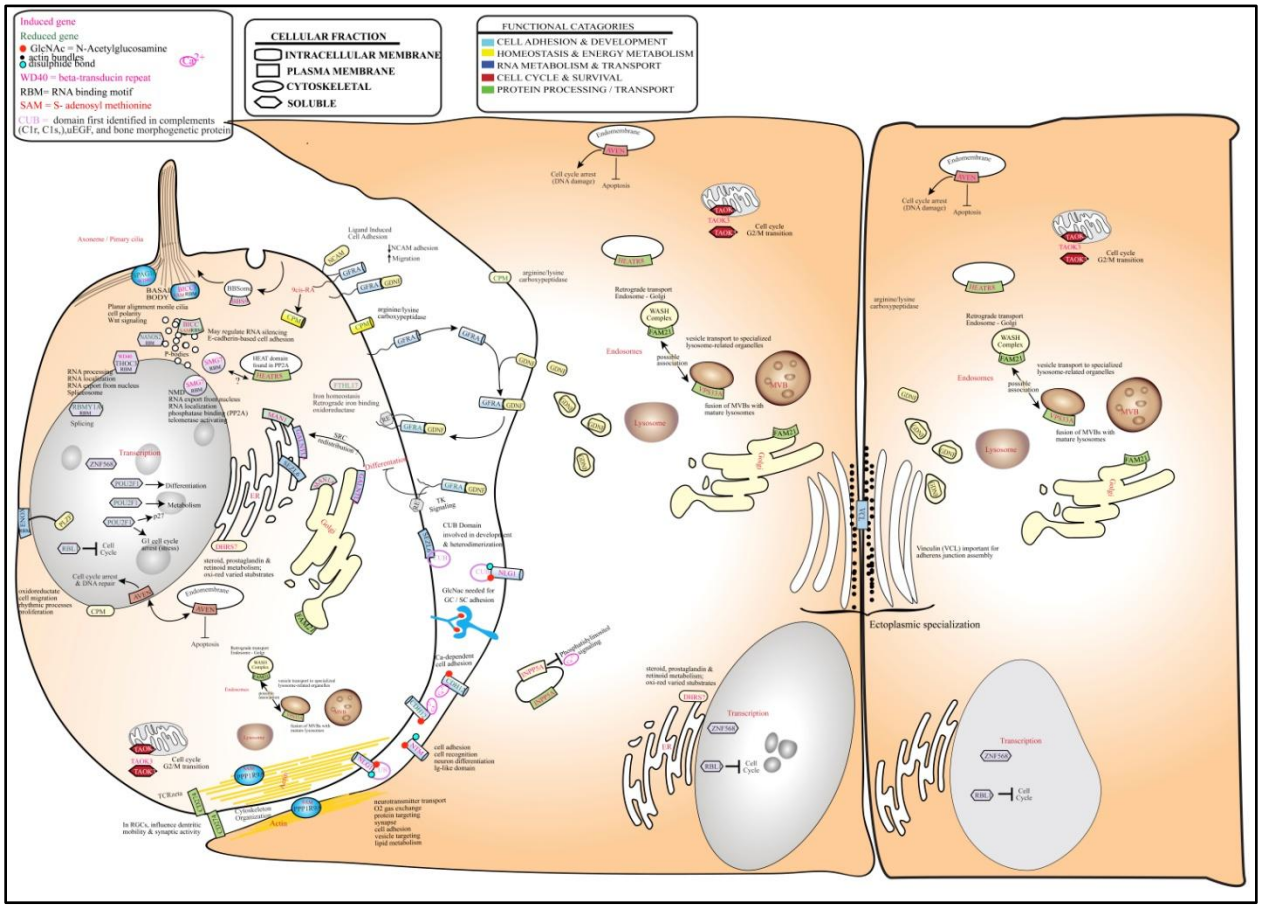

References

1. Bull JJ. Evolution of sex determining mechanisms. Menlo Park, Calif.: Benjamin/Cummings Pub. Co., Advanced Book Program; 1983.
2. Capel B. Sex in the 90s: SRY and the switch to the male pathway. Annu Rev Physiol 1998; 60:497-523.
3. Smith CA, Sinclair AH. Sex determination: insights from the chicken. Bioessays 2004; 26:120-132.
4. Pieau C, Girondot M, Richardmercier N, Desvages G, Dorizzi M, Zaborski P. Temperature Sensitivity of Sexual-Differentiation of Gonads in the European Pond Turtle - Hormonal Involvement. Journal of Experimental Zoology 1994; 270:86-94.
5. Gamble T, Zarkower D. Sex determination. Curr Biol 2012; 22:R257-262.
6. Angelopoulou R, Lavranos G, Manolakou P. Sex determination strategies in 2012: towards a common regulatory model? Reprod Biol Endocrinol 2012; 10:13.
7. Parisi M, Nuttall R, Edwards P, Minor J, Naiman D, Lu J, Doctolero M, Vainer M, Chan C, Malley J, Eastman S, Oliver B. A survey of ovary-, testis-, and soma-biased gene expression in Drosophila melanogaster adults. Genome Biol 2004; 5:R40.
8. Nanda I, Shan ZH, Schartl M, Burt DW, Koehler M, Nothwang HG, Grutzner F, Paton IR, Windsor D, Dunn I, Engel W, Staeheli P, et al. 300 million years of conserved synteny between chicken Z and human chromosome 9. Nature Genetics 1999; 21:258-259.
9. Chue J, Smith CA. Sex determination and sexual differentiation in the avian model. FEBS J 2011; 278:1027-1034.
10. Nordqvist K, Lovellbadge R. Setbacks on the Road to Sexual Fulfillment. Nature Genetics 1994; 7:7-9.
11. Gubbay J, Collignon J, Koopman P, Capel B, Economou A, Munsterberg A, Vivian N, Goodfellow P, Lovell-Badge R. A gene mapping to the sex-determining region of the mouse Y chromosome is a member of a novel family of embryonically expressed genes. Nature 1990; 346:245-250.
12. Koopman P, Munsterberg A, Capel B, Vivian N, Lovell-Badge R. Expression of a candidate sex-determining gene during mouse testis differentiation. Nature 1990; 348:450-452.
13. Sinclair AH, Berta P, Palmer MS, Hawkins JR, Griffiths BL, Smith MJ, Foster JW, Frischauf AM, Lovell-Badge R, Goodfellow PN. A gene from the human sex-determining region encodes a protein with homology to a conserved DNA-binding motif. Nature 1990; 346:240-244.
14. Koopman P, Gubbay J, Vivian N, Goodfellow P, Lovell-Badge R. Male development of chromosomally female mice transgenic for Sry. Nature 1991; 351:117-121.
15. Jeays-Ward K, Hoyle C, Brennan J, Dandonneau M, Alldus G, Capel B, Swain A. Endothelial and steroidogenic cell migration are regulated by WNT4 in the developing mammalian gonad. Development 2003; 130:3663-3670.
16. Nef S, Verma-Kurvari S, Merenmies J, Vassalli JD, Efstratiadis A, Accili D, Parada LF. Testis determination requires insulin receptor family function in mice. Nature 2003; 426:291-295.
17. Schmahl J, Kim Y, Colvin JS, Ornitz DM, Capel B. Fgf9 induces proliferation and nuclear localization of FGFR2 in Sertoli precursors during male sex determination. Development 2004; 131:3627-3636.
18. Capel B. The battle of the sexes. Mech Dev 2000; 92:89-103.
19. Grinspon RP, Rey RA. Anti-mullerian hormone and sertoli cell function in paediatric male hypogonadism. Horm Res Paediatr 2010; 73:81-92.
20. McLaren A. Germ and somatic cell lineages in the developing gonad. Mol Cell Endocrinol 2000; 163:3-9.

21. McCarrey JR, Abbott UK. Mechanisms of genetic sex determination, gonadal sex differentiation, and germ-cell development in animals. Adv Genet 1979; 20:217-290.
22. Kaufman MH, Bard JBL. The anatomical basis of mouse development. San Diego: Academic Press; 1999: pp.109-128.
23. McLaren A. Development of the mammalian gonad: the fate of the supporting cell lineage. Bioessays 1991; 13:151-156.
24. Albrecht KH, Eicher EM. Evidence that Sry is expressed in pre-Sertoli cells and Sertoli and granulosa cells have a common precursor. Dev Biol 2001; 240:92-107.
25. McLaren A. The fate of germ cells in the testis of fetal Sex-reversed mice. J Reprod Fertil 1981; 61:461-467.
26. Yao HH, DiNapoli L, Capel B. Meiotic germ cells antagonize mesonephric cell migration and testis cord formation in mouse gonads. Development 2003; 130:5895-5902.
27. Burgoyne PS, Buehr M, Koopman P, Rossant J, McLaren A. Cell-autonomous action of the testis-determining gene: Sertoli cells are exclusively XY in XX----XY chimaeric mouse testes. Development 1988; 102:443-450.
28. McLaren A. Sexual differentiation. Of MIS and the mouse. Nature 1990; 345:111.
29. Merchant H. Rat gonadal and ovarioan organogenesis with and without germ cells. An ultrastructural study. Dev Biol 1975; 44:1-21.
30. Merchant-Larios H, Centeno B. Morphogenesis of the ovary from the sterile W/Wv mouse. Prog Clin Biol Res 1981; 59B:383-392.
31. Palmer SJ, Burgoyne PS. In situ analysis of fetal, prepuberal and adult XX----XY chimaeric mouse testes: Sertoli cells are predominantly, but not exclusively, XY. Development 1991; 112:265-268.
32. Kreidberg JA, Sariola H, Loring JM, Maeda M, Pelletier J, Housman D, Jaenisch R. WT-1 is required for early kidney development. Cell 1993; 74:679-691.
33. Luo X, Ikeda Y, Parker KL. A cell-specific nuclear receptor is essential for adrenal and gonadal development and sexual differentiation. Cell 1994; 77:481-490.
34. Shawlot W, Behringer RR. Requirement for Lim1 in head-organizer function. Nature 1995; 374:425-430.
35. Tsang TE, Shawlot W, Kinder SJ, Kobayashi A, Kwan KM, Schughart K, Kania A, Jessell TM, Behringer RR, Tam PP. Lim1 activity is required for intermediate mesoderm differentiation in the mouse embryo. Dev Biol 2000; 223:77-90.
36. Miyamoto N, Yoshida M, Kuratani S, Matsuo I, Aizawa S. Defects of urogenital development in mice lacking Emx2. Development 1997; 124:1653-1664.
37. Birk OS, Casiano DE, Wassif CA, Cogliati T, Zhao L, Zhao Y, Grinberg A, Huang S, Kreidberg JA, Parker KL, Porter FD, Westphal H. The LIM homeobox gene Lhx9 is essential for mouse gonad formation. Nature 2000; 403:909-913.
38. Chaboissier MC, Kobayashi A, Vidal VI, Lutzkendorf S, van de Kant HJ, Wegner M, de Rooij DG, Behringer RR, Schedl A. Functional analysis of Sox8 and Sox9 during sex determination in the mouse. Development 2004; 131:1891-1901.
39. Vidal VP, Chaboissier MC, de Rooij DG, Schedl A. Sox9 induces testis development in XX transgenic mice. Nat Genet 2001; 28:216-217.
40. Swain A, Lovell-Badge R. Mammalian sex determination: a molecular drama. Genes Dev 1999; 13:755-767.
41. Skinner MK, Tung PS, Fritz IB. Cooperativity between Sertoli cells and testicular peritubular cells in the production and deposition of extracellular matrix components. J Cell Biol 1985; 100:1941-1947.
42. Byskov AG. Differentiation of mammalian embryonic gonad. Physiol Rev 1986; 66:71-117.
43. McLaren A. Primordial germ cells in the mouse. Dev Biol 2003; 262:1-15.

44. McLaren A, Southee D. Entry of mouse embryonic germ cells into meiosis. Dev Biol 1997; 187:107-113.
45. Arango NA, Lovell-Badge R, Behringer RR. Targeted mutagenesis of the endogenous mouse Mis gene promoter: in vivo definition of genetic pathways of vertebrate sexual development. Cell 1999; 99:409-419.
46. Jeays-Ward K, Dandonneau M, Swain A. Wnt4 is required for proper male as well as female sexual development. Dev Biol 2004; 276:431-440.
47. Meeks JJ, Crawford SE, Russell TA, Morohashi K, Weiss J, Jameson JL. Dax1 regulates testis cord organization during gonadal differentiation. Development 2003; 130:1029-1036.
48. Meeks JJ, Weiss J, Jameson JL. Dax1 is required for testis determination. Nature Genetics 2003; 34:32-33.
49. Nachtigal MW, Hirokawa Y, Enyeart-VanHouten DL, Flanagan JN, Hammer GD, Ingraham HA. Wilms' tumor 1 and Dax-1 modulate the orphan nuclear receptor SF-1 in sex-specific gene expression. Cell 1998; 93:445-454.
50. Raymond CS, Murphy MW, O'Sullivan MG, Bardwell VJ, Zarkower D. Dmrt1, a gene related to worm and fly sexual regulators, is required for mammalian testis differentiation. Genes Dev 2000; 14:2587-2595.
51. Shen WH, Moore CC, Ikeda Y, Parker KL, Ingraham HA. Nuclear receptor steroidogenic factor 1 regulates the mullerian inhibiting substance gene: a link to the sex determination cascade. Cell 1994; 77:651-661.
52. Peters H. Migration of gonocytes into the mammalian gonad and their differentiation. Philos Trans R Soc Lond B Biol Sci 1970; 259:91-101.
53. Buehr M, Gu S, McLaren A. Mesonephric contribution to testis differentiation in the fetal mouse. Development 1993; 117:273-281.
54. Koubova J, Menke DB, Zhou Q, Capel B, Griswold MD, Page DC. Retinoic acid regulates sex-specific timing of meiotic initiation in mice. Proc Natl Acad Sci U S A 2006; 103:2474-2479.
55. Bowles J, Knight D, Smith C, Wilhelm D, Richman J, Mamiya S, Yashiro K, Chawengsaksophak K, Wilson MJ, Rossant J, Hamada H, Koopman P. Retinoid signaling determines germ cell fate in mice. Science 2006; 312:596-600.
56. Bowles J, Koopman P. Retinoic acid, meiosis and germ cell fate in mammals. Development 2007; 134:3401-3411.
57. de Sousa Lopes SM, Roelen BA, Monteiro RM, Emmens R, Lin HY, Li E, Lawson KA, Mummery CL. BMP signaling mediated by ALK2 in the visceral endoderm is necessary for the generation of primordial germ cells in the mouse embryo. Genes Dev 2004; 18:1838-1849.
58. Lawson KA, Dunn NR, Roelen BA, Zeinstra LM, Davis AM, Wright CV, Korving JP, Hogan BL. Bmp4 is required for the generation of primordial germ cells in the mouse embryo. Genes Dev 1999; 13:424-436.
59. Ying Y, Liu XM, Marble A, Lawson KA, Zhao GQ. Requirement of Bmp8b for the generation of primordial germ cells in the mouse. Mol Endocrinol 2000; 14:1053-1063.
60. Ying Y, Qi XX, Zhao GQ. Induction of primordial germ cells from murine epiblasts by synergistic action of BMP4 and BMP8B signaling pathways. Proceedings of the National Academy of Sciences of the United States of America 2001; 98:7858-7862.
61. Ying Y, Zhao GQ. Cooperation of endoderm-derived BMP2 and extraembryonic ectoderm-derived BMP4 in primordial germ cell generation in the mouse. Dev Biol 2001; 232:484-492.
62. Ohinata Y, Ohta H, Shigeta M, Yamanaka K, Wakayama T, Saitou M. A signaling principle for the specification of the germ cell lineage in mice. Cell 2009; 137:571-584.
63. Lange UC, Adams DJ, Lee C, Barton S, Schneider R, Bradley A, Surani MA. Normal germ line establishment in mice carrying a deletion of the Ifitm/Fragilis gene family cluster. Mol Cell Biol 2008; 28:4688-4696.

64. Saitou M, Barton SC, Surani MA. A molecular programme for the specification of germ cell fate in mice. Nature 2002; 418:293-300.
65. Ohinata Y, Payer B, O'Carroll D, Ancelin K, Ono Y, Sano M, Barton SC, Obukhanych T, Nussenzweig M, Tarakhovsky A, Saitou M, Surani MA. Blimp1 is a critical determinant of the germ cell lineage in mice. Nature 2005; 436:207-213.
66. Saitou M, Payer B, O'Carroll D, Ohinata Y, Surani MA. Blimp1 and the emergence of the germ line during development in the mouse. Cell Cycle 2005; 4:1736-1740.
67. Bortvin A, Goodheart M, Liao M, Page DC. Dppa3 / Pgc7 / stella is a maternal factor and is not required for germ cell specification in mice. BMC Dev Biol 2004; 4:2.
68. MacGregor GR, Zambrowicz BP, Soriano P. Tissue non-specific alkaline phosphatase is expressed in both embryonic and extraembryonic lineages during mouse embryogenesis but is not required for migration of primordial germ cells. Development 1995; 121:1487-1496.
69. West JA, Viswanathan SR, Yabuuchi A, Cunniff K, Takeuchi A, Park IH, Sero JE, Zhu H, Perez-Atayde A, Frazier AL, Surani MA, Daley GQ. A role for Lin28 in primordial germ-cell development and germ-cell malignancy. Nature 2009; 460:909-913.
70. Yamaji M, Seki Y, Kurimoto K, Yabuta Y, Yuasa M, Shigeta M, Yamanaka K, Ohinata Y, Saitou M. Critical function of Prdm14 for the establishment of the germ cell lineage in mice. Nature Genetics 2008; 40:1016-1022.
71. Ancelin K, Lange UC, Hajkova P, Schneider R, Bannister AJ, Kouzarides T, Surani MA. Blimp1 associates with Prmt5 and directs histone arginine methylation in mouse germ cells. Nat Cell Biol 2006; 8:623-630.
72. Ginsburg M, Snow MH, McLaren A. Primordial germ cells in the mouse embryo during gastrulation. Development 1990; 110:521-528.
73. Scholer HR, Dressler GR, Balling R, Rohdewohld H, Gruss P. Oct-4: a germline-specific transcription factor mapping to the mouse t-complex. EMBO J 1990; 9:2185-2195.
74. Lawson KA, Hage WJ. Clonal analysis of the origin of primordial germ cells in the mouse. Ciba Found Symp 1994; 182:68-84; discussion 84-91.
75. McLaren A. Gonad development: assembling the mammalian testis. Curr Biol 1998; 8:R175-177.
76. McLaren A. Development of primordial germ cells in the mouse. Andrologia 1992; 24:243-247.
77. Seki Y, Yamaji M, Yabuta Y, Sano M, Shigeta M, Matsui Y, Saga Y, Tachibana M, Shinkai Y, Saitou M. Cellular dynamics associated with the genome-wide epigenetic reprogramming in migrating primordial germ cells in mice. Development 2007; 134:2627-2638.
78. Tam PP, Snow MH. Proliferation and migration of primordial germ cells during compensatory growth in mouse embryos. J Embryol Exp Morphol 1981; 64:133-147.
79. Burlacu A. Regulation of apoptosis by Bcl-2 family proteins. J Cell Mol Med 2003; 7:249-257.
80. Donovan PJ. Growth factor regulation of mouse primordial germ cell development. Curr Top Dev Biol 1994; 29:189-225.
81. Elmore S. Apoptosis: a review of programmed cell death. Toxicol Pathol 2007; 35:495-516.
82. Matsui Y, Toksoz D, Nishikawa S, Williams D, Zsebo K, Hogan BL. Effect of Steel factor and leukaemia inhibitory factor on murine primordial germ cells in culture. Nature 1991; 353:750-752.
83. Suzuki H, Tsuda M, Kiso M, Saga Y. Nanos3 maintains the germ cell lineage in the mouse by suppressing both Bax-dependent and -independent apoptotic pathways. Dev Biol 2008; 318:133-142.
84. Youngren KK, Coveney D, Peng X, Bhattacharya C, Schmidt LS, Nickerson ML, Lamb BT, Deng JM, Behringer RR, Capel B, Rubin EM, Nadeau JH, et al. The Ter mutation in the dead end gene causes germ cell loss and testicular germ cell tumours. Nature 2005; 435:360-364.
85. Bremner WJ, Millar MR, Sharpe RM, Saunders PT. Immunohistochemical localization of androgen receptors in the rat testis: evidence for stage-dependent expression and regulation by androgens. Endocrinology 1994; 135:1227-1234.

86. Sharpe RM, McKinnell C, Kivlin C, Fisher JS. Proliferation and functional maturation of Sertoli cells, and their relevance to disorders of testis function in adulthood. Reproduction 2003; 125:769-784.
87. Tan KA, De Gendt K, Atanassova N, Walker M, Sharpe RM, Saunders PT, Denolet E, Verhoeven G. The role of androgens in sertoli cell proliferation and functional maturation: studies in mice with total or Sertoli cell-selective ablation of the androgen receptor. Endocrinology 2005; 146:2674-2683.
88. Orth JM, Gunsalus GL, Lamperti AA. Evidence from Sertoli cell-depleted rats indicates that spermatid number in adults depends on numbers of Sertoli cells produced during perinatal development. Endocrinology 1988; 122:787-794.
89. Sharpe RM, Millar M, McKinnell C. Relative roles of testosterone and the germ cell complement in determining stage-dependent changes in protein secretion by isolated rat seminiferous tubules. Int J Androl 1993; 16:71-81.
90. Orth JM. Proliferation of Sertoli cells in fetal and postnatal rats: a quantitative autoradiographic study. Anat Rec 1982; 203:485-492.
91. Kluin PM, Kramer MF, de Rooij DG. Proliferation of spermatogonia and Sertoli cells in maturing mice. Anat Embryol (Berl) 1984; 169:73-78.
92. Guitton N, Touzalin AM, Sharpe RM, Cheng CY, Pinon-Lataillade G, Meritte H, Chenal C, Jegou B. Regulatory influence of germ cells on sertoli cell function in the pre-pubertal rat after acute irradiation of the testis. Int J Androl 2000; 23:332-339.
93. Steger K, Rey R, Kliesch S, Louis F, Schleicher G, Bergmann M. Immunohistochemical detection of immature Sertoli cell markers in testicular tissue of infertile adult men: a preliminary study. Int J Androl 1996; 19:122-128.
94. Steger K, Rey R, Louis F, Kliesch S, Behre HM, Nieschlag E, Hoepffner W, Bailey D, Marks A, Bergmann M. Reversion of the differentiated phenotype and maturation block in Sertoli cells in pathological human testis. Hum Reprod 1999; 14:136-143.
95. Brehm R, Marks A, Rey R, Kliesch S, Bergmann M, Steger K. Altered expression of connexins 26 and 43 in Sertoli cells in seminiferous tubules infiltrated with carcinoma-in-situ or seminoma. J Pathol 2002; 197:647-653.
96. Brehm R, Steger K. Regulation of Sertoli cell and germ cell differentation. Adv Anat Embryol Cell Biol 2005; 181:1-93.
97. Kliesch S, Behre HM, Hertle L, Bergmann M. Alteration of Sertoli cell differentiation in the presence of carcinoma in situ in human testes. J Urol 1998; 160:1894-1898.
98. Means AR, Fakunding JL, Huckins C, Tindall DJ, Vitale R. Follicle-stimulating hormone, the Sertoli cell, and spermatogenesis. Recent Progress in Hormone Research, Vol 48 1976; 32:477-527.
99. Clermont Y, Perey B. Quantitative study of the cell population of the seminiferous tubules in immature rats. Am J Anat 1957; 100:241-267.
100. Huckins C, Clermont Y. Evolution of gonocytes in the rat testis during late embryonic and early post-natal life. Arch Anat Histol Embryol 1968; 51:341-354.
101. Hilscher B, Hilscher W, Bulthoff-Ohnolz B, Kramer U, Birke A, Pelzer H, Gauss G. Kinetics of gametogenesis. I. Comparative histological and autoradiographic studies of oocytes and transitional prospermatogonia during oogenesis and prespermatogenesis. Cell Tissue Res 1974; 154:443-470.
102. Bellve AR, Cavicchia JC, Millette CF, O'Brien DA, Bhatnagar YM, Dym M. Spermatogenic cells of the prepuberal mouse. Isolation and morphological characterization. J Cell Biol 1977; 74:68-85.
103. Roosenru.Ec, Leik J. Gonocyte Degeneration in Postnatal Male Rat. American Journal of Anatomy 1968; 122:275-&.
104. de Rooij DG. Stem cells in the testis. Int J Exp Pathol 1998; 79:67-80.

105. Sada A, Hasegawa K, Pin PH, Saga Y. NANOS2 Acts Downstream of GDNF Signaling to Suppress Differentiation of Spermatogonial Stem Cells. Stem Cells 2011.
106. Saga Y. Function of Nanos2 in the male germ cell lineage in mice. Cell Mol Life Sci 2010; 67:3815-3822.
107. Sada A, Suzuki A, Suzuki H, Saga Y. The RNA-binding protein NANOS2 is required to maintain murine spermatogonial stem cells. Science 2009; 325:1394-1398.
108. de Rooij DG, Russell LD. All you wanted to know about spermatogonia but were afraid to ask. J Androl 2000; 21:776-798.
109. Nakagawa T, Sharma M, Nabeshima Y, Braun RE, Yoshida S. Functional hierarchy and reversibility within the murine spermatogenic stem cell compartment. Science 2010; 328:62-67.
110. Yoshida S, Sukeno M, Nakagawa T, Ohbo K, Nagamatsu G, Suda T, Nabeshima Y. The first round of mouse spermatogenesis is a distinctive program that lacks the self-renewing spermatogonia stage. Development 2006; 133:1495-1505.
111. Shen MM, Hodgkin J. mab-3, a gene required for sex-specific yolk protein expression and a male-specific lineage in C. elegans. Cell 1988; 54:1019-1031.
112. Raymond CS, Shamu CE, Shen MM, Seifert KJ, Hirsch B, Hodgkin J, Zarkower D. Evidence for evolutionary conservation of sex-determining genes. Nature 1998; 391:691-695.
113. Erdman SE, Burtis KC. The Drosophila doublesex proteins share a novel zinc finger related DNA binding domain. EMBO J 1993; 12:527-535.
114. Zhu L, Wilken J, Phillips NB, Narendra U, Chan G, Stratton SM, Kent SB, Weiss MA. Sexual dimorphism in diverse metazoans is regulated by a novel class of intertwined zinc fingers. Genes Dev 2000; 14:1750-1764.
115. De Grandi A, Calvari V, Bertini V, Bulfone A, Peverali G, Camerino G, Borsani G, Guioli S. The expression pattern of a mouse doublesex-related gene is consistent with a role in gonadal differentiation. Mech Dev 2000; 90:323-326.
116. Calvari V, Bertini V, De Grandi A, Peverali G, Zuffardi O, Ferguson-Smith M, Knudtzon J, Camerino G, Borsani G, Guioli S. A new submicroscopic deletion that refines the 9p region for sex reversal. Genomics 2000; 65:203-212.
117. Ottolenghi C, Veitia R, Barbieri M, Fellous M, McElreavey K. The human doublesex-related gene, DMRT2, is homologous to a gene involved in somitogenesis and encodes a potential bicistronic transcript. Genomics 2000; 64:179-186.
118. Veyrunes F, Waters PD, Miethke P, Rens W, McMillan D, Alsop AE, Grutzner F, Deakin JE, Whittington CM, Schatzkamer K, Kremitzki CL, Graves T, et al. Bird-like sex chromosomes of platypus imply recent origin of mammal sex chromosomes. Genome Res 2008; 18:965-973.
119. Raymond CS, Parker ED, Kettlewell JR, Brown LG, Page DC, Kusz K, Jaruzelska J, Reinberg Y, Flejter WL, Bardwell VJ, Hirsch B, Zarkower D. A region of human chromosome 9p required for testis development contains two genes related to known sexual regulators. Hum Mol Genet 1999; 8:989-996.
120. Garcia-Heras J, Corley N, Garcia MF, Kukolich MK, Smith KG, Day DW. De novo partial duplications 1p: report of two new cases and review. Am J Med Genet 1999; 82:261-264.
121. Simpson JL, Rajkovic A. Ovarian differentiation and gonadal failure. Am J Med Genet 1999; 89:186-200.
122. Bennett CP, Docherty Z, Robb SA, Ramani P, Hawkins JR, Grant D. Deletion 9p and sex reversal. J Med Genet 1993; 30:518-520.
123. Wilkie AO, Campbell FM, Daubeney P, Grant DB, Daniels RJ, Mullarkey M, Affara NA, Fitchett M, Huson SM. Complete and partial XY sex reversal associated with terminal deletion of 10q: report of 2 cases and literature review. Am J Med Genet 1993; 46:597-600.
124. Guioli S, Schmitt K, Critcher R, Bouzyk M, Spurr NK, Ogata T, Hoo JJ, Pinsky L, Gimelli G, Pasztor L, Goodfellow PN. Molecular analysis of 9p deletions associated with XY sex reversal:

refining the localization of a sex-determining gene to the tip of the chromosome. Am J Hum Genet 1998; 63:905-908.
125. Veitia RA, Nunes M, Quintana-Murci L, Rappaport R, Thibaud E, Jaubert F, Fellous M, McElreavey K, Goncalves J, Silva M, Rodrigues JC, Caspurro M, et al. Swyer syndrome and 46,XY partial gonadal dysgenesis associated with 9p deletions in the absence of monosomy-9p syndrome. Am J Hum Genet 1998; 63:901-905.
126. Veitia R, Nunes M, Brauner R, Doco-Fenzy M, Joanny-Flinois O, Jaubert F, Lortat-Jacob S, Fellous M, McElreavey K. Deletions of distal 9p associated with 46,XY male to female sex reversal: definition of the breakpoints at 9p23.3-p24.1. Genomics 1997; 41:271-274.
127. Flejter WL, Fergestad J, Gorski J, Varvill T, Chandrasekharappa S. A gene involved in XY sex reversal is located on chromosome 9, distal to marker D9S1779. Am J Hum Genet 1998; 63:794-802.
128. Moniot B, Berta P, Scherer G, Sudbeck P, Poulat F. Male specific expression suggests role of DMRT1 in human sex determination. Mech Dev 2000; 91:323-325.
129. Brunner B, Hornung U, Shan Z, Nanda I, Kondo M, Zend-Ajusch E, Haaf T, Ropers HH, Shima A, Schmid M, Kalscheuer VM, Schartl M. Genomic organization and expression of the doublesex-related gene cluster in vertebrates and detection of putative regulatory regions for DMRT1. Genomics 2001; 77:8-17.
130. Lei N, Hornbaker KI, Rice DA, Karpova T, Agbor VA, Heckert LL. Sex-specific differences in mouse DMRT1 expression are both cell type- and stage-dependent during gonad development. Biol Reprod 2007; 77:466-475.
131. Kim S, Bardwell VJ, Zarkower D. Cell type-autonomous and non-autonomous requirements for Dmrt1 in postnatal testis differentiation. Dev Biol 2007; 307:314-327.
132. Fahrioglu U, Murphy MW, Zarkower D, Bardwell VJ. mRNA expression analysis and the molecular basis of neonatal testis defects in Dmrt1 mutant mice. Sex Dev 2007; 1:42-58.
133. Krentz AD, Murphy MW, Kim S, Cook MS, Capel B, Zhu R, Matin A, Sarver AL, Parker KL, Griswold MD, Looijenga LH, Bardwell VJ, et al. The DM domain protein DMRT1 is a dose-sensitive regulator of fetal germ cell proliferation and pluripotency. Proc Natl Acad Sci U S A 2009; 106:22323-22328.
134. Matson CK, Murphy MW, Griswold MD, Yoshida S, Bardwell VJ, Zarkower D. The mammalian doublesex homolog DMRT1 is a transcriptional gatekeeper that controls the mitosis versus meiosis decision in male germ cells. Dev Cell 2010; 19:612-624.
135. Matson CK, Murphy MW, Sarver AL, Griswold MD, Bardwell VJ, Zarkower D. DMRT1 prevents female reprogramming in the postnatal mammalian testis. Nature 2011; 476:101-104.
136. Murphy MW, Sarver AL, Rice D, Hatzi K, Ye K, Melnick A, Heckert LL, Zarkower D, Bardwell VJ. Genome-wide analysis of DNA binding and transcriptional regulation by the mammalian Doublesex homolog DMRT1 in the juvenile testis. Proc Natl Acad Sci U S A 2010; 107:13360-13365.
137. Krentz AD, Murphy MW, Sarver AL, Griswold MD, Bardwell VJ, Zarkower D. DMRT1 promotes oogenesis by transcriptional activation of Stra8 in the mammalian fetal ovary. Dev Biol 2011.
138. Lei N, Heckert LL. Sp1 and Egr1 regulate transcription of the Dmrt1 gene in Sertoli cells. Biol Reprod 2002; 66:675-684.
139. Lei N, Heckert LL. Gata4 regulates testis expression of Dmrt1. Mol Cell Biol 2004; 24:377-388.
140. Lei N, Karpova T, Hornbaker KI, Rice DA, Heckert LL. Distinct transcriptional mechanisms direct expression of the rat Dmrt1 promoter in sertoli cells and germ cells of transgenic mice. Biol Reprod 2009; 81:118-125.
141. Raymond CS, Kettlewell JR, Hirsch B, Bardwell VJ, Zarkower D. Expression of Dmrt1 in the genital ridge of mouse and chicken embryos suggests a role in vertebrate sexual development. Dev Biol 1999; 215:208-220.

142. Brugh VM, 3rd, Lipshultz LI. Male factor infertility: evaluation and management. Med Clin North Am 2004; 88:367-385.
143. Matzuk MM, Lamb DJ. The biology of infertility: research advances and clinical challenges. Nat Med 2008; 14:1197-1213.
144. Ferguson-Smith M. The evolution of sex chromosomes and sex determination in vertebrates and the key role of DMRT1. Sex Dev 2007; 1:2-11.
145. Marchand O, Govoroun M, D'Cotta H, McMeel O, Lareyre J, Bernot A, Laudet V, Guiguen Y. DMRT1 expression during gonadal differentiation and spermatogenesis in the rainbow trout, Oncorhynchus mykiss. Biochim Biophys Acta 2000; 1493:180-187.
146. Volff JN, Zarkower D, Bardwell VJ, Schartl M. Evolutionary dynamics of the DM domain gene family in metazoans. J Mol Evol 2003; 57 Suppl 1:S241-249.
147. Bratus A, Slota E. DMRT1/Dmrt1, the sex determining or sex differentiating gene in Vertebrata. Folia Biol (Krakow) 2006; 54:81-86.
148. Nagahama Y. Molecular mechanisms of sex determination and gonadal sex differentiation in fish. Fish Physiol Biochem 2005; 31:105-109.
149. Sinclair A, Smith C, Western P, McClive P. A comparative analysis of vertebrate sex determination. Novartis Found Symp 2002; 244:102-111; discussion 111-104, 203-106, 253-107.
150. Smith CA, McClive PJ, Western PS, Reed KJ, Sinclair AH. Conservation of a sex-determining gene. Nature 1999; 402:601-602.
151. Boyer A, Dornan S, Daneau I, Lussier J, Silversides DW. Conservation of the function of DMRT1 regulatory sequences in mammalian sex differentiation. Genesis 2002; 34:236-243.
152. Hong CS, Park BY, Saint-Jeannet JP. The function of Dmrt genes in vertebrate development: it is not just about sex. Dev Biol 2007; 310:1-9.
153. Lints R, Emmons SW. Regulation of sex-specific differentiation and mating behavior in C. elegans by a new member of the DM domain transcription factor family. Genes Dev 2002; 16:2390-2402.
154. Zhang W, Li B, Singh R, Narendra U, Zhu L, Weiss MA. Regulation of sexual dimorphism: mutational and chemogenetic analysis of the doublesex DM domain. Mol Cell Biol 2006; 26:535-547.
155. Herpin A, Schartl M. Molecular mechanisms of sex determination and evolution of the Y-chromosome: insights from the medakafish (Oryzias latipes). Mol Cell Endocrinol 2009; 306:51-58.
156. Koopman P. The delicate balance between male and female sex determining pathways: potential for disruption of early steps in sexual development. Int J Androl 2010; 33:252-258.
157. Rhen T, Schroeder A. Molecular mechanisms of sex determination in reptiles. Sex Dev 2010; 4:16-28.
158. Smith CA, Roeszler KN, Ohnesorg T, Cummins DM, Farlie PG, Doran TJ, Sinclair AH. The avian Z-linked gene DMRT1 is required for male sex determination in the chicken. Nature 2009; 461:267-271.
159. Kettlewell JR, Raymond CS, Zarkower D. Temperature-dependent expression of turtle Dmrt1 prior to sexual differentiation. Genesis 2000; 26:174-178.
160. Repetto GM, Wagstaff J, Korf BR, Knoll JH. Complex familial rearrangement of chromosome 9p24.3 detected by FISH. Am J Med Genet 1998; 76:306-309.
161. Christ LA, Crowe CA, Micale MA, Conroy JM, Schwartz S. Chromosome breakage hotspots and delineation of the critical region for the 9p-deletion syndrome. Am J Hum Genet 1999; 65:1387-1395.
162. Swinkels ME, Simons A, Smeets DF, Vissers LE, Veltman JA, Pfundt R, de Vries BB, Faas BH, Schrander-Stumpel CT, McCann E, Sweeney E, May P, et al. Clinical and cytogenetic characterization of 13 Dutch patients with deletion 9p syndrome: Delineation of the critical region for a consensus phenotype. Am J Med Genet A 2008; 146A:1430-1438.

163. Barbaro M, Balsamo A, Anderlid BM, Myhre AG, Gennari M, Nicoletti A, Pittalis MC, Oscarson M, Wedell A. Characterization of deletions at 9p affecting the candidate regions for sex reversal and deletion 9p syndrome by MLPA. Eur J Hum Genet 2009; 17:1439-1447.
164. Vinci G, Chantot-Bastaraud S, El Houate B, Lortat-Jacob S, Brauner R, McElreavey K. Association of deletion 9p, 46,XY gonadal dysgenesis and autistic spectrum disorder. Mol Hum Reprod 2007; 13:685-689.
165. Vasquez-Velasquez AI, Arnaud-Lopez L, Figuera LE, Padilla-Gutierrez JR, Rivas F, Rivera H. Ambiguous genitalia by 9p deletion inherent to a dic(Y;9)(q12;p24). J Appl Genet 2005; 46:415-418.
166. Ounap K, Uibo O, Zordania R, Kiho L, Ilus T, Oiglane-Shlik E, Bartsch O. Three patients with 9p deletions including DMRT1 and DMRT2: a girl with XY complement, bilateral ovotestes, and extreme growth retardation, and two XX females with normal pubertal development. Am J Med Genet A 2004; 130A:415-423.
167. Vialard F, Ottolenghi C, Gonzales M, Choiset A, Girard S, Siffroi JP, McElreavey K, Vibert-Guigue C, Sebaoun M, Joye N, Portnoi MF, Jaubert F, et al. Deletion of 9p associated with gonadal dysfunction in 46,XY but not in 46,XX human fetuses. J Med Genet 2002; 39:514-518.
168. Shetty S, Kirby P, Zarkower D, Graves JA. DMRT1 in a ratite bird: evidence for a role in sex determination and discovery of a putative regulatory element. Cytogenetic and genome research 2002; 99:245-251.
169. Yi W, Zarkower D. Similarity of DNA binding and transcriptional regulation by Caenorhabditis elegans MAB-3 and Drosophila melanogaster DSX suggests conservation of sex determining mechanisms. Development 1999; 126:873-881.
170. Raymond CS. Dmrt1, a gene related to worm and fly sexual regulators, is required for mammalian testis differentiation. Genes & Development 2000; 14:2587-2595.
171. Herpin A, Schartl M. Dmrt1 genes at the crossroads: a widespread and central class of sexual development factors in fish. The FEBS journal 2011; 278:1010-1019.
172. Koopman P. Sex determination: the power of DMRT1. Trends Genet 2009; 25:479-481.
173. Krentz AD, Murphy MW, Sarver AL, Griswold MD, Bardwell VJ, Zarkower D. DMRT1 promotes oogenesis by transcriptional activation of Stra8 in the mammalian fetal ovary. Developmental biology 2011; 356:63-70.
174. Yoshida S, Takakura A, Ohbo K, Abe K, Wakabayashi J, Yamamoto M, Suda T, Nabeshima Y. Neurogenin3 delineates the earliest stages of spermatogenesis in the mouse testis. Dev Biol 2004; 269:447-458.
175. Karpova T, Presley J, Manimaran RR, Scherrer SP, Tejada L, Peterson KR, Heckert LL. A FTZ-F1-containing yeast artificial chromosome recapitulates expression of steroidogenic factor 1 in vivo. Mol Endocrinol 2005; 19:2549-2563.
176. Godwin AR, Capecchi MR. Hoxc13 mutant mice lack external hair. Genes Dev 1998; 12:11-20.
177. Poorkaj P, Peterson KR, Schellenberg GD. Single-step conversion of P1 and P1 artificial chromosome clones into yeast artificial chromosomes. Genomics 2000; 68:106-110.
178. Burgers PM, Percival KJ. Transformation of yeast spheroplasts without cell fusion. Anal Biochem 1987; 163:391-397.
179. Peterson KR, Clegg CH, Li Q, Stamatoyannopoulos G. Production of transgenic mice with yeast artificial chromosomes. Trends Genet 1997; 13:61-66.
180. Peterson KR. Production and analysis of transgenic mice containing yeast artificial chromosomes. Genet Eng (N Y) 1997; 19:235-255.
181. Thomas KR, Deng C, Capecchi MR. High-fidelity gene targeting in embryonic stem cells by using sequence replacement vectors. Mol Cell Biol 1992; 12:2919-2923.
182. Hermann BP, Hornbaker KI, Maran RR, Heckert LL. Distal regulatory elements are required for Fshr expression, in vivo. Mol Cell Endocrinol 2007; 260-262:49-58.

183. Jimenez T, Sanchez G, Wertheimer E, Blanco G. Activity of the Na,K-ATPase alpha4 isoform is important for membrane potential, intracellular Ca2+, and pH to maintain motility in rat spermatozoa. Reproduction 2010; 139:835-845.
184. Heckert LL, Sawadogo M, Daggett MA, Chen JK. The USF proteins regulate transcription of the follicle-stimulating hormone receptor but are insufficient for cell-specific expression. Mol Endocrinol 2000; 14:1836-1848.
185. Gifford CA, Racicot K, Clark DS, Austin KJ, Hansen TR, Lucy MC, Davies CJ, Ott TL. Regulation of interferon-stimulated genes in peripheral blood leukocytes in pregnant and bred, nonpregnant dairy cows. J Dairy Sci 2007; 90:274-280.
186. Livak KJ, Schmittgen TD. Analysis of relative gene expression data using real-time quantitative PCR and the 2(-Delta Delta C(T)) Method. Methods 2001; 25:402-408.
187. Moore AW, Schedl A, McInnes L, Doyle M, Hecksher-Sorensen J, Hastie ND. YAC transgenic analysis reveals Wilms' tumour 1 gene activity in the proliferating coelomic epithelium, developing diaphragm and limb. Mech Dev 1998; 79:169-184.
188. Nagano R, Tabata S, Nakanishi Y, Ohsako S, Kurohmaru M, Hayashi Y. Reproliferation and relocation of mouse male germ cells (gonocytes) during prespermatogenesis. Anat Rec 2000; 258:210-220.
189. Tarulli GA, Stanton PG, Lerchl A, Meachem SJ. Adult sertoli cells are not terminally differentiated in the Djungarian hamster: effect of FSH on proliferation and junction protein organization. Biol Reprod 2006; 74:798-806.
190. Yomogida K, Ohtani H, Harigae H, Ito E, Nishimune Y, Engel JD, Yamamoto M. Developmental stage- and spermatogenic cycle-specific expression of transcription factor GATA-1 in mouse Sertoli cells. Development 1994; 120:1759-1766.
191. Russell LD, Bartke A, Goh JC. Postnatal development of the Sertoli cell barrier, tubular lumen, and cytoskeleton of Sertoli and myoid cells in the rat, and their relationship to tubular fluid secretion and flow. Am J Anat 1989; 184:179-189.
192. Cheng CY, Mruk DD. Regulation of spermiogenesis, spermiation and blood-testis barrier dynamics: novel insights from studies on Eps8 and Arp3. Biochem J 2011; 435:553-562.
193. Cheng CY, Mruk DD. Cell junction dynamics in the testis: Sertoli-germ cell interactions and male contraceptive development. Physiol Rev 2002; 82:825-874.
194. Mruk DD, Cheng CY. Tight junctions in the testis: new perspectives. Philos Trans R Soc Lond B Biol Sci 2010; 365:1621-1635.
195. Imai T, Kawai Y, Tadokoro Y, Yamamoto M, Nishimune Y, Yomogida K. In vivo and in vitro constant expression of GATA-4 in mouse postnatal Sertoli cells. Mol Cell Endocrinol 2004; 214:107-115.
196. Montoliu L. Gene transfer strategies in animal transgenesis. Cloning Stem Cells 2002; 4:39-46.
197. Mundlos S, Pelletier J, Darveau A, Bachmann M, Winterpacht A, Zabel B. Nuclear localization of the protein encoded by the Wilms' tumor gene WT1 in embryonic and adult tissues. Development 1993; 119:1329-1341.
198. Pelletier J, Schalling M, Buckler AJ, Rogers A, Haber DA, Housman D. Expression of the Wilms' tumor gene WT1 in the murine urogenital system. Genes Dev 1991; 5:1345-1356.
199. Lei N. Characterization of Dmrt1 in testis differentiation. United States -- Kansas: The University of Kansas; 2006. 3209838.
200. Lomeli H, Ramos-Mejia V, Gertsenstein M, Lobe CG, Nagy A. Targeted insertion of Cre recombinase into the TNAP gene: excision in primordial germ cells. Genesis 2000; 26:116-117.
201. Kubota H, Avarbock MR, Schmidt JA, Brinster RL. Spermatogonial stem cells derived from infertile Wv/Wv mice self-renew in vitro and generate progeny following transplantation. Biol Reprod 2009; 81:293-301.

202. Regadera J, Martinez-Garcia F, Gonzalez-Peramato P, Serrano A, Nistal M, Suarez-Quian C. Androgen receptor expression in sertoli cells as a function of seminiferous tubule maturation in the human cryptorchid testis. J Clin Endocrinol Metab 2001; 86:413-421.
203. Armstrong JF, Pritchard-Jones K, Bickmore WA, Hastie ND, Bard JB. The expression of the Wilms' tumour gene, WT1, in the developing mammalian embryo. Mech Dev 1993; 40:85-97.
204. Ketola I, Anttonen M, Vaskivuo T, Tapanainen JS, Toppari J, Heikinheimo M. Developmental expression and spermatogenic stage specificity of transcription factors GATA-1 and GATA-4 and their cofactors FOG-1 and FOG-2 in the mouse testis. Eur J Endocrinol 2002; 147:397-406.
205. LaVoie HA. The role of GATA in mammalian reproduction. Exp Biol Med (Maywood) 2003; 228:1282-1290.
206. Maga G, Hubscher U. Proliferating cell nuclear antigen (PCNA): a dancer with many partners. J Cell Sci 2003; 116:3051-3060.
207. Bar-Shira Maymon B, Paz G, Elliott DJ, Hammel I, Kleiman SE, Yogev L, Hauser R, Botchan A, Yavetz H. Maturation phenotype of Sertoli cells in testicular biopsies of azoospermic men. Hum Reprod 2000; 15:1537-1542.
208. Capo-chichi CD, Roland IH, Vanderveer L, Bao R, Yamagata T, Hirai H, Cohen C, Hamilton TC, Godwin AK, Xu XX. Anomalous expression of epithelial differentiation-determining GATA factors in ovarian tumorigenesis. Cancer Res 2003; 63:4967-4977.
209. Russell LD, Griswold MD. The Sertoli cell. Clearwater, FL: Cache River Press; 1993.
210. Schulze C. Response of the human testis to long-term estrogen treatment: morphology of Sertoli cells, Leydig cells and spermatogonial stem cells. Cell Tissue Res 1988; 251:31-43.
211. Wistuba J, Luetjens CM, Stukenborg JB, Poplinski A, Werler S, Dittmann M, Damm OS, Hamalainen T, Simoni M, Gromoll J. Male 41, XXY* mice as a model for klinefelter syndrome: hyperactivation of leydig cells. Endocrinology 2010; 151:2898-2910.
212. Lue Y, Rao PN, Sinha Hikim AP, Im M, Salameh WA, Yen PH, Wang C, Swerdloff RS. XXY male mice: an experimental model for Klinefelter syndrome. Endocrinology 2001; 142:1461-1470.
213. Lewejohann L, Damm OS, Luetjens CM, Hamalainen T, Simoni M, Nieschlag E, Gromoll J, Wistuba J. Impaired recognition memory in male mice with a supernumerary X chromosome. Physiol Behav 2009; 96:23-29.
214. Lue Y, Jentsch JD, Wang C, Rao PN, Hikim AP, Salameh W, Swerdloff RS. XXY mice exhibit gonadal and behavioral phenotypes similar to Klinefelter syndrome. Endocrinology 2005; 146:4148-4154.
215. Lue YH, Wang C, Liu PY, Erkilla K, Swerdloff RS. Insights into the pathogenesis of XXY phenotype from comparison of the clinical syndrome with an experimental XXY mouse model. Pediatr Endocrinol Rev 2010; 8 Suppl 1:140-144.
216. Guan G, Kobayashi T, Nagahama Y. Sexually dimorphic expression of two types of DM (Doublesex/Mab-3)-domain genes in a teleost fish, the Tilapia (Oreochromis niloticus). Biochem Biophys Res Commun 2000; 272:662-666.
217. Matsuda M, Nagahama Y, Shinomiya A, Sato T, Matsuda C, Kobayashi T, Morrey CE, Shibata N, Asakawa S, Shimizu N, Hori H, Hamaguchi S, et al. DMY is a Y-specific DM-domain gene required for male development in the medaka fish. Nature 2002; 417:559-563.
218. Nanda I, Kondo M, Hornung U, Asakawa S, Winkler C, Shimizu A, Shan Z, Haaf T, Shimizu N, Shima A, Schmid M, Schartl M. A duplicated copy of DMRT1 in the sex-determining region of the Y chromosome of the medaka, Oryzias latipes. Proc Natl Acad Sci U S A 2002; 99:11778-11783.
219. Kim S, Namekawa SH, Niswander LM, Ward JO, Lee JT, Bardwell VJ, Zarkower D. A mammal-specific Doublesex homolog associates with male sex chromatin and is required for male meiosis. PLoS Genet 2007; 3:e62.

220. Byers S, Graham R, Dai HN, Hoxter B. Development of Sertoli cell junctional specializations and the distribution of the tight-junction-associated protein ZO-1 in the mouse testis. Am J Anat 1991; 191:35-47.
221. Mulholland DJ, Dedhar S, Vogl AW. Rat seminiferous epithelium contains a unique junction (Ectoplasmic specialization) with signaling properties both of cell/cell and cell/matrix junctions. Biol Reprod 2001; 64:396-407.
222. Wang CQ, Cheng CY. A seamless trespass: germ cell migration across the seminiferous epithelium during spermatogenesis. J Cell Biol 2007; 178:549-556.
223. Mueller S, Rosenquist TA, Takai Y, Bronson RA, Wimmer E. Loss of nectin-2 at Sertoli-spermatid junctions leads to male infertility and correlates with severe spermatozoan head and midpiece malformation, impaired binding to the zona pellucida, and oocyte penetration. Biol Reprod 2003; 69:1330-1340.
224. Leblond CP, Clermont Y. Definition of the stages of the cycle of the seminiferous epithelium in the rat. Ann N Y Acad Sci 1952; 55:548-573.
225. Russell LD, Peterson RN. Sertoli cell junctions: morphological and functional correlates. Int Rev Cytol 1985; 94:177-211.
226. Vogl AW. Distribution and function of organized concentrations of actin filaments in mammalian spermatogenic cells and Sertoli cells. Int Rev Cytol 1989; 119:1-56.
227. Leblond CP, Clermont Y. Spermiogenesis of rat, mouse, hamster and guinea pig as revealed by the periodic acid-fuchsin sulfurous acid technique. Am J Anat 1952; 90:167-215.
228. Vogl AW, Pfeiffer DC, Redenbach DM. Ectoplasmic ("junctional") specializations in mammalian Sertoli cells: influence on spermatogenic cells. Ann N Y Acad Sci 1991; 637:175-202.
229. Dym M, Fawcett DW. The blood-testis barrier in the rat and the physiological compartmentation of the seminiferous epithelium. Biol Reprod 1970; 3:308-326.
230. Wong CH, Cheng CY. The blood-testis barrier: its biology, regulation, and physiological role in spermatogenesis. Curr Top Dev Biol 2005; 71:263-296.
231. Sprando RL, Heidinger RC, Russell LD. Spermiogenesis in the bluegill (Lepomis macrochirus): a study of cytoplasmic events including cell volume changes and cytoplasmic elimination. J Morphol 1988; 198:165-177.
232. Stanley HP, Lambert CC. The role of a Sertoli cell actin-myosin system in sperm bundle formation in the ratfish, Hydrolagus colliei (Chondrichthyes, Holocephali). J Morphol 1985; 186:223-236.
233. Fawcett DW, Anderson WA, Phillips DM. Morphogenetic factors influencing the shape of the sperm head. Dev Biol 1971; 26:220-251.
234. Vogl AW, Soucy LJ. Arrangement and possible function of actin filament bundles in ectoplasmic specializations of ground squirrel Sertoli cells. J Cell Biol 1985; 100:814-825.
235. Russell L. Observations on rat Sertoli ectoplasmic ('junctional') specializations in their association with germ cells of the rat testis. Tissue Cell 1977; 9:475-498.
236. O'Donnell L, McLachlan RI, Wreford NG, de Kretser DM, Robertson DM. Testosterone withdrawal promotes stage-specific detachment of round spermatids from the rat seminiferous epithelium. Biol Reprod 1996; 55:895-901.
237. Maekawa M, Ito C, Toyama Y, Suzuki-Toyota F, Fujita E, Momoi T, Toshimori K. Localisation of RA175 (Cadm1), a cell adhesion molecule of the immunoglobulin superfamily, in the mouse testis, and analysis of male infertility in the RA175-deficient mouse. Andrologia 2011; 43:180-188.
238. Miyahara M, Nakanishi H, Takahashi K, Satoh-Horikawa K, Tachibana K, Takai Y. Interaction of nectin with afadin is necessary for its clustering at cell-cell contact sites but not for its cis dimerization or trans interaction. J Biol Chem 2000; 275:613-618.

239. Mueller S, Wimmer E. Recruitment of nectin-3 to cell-cell junctions through trans-heterophilic interaction with CD155, a vitronectin and poliovirus receptor that localizes to alpha(v)beta3 integrin-containing membrane microdomains. J Biol Chem 2003; 278:31251-31260.
240. Ozaki-Kuroda K, Nakanishi H, Ohta H, Tanaka H, Kurihara H, Mueller S, Irie K, Ikeda W, Sakai T, Wimmer E, Nishimune Y, Takai Y. Nectin couples cell-cell adhesion and the actin scaffold at heterotypic testicular junctions. Curr Biol 2002; 12:1145-1150.
241. Toyama Y, Suzuki-Toyota F, Maekawa M, Ito C, Toshimori K. Disruption of ectoplasmic specializations between Sertoli cells and maturing spermatids by anti-nectin-2 and anti-nectin-3 antibodies. Asian J Androl 2008; 10:577-584.
242. Satoh-Horikawa K, Nakanishi H, Takahashi K, Miyahara M, Nishimura M, Tachibana K, Mizoguchi A, Takai Y. Nectin-3, a new member of immunoglobulin-like cell adhesion molecules that shows homophilic and heterophilic cell-cell adhesion activities. J Biol Chem 2000; 275:10291-10299.
243. Myers M, Ebling FJ, Nwagwu M, Boulton R, Wadhwa K, Stewart J, Kerr JB. Atypical development of Sertoli cells and impairment of spermatogenesis in the hypogonadal (hpg) mouse. J Anat 2005; 207:797-811.
244. Hosoi I, Toyama Y, Maekawa M, Ito H, Yuasa S. Development of the blood-testis barrier in the mouse is delayed by neonatally administered diethylstilbestrol but not by beta-estradiol 3-benzoate. Andrologia 2002; 34:255-262.
245. Etienne-Manneville S. Control of polarized cell morphology and motility by adherens junctions. Semin Cell Dev Biol 2011; 22:850-857.
246. Moroi S, Saitou M, Fujimoto K, Sakakibara A, Furuse M, Yoshida O, Tsukita S. Occludin is concentrated at tight junctions of mouse/rat but not human/guinea pig Sertoli cells in testes. Am J Physiol 1998; 274:C1708-1717.
247. Cyr DG, Hermo L, Egenberger N, Mertineit C, Trasler JM, Laird DW. Cellular immunolocalization of occludin during embryonic and postnatal development of the mouse testis and epididymis. Endocrinology 1999; 140:3815-3825.
248. Morita K, Sasaki H, Fujimoto K, Furuse M, Tsukita S. Claudin-11/OSP-based tight junctions of myelin sheaths in brain and Sertoli cells in testis. J Cell Biol 1999; 145:579-588.
249. Gow A, Southwood CM, Li JS, Pariali M, Riordan GP, Brodie SE, Danias J, Bronstein JM, Kachar B, Lazzarini RA. CNS myelin and sertoli cell tight junction strands are absent in Osp/claudin-11 null mice. Cell 1999; 99:649-659.
250. Bartles JR, Wierda A, Zheng L. Identification and characterization of espin, an actin-binding protein localized to the F-actin-rich junctional plaques of Sertoli cell ectoplasmic specializations. J Cell Sci 1996; 109 (Pt 6):1229-1239.
251. Chen B, Li A, Wang D, Wang M, Zheng L, Bartles JR. Espin contains an additional actin-binding site in its N terminus and is a major actin-bundling protein of the Sertoli cell-spermatid ectoplasmic specialization junctional plaque. Mol Biol Cell 1999; 10:4327-4339.
252. Toyama Y, Maekawa M, Yuasa S. Ectoplasmic specializations in the Sertoli cell: new vistas based on genetic defects and testicular toxicology. Anat Sci Int 2003; 78:1-16.
253. Lyon MF, Hawkes SG. X-linked gene for testicular feminization in the mouse. Nature 1970; 227:1217-1219.
254. Irizarry RA, Bolstad BM, Collin F, Cope LM, Hobbs B, Speed TP. Summaries of Affymetrix GeneChip probe level data. Nucleic Acids Res 2003; 31:e15.
255. Bolstad BM, Irizarry RA, Astrand M, Speed TP. A comparison of normalization methods for high density oligonucleotide array data based on variance and bias. Bioinformatics 2003; 19:185-193.
256. Tukey JW. Exploratory data analysis. Reading, Mass.: Addison-Wesley Pub. Co.; 1977.
257. Gautier L, Cope L, Bolstad BM, Irizarry RA. affy - analysis of Affymetrix GeneChip data at the probe level. Bioinformatics 2004; 20:307-315.

258. Benjamini Y, Hochberg Y. Controlling the False Discovery Rate - a Practical and Powerful Approach to Multiple Testing. Journal of the Royal Statistical Society Series B-Methodological 1995; 57:289-300.
259. Smyth GK. Linear models and empirical bayes methods for assessing differential expression in microarray experiments. Stat Appl Genet Mol Biol 2004; 3:Article3.
260. Dennis G, Jr., Sherman BT, Hosack DA, Yang J, Gao W, Lane HC, Lempicki RA. DAVID: Database for Annotation, Visualization, and Integrated Discovery. Genome Biol 2003; 4:P3.
261. Mathivanan S, Simpson RJ. ExoCarta: A compendium of exosomal proteins and RNA. Proteomics 2009; 9:4997-5000.
262. Mathivanan S, Fahner CJ, Reid GE, Simpson RJ. ExoCarta 2012: database of exosomal proteins, RNA and lipids. Nucleic Acids Res 2012; 40:D1241-1244.
263. Li X, Wong J, Tsai SY, Tsai MJ, O'Malley BW. Progesterone and glucocorticoid receptors recruit distinct coactivator complexes and promote distinct patterns of local chromatin modification. Mol Cell Biol 2003; 23:3763-3773.
264. Hiroi H, Christenson LK, Chang L, Sammel MD, Berger SL, Strauss JF, 3rd. Temporal and spatial changes in transcription factor binding and histone modifications at the steroidogenic acute regulatory protein (stAR) locus associated with stAR transcription. Mol Endocrinol 2004; 18:791-806.
265. Hermann BP, Hornbaker K, Rice DA, Sawadogo M, Heckert LL. In vivo regulation of follicle-stimulating hormone receptor by the transcription factors upstream stimulatory factor 1 and upstream stimulatory factor 2 is cell specific. Endocrinology 2008; 149:5297-5306.
266. Langmead B, Trapnell C, Pop M, Salzberg SL. Ultrafast and memory-efficient alignment of short DNA sequences to the human genome. Genome Biol 2009; 10:R25.
267. Hesselberth JR, Chen X, Zhang Z, Sabo PJ, Sandstrom R, Reynolds AP, Thurman RE, Neph S, Kuehn MS, Noble WS, Fields S, Stamatoyannopoulos JA. Global mapping of protein-DNA interactions in vivo by digital genomic footprinting. Nat Methods 2009; 6:283-289.
268. Leleu M, Lefebvre G, Rougemont J. Processing and analyzing ChIP-seq data: from short reads to regulatory interactions. Brief Funct Genomics 2010; 9:466-476.
269. Rye MB, Saetrom P, Drablos F. A manually curated ChIP-seq benchmark demonstrates room for improvement in current peak-finder programs. Nucleic Acids Res 2011; 39:e25.
270. Fujita PA, Rhead B, Zweig AS, Hinrichs AS, Karolchik D, Cline MS, Goldman M, Barber GP, Clawson H, Coelho A, Diekhans M, Dreszer TR, et al. The UCSC Genome Browser database: update 2011. Nucleic Acids Res 2011; 39:D876-882.
271. Dreszer TR, Karolchik D, Zweig AS, Hinrichs AS, Raney BJ, Kuhn RM, Meyer LR, Wong M, Sloan CA, Rosenbloom KR, Roe G, Rhead B, et al. The UCSC Genome Browser database: extensions and updates 2011. Nucleic Acids Res 2012; 40:D918-923.
272. Bailey TL, Williams N, Misleh C, Li WW. MEME: discovering and analyzing DNA and protein sequence motifs. Nucleic Acids Res 2006; 34:W369-373.
273. Gupta S, Stamatoyannopoulos JA, Bailey TL, Noble WS. Quantifying similarity between motifs. Genome Biology 2007; 8.
274. Murphy MW, Zarkower D, Bardwell VJ. Vertebrate DM domain proteins bind similar DNA sequences and can heterodimerize on DNA. BMC Mol Biol 2007; 8:58.
275. Qin J, Li MJ, Wang P, Zhang MQ, Wang J. ChIP-Array: combinatory analysis of ChIP-seq/chip and microarray gene expression data to discover direct/indirect targets of a transcription factor. Nucleic Acids Res 2011; 39:W430-436.
276. Shima JE, McLean DJ, McCarrey JR, Griswold MD. The murine testicular transcriptome: characterizing gene expression in the testis during the progression of spermatogenesis. Biol Reprod 2004; 71:319-330.
277. VanGompel MJ, Xu EY. A novel requirement in mammalian spermatid differentiation for the DAZ-family protein Boule. Hum Mol Genet 2010; 19:2360-2369.

278. Lee KH, Song GJ, Kang IS, Kim SW, Paick JS, Chung CH, Rhee K. Ubiquitin-specific protease activity of USP9Y, a male infertility gene on the Y chromosome. Reprod Fertil Dev 2003; 15:129-133.
279. Hoffmann SC, Schellack C, Textor S, Konold S, Schmitz D, Cerwenka A, Pflanz S, Watzl C. Identification of CLEC12B, an inhibitory receptor on myeloid cells. J Biol Chem 2007; 282:22370-22375.
280. Setoguchi K, Misaki Y, Kawahata K, Shimada K, Juji T, Tanaka S, Oda H, Shukunami C, Nishizaki Y, Hiraki Y, Yamamoto K. Suppression of T cell responses by chondromodulin I, a cartilage-derived angiogenesis inhibitory factor: therapeutic potential in rheumatoid arthritis. Arthritis Rheum 2004; 50:828-839.
281. Ohnishi S, Okabe K, Obata H, Otani K, Ishikane S, Ogino H, Kitamura S, Nagaya N. Involvement of tazarotene-induced gene 1 in proliferation and differentiation of human adipose tissue-derived mesenchymal stem cells. Cell Prolif 2009; 42:309-316.
282. Paratcha G, Ledda F. GDNF and GFRalpha: a versatile molecular complex for developing neurons. Trends Neurosci 2008; 31:384-391.
283. Zhang Z, Kostetskii I, Tang W, Haig-Ladewig L, Sapiro R, Wei Z, Patel AM, Bennett J, Gerton GL, Moss SB, Radice GL, Strauss JF, 3rd. Deficiency of SPAG16L causes male infertility associated with impaired sperm motility. Biol Reprod 2006; 74:751-759.
284. Zhang Z, Shen X, Gude DR, Wilkinson BM, Justice MJ, Flickinger CJ, Herr JC, Eddy EM, Strauss JF, 3rd. MEIG1 is essential for spermiogenesis in mice. Proc Natl Acad Sci U S A 2009; 106:17055-17060.
285. Krizsan-Agbas D, Pedchenko T, Smith PG. Neurotrimin is an estrogen-regulated determinant of peripheral sympathetic innervation. J Neurosci Res 2008; 86:3086-3095.
286. Struyk AF, Canoll PD, Wolfgang MJ, Rosen CL, D'Eustachio P, Salzer JL. Cloning of neurotrimin defines a new subfamily of differentially expressed neural cell adhesion molecules. J Neurosci 1995; 15:2141-2156.
287. Lin YM, Chung CL, Cheng YS. Posttranscriptional regulation of CDC25A by BOLL is a conserved fertility mechanism essential for human spermatogenesis. J Clin Endocrinol Metab 2009; 94:2650-2657.
288. Doyle JM, Gao J, Wang J, Yang M, Potts PR. MAGE-RING protein complexes comprise a family of E3 ubiquitin ligases. Mol Cell 2010; 39:963-974.
289. McLaren A. Mammalian germ cells: birth, sex, and immortality. Cell Struct Funct 2001; 26:119-122.
290. Gassei K, Schlatt S. Testicular morphogenesis: comparison of in vivo and in vitro models to study male gonadal development. Ann N Y Acad Sci 2007; 1120:152-167.
291. Ross AJ, Capel B. Signaling at the crossroads of gonad development. Trends Endocrinol Metab 2005; 16:19-25.
292. Moreno-Mendoza N, Torres-Maldonado L, Chimal-Monroy J, Harley V, Merchant-Larios H. Disturbed expression of Sox9 in pre-sertoli cells underlies sex-reversal in mice b6.Ytir. Biol Reprod 2004; 70:114-122.
293. Anderson EL, Baltus AE, Roepers-Gajadien HL, Hassold TJ, de Rooij DG, van Pelt AM, Page DC. Stra8 and its inducer, retinoic acid, regulate meiotic initiation in both spermatogenesis and oogenesis in mice. Proc Natl Acad Sci U S A 2008; 105:14976-14980.
294. Mark M, Jacobs H, Oulad-Abdelghani M, Dennefeld C, Feret B, Vernet N, Codreanu CA, Chambon P, Ghyselinck NB. STRA8-deficient spermatocytes initiate, but fail to complete, meiosis and undergo premature chromosome condensation. J Cell Sci 2008; 121:3233-3242.
295. Suzuki A, Saga Y. Nanos2 suppresses meiosis and promotes male germ cell differentiation. Genes Dev 2008; 22:430-435.
296. Shen R, Xie T. NANOS: a germline stem cell's Guardian Angel. J Mol Cell Biol 2010; 2:76-77.

297. Gearhart MD, Corcoran CM, Wamstad JA, Bardwell VJ. Polycomb group and SCF ubiquitin ligases are found in a novel BCOR complex that is recruited to BCL6 targets. Mol Cell Biol 2006; 26:6880-6889.
298. Hofmann MC, Narisawa S, Hess RA, Millan JL. Immortalization of Germ-Cells and Somatic Testicular Cells Using the Sv40 Large T-Antigen. Experimental Cell Research 1992; 201:417-435.
299. Daggett MA, Rice DA, Heckert LL. Expression of steroidogenic factor 1 in the testis requires an E box and CCAAT box in its promoter proximal region. Biol Reprod 2000; 62:670-679.
300. Suzuki A, Igarashi K, Aisaki K, Kanno J, Saga Y. NANOS2 interacts with the CCR4-NOT deadenylation complex and leads to suppression of specific RNAs. Proc Natl Acad Sci U S A 2010; 107:3594-3599.
301. Barrios F, Filipponi D, Pellegrini M, Paronetto MP, Di Siena S, Geremia R, Rossi P, De Felici M, Jannini EA, Dolci S. Opposing effects of retinoic acid and FGF9 on Nanos2 expression and meiotic entry of mouse germ cells. J Cell Sci 2010; 123:871-880.
302. Suzuki A, Tsuda M, Saga Y. Functional redundancy among Nanos proteins and a distinct role of Nanos2 during male germ cell development. Development 2007; 134:77-83.
303. Lin Y, Gill ME, Koubova J, Page DC. Germ cell-intrinsic and -extrinsic factors govern meiotic initiation in mouse embryos. Science 2008; 322:1685-1687.
304. Kobayashi S, Yamada M, Asaoka M, Kitamura T. Essential role of the posterior morphogen nanos for germline development in Drosophila. Nature 1996; 380:708-711.
305. Tsuda M, Sasaoka Y, Kiso M, Abe K, Haraguchi S, Kobayashi S, Saga Y. Conserved role of nanos proteins in germ cell development. Science 2003; 301:1239-1241.
306. Murata Y, Wharton RP. Binding of pumilio to maternal hunchback mRNA is required for posterior patterning in Drosophila embryos. Cell 1995; 80:747-756.
307. Asaoka M, Sano H, Obara Y, Kobayashi S. Maternal Nanos regulates zygotic gene expression in germline progenitors of Drosophila melanogaster. Mech Dev 1998; 78:153-158.
308. Asaoka-Taguchi M, Yamada M, Nakamura A, Hanyu K, Kobayashi S. Maternal Pumilio acts together with Nanos in germline development in Drosophila embryos. Nat Cell Biol 1999; 1:431-437.
309. Sato K, Hayashi Y, Ninomiya Y, Shigenobu S, Arita K, Mukai M, Kobayashi S. Maternal Nanos represses hid/skl-dependent apoptosis to maintain the germ line in Drosophila embryos. Proc Natl Acad Sci U S A 2007; 104:7455-7460.
310. Wreden C, Verrotti AC, Schisa JA, Lieberfarb ME, Strickland S. Nanos and pumilio establish embryonic polarity in Drosophila by promoting posterior deadenylation of hunchback mRNA. Development 1997; 124:3015-3023.
311. Suzuki H, Sada A, Yoshida S, Saga Y. The heterogeneity of spermatogonia is revealed by their topology and expression of marker proteins including the germ cell-specific proteins Nanos2 and Nanos3. Dev Biol 2009; 336:222-231.
312. Kadyrova LY, Habara Y, Lee TH, Wharton RP. Translational control of maternal Cyclin B mRNA by Nanos in the Drosophila germline. Development 2007; 134:1519-1527.
313. Sonoda J, Wharton RP. Drosophila Brain Tumor is a translational repressor. Genes Dev 2001; 15:762-773.
314. Parker R, Sheth U. P bodies and the control of mRNA translation and degradation. Mol Cell 2007; 25:635-646.
315. Wharton RP, Struhl G. RNA regulatory elements mediate control of Drosophila body pattern by the posterior morphogen nanos. Cell 1991; 67:955-967.
316. Zhong XP, Krangel MS. An enhancer-blocking element between alpha and delta gene segments within the human T cell receptor alpha/delta locus. Proc Natl Acad Sci U S A 1997; 94:5219-5224.

317. Fromm M, Berg P. Deletion mapping of DNA regions required for SV40 early region promoter function in vivo. J Mol Appl Genet 1982; 1:457-481.
318. Fujino RS, Tanaka K, Morimatsu M, Tamura K, Kogo H, Hara T. Spermatogonial cell-mediated activation of an IkappaBzeta-independent nuclear factor-kappaB pathway in Sertoli cells induces transcription of the lipocalin-2 gene. Mol Endocrinol 2006; 20:904-915.
319. Kim S, Kettlewell JR, Anderson RC, Bardwell VJ, Zarkower D. Sexually dimorphic expression of multiple doublesex-related genes in the embryonic mouse gonad. Gene Expr Patterns 2003; 3:77-82.
320. Lanfranco F, Kamischke A, Zitzmann M, Nieschlag E. Klinefelter's syndrome. Lancet 2004; 364:273-283.
321. Aksglaede L, Wikstrom AM, Rajpert-De Meyts E, Dunkel L, Skakkebaek NE, Juul A. Natural history of seminiferous tubule degeneration in Klinefelter syndrome. Hum Reprod Update 2006; 12:39-48.
322. Wikstrom AM, Dunkel L. Testicular function in Klinefelter syndrome. Horm Res 2008; 69:317-326.
323. Palombi F, Salanova M, Tarone G, Farini D, Stefanini M. Distribution of beta 1 integrin subunit in rat seminiferous epithelium. Biol Reprod 1992; 47:1173-1182.
324. Salanova M, Stefanini M, De Curtis I, Palombi F. Integrin receptor alpha 6 beta 1 is localized at specific sites of cell-to-cell contact in rat seminiferous epithelium. Biol Reprod 1995; 52:79-87.
325. Takahashi K, Nakanishi H, Miyahara M, Mandai K, Satoh K, Satoh A, Nishioka H, Aoki J, Nomoto A, Mizoguchi A, Takai Y. Nectin/PRR: an immunoglobulin-like cell adhesion molecule recruited to cadherin-based adherens junctions through interaction with Afadin, a PDZ domain-containing protein. J Cell Biol 1999; 145:539-549.
326. Bouchard MJ, Dong Y, McDermott BM, Jr., Lam DH, Brown KR, Shelanski M, Bellve AR, Racaniello VR. Defects in nuclear and cytoskeletal morphology and mitochondrial localization in spermatozoa of mice lacking nectin-2, a component of cell-cell adherens junctions. Mol Cell Biol 2000; 20:2865-2873.
327. Ikeda W, Nakanishi H, Miyoshi J, Mandai K, Ishizaki H, Tanaka M, Togawa A, Takahashi K, Nishioka H, Yoshida H, Mizoguchi A, Nishikawa S, et al. Afadin: A key molecule essential for structural organization of cell-cell junctions of polarized epithelia during embryogenesis. J Cell Biol 1999; 146:1117-1132.
328. Sekerkova G, Zheng L, Loomis PA, Changyaleket B, Whitlon DS, Mugnaini E, Bartles JR. Espins are multifunctional actin cytoskeletal regulatory proteins in the microvilli of chemosensory and mechanosensory cells. J Neurosci 2004; 24:5445-5456.
329. Inagaki M, Irie K, Ishizaki H, Tanaka-Okamoto M, Morimoto K, Inoue E, Ohtsuka T, Miyoshi J, Takai Y. Roles of cell-adhesion molecules nectin 1 and nectin 3 in ciliary body development. Development 2005; 132:1525-1537.
330. Tozeren A, Wu S, Hoxter B, Xu W, Adamson ED, Byers SW. Vinculin and cell-cell adhesion. Cell Adhes Commun 1998; 5:49-59.
331. Palovuori R, Myrsky E, Eskelinen S. Membrane potential and endocytic activity control disintegration of cell-cell adhesion and cell fusion in vinculin-injected MDBK cells. J Cell Physiol 2004; 200:417-427.
332. Sumida GM, Tomita TM, Shih W, Yamada S. Myosin II activity dependent and independent vinculin recruitment to the sites of E-cadherin-mediated cell-cell adhesion. BMC Cell Biol 2011; 12:48.
333. Dikic I, Wakatsuki S, Walters KJ. Ubiquitin-binding domains - from structures to functions. Nat Rev Mol Cell Biol 2009; 10:659-671.
334. Welchman RL, Gordon C, Mayer RJ. Ubiquitin and ubiquitin-like proteins as multifunctional signals. Nat Rev Mol Cell Biol 2005; 6:599-609.

335. Ikeda F, Dikic I. Atypical ubiquitin chains: new molecular signals. 'Protein Modifications: Beyond the Usual Suspects' review series. EMBO Rep 2008; 9:536-542.
336. Ikeda F, Crosetto N, Dikic I. What determines the specificity and outcomes of ubiquitin signaling? Cell 2010; 143:677-681.
337. Iwai K, Tokunaga F. Linear polyubiquitination: a new regulator of NF-kappaB activation. EMBO Rep 2009; 10:706-713.
338. Plasterk RH. Micro RNAs in animal development. Cell 2006; 124:877-881.
339. Tolia NH, Joshua-Tor L. Slicer and the argonautes. Nat Chem Biol 2007; 3:36-43.
340. Aravin A, Gaidatzis D, Pfeffer S, Lagos-Quintana M, Landgraf P, Iovino N, Morris P, Brownstein MJ, Kuramochi-Miyagawa S, Nakano T, Chien M, Russo JJ, et al. A novel class of small RNAs bind to MILI protein in mouse testes. Nature 2006; 442:203-207.
341. Girard A, Sachidanandam R, Hannon GJ, Carmell MA. A germline-specific class of small RNAs binds mammalian Piwi proteins. Nature 2006; 442:199-202.
342. Grivna ST, Beyret E, Wang Z, Lin H. A novel class of small RNAs in mouse spermatogenic cells. Genes Dev 2006; 20:1709-1714.
343. Grivna ST, Pyhtila B, Lin H. MIWI associates with translational machinery and PIWI-interacting RNAs (piRNAs) in regulating spermatogenesis. Proc Natl Acad Sci U S A 2006; 103:13415-13420.
344. Lau NC, Seto AG, Kim J, Kuramochi-Miyagawa S, Nakano T, Bartel DP, Kingston RE. Characterization of the piRNA complex from rat testes. Science 2006; 313:363-367.
345. Klattenhoff C, Theurkauf W. Biogenesis and germline functions of piRNAs. Development 2008; 135:3-9.
346. Carmell MA, Girard A, van de Kant HJ, Bourc'his D, Bestor TH, de Rooij DG, Hannon GJ. MIWI2 is essential for spermatogenesis and repression of transposons in the mouse male germline. Dev Cell 2007; 12:503-514.
347. Wang J, Saxe JP, Tanaka T, Chuma S, Lin H. Mili interacts with tudor domain-containing protein 1 in regulating spermatogenesis. Curr Biol 2009; 19:640-644.
348. Bao J, Wang L, Lei J, Hu Y, Liu Y, Shen H, Yan W, Xu C. STK31(TDRD8) is dynamically regulated throughout mouse spermatogenesis and interacts with MIWI protein. Histochem Cell Biol 2012; 137:377-389.
349. Hayashi K, Chuva de Sousa Lopes SM, Kaneda M, Tang F, Hajkova P, Lao K, O'Carroll D, Das PP, Tarakhovsky A, Miska EA, Surani MA. MicroRNA biogenesis is required for mouse primordial germ cell development and spermatogenesis. PLoS One 2008; 3:e1738.
350. Shoji M, Tanaka T, Hosokawa M, Reuter M, Stark A, Kato Y, Kondoh G, Okawa K, Chujo T, Suzuki T, Hata K, Martin SL, et al. The TDRD9-MIWI2 complex is essential for piRNA-mediated retrotransposon silencing in the mouse male germline. Dev Cell 2009; 17:775-787.
351. Frost RJ, Hamra FK, Richardson JA, Qi X, Bassel-Duby R, Olson EN. MOV10L1 is necessary for protection of spermatocytes against retrotransposons by Piwi-interacting RNAs. Proc Natl Acad Sci U S A 2010; 107:11847-11852.
352. Sabeur K, Ball BA, Corbin CJ, Conley A. Characterization of a novel, testis-specific equine serine/threonine kinase. Mol Reprod Dev 2008; 75:867-873.
353. Ratajczak J, Wysoczynski M, Hayek F, Janowska-Wieczorek A, Ratajczak MZ. Membrane-derived microvesicles: important and underappreciated mediators of cell-to-cell communication. Leukemia 2006; 20:1487-1495.
354. Sullivan R, Saez F, Girouard J, Frenette G. Role of exosomes in sperm maturation during the transit along the male reproductive tract. Blood Cells Mol Dis 2005; 35:1-10.
355. Dowhan DH, Hong EP, Auboeuf D, Dennis AP, Wilson MM, Berget SM, O'Malley BW. Steroid hormone receptor coactivation and alternative RNA splicing by U2AF65-related proteins CAPERalpha and CAPERbeta. Mol Cell 2005; 17:429-439.

356. Liu L, Xie N, Rennie P, Challis JR, Gleave M, Lye SJ, Dong X. Consensus PP1 binding motifs regulate transcriptional corepression and alternative RNA splicing activities of the steroid receptor coregulators, p54nrb and PSF. Mol Endocrinol 2011; 25:1197-1210.
357. Collart MA, Panasenko OO. The Ccr4--not complex. Gene 2012; 492:42-53.
358. Collart MA. Global control of gene expression in yeast by the Ccr4-Not complex. Gene 2003; 313:1-16.
359. Winkler GS, Mulder KW, Bardwell VJ, Kalkhoven E, Timmers HT. Human Ccr4-Not complex is a ligand-dependent repressor of nuclear receptor-mediated transcription. EMBO J 2006; 25:3089-3099.
360. Neely GG, Kuba K, Cammarato A, Isobe K, Amann S, Zhang LY, Murata M, Elmen L, Gupta V, Arora S, Sarangi R, Dan D, et al. A Global In Vivo Drosophila RNAi Screen Identifies NOT3 as a Conserved Regulator of Heart Function. Cell 2010; 141:142-153.
361. Albert TK, Hanzawa H, Legtenberg YIA, de Ruwe MJ, van den Heuvel FAJ, Collart MA, Boelens R, Timmers HTM. Identification of a ubiquitin-protein ligase subunit within the CCR4-NOT transcription repressor complex. Embo Journal 2002; 21:355-364.
362. Hanzawa H, de Ruwe MJ, Albert TK, van der Vliet PC, Timmers HTM, Boelens R. The structure of the C4C4 RING finger of human NOT4 reveals features distinct from those of C3HC4 RING fingers. Journal of Biological Chemistry 2001; 276:10185-10190.
363. Masuda T, Itoh K, Higashitsuji H, Nakazawa N, Sakurai T, Liu Y, Tokuchi H, Fujita T, Zhao Y, Nishiyama H, Tanaka T, Fukumoto M, et al. Cold-inducible RNA-binding protein (Cirp) interacts with Dyrk1b/Mirk and promotes proliferation of immature male germ cells in mice. Proc Natl Acad Sci U S A 2012; 109:10885-10890.